

CENTRAL RESEARCH LIBRARY  
DOCUMENT COLLECTION

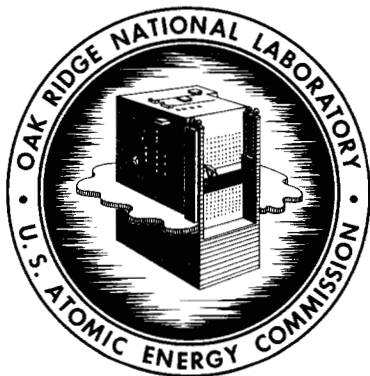


3 4456 0365259 9

ORNL-3383  
UC-32 - Mathematics and Computers

MONTE CARLO CALCULATIONS ON  
INTRANUCLEAR CASCADES

H. W. Bertini



**OAK RIDGE NATIONAL LABORATORY**

operated by

**UNION CARBIDE CORPORATION**

for the

**U.S. ATOMIC ENERGY COMMISSION**

Printed in USA. Price \$3.00 . Available from the Clearinghouse for Federal  
Scientific and Technical Information, National Bureau of Standards,  
U.S. Department of Commerce, Springfield, Virginia 22151

**LEGAL NOTICE**

This report was prepared as an account of Government sponsored work. Neither the United States, nor the Commission, nor any person acting on behalf of the Commission:

- A. Makes any warranty or representation, expressed or implied, with respect to the accuracy, completeness, or usefulness of the information contained in this report, or that the use of any information, apparatus, method, or process disclosed in this report may not infringe privately owned rights; or
- B. Assumes any liabilities with respect to the use of, or for damages resulting from the use of any information, apparatus, method, or process disclosed in this report.

As used in the above, "person acting on behalf of the Commission" includes any employee or contractor of the Commission, or employee of such contractor, to the extent that such employee or contractor of the Commission, or employee of such contractor prepares, disseminates, or provides access to, any information pursuant to his employment or contract with the Commission, or his employment with such contractor.

ORNL-3383

Contract No. W-7405-eng-26

Neutron Physics Division

MONTE CARLO CALCULATIONS ON INTRANUCLEAR CASCADES\*

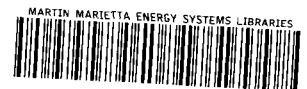
H. W. Bertini

Date Issued

APR 23 1963

\*Submitted to the University of Tennessee in partial fulfillment of the requirements for the degree of Doctor of Philosophy.

OAK RIDGE NATIONAL LABORATORY  
Oak Ridge, Tennessee  
operated by  
UNION CARBIDE CORPORATION  
for the  
U.S. ATOMIC ENERGY COMMISSION



3 4456 0365259 9



## ABSTRACT

The basic assumption of the Serber model in the description of high-energy nuclear reactions is that the interactions of incident particles with complex nuclei can be described in terms of individual particle-particle collisions within the nucleus. Calculations were performed in the past making use of this assumption, but using nuclear models that have properties that conflict with experimental evidence. Discrepancies observed between the results of the calculations performed previously and experimental data were attributed to the deficiencies of the nuclear model.

The present work makes use of a more realistic nuclear model, recent cross-section data, and an exact statistical sampling technique. The sampling technique has not been used previously in calculations of this type. Calculations were performed for incident  $\pi^+$ ,  $\pi^-$ , neutrons, and protons on nuclei from lithium to uranium. The energy range of the incident particles varied from about 50 to 350 Mev, i.e., the energy region in which pion production is not likely. Free-particle cross sections were used in determining the collisions within the nucleus, and statistical sampling techniques were used throughout. The problem was coded for the IBM-7090. Extensive comparisons with experiment were made and the results indicate that the calculation can be used to predict most of the cascade data for incident nucleons on complex nuclei, but only the gross features of the data are predictable for incident pions on nuclei. The effects of several nuclear configurations on the results of the calculations were investigated in some of the areas where discrepancies exist between the experimental results and those of the calculation. These configurations consisted of

uniform and nonuniform nucleon density distributions in spherically symmetric nuclei of various radii. The results of these investigations indicate that the greatest effect is due to the nuclear dimensions rather than the nucleon density distribution within the nucleus for a given nucleon volume.

## TABLE OF CONTENTS

CHAPTER	PAGE
I. INTRODUCTION .....	1
History .....	2
Limitations of Previous Calculations .....	3
Purpose of the Study .....	4
Justification for the Study .....	5
Definition of Terms .....	6
II. NUCLEAR MODEL .....	7
Nucleon Density Distribution Inside the Nucleus .....	7
Momentum Distribution of Nucleons Inside the Nucleus ....	9
Potential Energy Distribution Inside the Nucleus .....	11
III. CROSS-SECTION DATA .....	15
Nucleon-Nucleon Data .....	15
Total Cross Sections .....	15
Differential Scattering Cross Sections .....	19
Pion-Nucleon Data .....	22
Differential Scattering Cross Sections .....	22
Total Cross Sections .....	25
Pion Absorption Cross Section .....	26
IV. THE CALCULATION .....	31
General Description .....	31
Sampling Technique for Nucleon-Nucleon Scattering Angles...	34
Sampling Techniques for Pion-Nucleon Scattering Angles ....	37
Sampling Technique for Determining the Point of Collision and Type of Collision .....	38

CHAPTER	PAGE
Pion Absorption .....	42
Limitations .....	44
V. COMPARISONS WITH EXPERIMENT: INCIDENT NUCLEONS .....	46
Nonelastic Cross Sections .....	46
Excitation Energy of the Residual Nucleus .....	46
Spectra of Cascade Particles .....	53
Angular Distribution of Cascade Particles .....	55
Cascade Particle Multiplicities .....	56
(p,pn) Cross Sections .....	61
VI. COMPARISONS WITH EXPERIMENT: INCIDENT PIONS .....	114
Nonelastic Cross Sections .....	114
Energy Spectrum for Nonelastic Scattering .....	114
Angular Distribution of Nonelastic Pion Scattering .....	118
Pion Absorption .....	119
Pion Reactions Involving Charge Exchange .....	122
Errors .....	150
VII. SUMMARY AND CONCLUSIONS .....	152
BIBLIOGRAPHY .....	155
App. A. DERIVATION OF THE PION-NUCLEON DIFFERENTIAL SCATTERING CROSS SECTIONS IN TERMS OF THE PHASE SHIFTS .....	160
App. B. TWO-PARTICLE RELATIVISTIC KINEMATICS .....	178
App. C. SAMPLING TECHNIQUE FOR DETERMINING DISTANCE OF TRAVEL BETWEEN COLLISIONS, TYPE OF COLLISION, AND MOMENTUM OF STRUCK PARTICLE .....	185

CHAPTER	PAGE
App. D. LIST OF TABLES .....	195
App. E. LIST OF FIGURES .....	197
ACKNOWLEDGEMENTS .....	220



## CHAPTER I

### INTRODUCTION

In the present work calculations were performed on the interactions of  $\pi$ -mesons and nucleons with nuclei, and the results were compared with a large quantity of experimental data. The energy range of the incident particles was restricted to that in which pion production is not likely (i.e., 50 to 350 Mev).

The basic assumption of the method employed in the calculation was that the interactions of high-energy particles with the nucleus can be represented by free particle-particle collisions inside the nucleus, an approach first suggested by Serber.<sup>1</sup> The justification for the assumption is that the wave length of the incident particle is of the order of the internucleon distance ( $\sim 10^{-13}$  cm). The deBroglie wave length divided by  $2\pi$ ,  $\lambda$ , at a few energies is illustrated:

Energy (Mev)	$\lambda$ (cm)	
	Nucleon	$\pi$ -Meson
20	$1.02 \times 10^{-13}$	$2.55 \times 10^{-13}$
100	$4.45 \times 10^{-14}$	$1.02 \times 10^{-13}$
500	$1.82 \times 10^{-14}$	$3.17 \times 10^{-14}$

The physical process that can be approximately described by free-particle collisions within the nucleus is called the cascade. When the

---

<sup>1</sup>R. Serber, Phys. Rev. 72, 1114 (1947).

particle energy becomes relatively small it is assumed that this energy becomes distributed among all the nucleons in the nucleus, and descriptions of subsequent processes are usually given in terms of an evaporation model.

The present work represents calculations done on the cascade process. The statistical approach is used and Monte Carlo techniques are employed in carrying out the calculations.

## I. HISTORY

Goldberger<sup>2</sup> was one of the first to carry out calculations based on Serber's suggestion, and he initiated the statistical approach to this problem. His work required two weeks for two people in order to complete the hand calculations for one hundred incident-particle histories. Subsequently, similar calculations were performed by Bernardini, Booth, and Lindenbaum;<sup>3</sup> McManus, Sharp, and Gellman;<sup>4</sup> and Meadows<sup>5</sup> using the two-dimensional techniques of Bernardini *et al.*; and Ivanova and P'anov,<sup>6</sup> in Russia, who performed calculations using only fifty histories per case.

The most recent and the only detailed three-dimensional treatment using an electronic computer was that of Metropolis, Bivins, Storm,

---

<sup>2</sup>M. L. Goldberger, Phys. Rev. 74, 1268 (1948).

<sup>3</sup>G. Bernardini E. T. Booth, and S. J. Lindenbaum, Phys. Rev. 88, 1017 (1952).

<sup>4</sup>H. McManus, W. T. Sharp, and H. Gellman, Phys. Rev. 93, 924A (1954).

<sup>5</sup>J. W. Meadows, Phys. Rev. 98, 744 (1955).

<sup>6</sup>N. S. Ivanova and I. I. P'anov, Soviet Phys.-JETP 4, 367 (1957).

Turkevich, Miller, and Friedlander.<sup>7,8</sup> The present study is an attempt to improve on their work in the low-energy range.

## II. LIMITATIONS OF PREVIOUS CALCULATIONS

The limitations of the previous calculations are mainly in the nuclear models employed. Standard simplifying assumptions were made in constructing the models, but these generally conflict with experimental evidence. For example, it has been assumed that the nucleon density distribution inside the nucleus was uniform. However, Hofstadter<sup>9</sup> has found that a Fermi-type distribution function, i.e., a function in which the density varies with the radius in the same way that the Fermi energy distribution varies with the energy, could be used to improve the fit to the differential cross-section data obtained for the electron scattering from the nuclei. This distribution function is of the form

$$\rho(r) = \frac{\rho_1}{e^{(r-c)/z_1} + 1},$$

where  $c$  and  $z_1$  are parameters and  $\rho_1$  is a normalization constant.

In the previous calculations a momentum distribution obtained from a "zero-temperature" Fermi energy distribution was used to represent the momentum of the nucleons within the nucleus. There are several

---

<sup>7</sup>N. Metropolis et al., "Monte Carlo Calculations on Intranuclear Cascades. Part I. Low-Energy Studies," Phys. Rev. 110, 185 (1958).

<sup>8</sup>Ibid., "Part II. High-Energy Studies and Pion Processes," p. 204.

<sup>9</sup>R. Hofstadter, Revs. Modern Phys. 28, 214 (1956).

experimental papers on this subject,<sup>10</sup> the conclusions of each being that the experimental data can be fit most reasonably by a Gaussian momentum distribution, or, where it was tried, by a Fermi distribution for finite temperatures. The values of  $kT$  recommended for the Gaussian distributions ranged from 13 to 20 Mev.

In the work of Metropolis et al.<sup>8</sup> on pions there was no pion-nucleon potential employed, whereas analysis indicates that the potential is attractive and of magnitude 10 to 40 Mev. Fujii<sup>11</sup> calculated the pion potential by applying the optical model to his pion-nucleus scattering data. Other references to work of this type is included in a paper by Zerby.<sup>12</sup>

### III. PURPOSE OF THE STUDY

This work has several aims. One is to perform calculations using an improved nuclear model that incorporates the main features of the experimental work just mentioned.<sup>9-12</sup> An approximation to the diffuse nuclear surface is made. Along with this one obtains a nonuniform potential and a composite momentum distribution for the nucleons inside the nucleus which approximates a Gaussian. A potential for pions is included.

---

<sup>10</sup>L. S. Azhgirey et al., Nucl. Phys. 13, 258 (1959); J. D. Dowell et al., Pt. 1, Proc. Phys. Soc. 75, 24 (1960); J. M. Wilcox and B. J. Moyer, Phys. Rev. 99, 875 (1955).

<sup>11</sup>T. A. Fujii, Phys. Rev. 113, 695 (1959).

<sup>12</sup>C. D. Zerby, Phys. Rev. 124, 2029 (1961).

Another aim is to examine the areas of agreement or disagreement with experiment for this model. To this end rather exhaustive comparisons with experiments are made, and attention is directed to those areas where the changes in the model might influence the results.

Finally, it is desired to produce a computer program on intranuclear cascades which would be available for general use.

#### IV. JUSTIFICATION FOR THE STUDY

Since the publication of the work of Metropolis et al. a fairly large series of papers (about twenty) have been published which use that study as a basis or as an aid for comparing theory with experiment. In each case where there is a discrepancy between theory and experiment the deficiency of the nuclear model is noted as a possible source of discrepancy. In the present calculation the major deficiencies of the previous model have been removed and some of the major discrepancies between the calculations and experimental data can be investigated.

The machine for which the work of Metropolis et al. was coded (Maniac) has been dismantled. Thus, except for the cases already run and on file it is impossible to obtain additional information on the cascade process. In particular, there is a need for neutron and pion data and it is intended that the present program will satisfy that need.

In addition to the work reported here, an intermediate code has been written which transforms the data from the cascade process into suitable initial parameters for a calculation of the subsequent physical process which is assumed to be evaporation. A code for the evaporation

process has been written by Dresner<sup>13</sup> which incorporates the work of Dostrovsky et al.<sup>14</sup>

## V. DEFINITION OF TERMS

There is some overlap in the terminology which has been used to describe the high-energy nuclear processes. The terms "inelastic," "quasi-elastic," "absorption," and "nonelastic" have been used to describe the reactions which are not pure elastic scattering from the nucleus as a whole. The term "quasi-elastic," which is in considerable use, was proposed by Cladis et al.<sup>15</sup> to describe processes which are elastic on a particle-particle basis but inelastic in the sense that a rearrangement of the nucleus is brought about. "Absorption" is generally used to describe all nonelastic events when an optical model analysis is made. "Inelastic" has been carried over from its use in describing low-energy phenomena where the scattered particle retains its identity but leaves the nucleus in an excited state.

In this work the term "nonelastic" will be used to refer to all events which are not elastic scattering with the nucleus as a whole.

---

<sup>13</sup>L. Dresner, EVAP - A FORTRAN Program for Calculating the Evaporation of Various Particles from Excited Compound Nuclei, Oak Ridge National Laboratory Report ORNL-CF-61-12-30 (Dec. 19, 1961).

<sup>14</sup>I. Dostrovsky, Z. Fraenkel, and G. Friedlander, Phys. Rev. 116, 683 (1959).

<sup>15</sup>J. B. Cladis, W. N. Hess, and B. J. Moyer, Phys. Rev. 87, 425 (1952).

## CHAPTER II

### NUCLEAR MODEL

A description of the nuclear model is given here. It consists of the assumptions and illustrations related to the density distribution, the momentum distribution, and the potential energy distribution of the nucleons inside the nucleus.

#### I. NUCLEON DENSITY DISTRIBUTION INSIDE THE NUCLEUS

Hofstadter<sup>1</sup> has been quite successful in fitting the electron scattering data for medium- to heavy-weight nuclei with a nuclear charge distribution of the type

$$\rho(r) = \frac{\rho_1}{e^{(r-c)/z_1} + 1},$$

where  $c$  and  $z_1$  are parameters. If the skin thickness,  $t$ , is defined by the difference in the radii for which the charge density becomes 0.1 and 0.9 of its central density, then  $t$  is equal to  $4.40z_1$  for this distribution. The parameter  $c$  is the radius at which the charge density is one-half of its central value, and Hofstadter assumed that it varied with the atomic number,  $A$ , as  $r_1 A^{1/3}$ . By using a least-squares analysis on  $c$  and  $t$  to fit the experimental data he found that  $t$  and  $r_1 = c A^{-1/3}$  remained relatively constant over a broad range of nuclei. For the present

---

<sup>1</sup>See Ref. 9, Chapter I.

calculation  $r_1$  was taken to be  $1.07 \times 10^{-13}$  cm and  $z_1$  was taken to be  $0.545 \times 10^{-13}$  cm as representative values for these constants.

An approximation to this continuous distribution was made by using three concentric spheres. The density in each region (i.e., the central sphere and the two surrounding spherical annuli) was set equal to the average value of the continuous distribution in that region. The overall normalization was such that the sum of the products of the volume and the proton density for each region was equal to the number of protons in the nucleus being considered. The outer radius of each region was chosen by solving for  $r$  in the expression

$$\rho(r) = \alpha_i \rho(0), \quad i = 1, 2, 3,$$

where  $\alpha_1 = 0.9$ ,  $\alpha_2 = 0.2$ , and  $\alpha_3 = 0.01$  for the standard nuclear configuration used in this work. When the results for any other nuclear configuration are given, that configuration will be described. For instance, results are given in some cases where  $\alpha_1$ ,  $\alpha_2$ , and  $\alpha_3$  are all equal, which corresponds to a uniform density distribution.

The region boundaries were taken to be the same for neutrons and protons. The normalization for neutrons was similar to that for protons, which makes the ratio of neutrons to protons in all regions the same as the neutron-to-proton ratio of the nucleus. The nuclear surface effects have been given careful consideration since 1941,<sup>2</sup> and this work is

---

<sup>2</sup>E. Feenberg, Phys. Rev. 59, 593 (1941); E. Wigner, University of Pennsylvania Bicentennial Conference (1941).

summarized in a review article by Wilets.<sup>3</sup> The results of his most recent calculation included in that article indicate that for a heavy element ( $A = 225$ ,  $Z = 93$ ) the neutron and proton densities have about the same mean radius. When both density distributions are scaled to the same central value, the proton distribution has a slight hump and has a larger value in the region where the density begins to decrease, but the neutron distribution has a longer tail (approximately one Fermi). The distributions thus cross each other in the region of the nuclear surface with the neutron density somewhat larger at the outer edge. Therefore, this recent work indicates that there may not be a very large difference in the ratio of neutrons to protons at the surface of the nucleus from the ratio for the entire nucleus.

Effects arising from small differences in the neutron-to-proton ratios in this region would be completely masked in the present calculation. This is indicated later when the results of the calculation using a uniform nucleon density distribution and a nonuniform nucleon density distribution are compared.

An example of a few nuclear configurations is given in Figure 1.

## II. MOMENTUM DISTRIBUTION OF NUCLEONS INSIDE THE NUCLEUS

The neutrons and protons were assumed to have a zero-temperature Fermi momentum distribution in each region, i.e., the momentum distribution function,  $f(p)$ , was of the form

---

<sup>3</sup>L. Wilets, Revs. Modern Phys. 30, 542 (1958).

UNCLASSIFIED  
ORNL-LR-DWG-72979

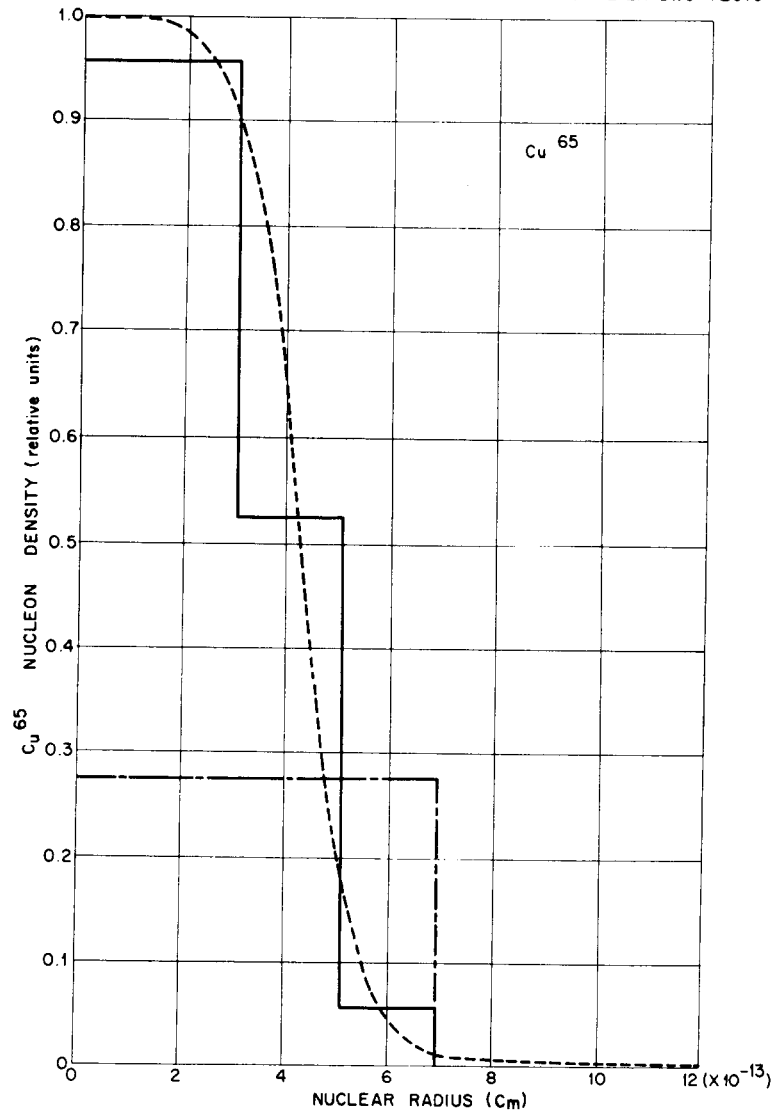


Figure 1. A Comparison of Various Nucleon Density Distributions for Nucleons Inside the Nucleus. — Standard three-region configuration; - - - uniform distribution; - . - . Hofstadter's curve [R. Hofstadter, Revs. Modern Phys. 28, 214 (1956)].

$$f(p) = c p^2,$$

where

$$\int_0^{p_f} f(p) dp = \text{total number of neutrons (protons) in that region, and}$$

$p_f$  is the momentum of a nucleon corresponding to the Fermi energy. This energy, which depends on the particle density, differed for each type of nucleon in each region. Hence, the composite momentum distribution for the entire nucleus is not a zero-temperature Fermi distribution. The composite distribution and a Maxwell-Boltzmann distribution with a  $kT$  value of 15 Mev are illustrated in Figure 2.

### III. POTENTIAL ENERGY DISTRIBUTION INSIDE THE NUCLEUS

The binding energy of the most loosely bound nucleon was taken to be 7 Mev and was assumed to be the same for all the regions and for all the nuclei. Therefore, one cannot account for symmetry effects, magic number effects, etc. The potential energy in each region was determined by the sum of the zero-temperature Fermi energy of the nucleons in each region plus the binding energy of the most loosely bound nucleon. This combination yields reasonable potentials for both the nucleons and the pions.<sup>4</sup> The pion potential in each region was taken to be the same as the potential

---

<sup>4</sup>See Ref. 11, Chapter I.

UNCLASSIFIED  
ORNL-LR-DWG 70413R1

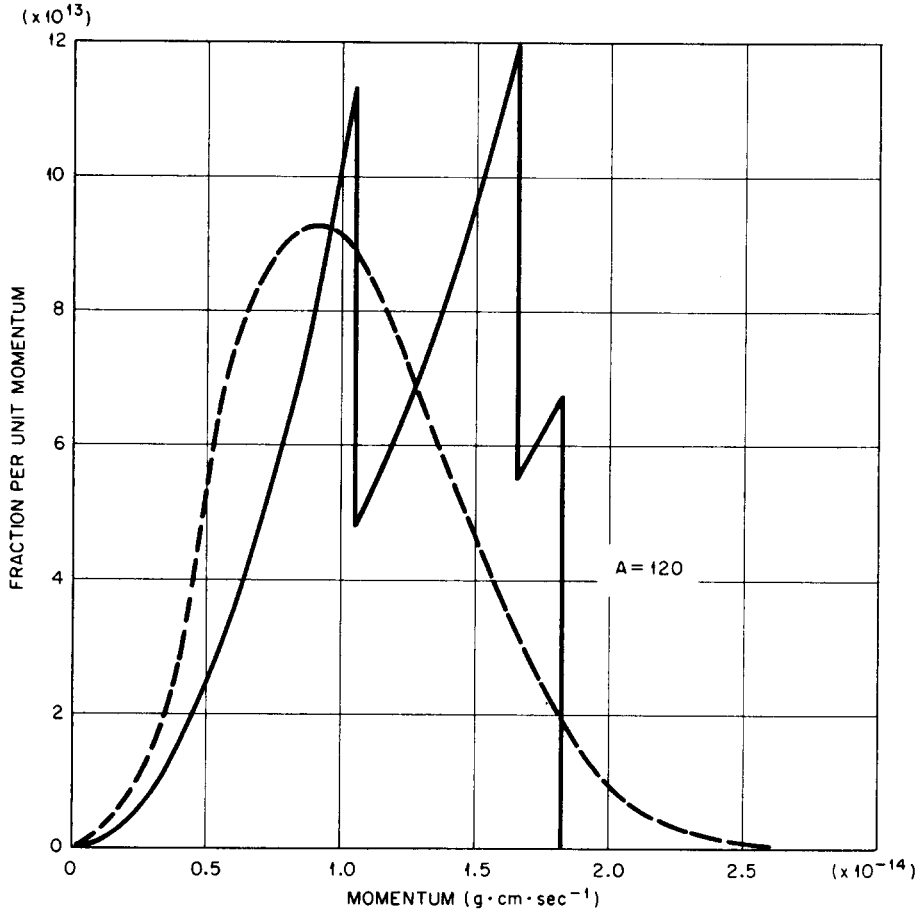


Figure 2. Momentum Distribution of Nucleons Inside the Nucleus.  
—— Composite distribution from three zero-temperature Fermi energy distributions; - - - Maxwell-Boltzmann distribution with kT value of 15 Mev.

of the nucleon with which it interacts. The potential values for a typical case are illustrated in Figure 3.

UNCLASSIFIED  
ORNL-LR-DWG 70431

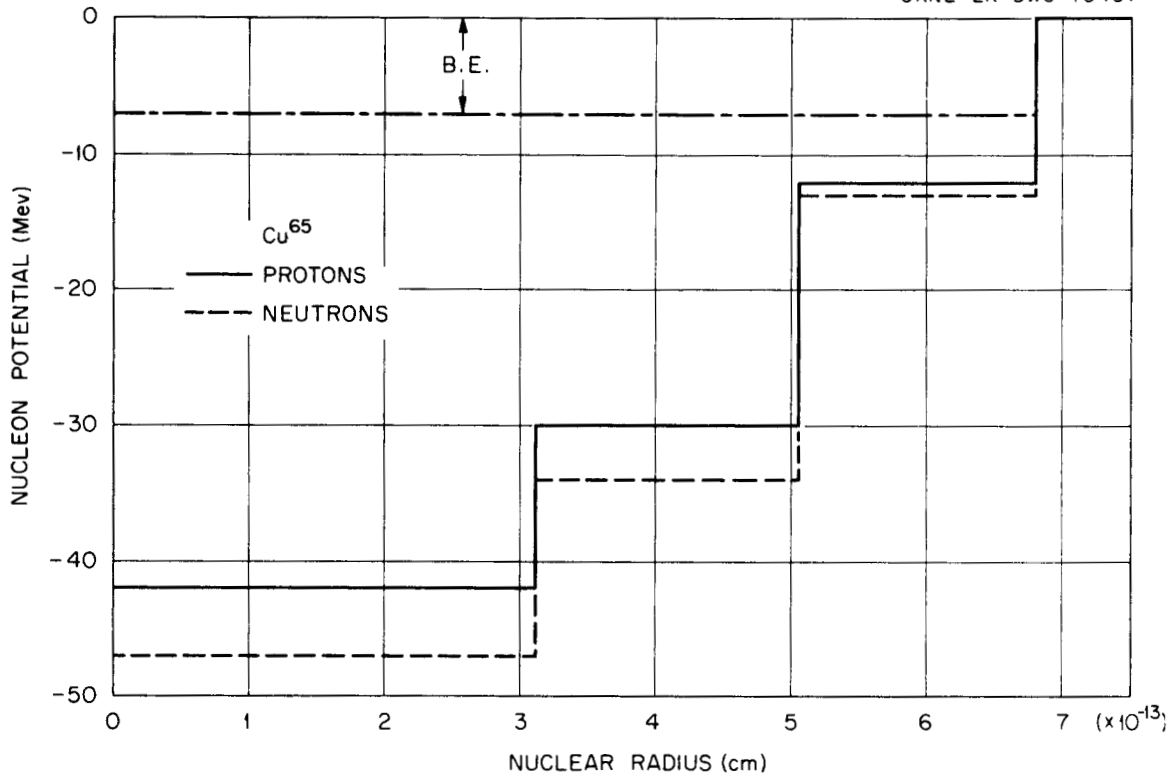


Figure 3. Nucleon Potential vs. Nuclear Radius for a Typical Nucleus. B. E. is the fixed binding energy of the most loosely bound nucleon.

## CHAPTER III

### CROSS-SECTION DATA

The free-particle cross sections that were used are illustrated or tabulated in this chapter. A description of the calculations and of the assumptions that were made to obtain the cross sections that were not available from experiments is given.

#### I. NUCLEON-NUCLEON DATA

##### A. Total Cross Sections

Figures 4 and 5 are graphs of the high-energy proton-proton and neutron-proton cross sections that were used in this work. The paper by Chen, Leavitt, and Shapiro<sup>1</sup> is an excellent source for these cross sections. Since pion production in any collision was not considered, the total cross sections were always employed when p-p cross-section data for any type was needed in the calculation. The cross sections that were used at the lower energies are given below.

---

<sup>1</sup>F. F. Chen, C. P. Leavitt, and A. M. Shapiro, Phys. Rev. 103, 211 (1956).

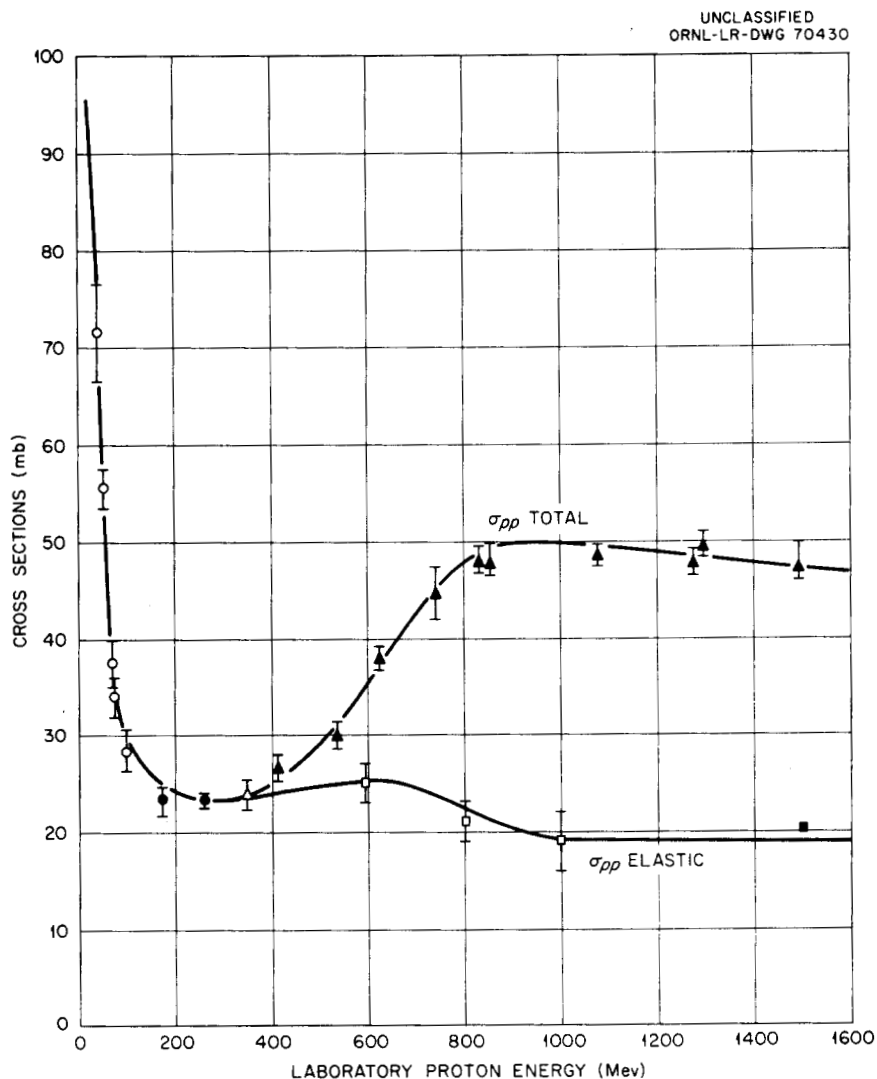


Figure 4. Proton-Proton Total and Elastic Cross Sections vs. Energy.  $\circ$  U. E. Kruse, J. M. Teem, and N. F. Ramsey, Phys. Rev. 101, 1079 (1956);  $\bullet$  O. Chamberlain and J. D. Garrison, Phys. Rev. 95 1349(L) (1954);  $\Delta$  O. Chamberlain, E. Segre', and C. Wiegand, Phys. Rev. 83, 923 (1951);  $\blacktriangle$  F. F. Chen, C. P. Leavitt, and A. M. Shapiro, Phys. Rev. 103, 211 (1956);  $\square$  L. W. Smith, A. W. McReynolds, and G. Snow, Phys. Rev. 97, 1186 (1955);  $\blacksquare$  W. B. Fowler et al., Phys. Rev. 103, 1479 (1956).

UNCLASSIFIED  
ORNL-LR-DWG 70429

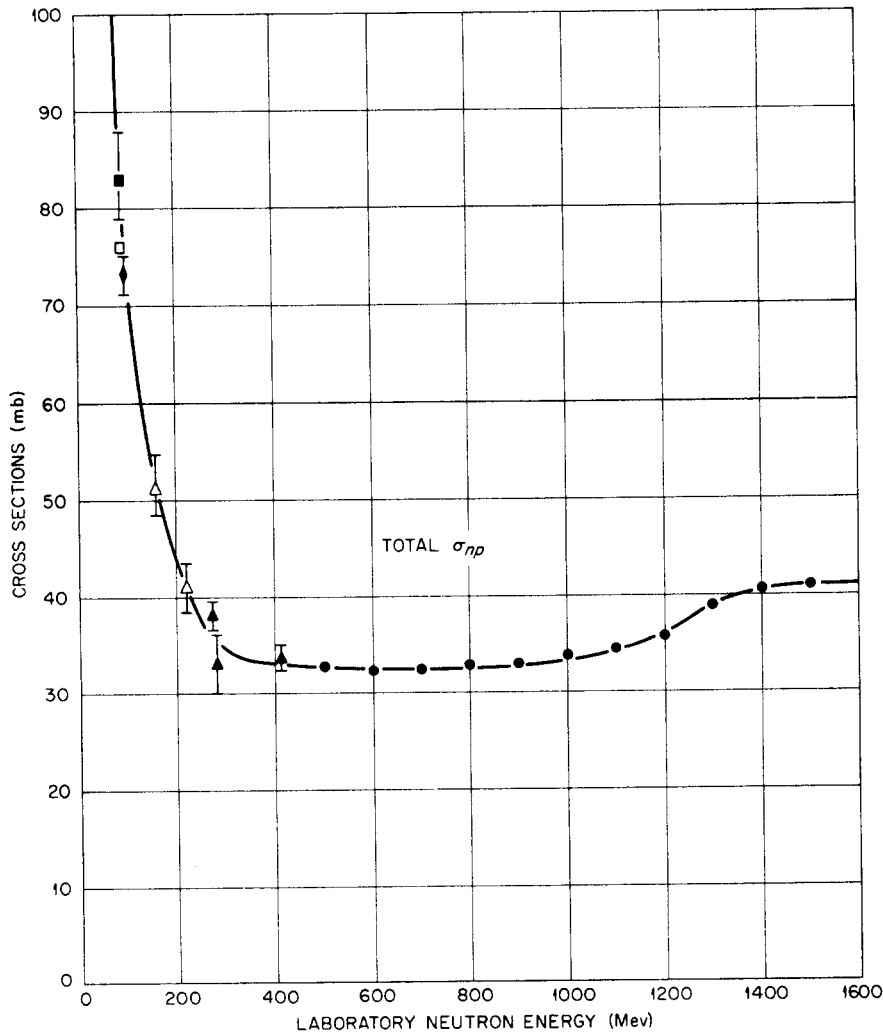


Figure 5. Neutron-Proton Total Cross Sections vs. Energy.

■ L. J. Cook *et al.*, Phys. Rev. 75, 7 (1949); □ J. Hadley *et al.*, Phys. Rev. 75, 351 (1949); ♦ J. DeJuren and N. Knable, Phys. Rev. 77, 606 (1950); △ J. DeJuren and B. J. Moyer, Phys. Rev. 81, 919 (1951); ▲ A. V. Nedzel, Phys. Rev. 94, 174 (1954); ● F. F. Chen, C. P. Leavitt, and A. M. Shapiro, Phys. Rev. 103, 211 (1956).

<u>Energy (Mev)</u>	<u>Total Cross Section (barns)</u>	
	<u>n-p</u>	<u>p-p</u>
0	2.000	0.700
20	0.480	0.160
40	0.220	0.072
60	0.140	
80	0.098	

The low-energy p-p cross sections were calculated from the differential cross sections given by Beretta et al.<sup>2</sup> An estimate of the average value of these differential cross sections in the range from about forty to ninety degrees was made, and the total p-p cross section was calculated by using this average value to represent the isotropic, noncoulomb part of the p-p cross section. This was done to eliminate coulomb effects from this cross section, for it was decided not to include these effects in the p-p reactions. A scattering due to coulomb forces alone would result in the particle being only slightly deflected from its original course since the differential cross section is highly peaked in the forward direction. In the present work this is equivalent to no scattering at all. The low-energy n-p cross sections were taken from the compilation of Hughes and Schwartz.<sup>3</sup> The n-n cross section was taken to be equal to the p-p cross section.

---

<sup>2</sup>L. Beretta, C. Villi, and F. Ferrari, Nuovo Cimento 12, S499 (1954).

<sup>3</sup>D. J. Hughes and R. B. Schwartz, Neutron Cross Sections, Brookhaven National Laboratory Report BNL-325 (July 1, 1958).

## B. Differential Scattering Cross Sections

The differential cross section for p-p scattering was assumed to be isotropic in the center-of-mass system for proton energies up to 500 Mev. For energies from 500 to 1,000 Mev semiempirical fits were made to the p-p cross-section data reported by Hess.<sup>4</sup> An expression of the form

$$\frac{d\sigma}{d\Omega} (p-p) = A + B\mu^3$$

was used, where  $\mu$  represents the cosine of the scattering angle in the center-of-mass system. Representative values of A and B that were used in this work are given in Table I. Again an attempt was made to eliminate the coulomb effects by ignoring the coulomb peak at small scattering angles.

Cross-section data is required at energies which are higher than the limiting value already given for the incident particles ( $\approx 350$  Mev) because the relative kinetic energy for colliding particles whose momenta are antiparallel will be larger than the energy of the incident particle alone. This energy can exceed the threshold for pion production, but the cross section for production is relatively small and reactions of this type are infrequent for the energy range to which the incident particles have been restricted.

The work of Hess<sup>4</sup> was also used as a source for the n-p differential scattering cross-section data. Four parameters were used to fit this data semiempirically. They are defined by the following:

---

<sup>4</sup>W. N. Hess, Revs. Modern Phys. 30, 368 (1958).

TABLE I

REPRESENTATIVE VALUES OF THE SEMIEMPIRICAL PARAMETERS USED  
TO DESCRIBE THE NUCLEON-NUCLEON DIFFERENTIAL  
SCATTERING CROSS SECTIONS<sup>a</sup>

Incident Particle Laboratory Energy (Mev)	n-p Parameters (mb/sr)				p-p Parameters (mb/sr)	
	A <sub>1</sub>	B <sub>1</sub>	B <sub>2</sub>	B <sub>3</sub>	A	B
0	1592.0	0	0	0		
40	12.0	7.0	7.0			
80	5.2	8.1	8.3			
120	3.3	6.6	9.0			
160	2.3	3.9	7.7			
200	2.0	3.6	6.5			
240	1.9	3.6	6.2			
280	1.8	3.6	6.0			
320	1.7	3.6		7.8		
360	1.5	3.6		7.4		
400	1.4	3.6		7.0		
440	1.3	3.6		6.7		
480	1.2	3.6		6.4		
520	1.1	3.6		6.1	3.88	1.70
560	1.0	3.6		5.8	3.19	4.00
600	1.0	3.6		5.6	2.60	5.60
640	0.9	3.6		5.4	2.25	6.85
680	0.8	3.6		5.1	1.92	7.95

TABLE I (continued)

Incident Particle Laboratory Energy (Mev)	n-p Parameters (mb/sr)				p-p Parameters (mb/sr)	
	A <sub>1</sub>	B <sub>1</sub>	B <sub>2</sub>	B <sub>3</sub>	A	B
720	0.7	3.6		4.9	1.64	8.75
760					1.40	9.40
800					1.20	9.70
840					0.99	9.85
880					0.80	9.90
920					0.69	9.90
980					0.60	9.90
1000					0.58	9.90

<sup>a</sup>Parameters defined in text on pages 19 and 22.

For  $0 \leq E_n \leq 740$  Mev,

$$\frac{d\sigma}{d\Omega} (n-p) = A_1 + B_1\mu^3 \quad 0 \leq \mu \leq 1.$$

For  $0 \leq E_n \leq 300$  Mev,

$$\frac{d\sigma}{d\Omega} (n-p) = A_1 + B_2\mu^4 \quad -1 \leq \mu \leq 0.$$

For  $300 \text{ Mev} \leq E_n \leq 740$  Mev,

$$\frac{d\sigma}{d\Omega} (n-p) = A_1 + B_3\mu^6 \quad -1 \leq \mu \leq 0.$$

The values of  $A_1$ ,  $B_1$ ,  $B_2$ , and  $B_3$  that were used are given at representative energies in Table I.

The binomial expressions along with these coefficients represent the experimental data either within or just outside of the experimental errors at all energies.

## II. PION-NUCLEON DATA

### A. Differential Scattering Cross Sections

For this work it is necessary to know all the pion-nucleon free-particle differential cross sections as a function of energy. The relationship between the cross sections of the various pion-nucleon combinations cannot be deduced as simply as was done for the nucleon-nucleon case where it was necessary only to invoke charge symmetry. In the pion-nucleon case charge independence is assumed and then the scattering amplitudes of the various pion-nucleon reactions are calculated and compared. This is the procedure that was used here. The details of

the calculation are given in Appendix A, and an outline of the method is given by Bethe and deHoffmann.<sup>5</sup>

One assumes that states higher than the  $P_{3/2}$  state do not contribute to the scattering at these energies,<sup>6</sup> and then only the phase shifts up to  $\delta_{33}$  are needed, where the first subscript is twice the isotopic spin of the state and the second is twice the angular momentum. The calculation establishes the following equalities:

$$\frac{d\sigma}{d\Omega} (\pi^+ + p) = \frac{d\sigma}{d\Omega} (\pi^- + n),$$

$$\frac{d\sigma}{d\Omega} (\pi^- + p)_{\text{elastic}} = \frac{d\sigma}{d\Omega} (\pi^+ + n)_{\text{elastic}},$$

$$\frac{d\sigma}{d\Omega} (\pi^0 + p)_{\text{elastic}} = \frac{d\sigma}{d\Omega} (\pi^0 + n)_{\text{elastic}}.$$

In addition, the calculations indicate that the differential scattering cross section for charge exchange scattering in the four last reactions are the same. It appears that one might have written these equations down directly. The  $\pi^0$  cross section is required because the half life is long enough to permit its escape from the nucleus.

The phase shifts that were used in calculating the differential cross sections are those of Orear.<sup>7</sup> He indicates that only a relatively few are needed for a description of the data, and these are depicted in Figure 6.

---

<sup>5</sup>H. A. Bethe and F. deHoffmann, Mesons and Fields (Row, Peterson and Company, Evanston, 1955), Vol. II, p. 63.

<sup>6</sup>H. L. Anderson et al., Phys. Rev. 91, 155 (1953).

<sup>7</sup>J. Orear, Phys. Rev. 100, 288 (1955).

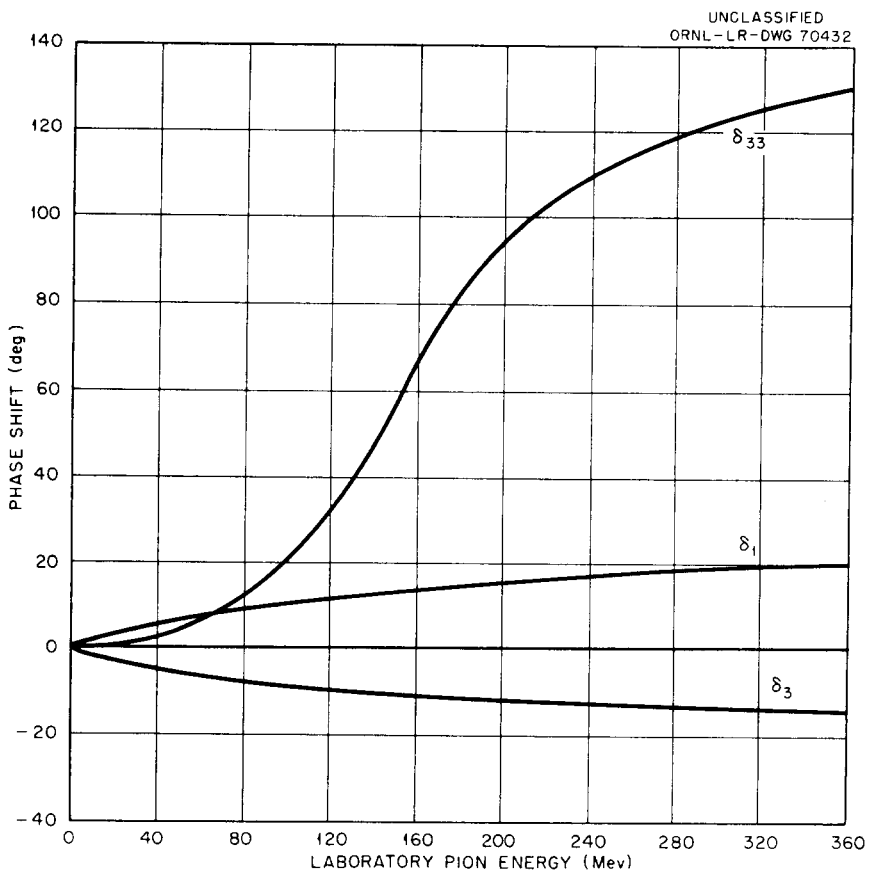


Figure 6. Phase Shifts for Pion-Proton Scattering vs. Pion Laboratory Energy [J. Orear, Phys. Rev. 100, 288 (1955)].

B. Total Cross Sections

Since the differential cross sections for charge exchange scattering are taken to be equal, the total cross sections are simply related. Namely,

$$\sigma_t(\pi^0 + p) = \frac{F_{-x}}{F_{ox}} \sigma_t(\pi^- + p),$$

where  $F_{-x}$  is the fraction of the exchange cross section plus elastic scattering cross section that is exchange for  $(\pi^- + p)$  scattering, and  $F_{ox}$  is the same fraction for  $(\pi^0 + p)$  scattering. These fractions were calculated by integrating the expressions for the differential cross sections derived in the appendix. For example,

$$F_{-x} = \frac{\int_{\Omega} \left[ \frac{d\sigma}{d\Omega} (\pi^- + p)_{\text{exchange}} \right] d\Omega}{\int_{\Omega} \left[ \frac{d\sigma}{d\Omega} (\pi^- + p)_{\text{exchange}} + \frac{d\sigma}{d\Omega} (\pi^- + p)_{\text{elastic}} \right] d\Omega} .$$

Then

$$\sigma_{\text{exchange}}(\pi^0 + p) = \sigma_{\text{exchange}}(\pi^- + p) = F_{-x} \sigma_t(\pi^- + p)$$

and

$$\sigma_{\text{elastic}}(\pi^0 + p) = \sigma_t(\pi^0 + p) - \sigma_{\text{exchange}}(\pi^0 + p).$$

The experimental total cross sections for  $\pi^+$ -proton and  $\pi^-$ -proton scattering are shown in Figure 7. The calculated cross sections are given in Figure 8.

### C. Pion Absorption Cross Section

The numerical work of Metropolis et al.<sup>8</sup> was used here for the pion absorption cross section which represents the average pion absorption cross section per proton in nuclear matter. A very brief history of its derivation is given here.

In 1951, Brueckner, Serber, and Watson<sup>9</sup> proposed a model for pion absorption in nuclear matter. This model is based on the assumptions that pion absorption takes place with a two-nucleon cluster within the nucleus and that the cross section for pion absorption is related to the deuteron absorption cross section in the following way:

$$\frac{1}{z} \sigma(\pi + \text{nucleus} \rightarrow \text{star}) = \Gamma \sigma(\pi^- + D \rightarrow 2 \text{ neutrons}),$$

where  $z$  is the nuclear charge and  $\Gamma$  is a proportionality constant which is independent of energy.

Later Gell-Mann and Watson<sup>10</sup> determined a semiempirical expression for the pion-deuteron absorption cross section, i.e.,

$$\sigma_D \propto \frac{1}{\eta} (0.14 + \eta^2); \quad \eta = k\hbar/m_\pi c,$$

---

<sup>8</sup> See Ref. 8, Chapter I.

<sup>9</sup> K. A. Brueckner, R. Serber, and K. M. Watson, Phys. Rev. 84, 258 (1951).

<sup>10</sup> M. Gell-Mann and K. M. Watson, Annual Review of Nuclear Science, Vol. 4 (Annual Reviews, Inc., Stanford, 1954), p. 219.

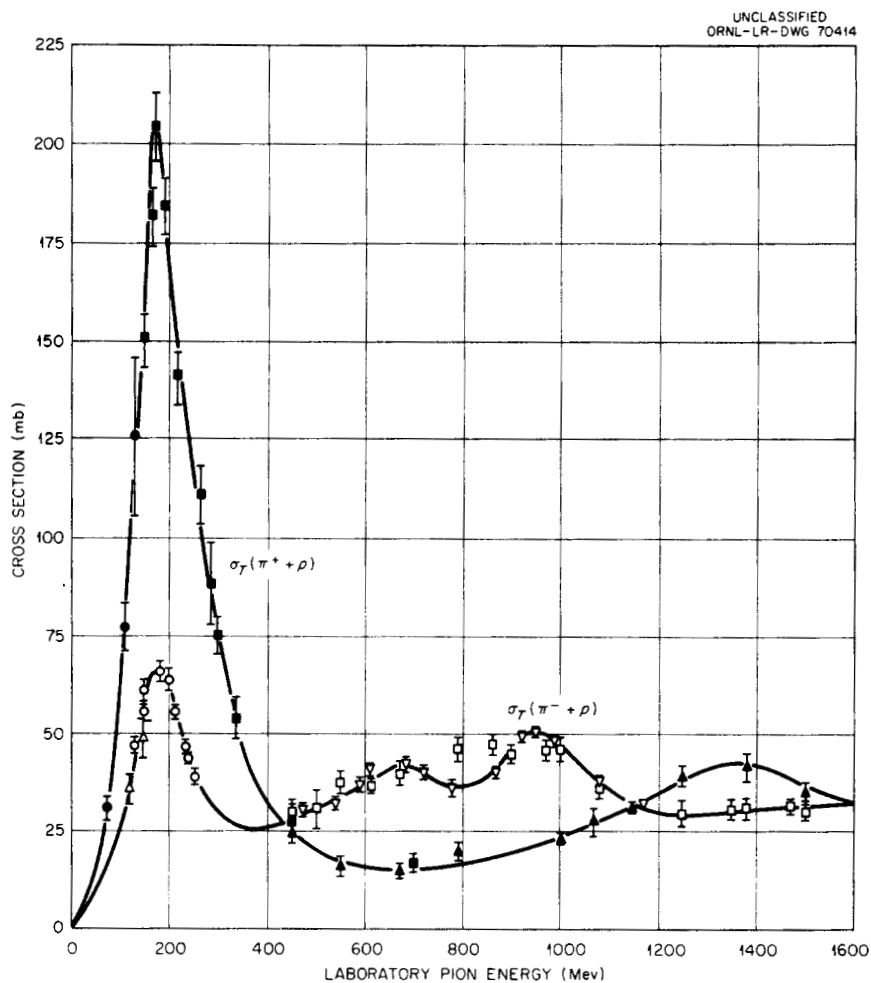


Figure 7.  $\pi^+$ -Proton and  $\pi^-$ -Proton Total Cross Sections vs. Energy. ●, △ H. L. Anderson *et al.*, Phys. Rev. 91, 155 (1953); ■ S. J. Lindenbaum and L. C. L. Yuan, Phys. Rev. 100, 306 (1955); ▲, □ R. Cool, O. Piccioni, and D. Clark, Phys. Rev. 103, 1082 (1956); ○ J. Ashkin *et al.*, Phys. Rev. 96, 1104 (1954); ▽ H. C. Burrowes *et al.*, Phys. Rev. Letters 2, 119 (1959).

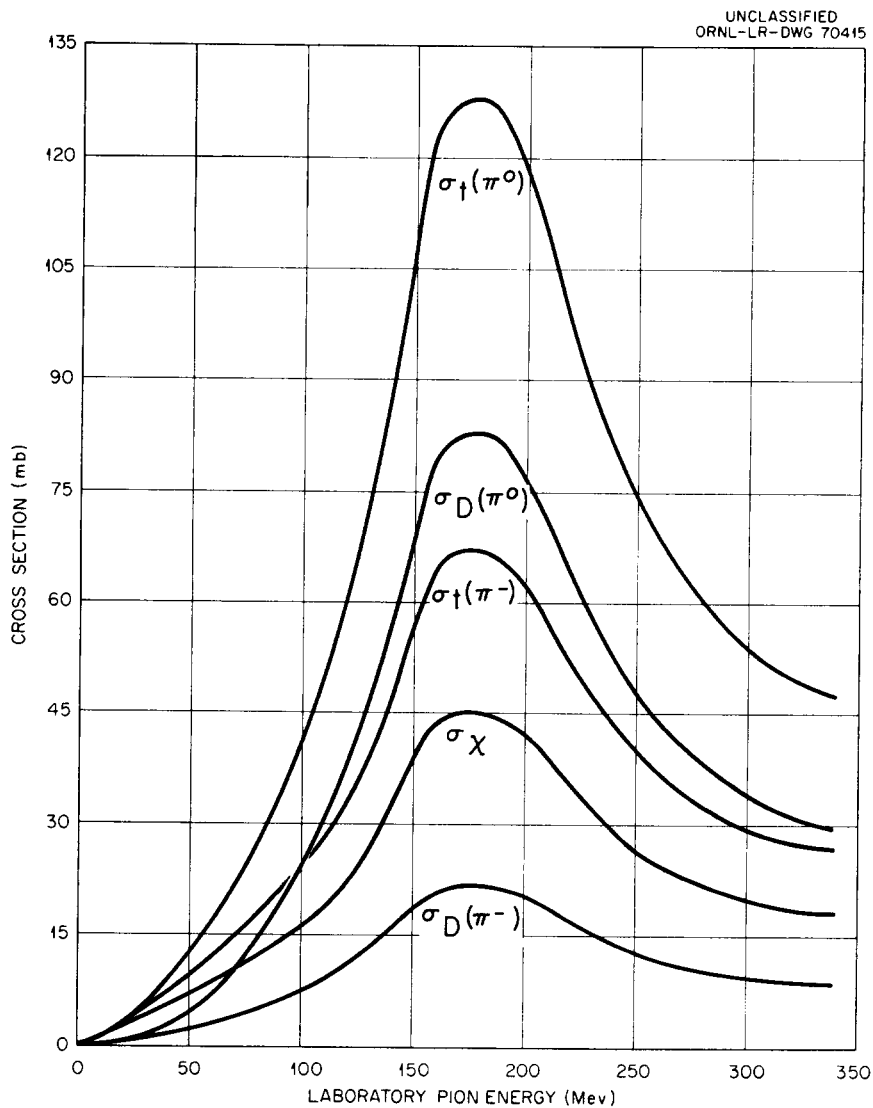


Figure 8. Calculated Pion-Proton Cross Sections vs. Pion Energy.  $\sigma_t(\pi^0)$ , total cross section for  $\pi^0 + p$  scattering;  $\sigma_D(\pi^0)$ , cross section for  $\pi^0 + p$  elastic scattering;  $\sigma_t(\pi^-)$ , experimental  $\pi^- + p$  total cross section included for comparison purposes;  $\sigma_\chi$ , cross section for  $\pi^- + p$ ,  $\pi^+ + n$ ,  $\pi^0 + p$ , and  $\pi^0 + n$  exchange scattering;  $\sigma_D(\pi^-)$ , cross section for  $\pi^- + p$  elastic scattering.

where  $k$  is the pion wave number divided by  $2\pi$  and  $\sigma_D$  is the cross section for either  $\pi^+ + D \rightarrow p + p$  or  $\pi^- + D \rightarrow n + n$ .

In their work on the pion-nucleus optical model potentials, Frank, Gammel, and Watson<sup>11</sup> used

$$\sigma_D = \frac{4.45}{\eta} (0.14 + \eta^2)$$

and they used  $\Gamma = 4$  in estimating the pion absorption mean-free-path length in nuclear matter.

This same combination was used by Metropolis et al. so that the pion absorption cross section per proton within the nucleus is assumed to be

$$\sigma_{\text{absorption}} = \frac{17.8}{\eta} (0.14 + \eta^2).$$

The mean free path for  $\pi^0$  absorption was arbitrarily assumed to be the same as that for the charged pions. The actual values of the pion absorption cross section per proton that were used in the work reported here are given in Table II.

---

<sup>11</sup> R. M. Frank, J. L. Gammel, and K. M. Watson, Phys. Rev. 101, 891 (1956).

TABLE II

PION ABSORPTION CROSS SECTION PER PROTON  
IN NUCLEAR MATTER

Pion Energy (Mev)	Absorption Cross Section (mb)
0	10
20	14
40	17
60	25
80	32
100	38
120	45
140	43
160	40
180	38
200	32
220	25
240	21
260	16
280	12
300	8
320	5
340	2
360	0

## CHAPTER IV

### THE CALCULATION

The general flow of the calculation is described here, and the Monte Carlo sampling techniques are discussed. The treatment given to pion absorption is noted, and the limitations of the calculation are listed.

#### I. GENERAL DESCRIPTION

In the calculation the incident particles enter the nucleus parallel to the z axis and are uniformly distributed over the projected area of the nucleus. The collision histories of each incident particle and all subsequent collision products are traced using Monte Carlo techniques.

As the incident particle moves from outside the nucleus to the inside and then from region to region the potential energy in each region is added to the kinetic energy measured with respect to the outside of the nucleus to give the kinetic energy inside.

The Monte Carlo sampling technique is such that the point of collision inside the nucleus and the collision reaction are chosen simultaneously.<sup>1</sup> If the reaction is a scattering reaction, the scattering angles are obtained by sampling from the appropriate differential scattering cross section. If the reaction is a pion absorption reaction, the collision products are emitted isotropically in the center-of-mass system. All

---

<sup>1</sup>C. D. Zerby, R. B. Curtis, and H. W. Bertini, The Relativistic Doppler Problem, Oak Ridge National Laboratory Report ORNL-CF-61-7-20 (July 12, 1961).

the kinematics are relativistic.

When the energies and vector momenta of the two collision products are determined, one collision product is stored temporarily. Starting from the point of collision the process is repeated for the other collision product which collides and makes additional collision products. In this way a cascade develops. This process is repeated for all the collision products.

An attempt is made to account for exclusion effects in the following way: The energy of each nucleon of the collision products is examined to see if it is greater than the Fermi energy in that region. If it is not greater, the collision is "forbidden," and the history of the colliding particle is traced as though the collision did not occur.

When the energy of a collision product measured with respect to the outside of the nucleus falls below some cutoff energy, the history of that particle is no longer traced. The implication is that the particle wave length is too large to permit the subsequent reactions to be represented by particle-particle collisions; hence, its energy contributes to the excitation energy of the residual nucleus. The cutoff energy was taken to be the same for all particles. It is one-half the coulomb potential at the surface of the nucleus. It might seem more appropriate to have chosen the entire coulomb potential at the surface as the cutoff energy for protons and to have used zero for the energy measured with respect to the outside of the nucleus as the cutoff energy for neutrons. This was not done because a proton with energy less than the coulomb potential might have a collision with a neutron where most or all of the proton energy is given to the neutrons which could then

escape or continue to have cascade collisions. In this situation the use of the entire coulomb potential for the cutoff energy would have stopped the calculation prematurely; therefore, one-half the coulomb potential was chosen as a compromise.

Another aspect related to the cutoff energy is the following: The particle wave lengths near the cutoff energy are of the order of the internucleon distance and so the calculation is being used somewhat beyond the limit of validity at this point. However, if the combined cascade and evaporation particle spectra and the number of cascade plus evaporation particles produced are examined as a function of cutoff energy one finds that both the combined spectra and the combined particle multiplicities are insensitive to the cutoff energy. This is true as long as the cutoff energy is of the order of the coulomb potential; otherwise, there is a gap in the combined spectra between the lowest cascade particle energy and the tail of the evaporation particle spectrum.

Proceeding with the calculation, if the particle escapes from the nucleus, the type, energy, direction cosines, and coordinates of the point of the last collision within the nucleus are recorded. This information is recorded on magnetic tape in one record for all the escaping cascade particles which result from one incident particle. There is one such record for every incident particle that makes an "allowed" collision inside the nucleus.

From this series of records representing the raw data of the cascade process, one can obtain a wealth of information by writing codes which process the data in any form desired.

## II. SAMPLING TECHNIQUE FOR NUCLEON-NUCLEON SCATTERING ANGLES

For sampling purposes the differential scattering cross section for neutron-proton scattering in the center-of-mass system is represented by five parameters which are tabulated at every 20-Mev interval. These parameters are calculated from the data represented in Table I. As has been stated, the semiempirical fits to the experimental data are of the form

$$0 \leq E_n \leq 300 \text{ Mev}$$

$$\begin{aligned} \frac{d\sigma}{d\Omega} (n-p) &= A_1 + B_1\mu^3 & 0 \leq \mu \leq 1 \\ &= A_1 + B_2\mu^4 & -1 \leq \mu < 0 \end{aligned}$$

$$300 < E_n \leq 740 \text{ Mev}$$

$$\begin{aligned} \frac{d\sigma}{d\Omega} (n-p) &= A_1 + B_1\mu^3 & 0 \leq \mu \leq 1 \\ &= A_1 + B_3\mu^6 & -1 \leq \mu < 0 \end{aligned}$$

where  $A_1$ ,  $B_1$ ,  $B_2$ , and  $B_3$  are functions of the energy. One of the five tabulated parameters is the fraction of the cross section representing the scattering in the backward hemisphere. This was obtained by integrating the above expressions. The other four parameters are obtained from the A's and B's above by normalization. For example, in

the energy range 0-300 Mev, the four parameters,  $A_F$ ,  $B_F$ ,  $A_B$ , and  $B_B$  are given by

$$A_F = \frac{A_1}{A_1 + B_1/4}$$

$$B_F = \frac{B_1}{A_1 + B_1/4}$$

$$A_B = \frac{A_1}{A_1 + B_2/5}$$

$$B_B = \frac{B_2}{A_1 + B_2/5} .$$

A normalized frequency distribution function representing the differential cross section curve in the forward direction is then

$$A_F + B_F \mu^3 ,$$

and for the backward direction

$$A_B + B_B \mu^4 .$$

Similar methods apply for the energy range 300-740 Mev.

Now the scattering angles  $\theta$  ( $\mu = \cos\theta$ ) and  $\phi$  in the center-of-mass system in an n-p collision are selected in the following way: The relative kinetic energy of the colliding particles is calculated, and the five parameters mentioned above are obtained at this energy from the values tabulated versus energy by linear interpolation. A pseudo random

number,<sup>2</sup>  $R$ , is selected. If it is less than the fraction scattered in the backward direction, the scattering is assumed to be backward; if not, the scattering is assumed to be forward. The appropriate values of  $A$  and  $B$  are then used as follows: Another random number is selected and tested against  $A$ . If  $A$  is the greater,  $\mu$  is selected from a distribution which is uniform from 0 to 1. If  $A$  is smaller,  $\mu$  is selected from the distribution  $(n + 1)\mu^n$  simply by choosing the largest of  $(n + 1)$  random numbers.<sup>3</sup> This method will select the random variable  $\mu$  from the normalized frequency distribution

$$f(\mu) d\mu = (A + B\mu^n) d\mu, \quad 0 \leq \mu \leq 1.$$

To illustrate this, consider that this function can be interpreted as the sum of a uniform distribution,  $d\mu$ , and a distribution,  $(n + 1)\mu^n d\mu$ , where the uniform distribution occurs with probability  $A$  and the distribution,  $(n + 1)\mu^n d\mu$ , occurs with probability  $B/(n + 1)$ . One first selects the forward or backward hemisphere of scattering with a probability determined by  $d\sigma/d\Omega$ . Then, using the appropriate values of  $A$  and  $B$  (i.e., forward or backward values of  $A$  and  $B$ ), one selects  $\mu$  from a uniform distribution with probability  $A$  or selects  $\mu$  from  $(n + 1)\mu^n$  with probability  $B/(n + 1)$ , where  $A + B/(n + 1) = 1$ . If the direction of scattering is forward the sign of  $\mu$  is left positive. If the scattering is

---

<sup>2</sup>A random number  $R$ , where  $0 \leq R \leq 1$ , is a number such that the probability of selecting  $R$  in  $dR$  is equal to  $dR$ . A pseudo random number is a number generated by the computer in a manner that approximates a true random number.

<sup>3</sup>Herman Kahn, Applications of Monte Carlo, Atomic Energy Commission Report AECU-3259 (April 19, 1954), p. 27.

backward the sign of  $\mu$  is made negative. Since the scattering is assumed to have azimuthal symmetry, the azimuthal angle  $\phi$  is chosen from a uniform distribution.

The proton-proton differential scattering cross section was assumed to be isotropic in the center-of-mass system for relative proton-proton energies up to 500 Mev.

The scattering angles for p-p collision at energies below 500 Mev were chosen from the appropriate uniform distributions. At higher energies the techniques used are as described above for neutron-proton collisions. Here only two parameters are tabulated, since the scattering is symmetric about ninety degrees and is forward with a probability of one half.

### III. SAMPLING TECHNIQUES FOR PION-NUCLEON SCATTERING ANGLES

The phase shift analysis gives the differential scattering cross section in the form

$$\frac{d\sigma}{d\Omega} = A + B\mu + C\mu^2.$$

$\mu$  is obtained by solving the equation

$$R = \frac{\int_0^\mu (A + B\mu + C\mu^2) d\mu}{A + C/3},$$

where  $R$  is a random number.<sup>4</sup> A table of  $\mu$  values was generated representing

---

<sup>4</sup>Ibid., p. 8.

solutions to the above for twenty-one values of R ranging from zero to one at 0.05 intervals. This was done for each different scattering reaction ( $\pi^+$  + p scattering,  $\pi^0$  + p elastic,  $\pi^-$  + p elastic, and  $\pi^-$  + p exchange) and at every 20-Mev interval.

When a value of  $\mu$  was needed it was obtained from the proper tables by first generating a random number, R, and then interpolating in R and in energy. The azimuthal angle  $\phi$  was chosen from a uniform distribution over its entire range.

#### IV. SAMPLING TECHNIQUE FOR DETERMINING THE POINT OF COLLISION AND TYPE OF COLLISION

The details of the sampling technique that was used to determine the point of collision and the type of collision are given in the paper by Zerby et al.<sup>1</sup> A brief outline of this method is given here, and a more complete derivation is given in Appendix C.

Let  $\bar{p}$  denote the initial vector momentum of the struck particle, and call the frame moving with the struck particle the  $\bar{p}$  system. One then chooses a fictitious cross section,  $\sigma^m$ , such that

$$|\bar{j}| N\sigma^m \geq |\bar{j}'(\bar{p})| N'\sigma(\bar{p})$$

for any  $\bar{p}$  that the struck particle may have. N is the target density in the laboratory system, N' the same density expressed in the  $\bar{p}$  system,  $\bar{j}$  the current of colliding particles measured in the laboratory system, and  $\bar{j}'(\bar{p})$  the same quantity measured in the  $\bar{p}$  system.  $\sigma(\bar{p})$  is the reaction cross section at the energy of the incident particle measured in the  $\bar{p}$  system.

The expression on the left represents a reaction rate per unit volume in the laboratory system. That on the right represents the same quantity in the  $\bar{p}$  system where it is assumed that all the target particles have momentum  $\bar{p}$ . The units need not be modified, for  $d\bar{x}/dt$  is relativistically invariant.

Let

$$\Sigma_i^m = N_i \sigma_i^m,$$

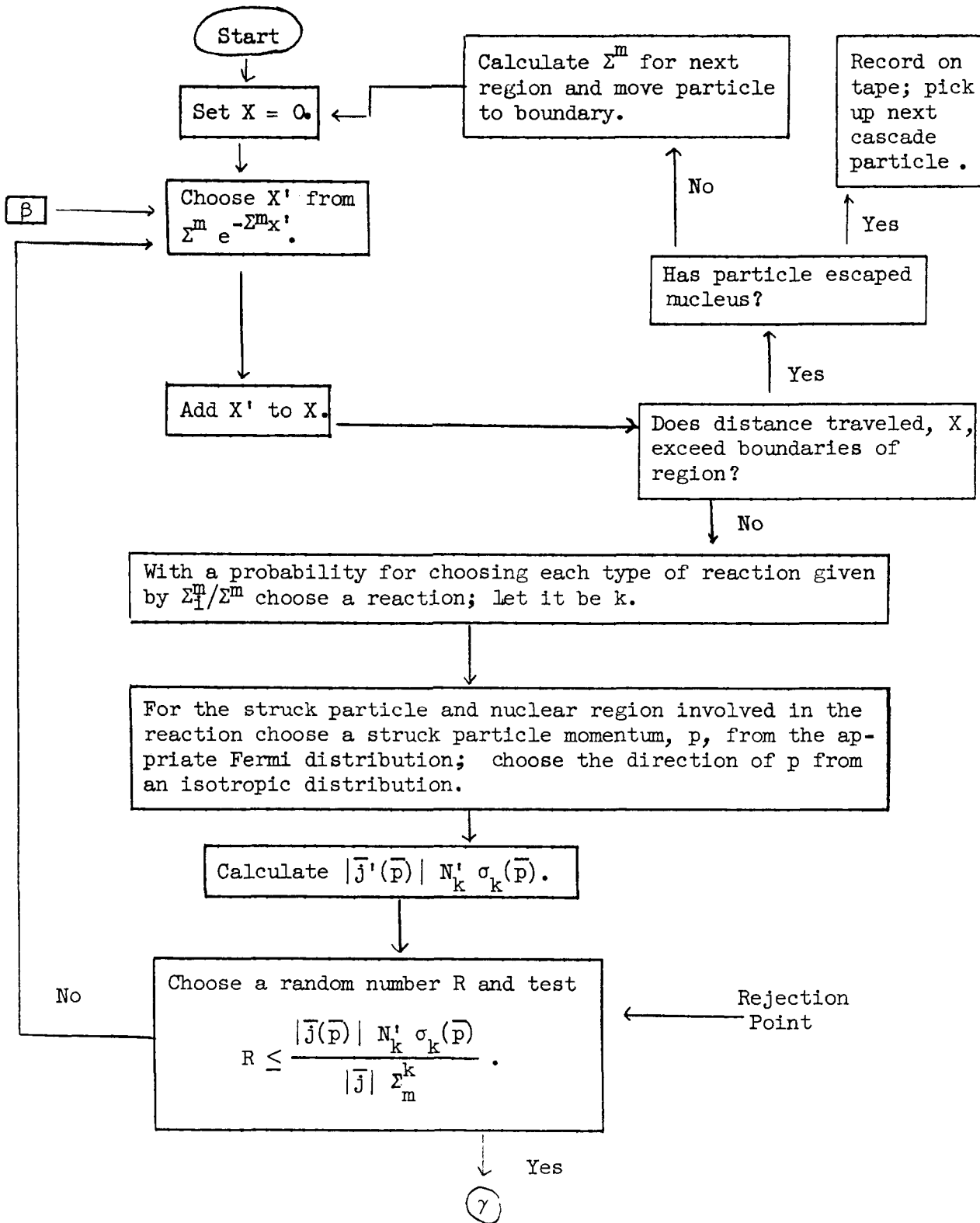
where  $i$  refers to all possible types of collisions that might occur such as  $\pi^+ + p$ ,  $\pi^+ + n$  elastic, and  $\pi^+ + n$  exchange. (Pion absorption is ignored in the following for brevity.)

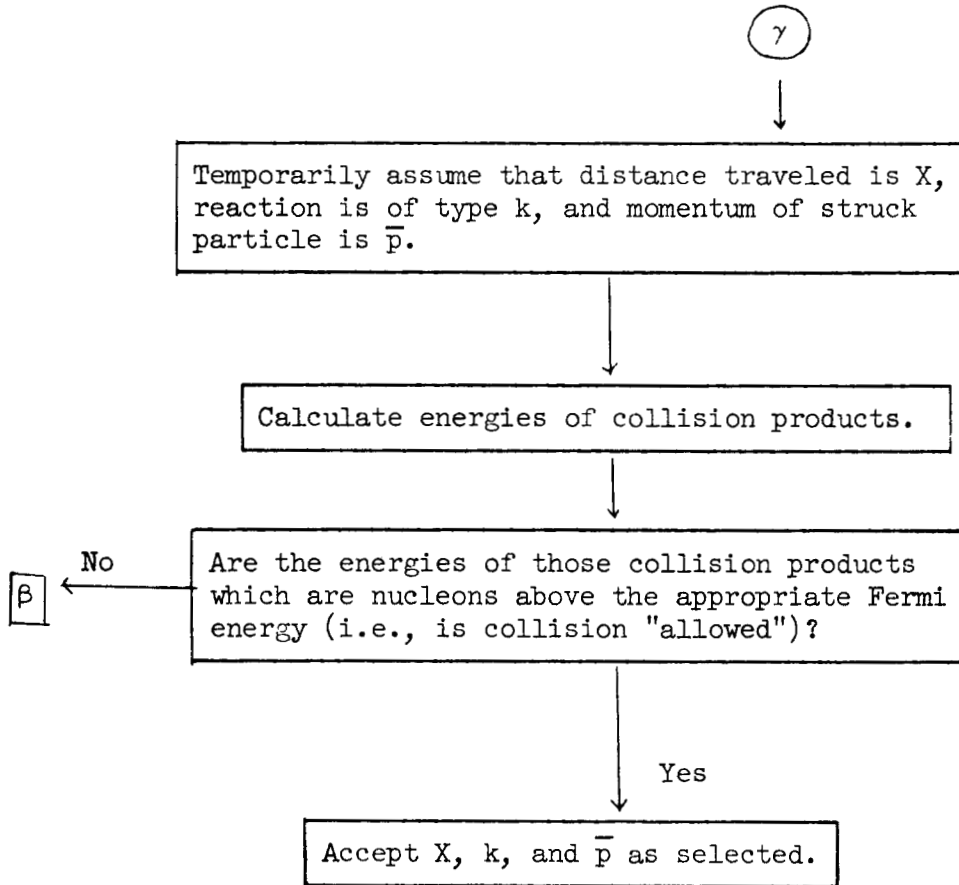
Let

$$\Sigma^m = \sum_i \Sigma_i^m,$$

and note that  $1/\Sigma^m = \lambda_m \leq \lambda$ , where  $\lambda$  is the actual mean free path of the incident particle.

The technique for selecting the point of collision and type of collision is illustrated schematically as follows:





## V. PION ABSORPTION

Pion absorption is treated somewhat differently than the other reactions. It is independent of the momentum of the nucleons in the nucleus, since the cross section applies to nuclear matter which presumably includes averaging over the momentum distribution. In the sampling technique for this reaction the test at the rejection point is bypassed, and there is no return to the entry point if the collision is forbidden. Instead, a new momentum for the two-nucleon cluster is selected until the collision is allowed.

The momentum of the two-nucleon cluster which acts as the collision partner for pion absorption is selected by sampling from the Fermi momentum distributions in the proper region to get the vector momenta of the two particles. The momentum of the cluster is then taken to be equal to the momentum of the center of mass of the two particles.

The type of two-nucleon cluster is chosen with a probability determined by the number of each particle-pair type within the nucleus (p-p, n-p, n-n). Pair types which would violate charge conservation are not included in the calculation of the probabilities (i.e.,  $\pi^+$  absorption on p-p pair, etc.). For example, consider the reaction  $\pi^+ + {}_{44}\text{Ru}^{100}$ .  $\pi^+$  absorption is allowed only on n-p and n-n pairs. The number of n-p pairs in Ru is the product of the number of neutrons, N, and the number of protons, Z. The number of n-n pairs is  $N(N - 1)/2$ . Therefore the probability for  $\pi^+$  absorption by

an n-p pair in  ${}_{44}\text{Ru}^{100}$  is given by

$$\frac{NZ}{NZ + N(N - 1)/2} = 0.616.$$

On the other hand,  $\pi^-$  absorption is allowed only on n-p and p-p pairs.

Therefore, in the reaction  $\pi^- + {}_{44}\text{Ru}^{100}$  the probability for  $\pi^-$  absorption by an n-p pair is

$$\frac{NZ}{NZ + Z(Z - 1)/2} = 0.723.$$

A few typical values are given here.

<u>Target</u>	<u>Probability of Absorption of <math>\pi^-</math> on n-p Pair</u>	<u>Probability of Absorption of <math>\pi^+</math> on n-p Pair</u>
C	0.706	0.706
Ru	0.723	0.616
Au	0.751	0.574

These values are in reasonable agreement with other work where estimates made of the fraction of pion absorption taking place with n-p pairs range from sixty to one hundred per cent.<sup>5</sup>

Special treatment is given to the collision products in pion absorption, and it is somewhat arbitrary. The difficulty lies in the fact that prior to the collision there are three particles, all in a potential field, and after the collision only two particles remain in a potential field.

---

<sup>5</sup>S. O. Zoki *et al.*, Phys. Rev. Letters 4, 533 (1960); N. I. Petrov, V. G. Ivanov, V. A. Rusakov, Soviet Phys.-JETP 37 (10), 682 (1960); G. A. Blinov *et al.*, Soviet Phys.-JETP 35 (8), 609 (1959); A. Tomasini, Nuovo Cimento 3, 160 (1956); V. De Sabbata, E. Monaresi, G. Puppi, Nuovo Cimento 10, 1704 (1953).

The potential energy of the missing particle is used in contributing to the energies of the remaining particles. As long as the energy inside the potential field is used as a basis there is no problem with energy conservation. But under these conditions energy is not conserved if it is measured with respect to the outside of the nucleus.

The energies of the collision products were compelled to be such that the total energy measured with respect to the outside of the nucleus was conserved. This was done to avoid the complications involved in dealing with negative excitation energies of the residual nuclei or to avoid modifying the initial conditions.

When the cluster contained a proton, the pion potential was taken to be that of protons. When the cluster consisted of two neutrons, the pion potential was taken to be equal to that of neutrons. There is no physical significance in these choices. They are arbitrary and were selected merely for convenience in the coding.

## VI. LIMITATIONS

There are several limitations to this calculation. One is that the effects of the pion potential alone cannot be separated. The pion potential is included for all pion reactions and cannot be switched out.

Another limitation is that the energy range of validity of the calculation is restricted to that for which pion production is not likely (< 350-Mev incident particle energy).

In addition, the following effects are not included:

1. Cluster formation: Pion absorption is assumed to occur with a two-nucleon cluster, but the possible scattering reaction of a nucleon or pion with other clusters (alpha particles, for example) is not included.

2. Refraction at the nuclear surface.

3. Nuclear depletion due to cascades: This effect was ignored because at the energies under consideration the velocity of the collision products resulting from a collision will in general be greater than the velocity of propagation of a disturbance in the nucleus resulting from the same collision. Therefore, for the most part the cascade particles will pass through undisturbed nuclear matter.

## CHAPTER V

### COMPARISONS WITH EXPERIMENT: INCIDENT NUCLEONS

The purpose of these comparisons is twofold: (1) to determine the practical limits of applicability of this model, and (2) to investigate those discrepancies with experimental data which have been attributed to the limitations of the previous models. An attempt has been made to examine systematically most of the pertinent experimental data. The comparisons with the calculations are illustrated and discussed. A brief section on the statistical errors is left to the end of Chapter VI.

#### I. NONELASTIC CROSS SECTIONS

Comparisons between the calculated and experimental cross sections for nonelastic scattering are given in Tables III and IV for incident protons and neutrons, respectively. The largest discrepancy is a 13 per cent difference between the calculated and experimental values for 95-Mev neutrons on carbon. All other discrepancies are smaller than this, and most of the values agree within the limits of the errors.

#### II. EXCITATION ENERGY OF THE RESIDUAL NUCLEUS

The most extensive experimental data on this quantity are those given by Gross.<sup>1,2</sup> The comparison of the calculated values with his data

---

<sup>1</sup>E. Gross, The Absolute Yield of Low Energy Neutrons from 190-Mev Proton Bombardment of Gold, Silver, Nickel, Aluminum, and Carbon, University of California Radiation Laboratory Report UCRL-3330 (Feb. 29, 1956).

<sup>2</sup>E. Gross, Absolute Neutron Spectra from 190-Mev Proton Bombardment of Uranium, University of California Radiation Laboratory Report UCRL-3337 (March 8, 1956).

TABLE III

CALCULATED AND EXPERIMENTAL TOTAL NONELASTIC  
CROSS SECTIONS FOR INCIDENT PROTONS

Proton Energy (Mev)	Target	Nonelastic Cross Section (mb)	
		Calculated <sup>a</sup>	Experimental <sup>b</sup>
185	Be	187 ± 7	172 ± 17
240		177 ± 7	169 ± 17
305		176 ± 7	151 ± 15
185	C	230 ± 6	204 ± 20
240		226 ± 8	202 ± 20
305		211 ± 8	187 ± 19
185	Al	417 ± 9	408 ± 41
230		415 ± 16	
240			383 ± 38
305		394 ± 11	334 ± 33
170	Cu	795 ± 23	
185			746 ± 75
196		741 ± 23	
240		747 ± 23	667 ± 67
305			608 ± 61
330		745 ± 23	
140	Ru	1049 ± 27	
140	Ag-Br(emulsions)		952 ± 124 <sup>c</sup>
185	Pb	1625 ± 26	1550 ± 155
240		1599 ± 26	1570 ± 157
305		1594 ± 26	1480 ± 148

Table III (continued)

Proton Energy (Mev)	Target	Nonelastic Cross Section (mb)	
		Calculated <sup>a</sup>	Experimental <sup>b</sup>
185	U	1825 ± 38	1900 ± 190
230			2030 ± 203
240		1756 ± 28	1770 ± 177
305		1754 ± 28	1600 ± 160

<sup>a</sup>The errors shown here are those for a confidence interval of 68%.

<sup>b</sup>Unless otherwise noted, all of this data comes from G. P. Millburn et al., Phys. Rev. 95, 1268 (1954).

<sup>c</sup>S. Jannelli and F. Mezzanares, Nuovo Cimento 4, S939 (1956).

TABLE IV

CALCULATED AND EXPERIMENTAL TOTAL NONELASTIC  
CROSS SECTIONS FOR INCIDENT NEUTRONS

Neutron Energy (Mev)	Target	Nonelastic Cross Section (mb)	
		Calculated <sup>a</sup>	Experimental
95	Be	217 ± 7	210 ± 8 <sup>b</sup>
95	C	267 ± 8	235 ± 9 <sup>b</sup>
95			224 ± 7 <sup>c</sup>
300		209 ± 8	203 ± 33 <sup>d</sup>
84	Al	502 ± 16	500 ± 50 <sup>d+</sup>
95		478 ± 11	418 ± 15 <sup>c</sup>
95			440 ± 18 <sup>b</sup>
300		383 ± 11	390 ± 23 <sup>d</sup>
84	Cu	825 ± 23	910 ± 50 <sup>d+</sup>
95		810 ± 16	815 ± 33 <sup>b</sup>
95			782 ± 10 <sup>c</sup>
270		739 ± 16	573 ± 24 <sup>d*</sup>
300		725 ± 16	755 ± 33 <sup>d</sup>
84	Pb	1654 ± 26	1850 ± 180 <sup>d+</sup>
95		1654 ± 26	1865 ± 75 <sup>b</sup>
95			1784 ± 45 <sup>c</sup>
270		1571 ± 26	1420 ± 60 <sup>d*</sup>
300		1552 ± 27	1720 ± 80 <sup>d</sup>

TABLE IV (continued)

Neutron Energy (Mev)	Target	Nonelastic Cross Section (mb)	
		Calculated <sup>a</sup>	Experimental
96	U	1815 ± 27	2028 ± 81 <sup>b</sup>

<sup>a</sup>See ref. a, Table III.

<sup>b</sup>P. E. Hodgson, Nucl. Phys. 21, 21 (1960).

<sup>c</sup>J. De Juren and N. Knable, Phys. Rev. 77, 606 (1950).

<sup>d</sup>G. P. Millburn et al., Phys. Rev. 95, 1268 (1954).

+Upper limit.

\*Lower limit.

are given in Table V. The agreement is quite good. Gross calculated the spectrum from his experimental data by making an energy balance using the results which were attributable to the evaporation process alone. These are distinguishable by the isotropy of the angular distribution in the center-of-mass system and by the low-energy peaks in the particle spectrum. The sum of the ground state energy of the average residual nucleus resulting from the cascade plus its average excitation energy were set equal to the sum of the average energy of the nucleus after the evaporation process was complete plus the average total energy of the evaporation particles.

In the present calculation the effect of the cutoff energy on the average excitation energy was examined for a medium weight element using 190-Mev incident protons. It was found that there was about a 1-Mev increase in the average excitation energy for every 1-Mev increase in the cutoff energy. This is not a very sensitive dependence.

Other experimental data has been given by Ostroumov.<sup>3</sup> Using photographic plate data, he calculated an average excitation energy for the heavy nuclei in emulsions for 130-Mev protons. His value was 48 Mev, and the present calculation yields 63 Mev for the same quantity, where  $Ru^{100}$  is used to represent the Ag-Br nuclei. Ostroumov used an iteration technique which involved an estimate of the velocity of the cascade residual nucleus, an estimate of the number of low-energy cascade protons, and a theoretical curve of the number of evaporated particles vs excitation energy. Considering the complete differences in the techniques involved, the above agreement is surprising.

---

<sup>3</sup>V. I. Ostroumov, Soviet Phys.-JETP 5, 12 (1957).

TABLE V

AVERAGE EXCITATION ENERGY (Mev) FOR 190-Mev  
INCIDENT PROTONS ON VARIOUS NUCLEI

Element	Calculated	Gross <sup>a, b</sup>
C	22	27 ± 5
Al	36	50 ± 8
Ni	59	57 ± 9
Ag	72	69 ± 12
Au	92	83 ± 17
U	95	88 ± 18

<sup>a</sup>E. Gross, The Absolute Yield of Low-Energy Neutrons from 190-Mev Proton Bombardment of Gold, Silver, Nickel, Aluminum, and Carbon, University of California Radiation Laboratory Report UCRL-3330 (Feb. 29, 1956).

<sup>b</sup>E. Gross, Absolute Neutron Spectra from 190-Mev Proton Bombardment of Uranium, University of California Radiation Laboratory Report UCRL-3337 (March 8, 1956).

### III. SPECTRA OF CASCADE PARTICLES

Comparisons between calculated cascade spectra and experimental values are given in Figures 9 through 43. Figures 9 through 34 contain comparisons for incident protons and the remainder comparisons for incident neutrons. The figures are arranged in sequence from low to high incident particle energy.

In most cases the agreement is excellent. The main area of disagreement is the spectra of cascade particles emitted at or near zero degrees for carbon and copper at relatively low energies. These disagreements are illustrated in Figures 9 and 10 for 50-Mev protons on carbon and in Figures 35, 36, 38, and 39 for 90-Mev neutrons on carbon and copper. The prediction of the calculations is that the spectrum of particles emitted near zero degrees will have a high-energy peak, and on a particle-particle collision basis this is understandable since particles scattered near zero degrees will suffer small energy losses. The experiments, however, do not show any such peaks.

The discrepancy between the calculations and the experiments for these two nuclei is probably due to the effects of nuclear structure. The continuum states for carbon and copper are approximately 20 Mev and 5 Mev above the ground state, respectively. The calculation can only be valid when the energy transfer from the incident particle to the nucleus is greater than the minimum continuum energy of the nucleus. For 50-Mev protons a 20-Mev energy loss for particle-particle collisions occurs at scattering angles of about forty degrees. For 90-Mev neutrons the same

energy loss would occur at about thirty degrees. To lose 5 Mev, a 90-Mev neutron would have to scatter at about fifteen degrees.

So for 50-Mev protons on carbon one would not expect agreement with experiment for emission angles of less than forty degrees. For 90-Mev neutrons on carbon and copper this angle would be thirty degrees and fifteen degrees, respectively. The agreement between the calculations and experiment for angles greater than this is illustrated in Figures 37 and 40.

When the calculation on copper is repeated with a nuclear configuration equivalent to that used by Metropolis et al. (smaller nuclear radius and a uniform nucleon density distribution within the nucleus),<sup>4</sup> the peak at zero degrees disappears (Figure 41). This is because the single-collision events which contribute to the peak are inhibited by the greater density of this configuration.

The experiments of Cassels et al.<sup>5</sup> indicate a high-energy peak near zero degrees for 171-Mev protons on carbon (Figure 19); however, the maximum value of the peak is about 30 to 40 Mev below the incident particle energy so that the energy transferred to the nucleus is above the minimum continuum energy. In this particular experiment the mean incident particle energy of the experimental beam inside the target was estimated to be 90 to 95 per cent of the incident beam energy outside the target (171 Mev). This would account for part of the discrepancy between the positions of the calculated and experimental peaks as indicated in Figures 19 and 20.

The calculations are compared with the experimental work of Strauch

---

<sup>4</sup>See ref. 7, Chapter I.

<sup>5</sup>J. M. Cassels et al., Phil. Mag. 42, 215 (1951).

and Titus<sup>6</sup> in Figures 13 through 18. The high-energy peaks in the experimental curves are due to elastic scattering, and the lower-energy peaks are caused by nuclear structure. Comparisons with the calculations should be made with that part of the spectrum that is not due to structure.

The experimental data of Bailey<sup>7</sup> is used as the basis for comparison in Figures 21 through 32. All the low-energy peaks in the experimental curves, except for the case of gold, are due to nuclear evaporation. The potential barrier of gold is high enough to inhibit the evaporation of protons so that almost all the protons come from the cascade. In this set the comparisons with the calculated values should be made in the energy region above about 15 Mev.

#### IV. ANGULAR DISTRIBUTION OF CASCADE PARTICLES

The comparisons between the calculated and experimental angular distributions are illustrated in Figures 44 through 50. The calculated distributions for the cascade particles of various energies are in very good agreement with the experimental data. The terminology used in some of these figures is defined as follows: The term "sparse black prongs" refer to tracks in photographic emulsions attributed to protons with energies between 30 and 100 Mev, the term "gray prongs" to those due to protons with energies above 100 Mev. There is one exception to the good agreement. It is shown in Figure 48 for the case of 90-Mev neutrons on lead,

---

<sup>6</sup>K. Strauch and F. Titus, Phys. Rev. 104, 191 (1956).

<sup>7</sup>L. E. Bailey, Angle and Energy Distributions of Charged Particles from the High Energy Nuclear Bombardment of Various Elements, University of California Radiation Laboratory Report UCRL-3334 (March 1, 1956).

and the discrepancy is most glaring for protons emitted at small angles. The high experimental cross section at these angles has been a source of trouble since the calculation of Goldberger.<sup>8</sup> Serber<sup>9</sup> has suggested that refraction effects at the nuclear surface might be the cause, but this cannot be tested with the present calculation. The diffuse nuclear edge used here does not alleviate the situation.

## V. CASCADE PARTICLE MULTIPLICITIES

Comparisons of the multiplicities of escaping cascade particles from the calculations with the photographic plate data of Bernardini et al.<sup>10</sup> are illustrated in Tables VI-IX. In all the calculations  ${}_{44}\text{Ru}^{100}$  was taken to represent the heavy nuclei in emulsions. In the tables the term "fast prongs" refer to the gray plus the sparse black tracks.

In addition to the data of Bernardini et al.,<sup>3</sup> Ostroumov<sup>3</sup> measured the average number of protons with energies greater than 30 Mev for 130-Mev protons on heavy emulsion nuclei. He obtained a value of 0.40, which is to be compared with a calculated value of 0.38 for 135-Mev protons on  $\text{Ru}^{100}$ .

The agreement between the experiments and the calculations is quite reasonable for the proton-induced tracks. For neutron-induced reactions, however, the number of fast protons emitted tends to be somewhat lower

---

<sup>8</sup>See ref. 2, Chapter I.

<sup>9</sup>R. Serber, as quoted by J. Hadley and H. York, Phys. Rev. 80, 345 (1950).

<sup>10</sup>G. Bernardini, E. T. Booth, and S. J. Lindenbaum, Phys. Rev. 85, 826 (1952).

TABLE VI

COMPARISON OF CALCULATED AND EXPERIMENTAL MEAN PRONG  
NUMBERS FOR 375-Mev PROTONS ON  
HEAVY EMULSION NUCLEI

Type	Mean Prong Number	
	Calculated	Experimental
Sparse Black	0.38	$0.39 \pm 0.04$
Gray	0.60	$0.46 \pm 0.04$
Fast	0.98	$0.85 \pm 0.07$

TABLE VII

COMPARISON OF CALCULATED AND EXPERIMENTAL MEAN PRONG  
NUMBERS FOR 300-Mev NEUTRONS ON  
HEAVY EMULSION NUCLEI

Type	Mean Prong Number	
	Calculated	Experimental
Sparse Black	0.27	$0.41 \pm 0.04$
Gray	0.23	$0.33 \pm 0.05$
Fast	0.50	$0.74 \pm 0.07$

TABLE VIII

GRAY PRONG DISTRIBUTION FOR 375-Mev PROTONS ON  
HEAVY EMULSION NUCLEI

Number of Gray Prongs	Percentage of Events	
	Calculated	Experimental
0	45	$57 \pm 4$
1	50	$40 \pm 4$
2	5	$2.4 \pm 1$
3	0	

TABLE IX  
FAST PRONG DISTRIBUTION FOR  
HEAVY EMULSION NUCLEI

Number of Fast Prongs	Percentage of Stars Induced			
	By 300-Mev Neutrons		By 375-Mev Protons	
	Calculated	Experimental	Calculated	Experimental
0	54	$30 \pm 4$	14	$29 \pm 3$
1	42	$63 \pm 5$	76	$60 \pm 4$
2	4	$7 \pm 2$	10	$9 \pm 2$
3	0	0	0.5	$2 \pm 1$

than the experimental values. Also, the experiments indicate a complete similarity between neutron- and proton-initiated events, while the calculations indicate a difference (Table IX). This difference seems to be a peculiarity of the theoretical calculations, since it was also observed by Metropolis et al. It manifested itself by a difference of a factor of two in the neutron-to-proton ratios for neutron-induced and proton-induced reactions on ruthenium at these energies, while the total number of nucleons emitted remained about the same.

Bernardini et al.<sup>10</sup> have attributed the similarity between the neutron- and proton-initiated events to the average number of collision stages per event. They estimated the value of this number to be between two and three, which would be sufficient to eliminate any observable asymmetry. The calculation, on the other hand, indicates that this average value is between one and two for escaping particles whose energies are above 30 Mev. Another experimental check on this point would be of use.

## VI. (p,pn) CROSS SECTIONS

The radiochemical cross sections examined here were calculated with an auxiliary code which transformed the cascade data into a form suitable for use as input data for the evaporation code which was written by Dresner.<sup>11</sup>

The (p,pn) cross section is one of the products for which the effect of the diffuse edge was expected to be quite large. A total of six nuclear configurations were used to examine this effect. They consisted of a

---

<sup>11</sup>See ref. 13, Chapter I.

uniform and a nonuniform density distribution for each of three outer nuclear radii identified as small, medium, and large. The small radius is given by  $r = r_0 A^{1/3}$ , with  $r_0 = 1.3 \times 10^{-13}$ . The medium and larger radii were determined from the Hofstadter curve (see Chapter II). The medium radius, the one for the standard configuration, is the radius at which the curve is 0.01 of its central value. The large radius is that at which the curve is 0.0001 of its central value, and it was used to represent the effects of an extreme nuclear edge. Configurations for copper and gold are shown in Figures 51 through 56, these two elements being chosen because the previous discrepancies between calculations and experiments are greatest for them.

The results of the calculations are illustrated in Tables X and XI, and are compared with the experimental data of Yule and Turkevich.<sup>12</sup> One can draw the following conclusions from this comparison:

1. The effect of nuclear size on this reaction is greater than the effect of nuclear edge.
2. With the volume kept constant the expected increase in the cross section as the density is changed from a uniform to a nonuniform distribution occurs consistently only in the case of gold. For the case of copper the cross section remains the same or decreases in all but one case. Although the nonelastic cross section decreases in every case, the excitation energies of gold remaining after the cascade process is complete are such that the probability for evaporating the proper particle is enhanced

---

<sup>12</sup>H. P. Yule and A. Turkevich, Phys. Rev. 118, 1591 (1960).

TABLE X  
 CROSS SECTIONS FOR THE  $\text{Cu}^{65}(\text{p,pn})\text{Cu}^{64}$  REACTION AND FOR  
 THE TOTAL NONELASTIC SCATTERING AS A FUNCTION OF  
 PROTON ENERGY AND NUCLEAR CONFIGURATION

Proton Energy (Mev)	Nuclear Configuration	(p,pn) Cross Section (mb)		Calculated Nonelastic Cross Section (mb)	Ratio of Calculated (p,pn) to Nonelastic Cross Section
		Calculated	Experimental <sup>a</sup>		
82	Small, uniform	26 ± 2	108.4 ± 4.2	740	0.0351
	Small, nonuniform	32 ± 3		701	0.0457
	Medium, uniform	72 ± 3		1119.0	0.0643
	Medium, nonuniform <sup>b</sup>	71 ± 3		876	0.0811
	Large, uniform	224 ± 12		1751	0.1279
	Large, nonuniform	183 ± 11		1087	0.1684
196	Medium, nonuniform	54 ± 4	64.3 ± 2.5	763	0.0708
330	Small, uniform	21 ± 2	55.9 ± 2.2	693	0.0303
	Small, nonuniform	19 ± 2		642	0.0296
	Medium, uniform	66 ± 3		939	0.0703
	Medium, nonuniform	51 ± 3		750	0.0680
	Large, uniform	225 ± 12		1272	0.1769
	Large, nonuniform	134 ± 9		844	0.1588

<sup>a</sup>H. P. Yule and A. Turkevich, Phys. Rev. 118, 1591 (1960).

<sup>b</sup>Standard nuclear configuration adopted for this report.

TABLE XI  
 CROSS SECTIONS FOR THE Au<sup>197</sup>(p,pn)Au<sup>196</sup> REACTION AND FOR  
 THE TOTAL NONELASTIC SCATTERING AS A FUNCTION OF  
 PROTON ENERGY AND NUCLEAR CONFIGURATION

Proton Energy (Mev)	Nuclear Configuration	(p,pn) Cross Section (mb)		Calculated Nonelastic Cross Section (mb)	Ratio of Calculated (p,pn) to Nonelastic Cross Section
		Calculated	Experimental <sup>a</sup>		
82	Small, uniform	13 ± 2	121.6 ± 9.8	1669	0.0078
	Small, nonuniform	23 ± 3		1534	0.0150
	Medium, uniform	15 ± 2		2139	0.0070
	Medium, nonuniform <sup>b</sup>	58 ± 4		1737	0.0334
	Large, uniform	98 ± 10		3411	0.0287
	Large, nonuniform	182 ± 13		2229	0.0817
210	Medium, nonuniform	49 ± 4	73.6 ± 6.0	1553	0.0316
282	Small, uniform	10 ± 2	71.0 ± 5.7	1582	0.0063
	Small, nonuniform	18 ± 3		1427	0.0126
	Medium, Uniform	31 ± 3		1972	0.0157
	Medium, nonuniform	50 ± 4		1553	0.0322
	Large, uniform	131 ± 11		2815	0.0465
	Large, nonuniform	166 ± 13		1746	0.0951

<sup>a</sup>H. P. Yule and A. Turkevich, Phys. Rev. 118, 1591 (1960).

<sup>b</sup>Standard nuclear configuration adopted for this report.

while just the opposite is true for copper. So the (p,pn) cross section becomes a larger fraction of the total nonelastic cross section for the case of gold in every case, while this trend is reversed in going to the higher energies in the case of copper.

3. The change in the cross section in going to the diffuse edge was only partially successful in accounting for the discrepancy with experiments.

This cross section appears to be very sensitive to the nuclear model and it is the author's opinion that it is beyond the capacity of the present model to predict its value with an accuracy better than a factor of two.

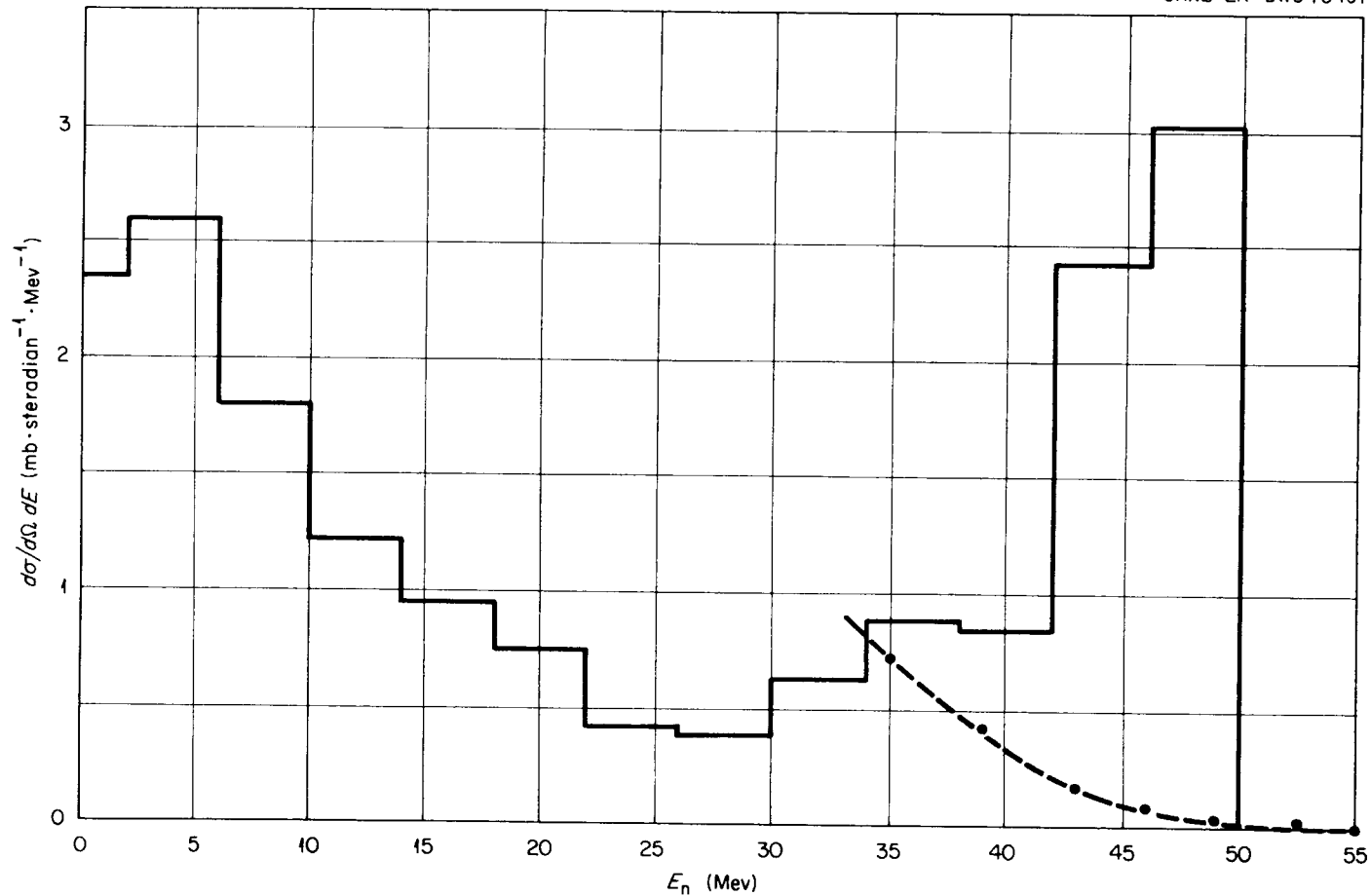


Figure 9. Neutron Spectra at  $0^\circ$  from 50-Mev Protons on Carbon. Dashed curve: Hofmann's experimental results [J. A. Hofmann, Neutrons Ejected from Nuclei by 50-Mev Protons, A Ph.D. Thesis submitted to the Faculty of Arts and Sciences of Harvard University, Cambridge (August, 1952)]; solid lines: calculated spectrum for neutrons emitted in the angular interval  $0^\circ$  to  $11^\circ$ .

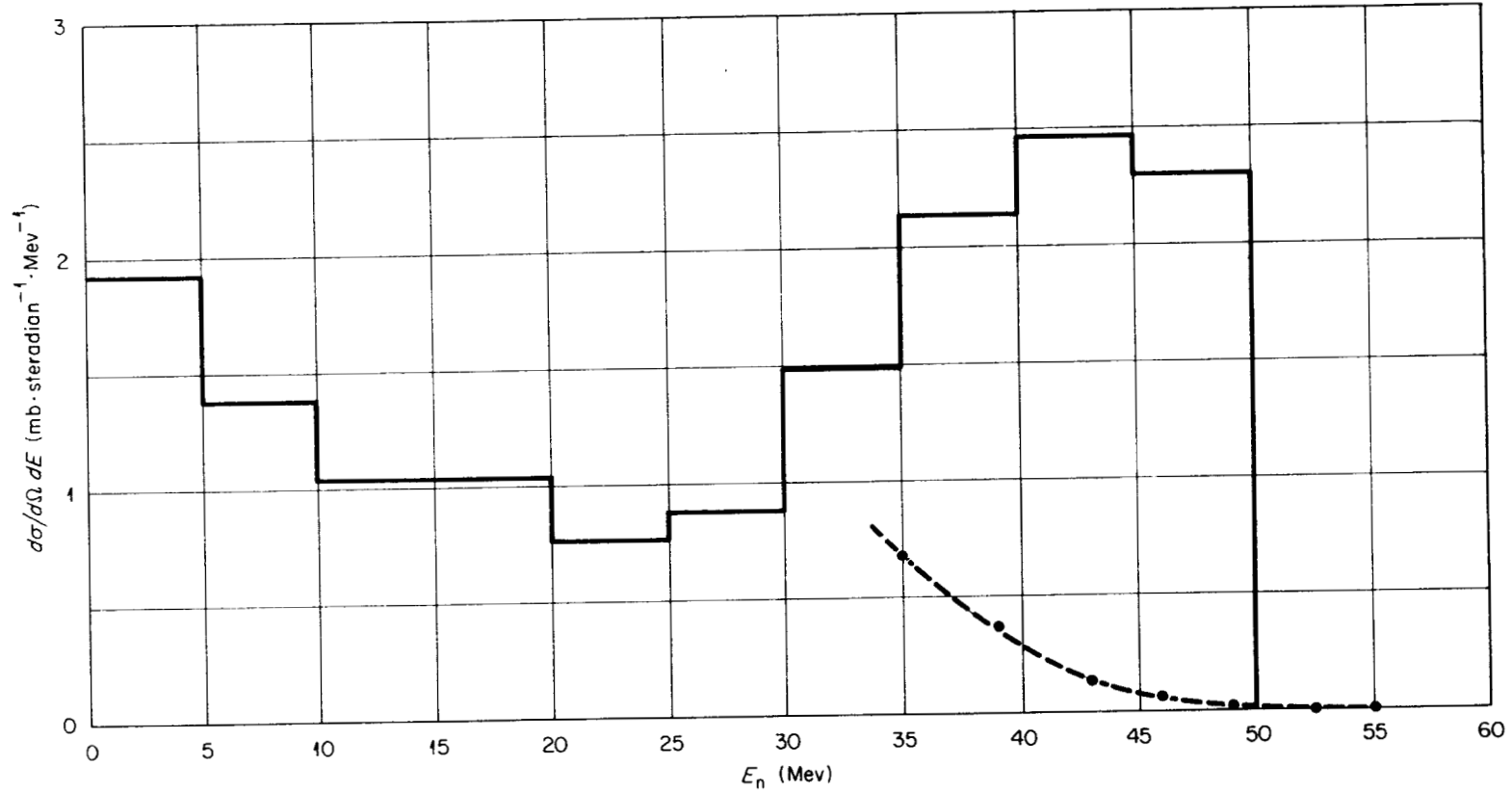


Figure 10. Neutron Spectra at  $16^\circ$  from 50-Mev Protons on Carbon. Dashed curve: Hofmann's experimental results [J. A. Hofmann, Neutrons Ejected from Nuclei by 50-Mev Protons, A Ph.D. Thesis submitted to the Faculty of Arts and Sciences of Harvard University, Cambridge (August, 1952)]; solid lines: calculated spectrum for neutrons emitted in the angular interval  $5^\circ$  to  $25^\circ$ .

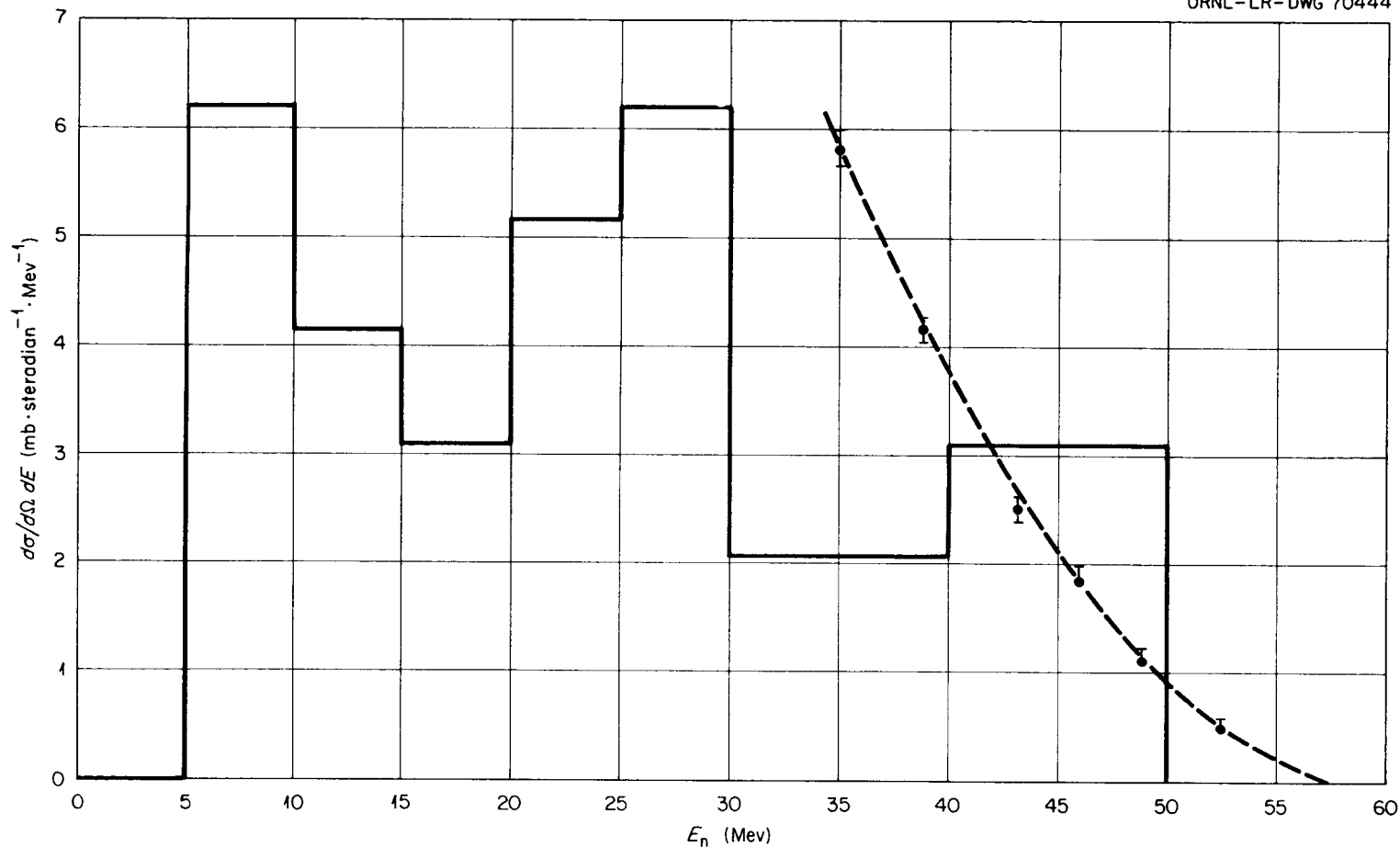


Figure 11. Neutron Spectra at  $0^\circ$  from 50-Mev Protons on Lead. Dashed curve: Hofmann's experimental results [J. A. Hofmann, Neutrons Ejected from Nuclei by 50-Mev Protons, A Ph.D. Thesis submitted to the Faculty of Arts and Sciences of Harvard University, Cambridge (August, 1952)]; solid lines: calculated spectrum for neutrons emitted in the interval  $0^\circ$  to  $10^\circ$ .

UNCLASSIFIED  
ORNL-LR-DWG 70443

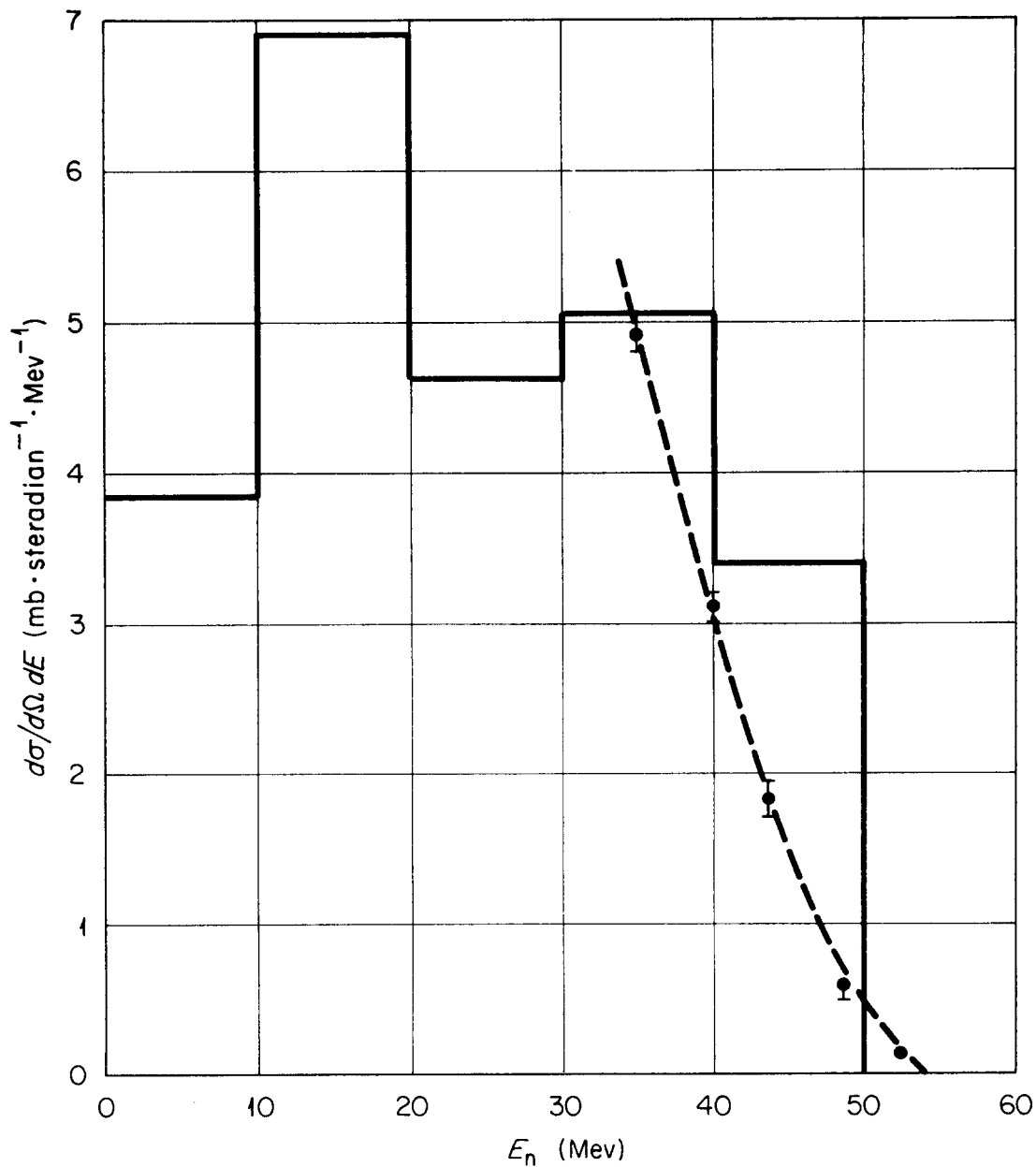


Figure 12. Neutron Spectra at  $16^\circ$  from 50-Mev Protons on Lead. Dashed curve: Hofmann's experimental results [J. A. Hofmann, Neutrons Ejected from Nuclei by 50-Mev Protons, A Ph.D. Thesis submitted to the Faculty of Arts and Sciences of Harvard University, Cambridge (August, 1952)]; solid lines: calculated spectra for neutrons emitted in the angular interval  $5^\circ$  to  $25^\circ$ .

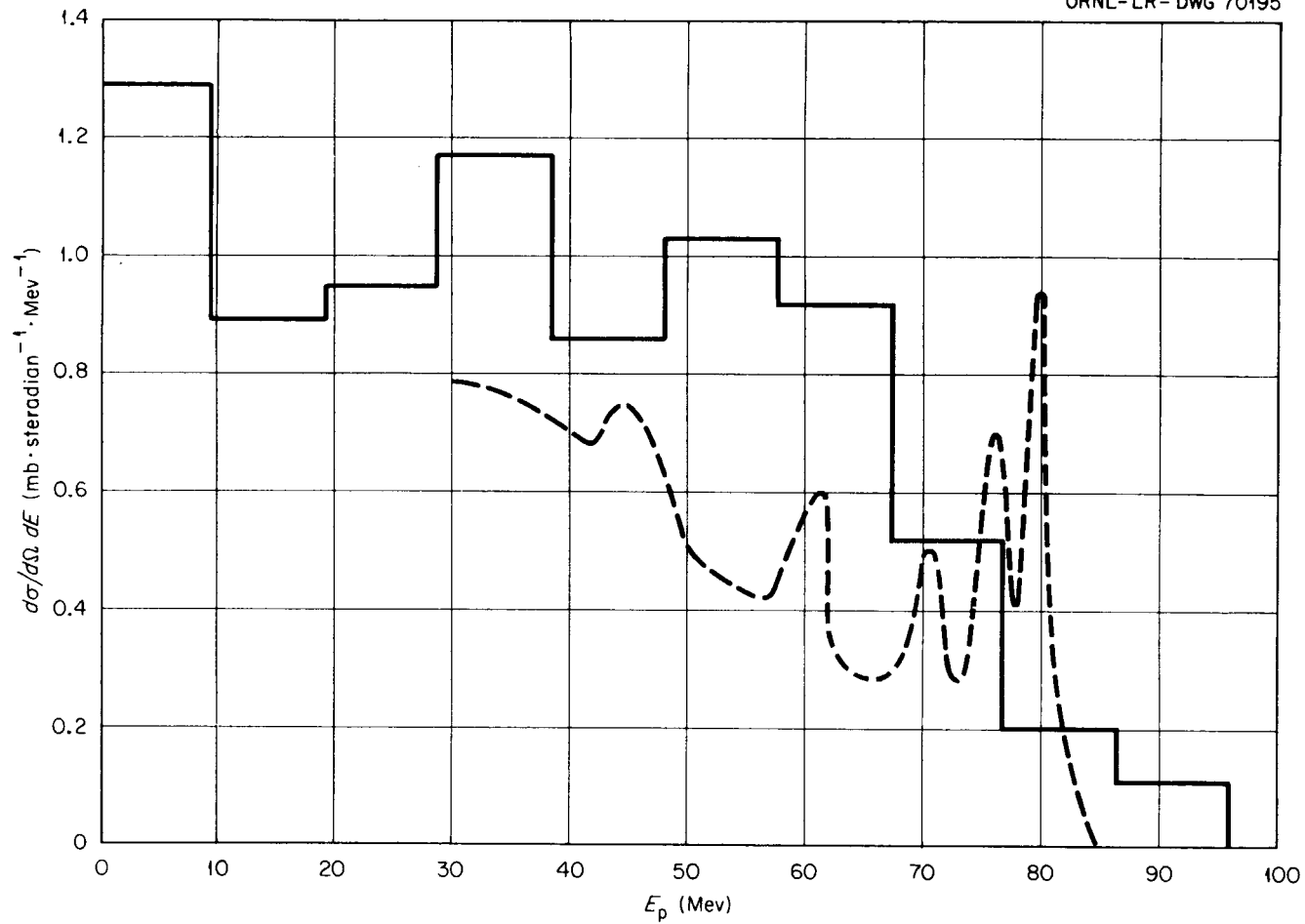


Figure 13. Proton Spectra at  $40^\circ$  from 96-Mev Protons on Carbon. Dashed curve: experimental results of Strauch and Titus [K. Strauch and F. Titus, Phys. Rev. 104, 191 (1956)]; solid lines: calculated spectrum of protons emitted in the angular interval  $30^\circ$  to  $50^\circ$ .

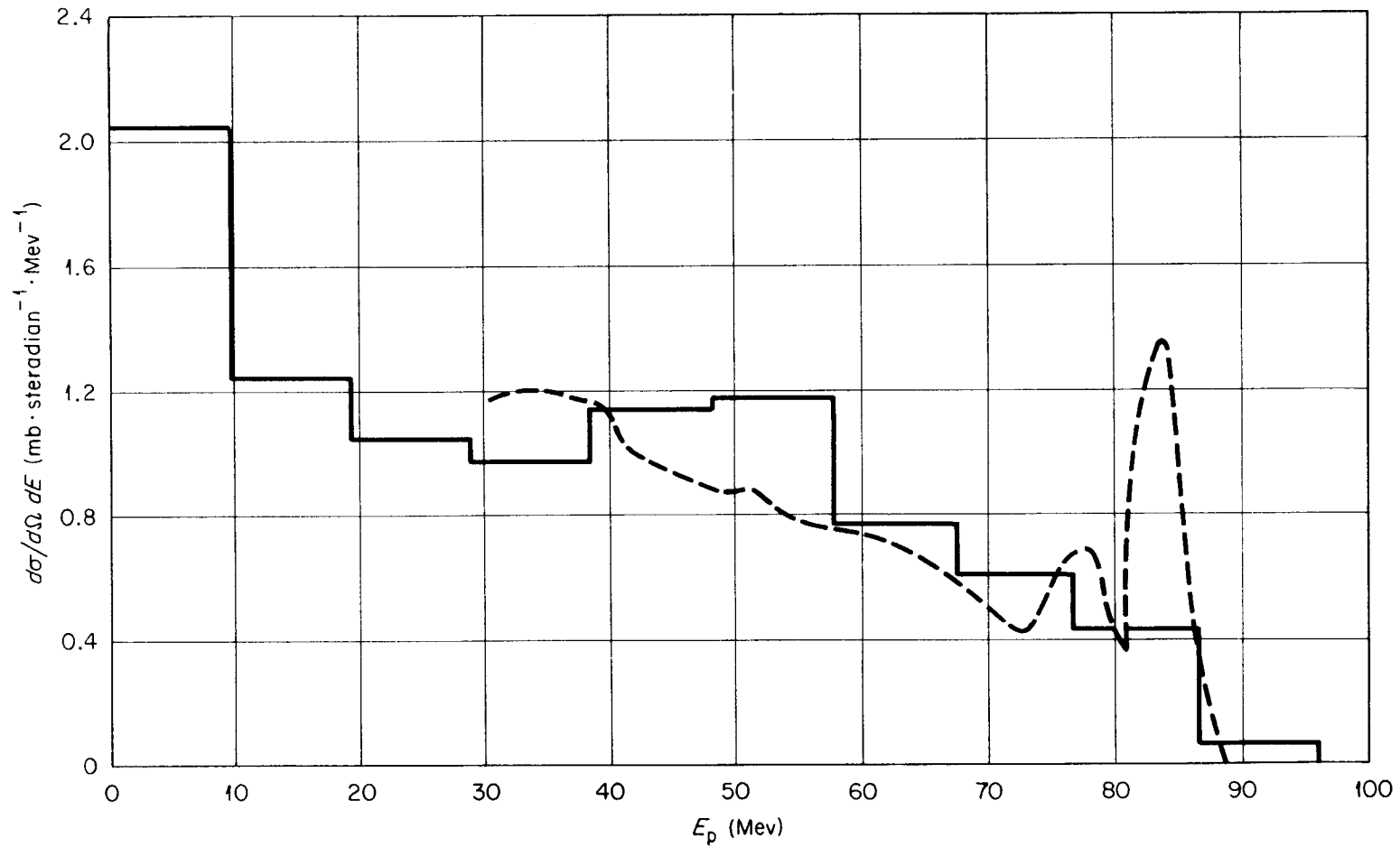


Figure 14. Proton Spectra at  $40^\circ$  from 96-Mev Protons on Fluorine. Dashed curve: experimental results of Strauch and Titus [K. Strauch and F. Titus, Phys. Rev. 104, 191 (1956)]; solid lines: calculated spectrum of protons emitted in the angular interval  $30^\circ$  to  $50^\circ$ .

UNCLASSIFIED  
ORNL-LR-DWG 70194

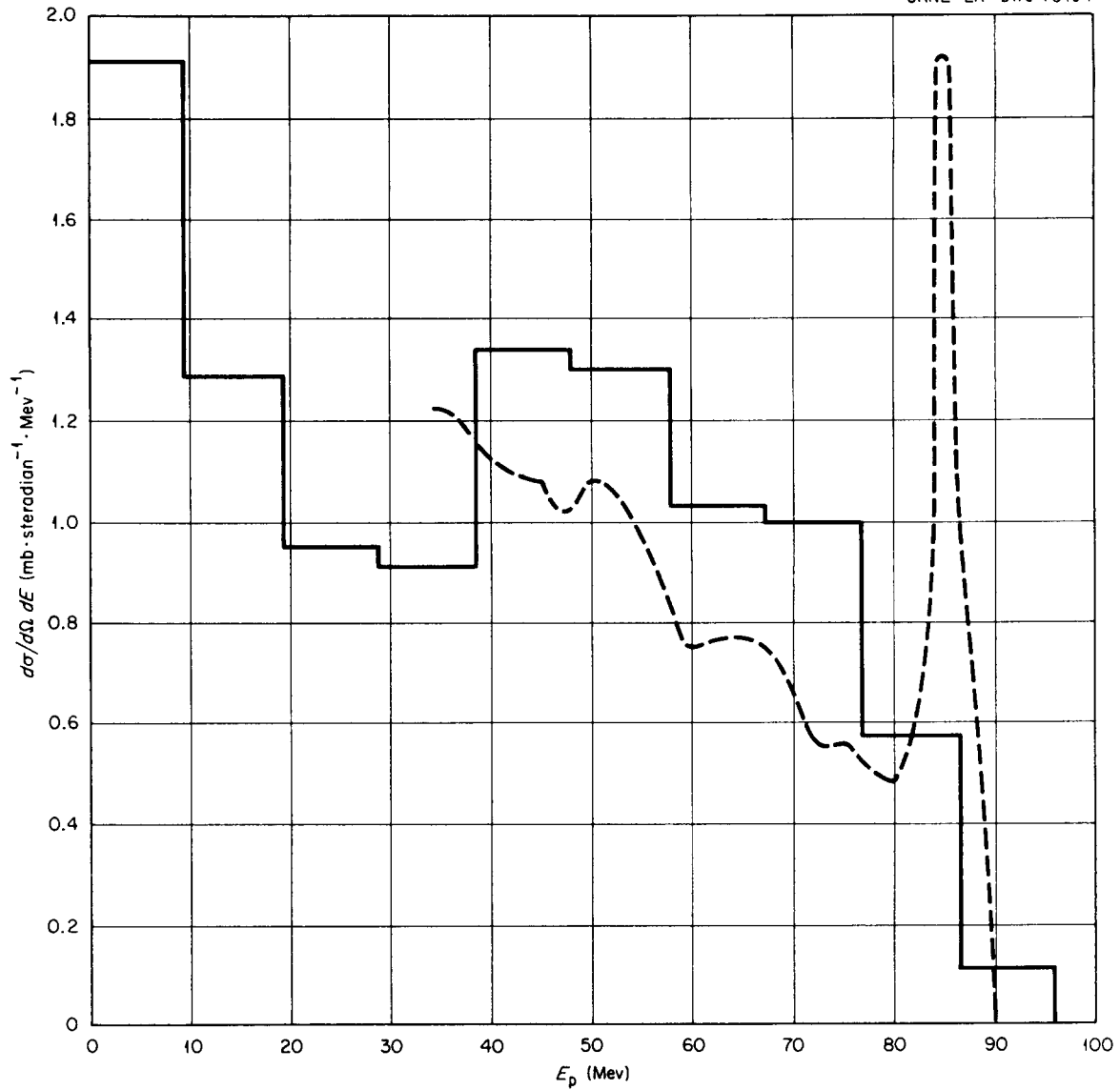


Figure 15. Proton Spectra at  $40^\circ$  from 96-Mev Protons on Aluminum. Dashed curve: experimental results of Strauch and Titus [K. Strauch and F. Titus, Phys. Rev. 104, 191 (1956)]; solid lines: calculated spectrum of protons emitted in the angular interval  $30^\circ$  to  $50^\circ$ .

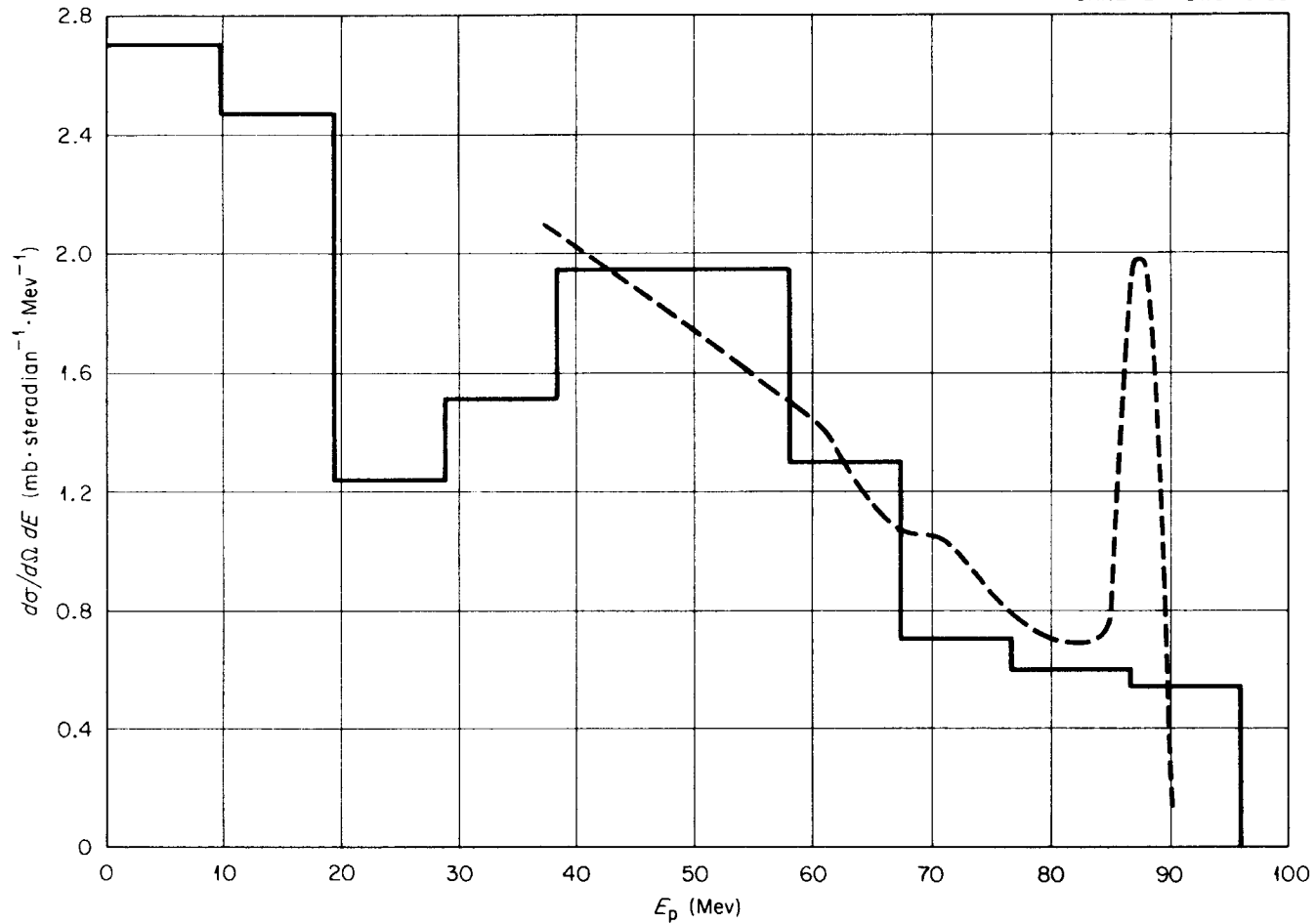


Figure 16. Proton Spectra at  $40^\circ$  from 96-Mev Protons on Copper. Dashed curve: experimental results of Strauch and Titus [K. Strauch and F. Titus, Phys. Rev. 104, 191 (1956)]; solid lines: calculated spectrum of protons emitted in the angular interval  $30^\circ$  to  $50^\circ$ .

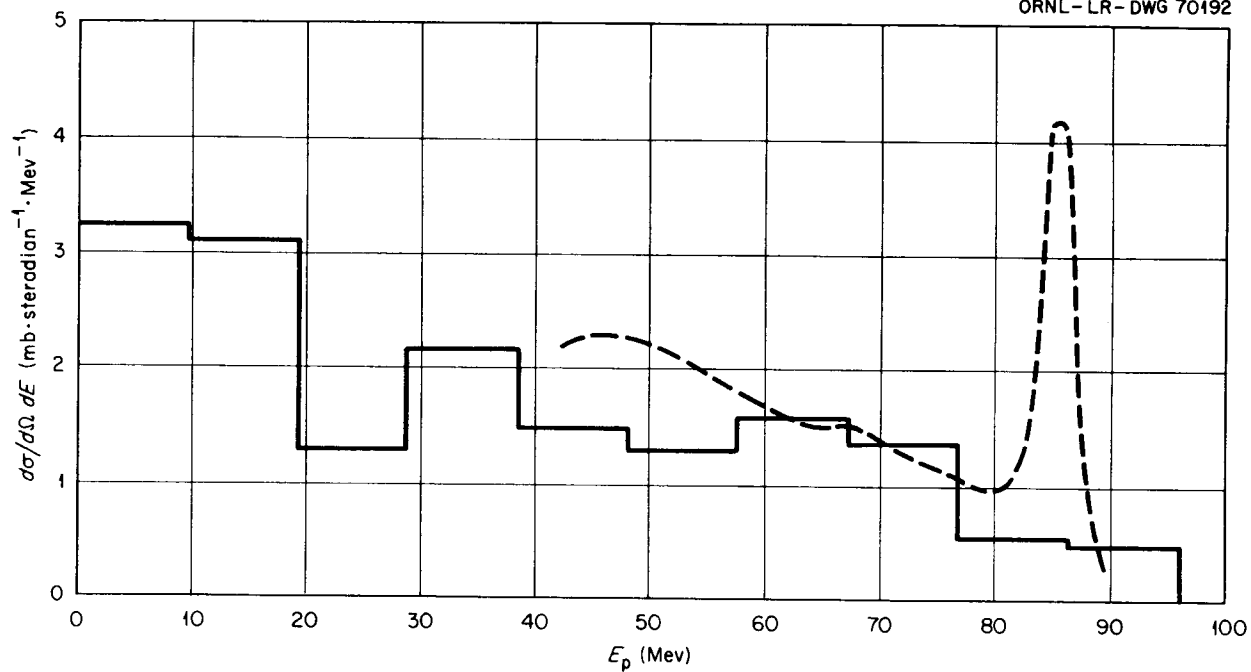


Figure 17. Proton Spectra at  $40^\circ$  from 96-Mev Protons on Silver. Dashed curve: experimental results of Strauch and Titus [K. Strauch and F. Titus, Phys. Rev. 104, 191 (1956)]; solid lines: calculated spectrum of protons emitted in angular interval  $30^\circ$  to  $50^\circ$ .

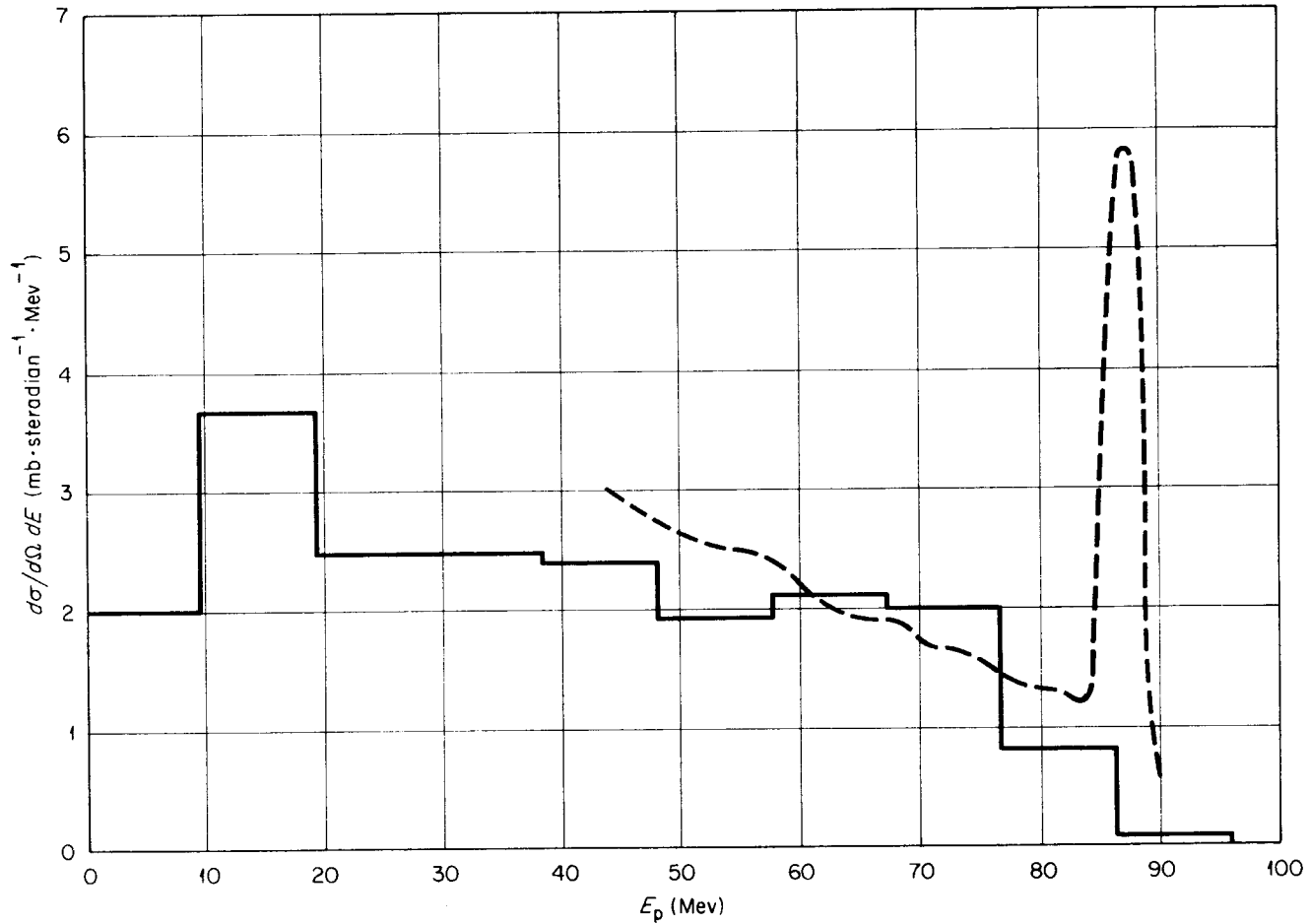


Figure 18. Proton Spectra at  $40^\circ$  from 96-Mev Protons on Bismuth. Dashed curve: experimental results of Strauch and Titus [K. Strauch and F. Titus, Phys. Rev. 104, 191 (1956)]; solid lines: calculated spectrum of protons emitted in the angular interval  $30^\circ$  to  $50^\circ$ .

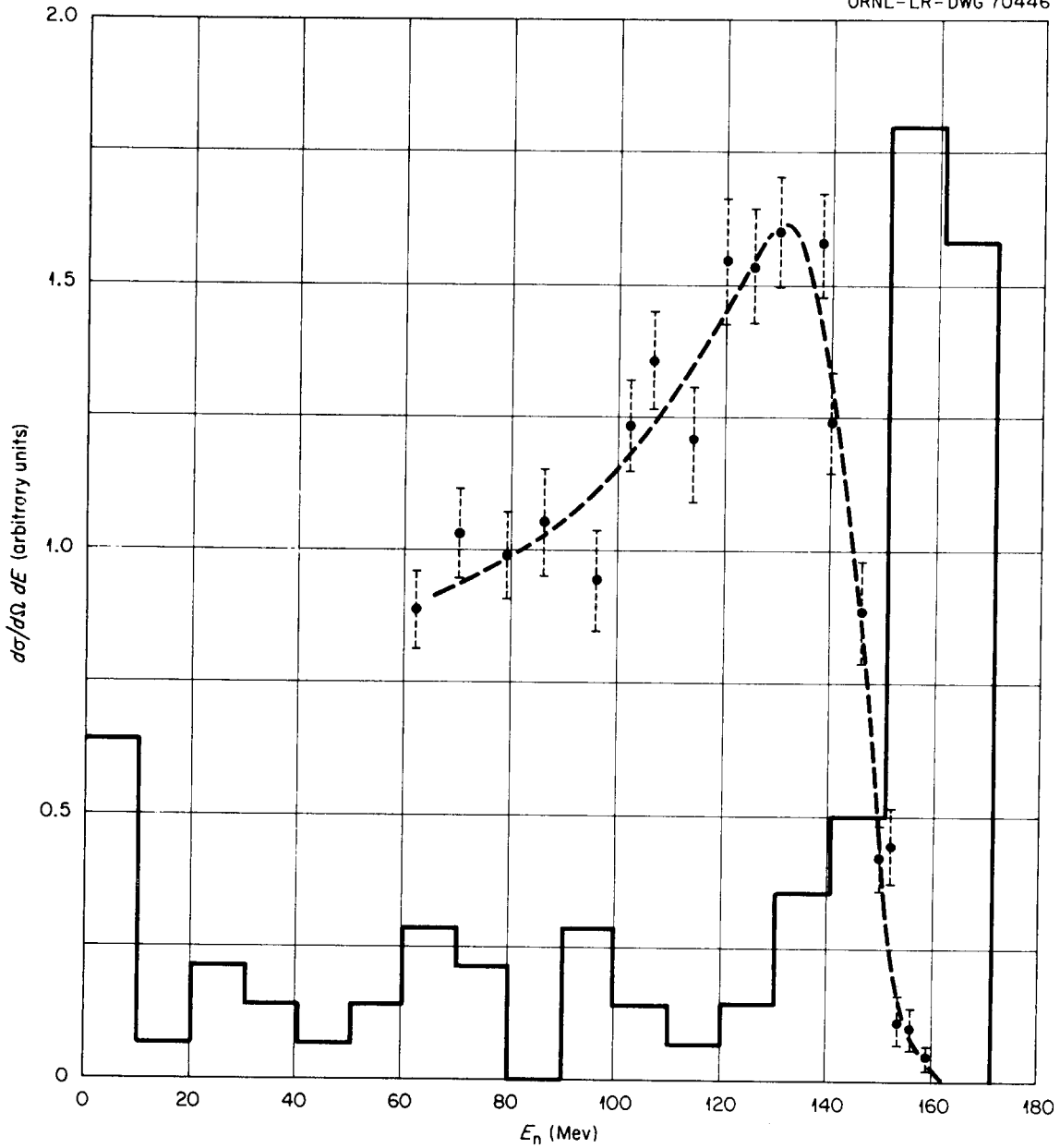


Figure 19. Neutron Spectra at  $2.5^\circ$  from 171-Mev Protons on Carbon. Dashed curve: experimental results of Cassels et al. [J. M. Cassels et al., *Phil. Mag.* 42, 215 (1951)]; solid lines: calculated spectrum of neutrons emitted in the angular interval  $0^\circ$  to  $15^\circ$ . The units of the ordinate scale are arbitrary.

UNCLASSIFIED  
ORNL-LR-DWG 70306R1

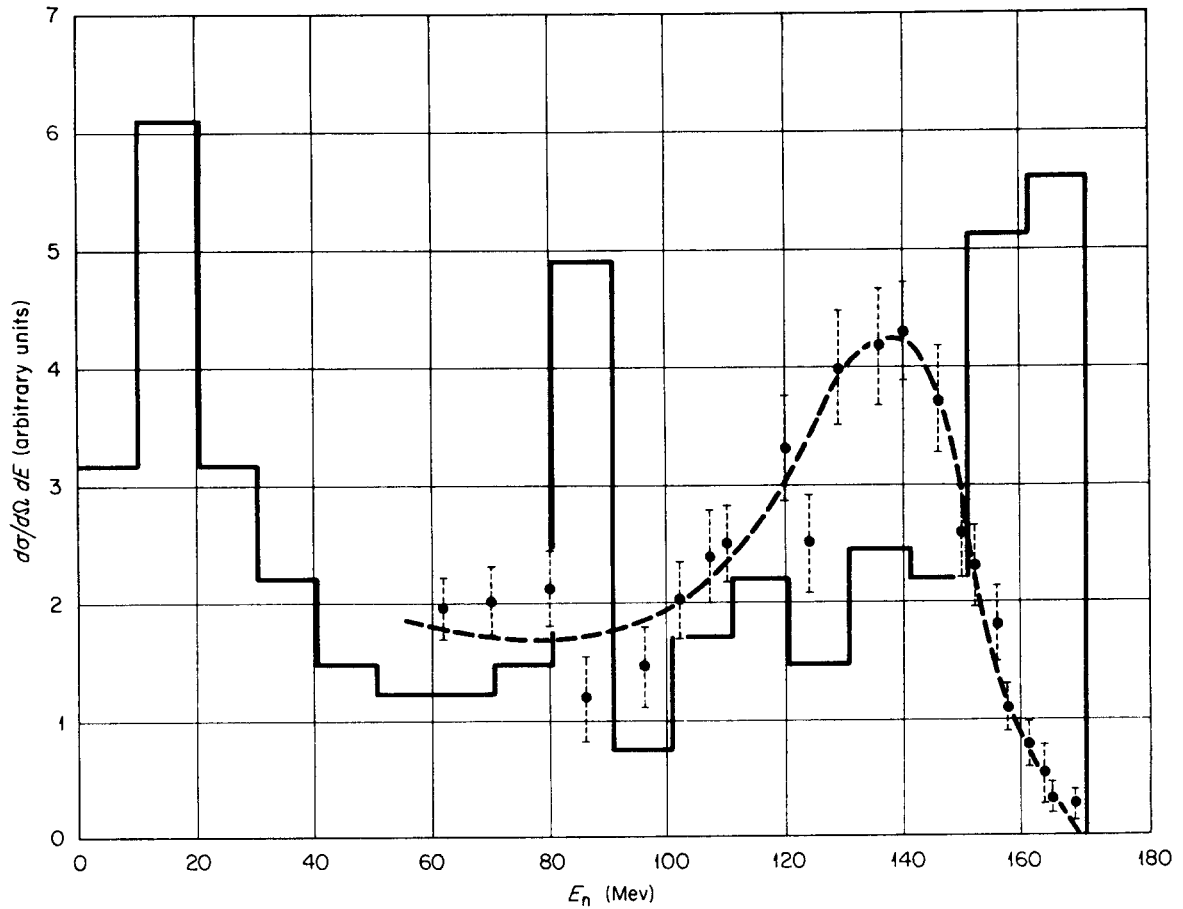


Figure 20. Neutron Spectra at  $2.5^\circ$  from 171-Mev Protons on Uranium. Dashed curve: experimental results of Cassels et al. [J. M. Cassels et al., Phil. Mag. 42, 215 (1951)]; solid lines: calculated spectrum of neutrons emitted in the angular interval  $0^\circ$  to  $15^\circ$ . The units of the ordinate scale are arbitrary.

UNCLASSIFIED  
ORNL-LR-DWG 70436

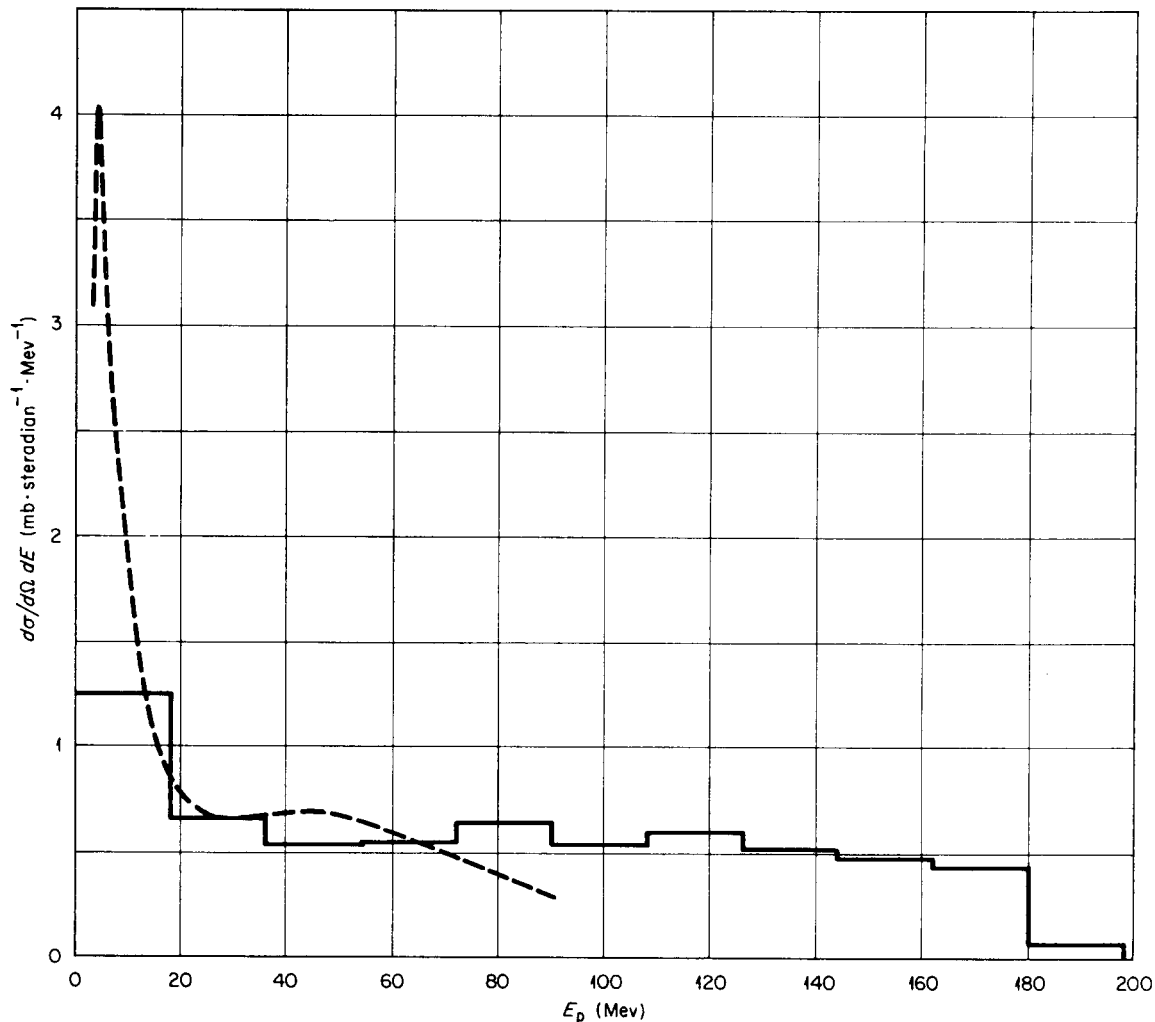


Figure 21. Proton Spectra from  $0^\circ$  to  $65^\circ$  for 190-Mev Protons on Aluminum. Dashed curve: experimental results of Bailey [L. E. Bailey, Angle and Energy Distributions of Charged Particles from the High Energy Nuclear Bombardment of Various Elements, University of California Radiation Laboratory Report UCRL-3334 (March 1, 1956)]; solid lines: calculated spectrum.

UNCLASSIFIED  
ORNL-LR-DWG 70311

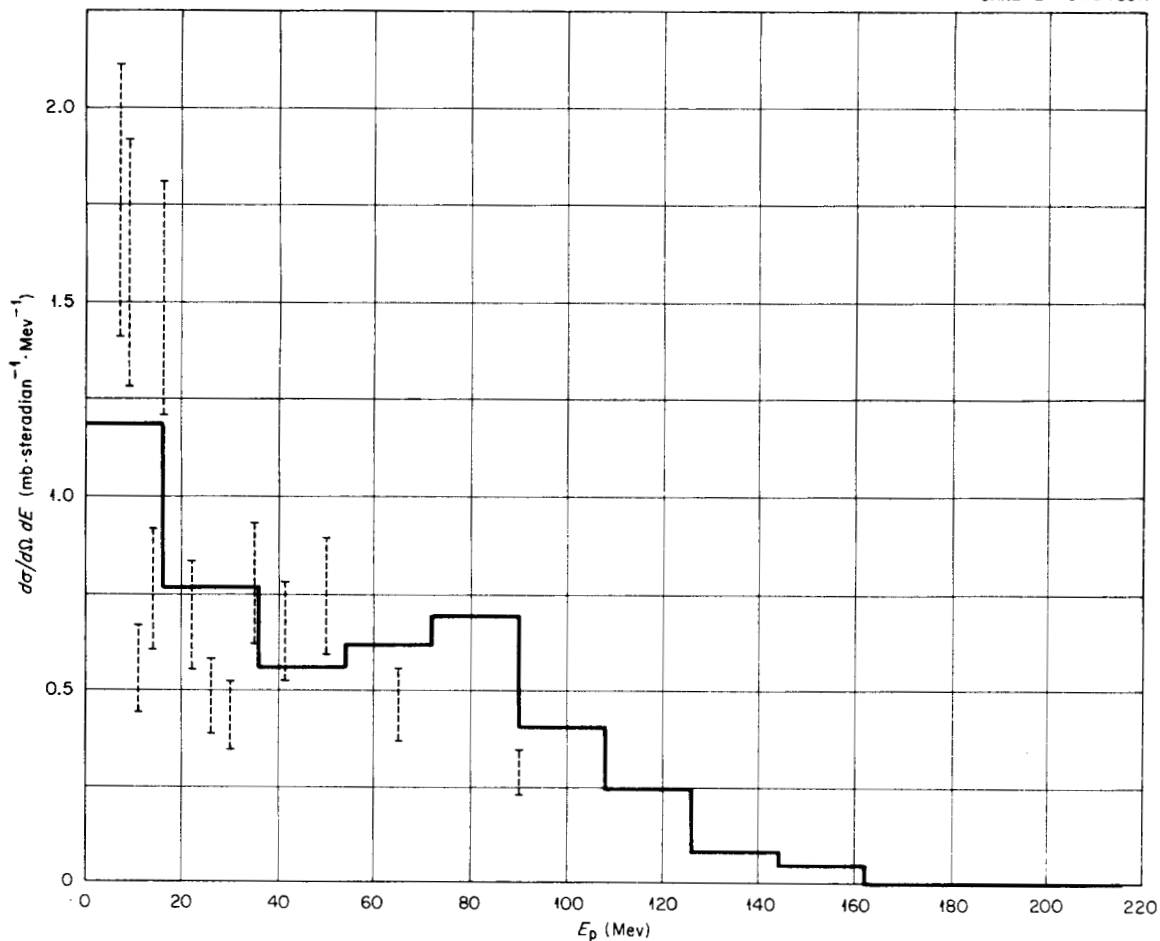


Figure 22. Proton Spectra from  $46^\circ$  to  $65^\circ$  for 190-Mev Protons on Aluminum. Error bars: experimental results of Bailey [L. E. Bailey, Angle and Energy Distributions of Charged Particles from the High Energy Nuclear Bombardment of Various Elements, University of California Radiation Laboratory UCRL-3334 (March 1, 1956)]; solid lines: calculated spectrum.

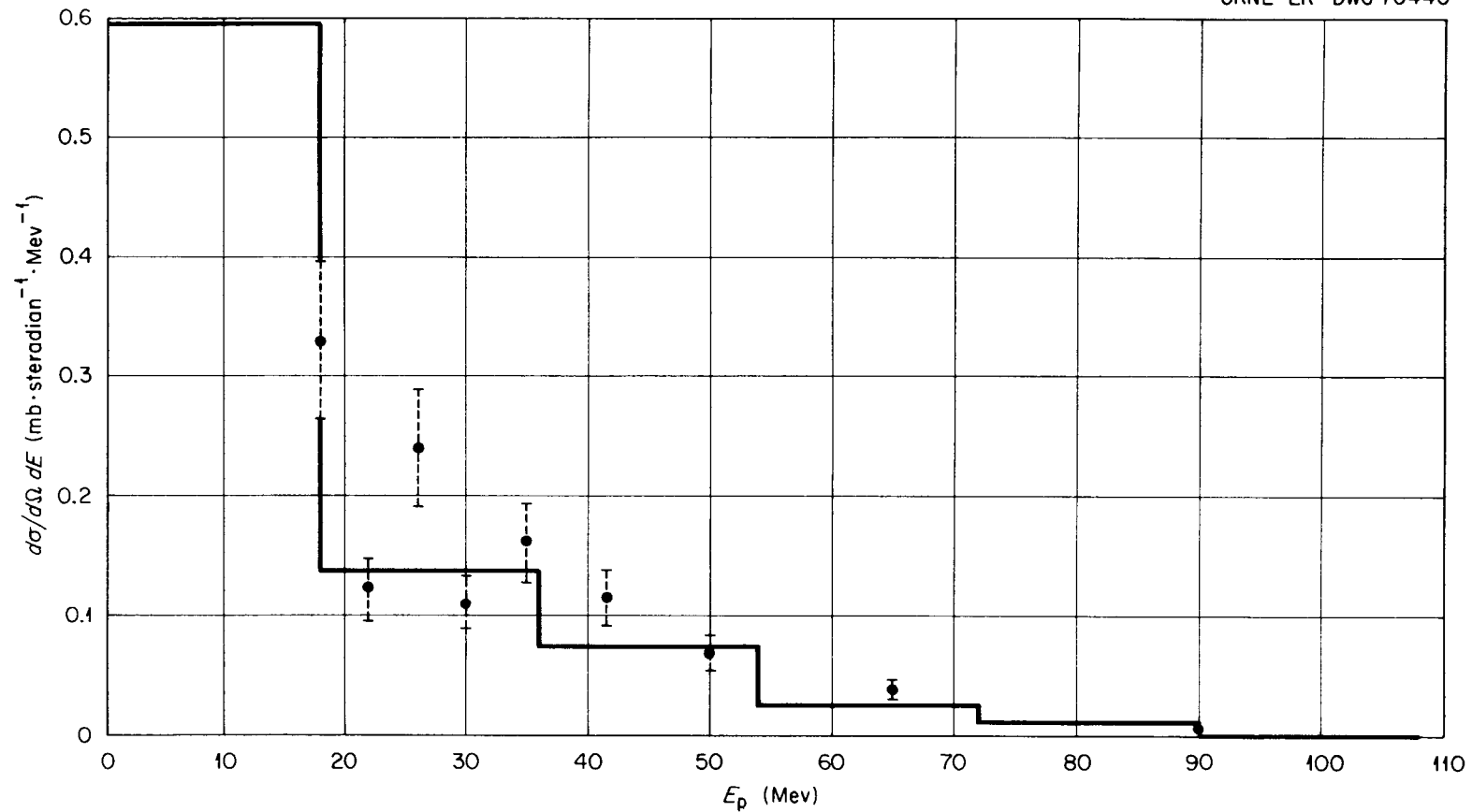


Figure 23. Proton Spectra from  $102^\circ$  to  $117^\circ$  for 190-Mev Protons on Aluminum. Points: experimental results of Bailey [L. E. Bailey, Angle and Energy Distributions of Charged Particles from the High Energy Nuclear Bombardment of Various Elements, University of California Radiation Laboratory Report UCRL-3334 (March 1, 1956)]; solid lines: calculated spectrum.

UNCLASSIFIED  
ORNL-LR-DWG 70416

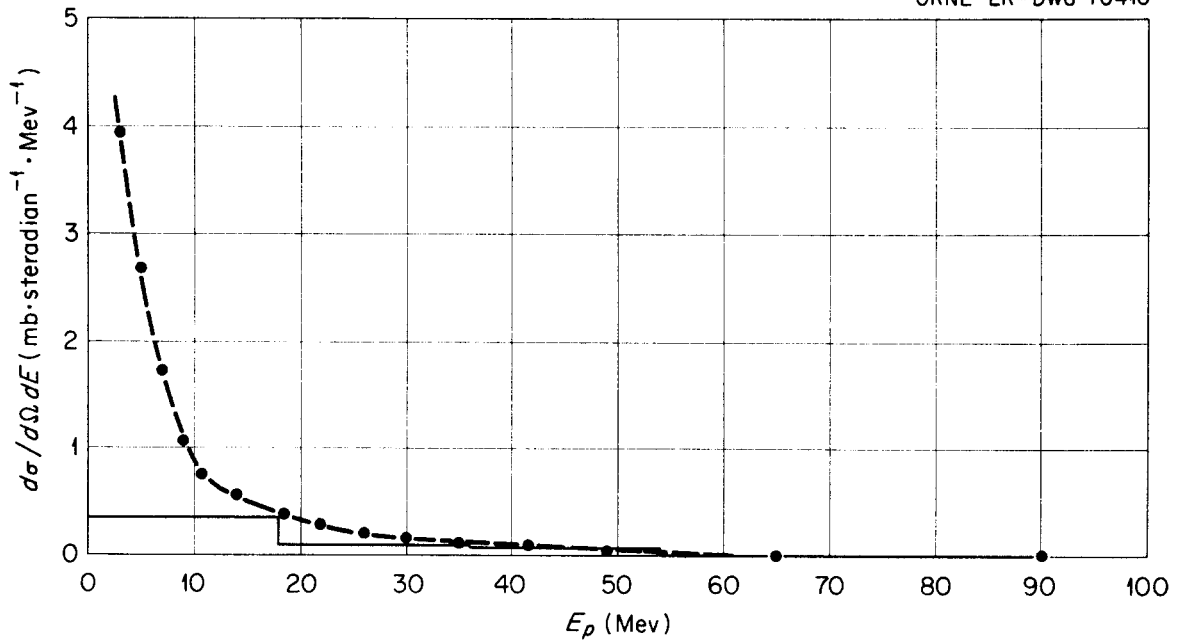


Figure 24. Proton Spectra from  $100^\circ$  to  $180^\circ$  for 190-Mev Protons on Aluminum. Dashed curve: experimental results of Bailey [L. E. Bailey, Angle and Energy Distributions of Charged Particles from the High Energy Nuclear Bombardment of Various Elements, University of California Radiation Laboratory Report UCRL-3334 (March 1, 1956)]; solid lines: calculated spectrum.

UNCLASSIFIED  
ORNL-LR-DWG 70442

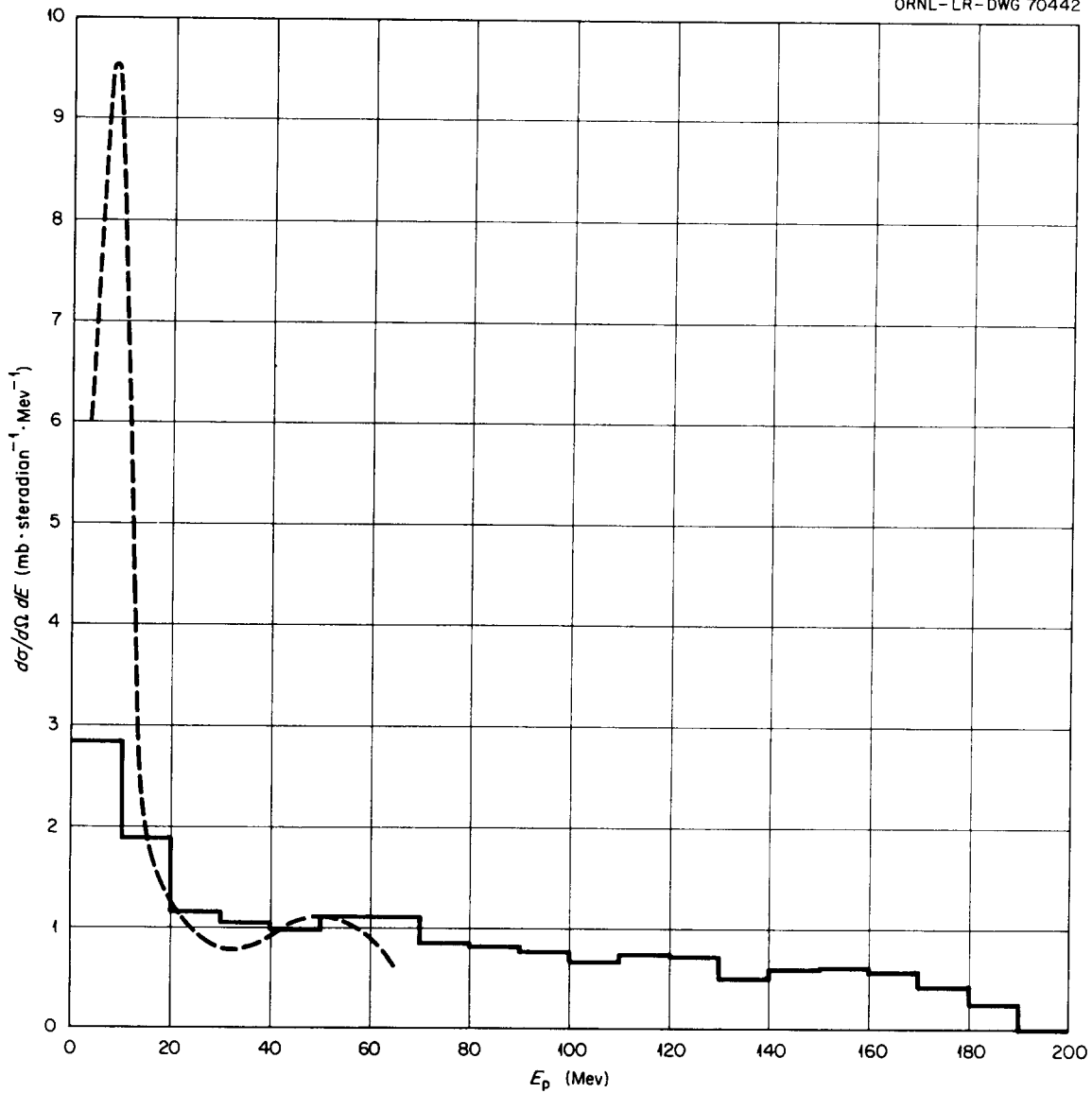


Figure 25. Proton Spectra from  $0^\circ$  to  $65^\circ$  for 190-Mev Protons on Nickel. Dashed curve: experimental results of Bailey [L. E. Bailey, Angle and Energy Distributions of Charged Particles from the High Energy Nuclear Bombardment of Various Elements, University of California Radiation Laboratory Report UCRL-3334 (March 1, 1956)]; solid lines: calculated spectrum.

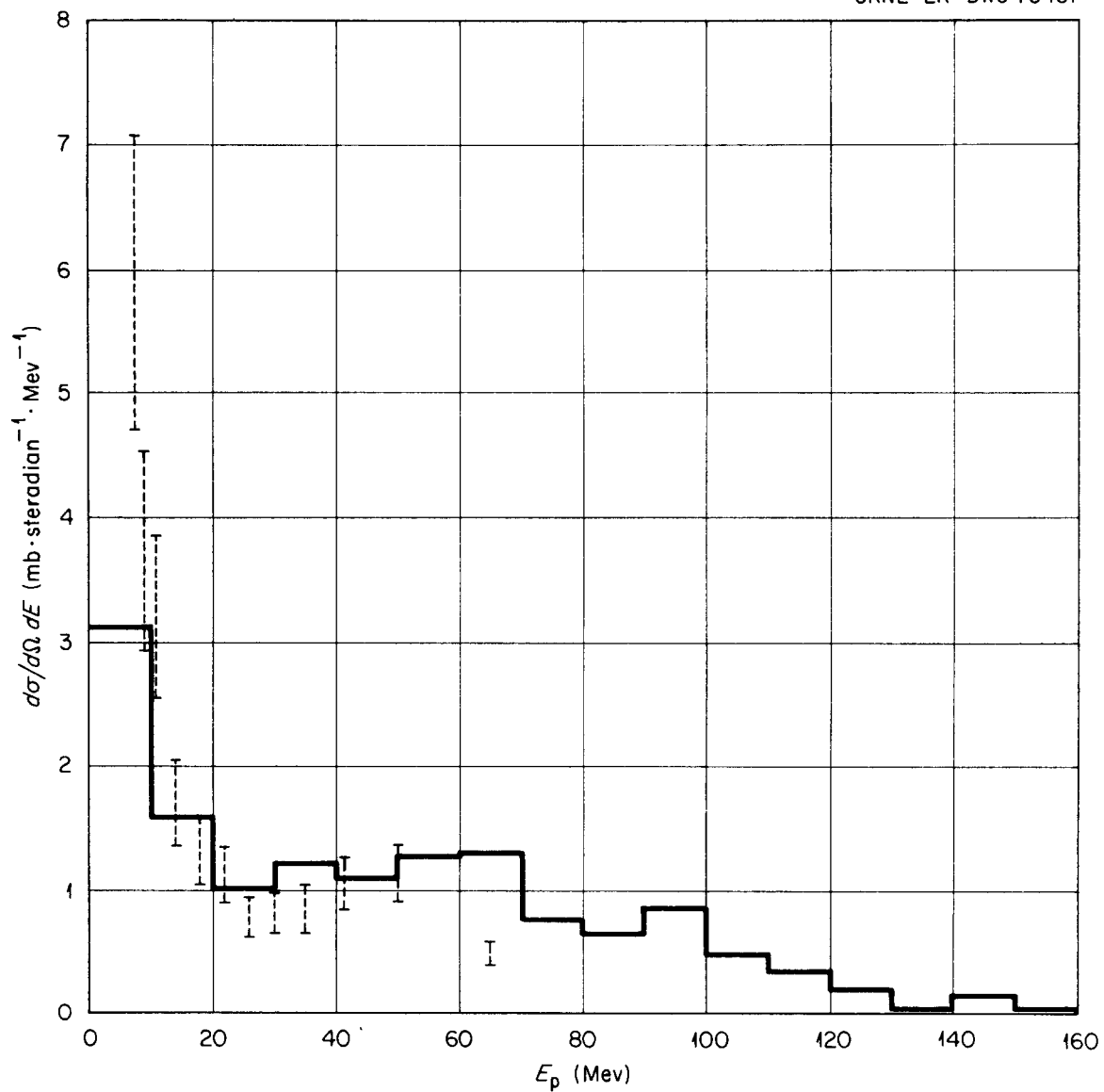


Figure 26. Proton Spectra from  $46^\circ$  to  $65^\circ$  for 190-Mev Protons on Nickel. Error bars: experimental results of Bailey [L. E. Bailey, Angle and Energy Distributions of Charged Particles from the High Energy Nuclear Bombardment of Various Elements, University of California Radiation Laboratory Report UCRL-3334 (March 1, 1956)]; solid lines: calculated spectrum.

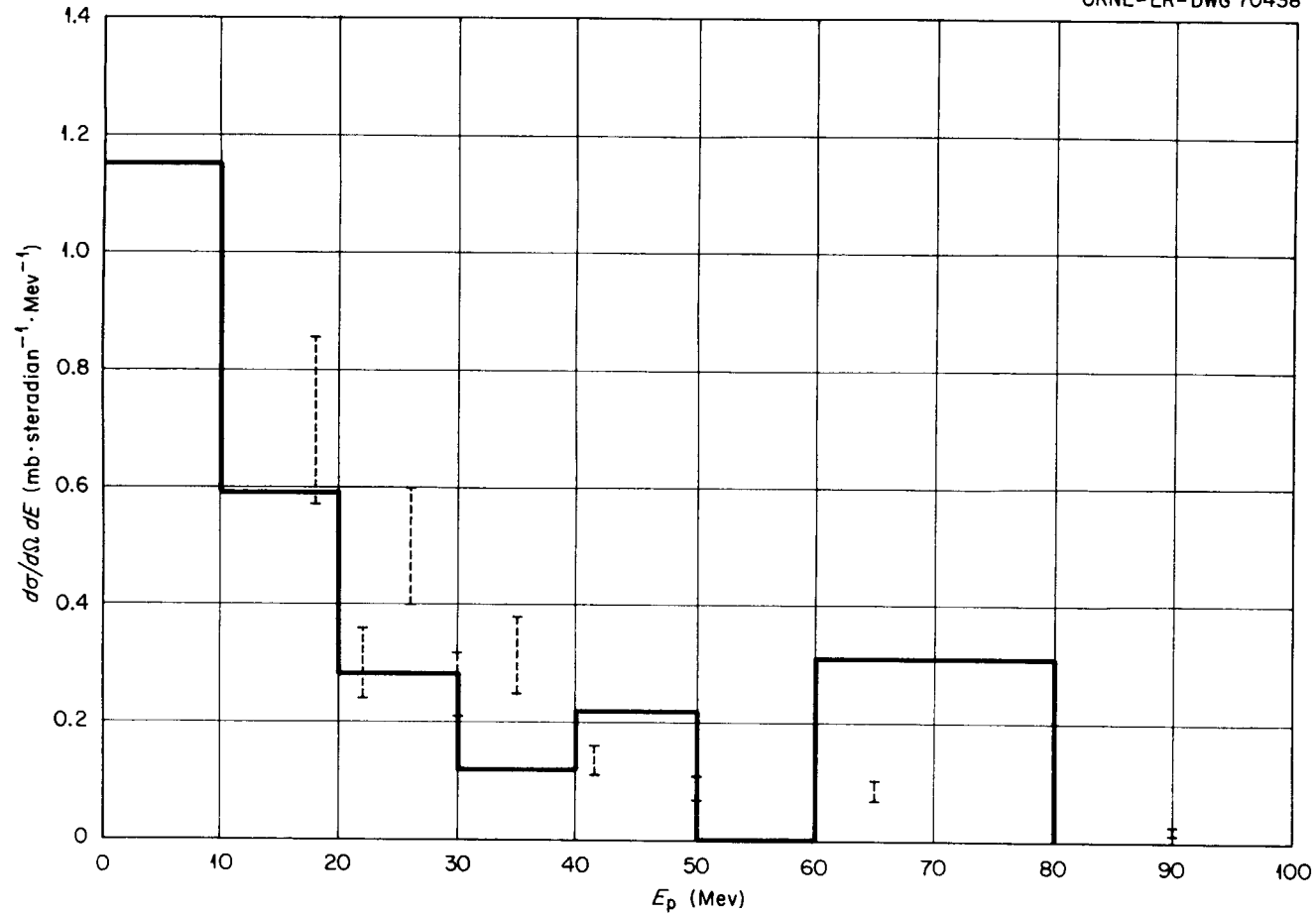


Figure 27. Proton Spectra from  $102^\circ$  to  $117^\circ$  for 190-Mev Protons on Nickel. Error bars: experimental results of Bailey [L. E. Bailey, Angle and Energy Distributions of Charged Particles from the High Energy Nuclear Bombardment of Various Elements, University of California Radiation Laboratory Report UCRL-3334 (March 1, 1956)]; solid lines: calculated spectrum.

UNCLASSIFIED  
ORNL-LR-DWG 70444

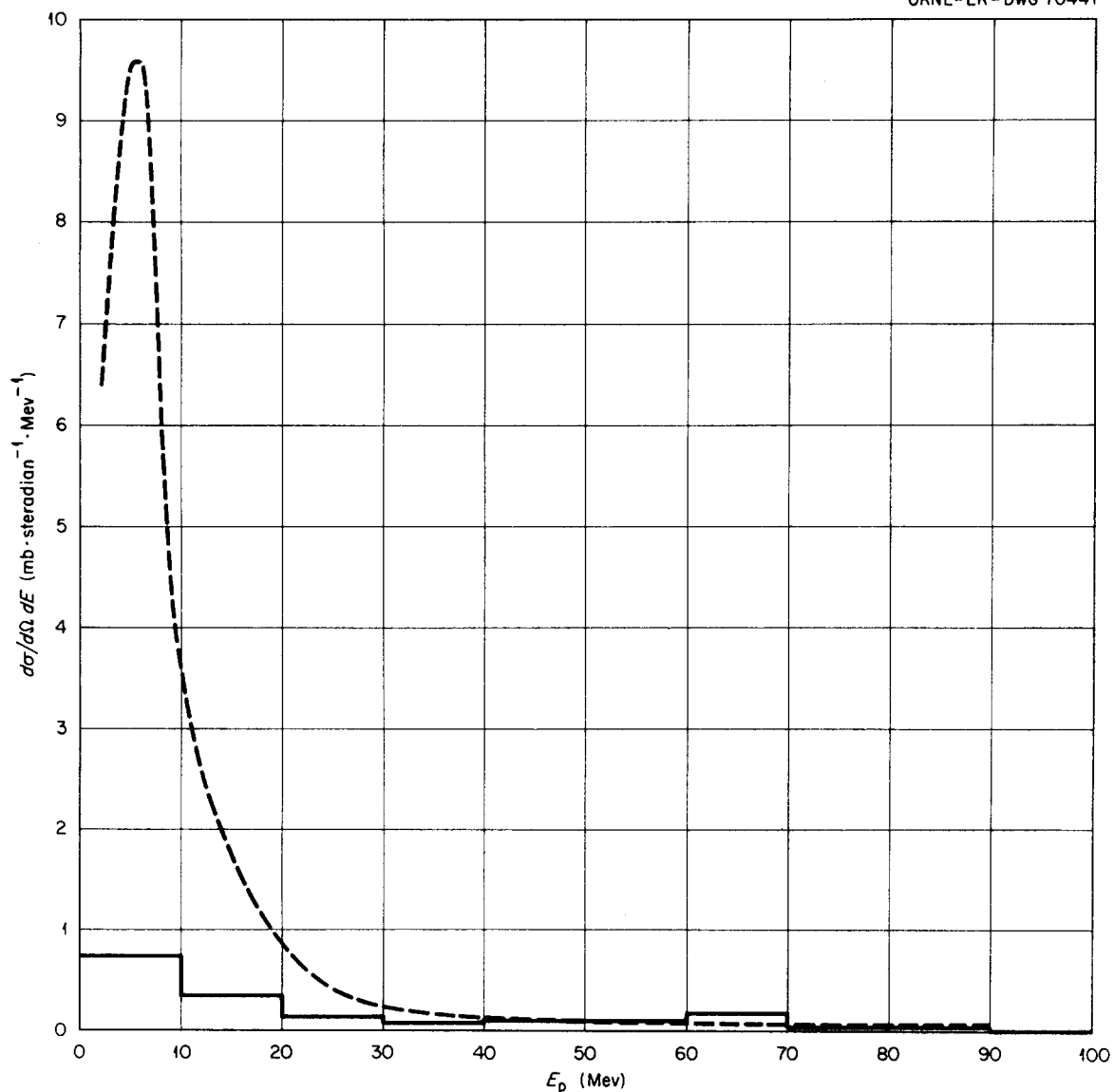


Figure 28. Proton Spectra from  $100^\circ$  to  $180^\circ$  for 190-Mev Protons on Nickel. Dashed curve: experimental results of Bailey [L. E. Bailey, Angle and Energy Distributions of Charged Particles from the High Energy Nuclear Bombardment of Various Elements, University of California Radiation Laboratory Report UCRL-3334 (March 1, 1956)]; solid lines: calculated spectrum.

UNCLASSIFIED  
ORNL-LR-DWG 70417

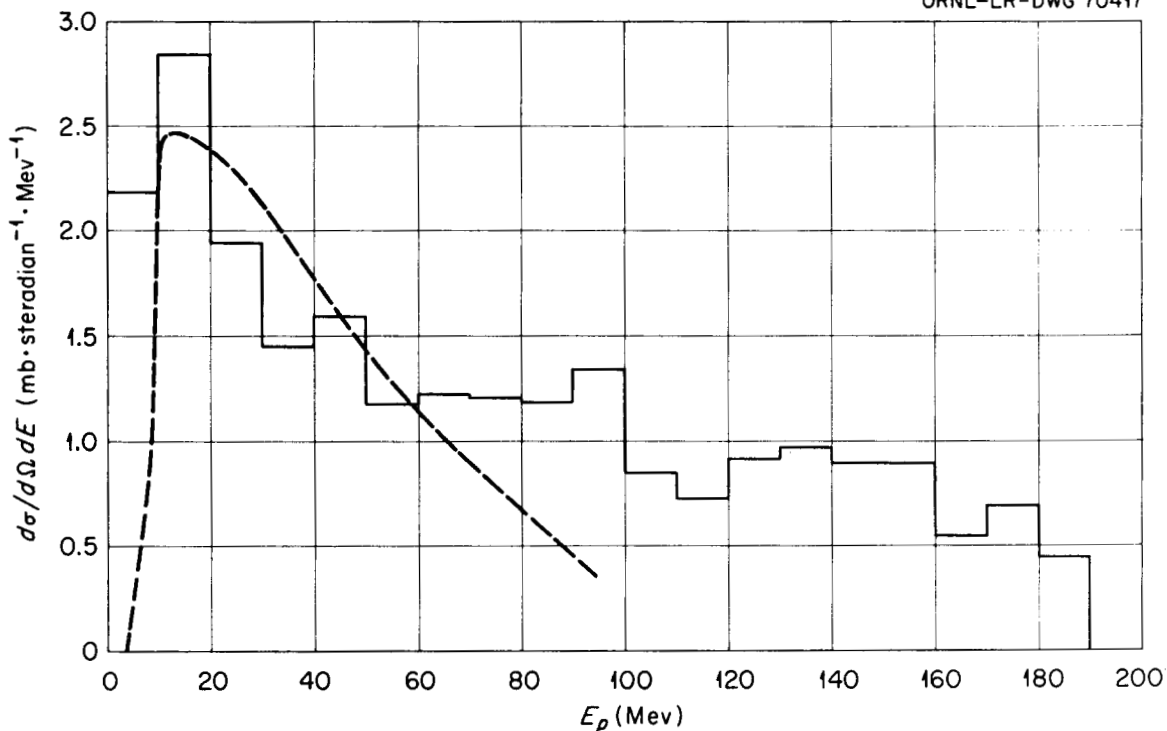


Figure 29. Proton Spectra from  $0^\circ$  to  $65^\circ$  for 190-Mev Protons on Gold. Dashed curve: experimental results of Bailey [L. E. Bailey, Angle and Energy Distributions of Charged Particles from the High Energy Nuclear Bombardment of Various Elements, University of California Radiation Laboratory Report UCRL-3334 (March 1, 1956)]; solid lines: calculated spectrum.

UNCLASSIFIED  
ORNL-LR-DWG 70439M

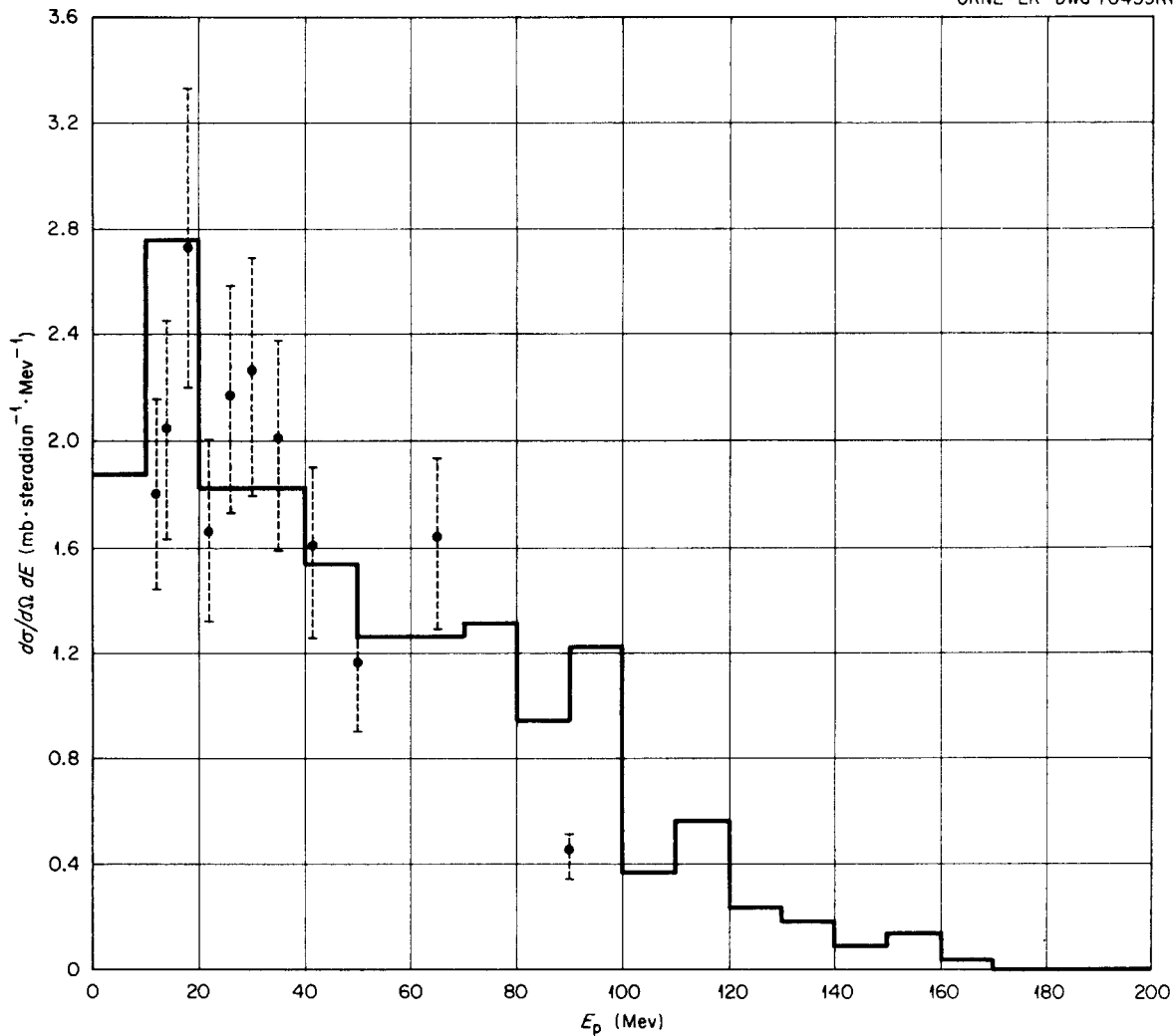


Figure 30. Proton Spectra from  $46^\circ$  to  $65^\circ$  for 190-Mev Protons on Gold. Points: experimental results of Bailey [L. E. Bailey, Angle and Energy Distributions of Charged Particles from the High Energy Nuclear Bombardment of Various Elements, University of California Radiation Laboratory Report UCRL-3334 (March 1, 1956)]; solid lines: calculated spectrum.

UNCLASSIFIED  
ORNL-LR-DWG 70316R1

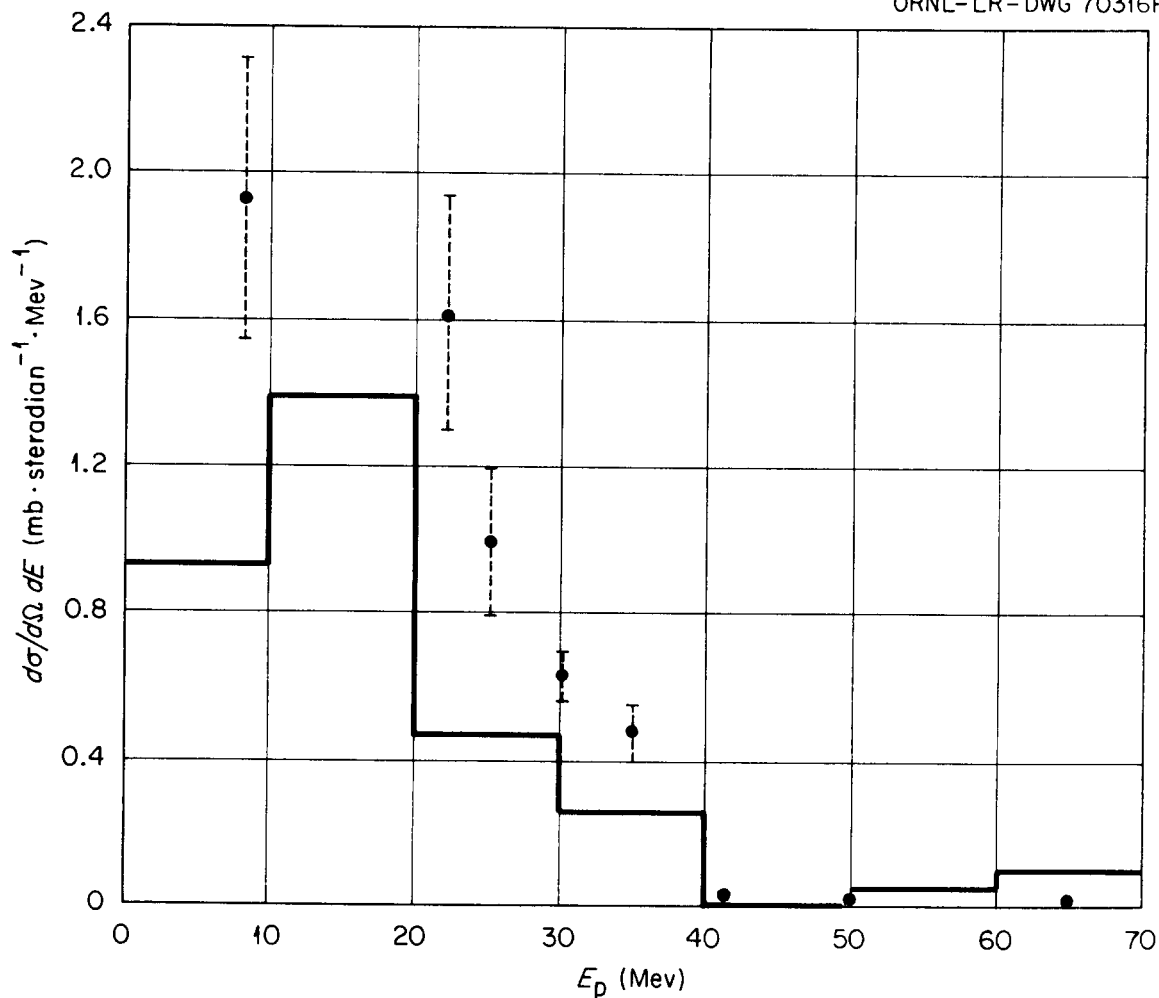


Figure 31. Proton Spectra from  $102^\circ$  to  $117^\circ$  for 190-Mev Protons on Gold. Points: experimental results of Bailey [L. E. Bailey, Angle and Energy Distributions of Charged Particles from the High Energy Nuclear Bombardment of Various Elements, University of California Radiation Laboratory Report UCRL-3334 (March 1, 1956)]; solid lines: calculated spectrum.

UNCLASSIFIED  
ORNL-LR-DWG 70418

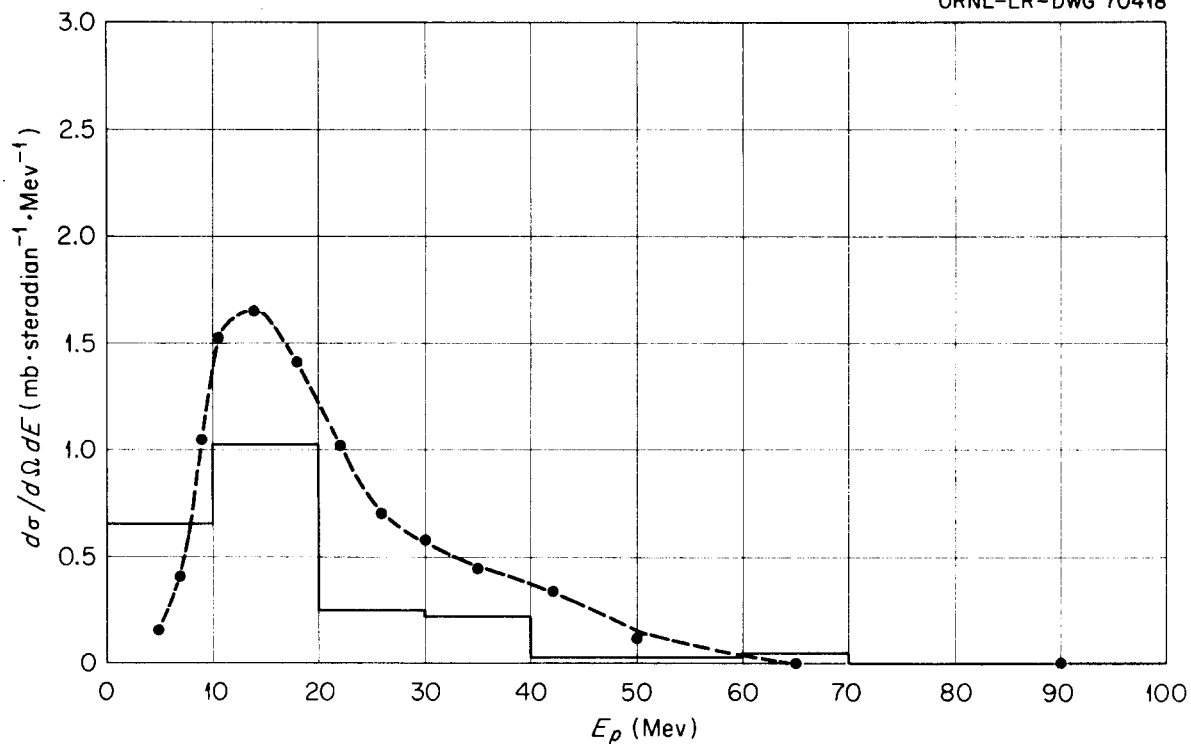


Figure 32. Proton Spectra from  $100^\circ$  to  $180^\circ$  for 190-Mev Protons on Gold. Dashed curve: experimental results of Bailey [L. E. Bailey, Angle and Energy Distributions of Charged Particles from the High Energy Nuclear Bombardment of Various Elements, University of California Radiation Laboratory Report UCRL-3334 (March 1, 1956)]; solid lines: calculated spectrum.

UNCLASSIFIED  
ORNL-LR-DWG 70445

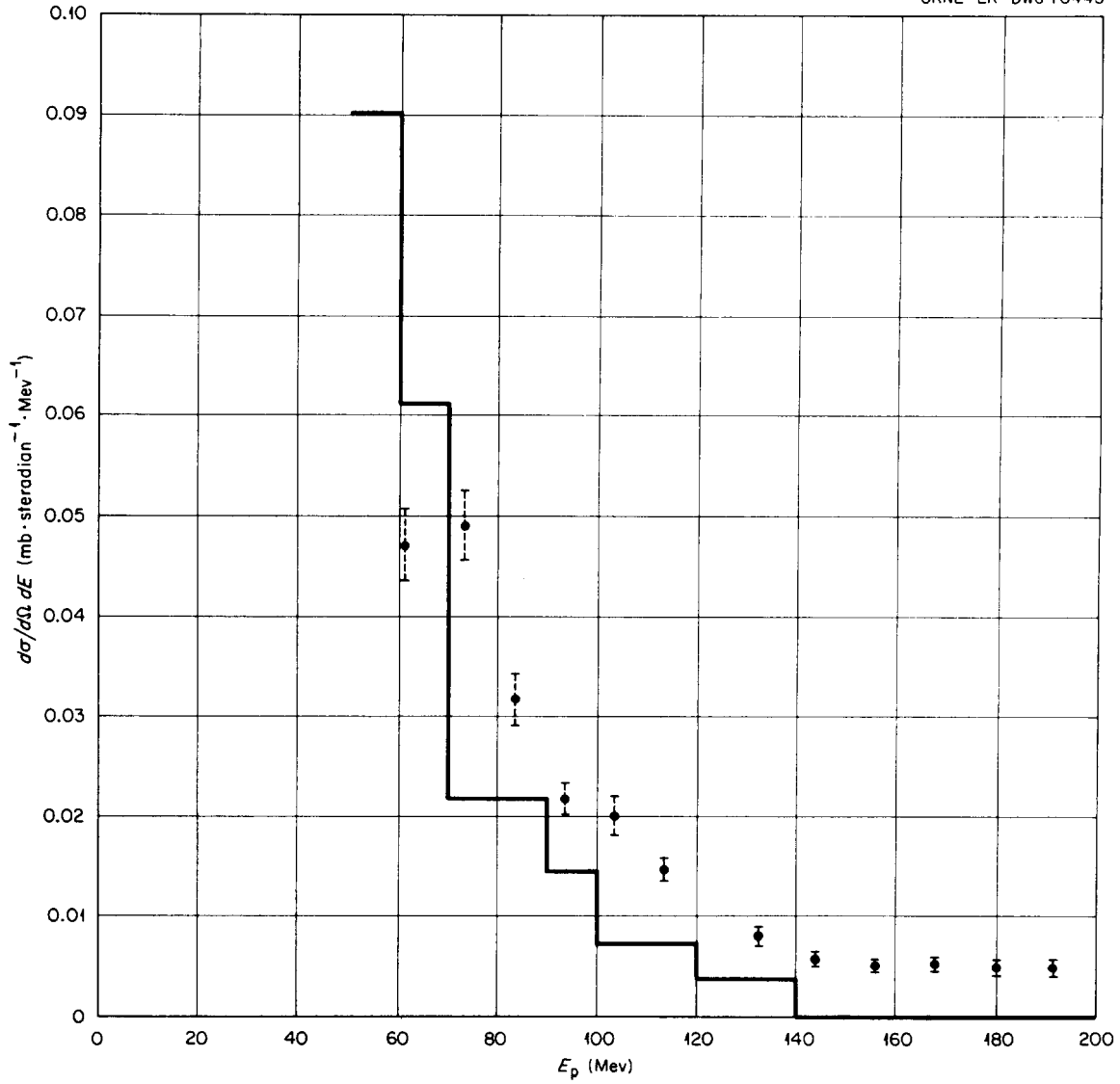


Figure 33. Proton Spectra at  $90^\circ$  from 240-Mev Protons on Carbon. Points: experimental values of Temmer [G. M. Temmer, Phys. Rev. 83, 1067 (1951)]; solid curve: calculated spectrum for protons emitted in the angular interval  $70^\circ$  to  $110^\circ$ .

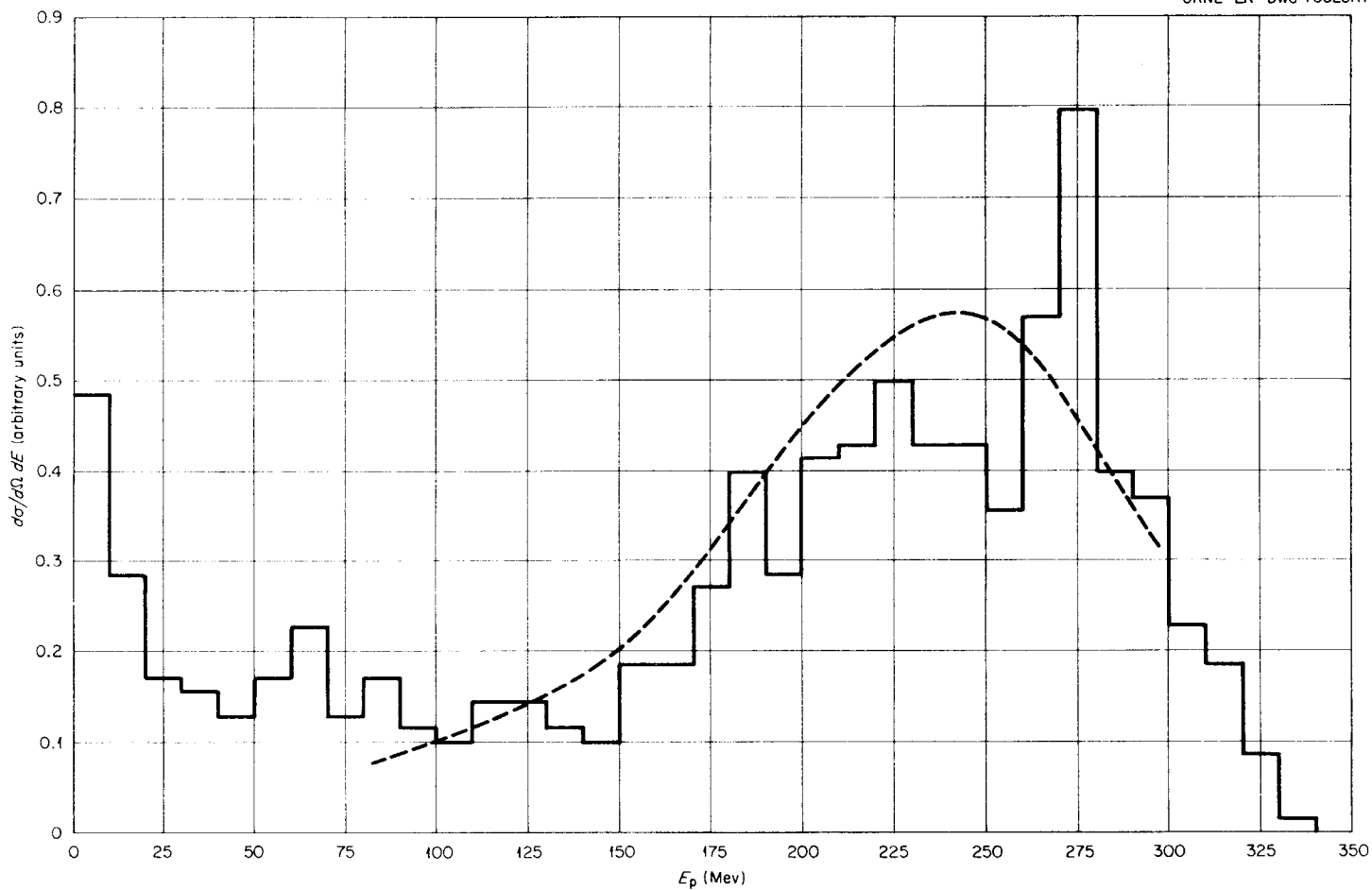


Figure 34. Proton Spectra at  $30^\circ$  from 340-Mev Protons on Carbon. Dashed curve: experimental spectrum of Cladis *et al.* [J. B. Cladis, W. N. Hess, and B. J. Moyer, *Phys. Rev.* 87, 425 (1952)]; solid lines: calculated spectrum of protons emitted in the angular interval  $20^\circ$  to  $40^\circ$ . The units of the ordinate scale are arbitrary.

UNCLASSIFIED  
ORNL-LR-DWG 70324

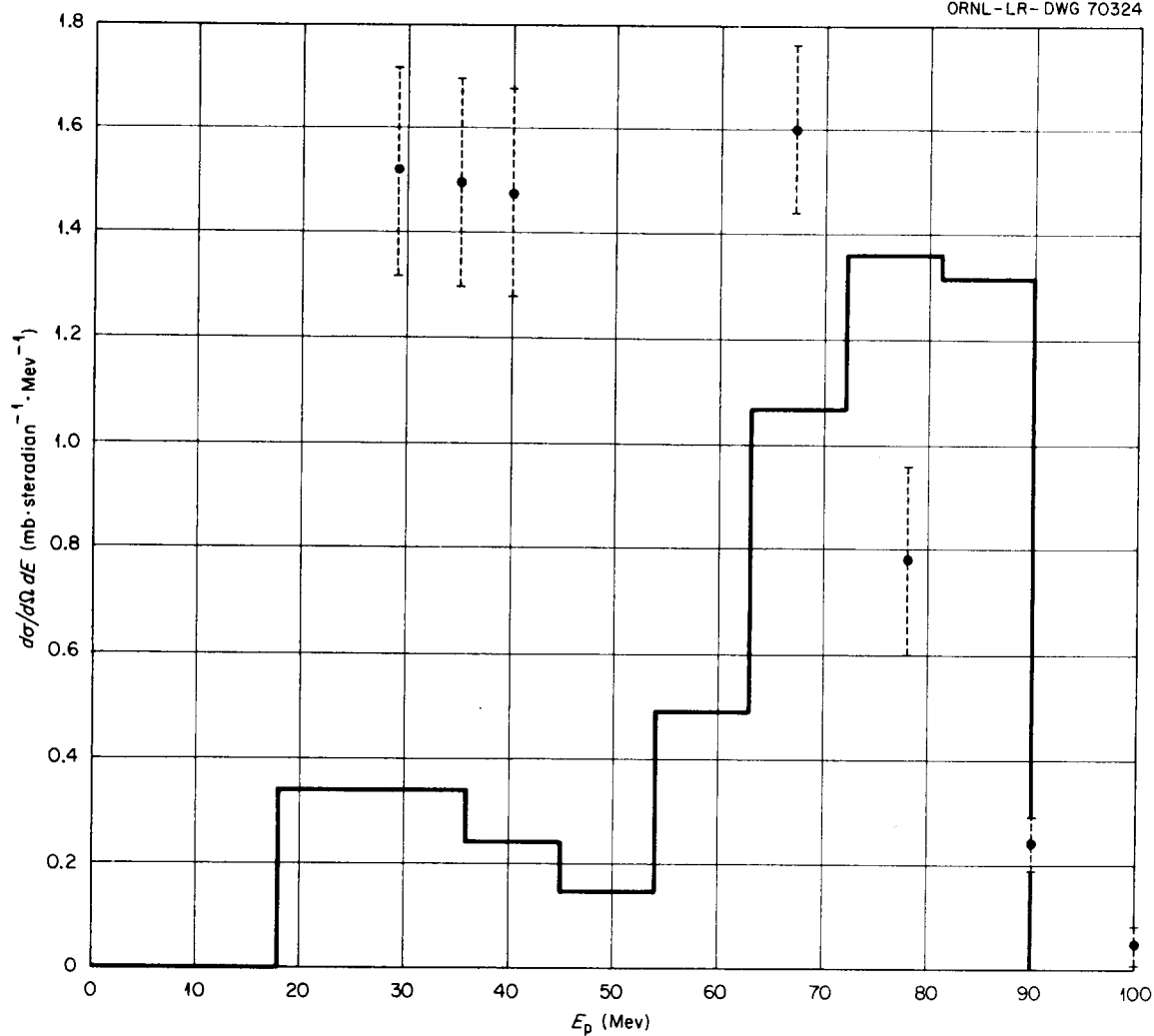


Figure 35. Proton Spectra at  $0^\circ$  for Protons with Energies Greater than 20 Mev from 90-Mev Neutrons on Carbon. Points: experimental results of Hadley and York [J. Hadley and H. York, Phys. Rev. 80, 345 (1950)]; solid lines: calculated spectrum of protons emitted in the angular interval from  $0^\circ$  to  $25^\circ$ .

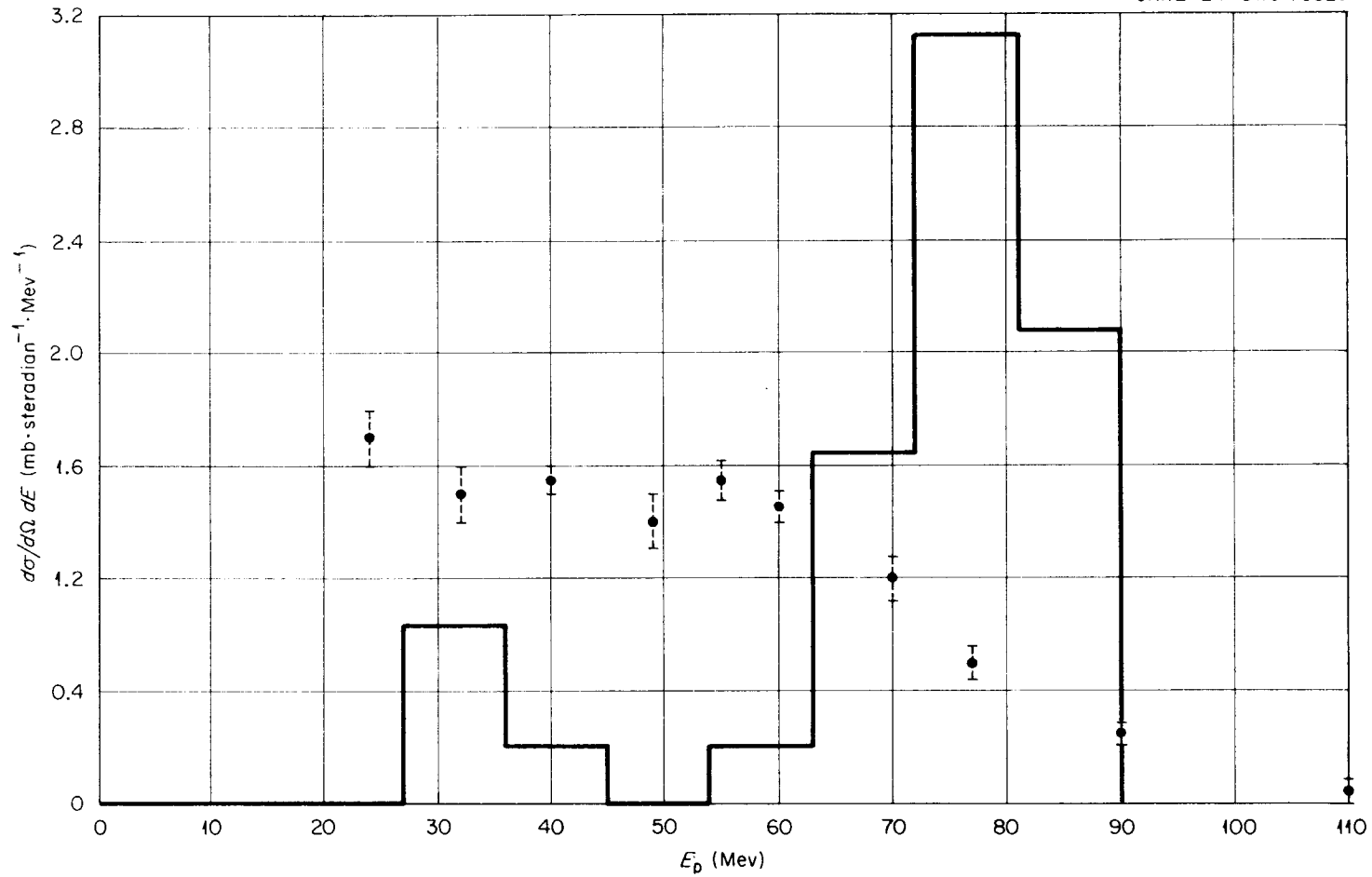


Figure 36. Proton Spectra at  $12^\circ$  for Protons with Energies Greater than 20 Mev from 90-Mev Neutrons on Carbon. Points: experimental results of Hadley and York [J. Hadley and H. York, Phys. Rev. 80, 345 (1950)]; solid lines: calculated spectrum of protons emitted in the angular interval from  $9^\circ$  to  $15^\circ$ .

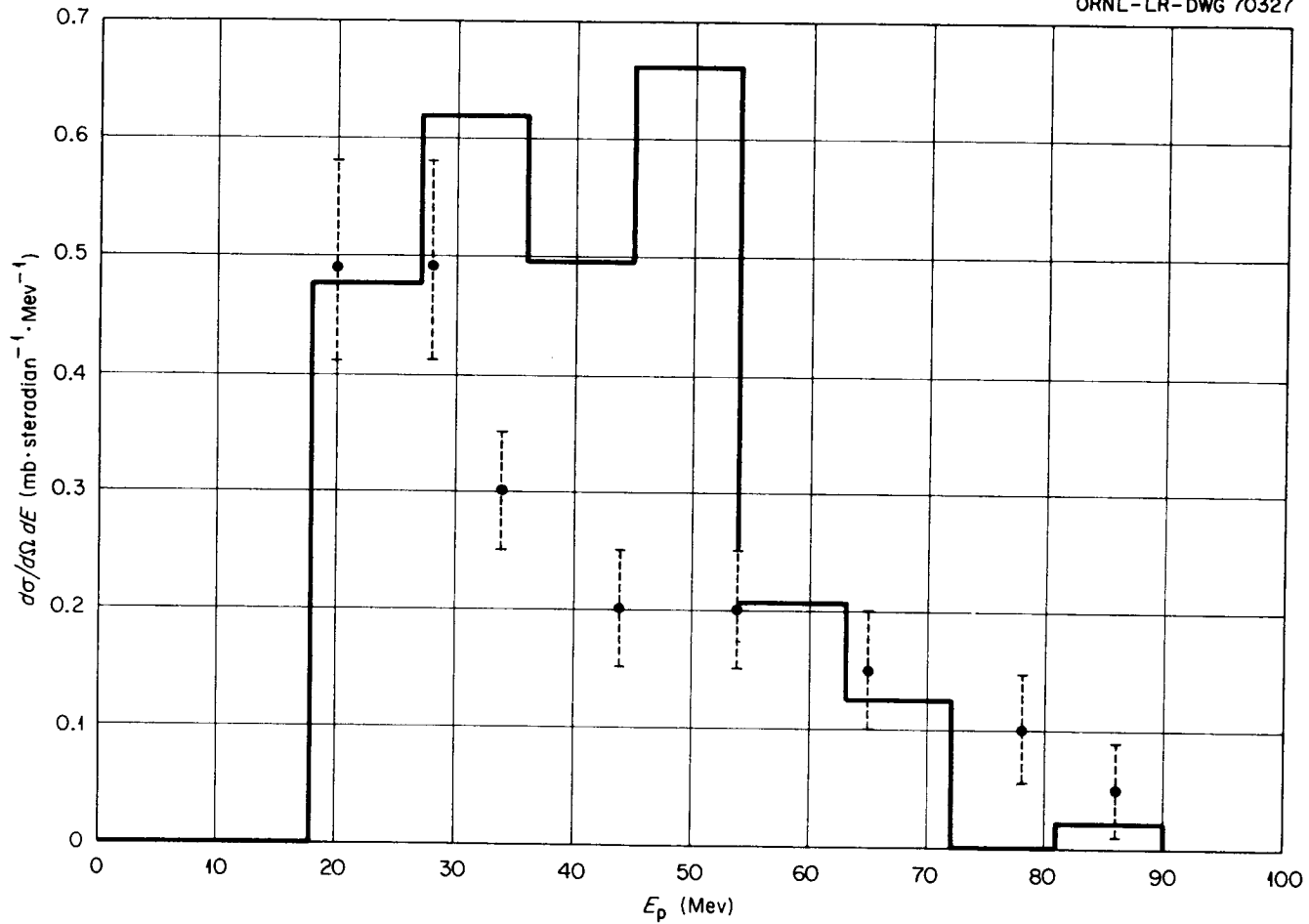


Figure 37. Proton Spectra at  $45^\circ$  for Protons with Energies Greater than 20 Mev from 90-Mev Neutrons on Carbon. Points: experimental results of Hadley and York (J. Hadley and H. York, Phys. Rev. 80, 345 (1950)]; solid lines: calculated spectrum of protons emitted in the angular interval from  $36^\circ$  to  $54^\circ$ .

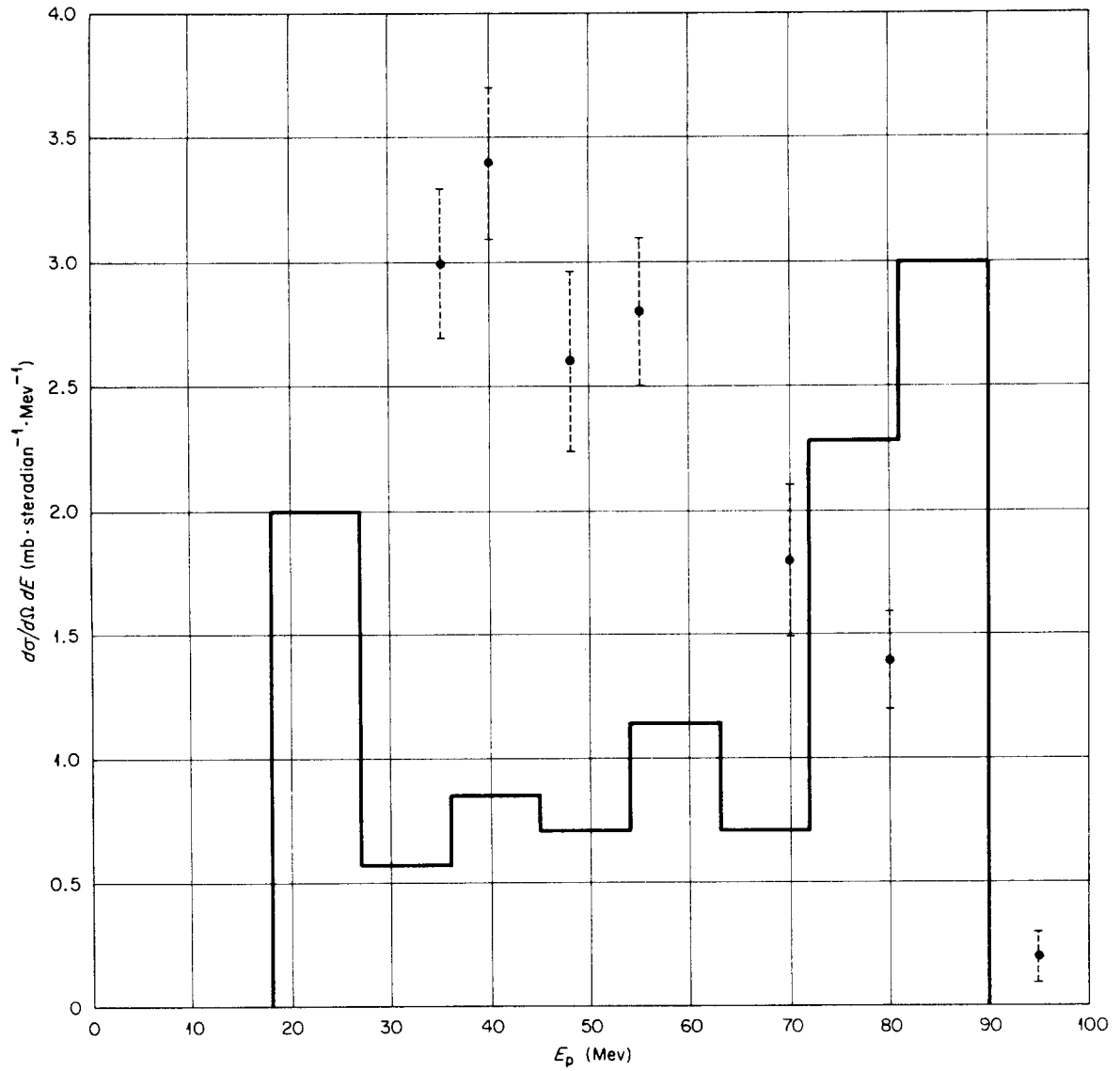


Figure 38. Proton Spectra at  $0^\circ$  for Protons with Energies Greater than 20 Mev from 90-Mev Neutrons on Copper. Points: experimental results of Hadley and York [J. Hadley and H. York, Phys. Rev. 80, 345 (1950)]; solid lines: calculated spectrum of protons emitted in the angular interval from  $0^\circ$  to  $20^\circ$ .

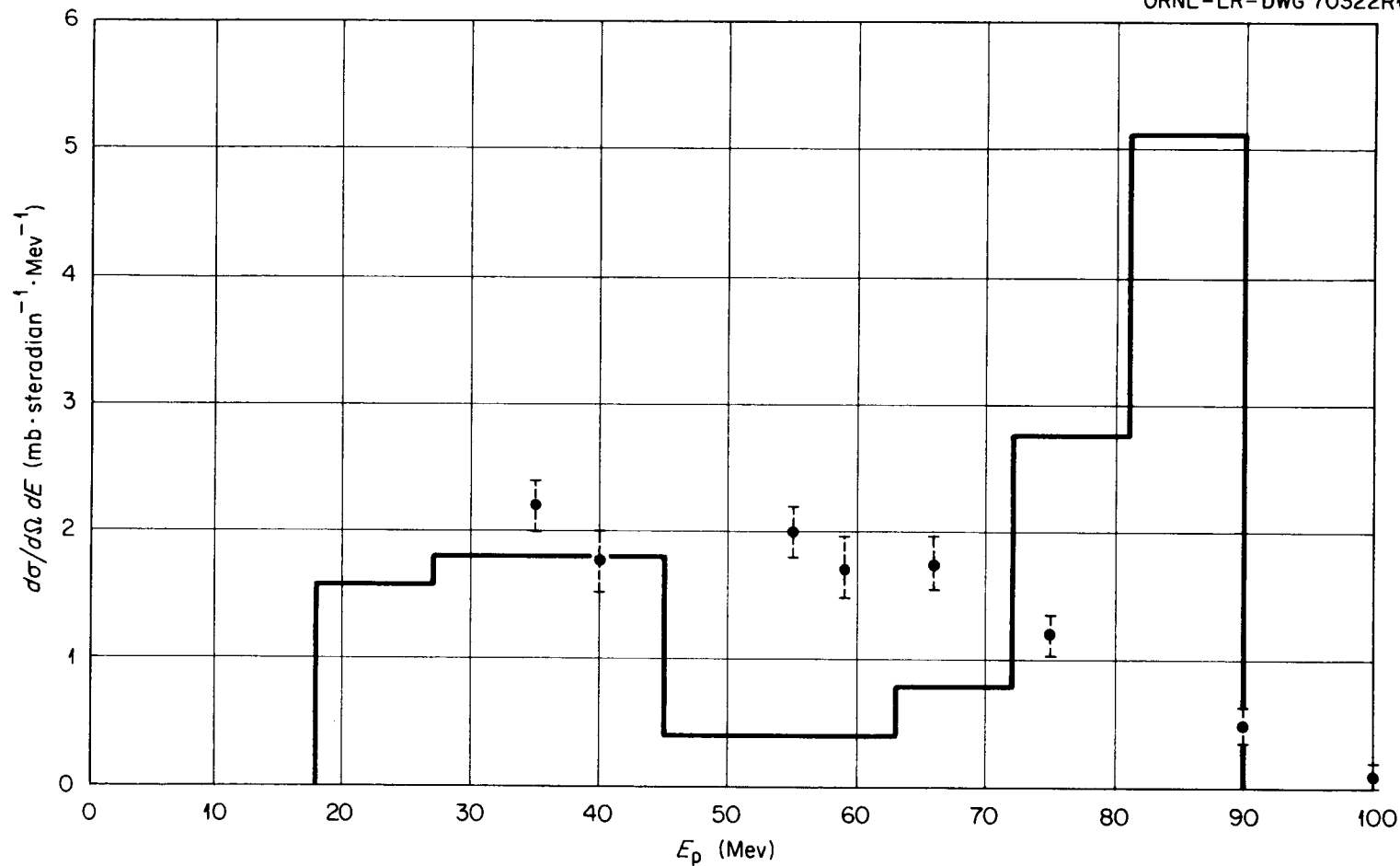


Figure 39. Proton Spectra at  $12^\circ$  for Protons with Energies Greater than 20 Mev from 90-Mev Neutrons on Copper. Points: experimental results of Hadley and York [J. Hadley and H. York, Phys. Rev. 80, 345 (1950)]; solid lines: calculated spectrum of protons emitted in the angular interval from  $9^\circ$  to  $15^\circ$ .

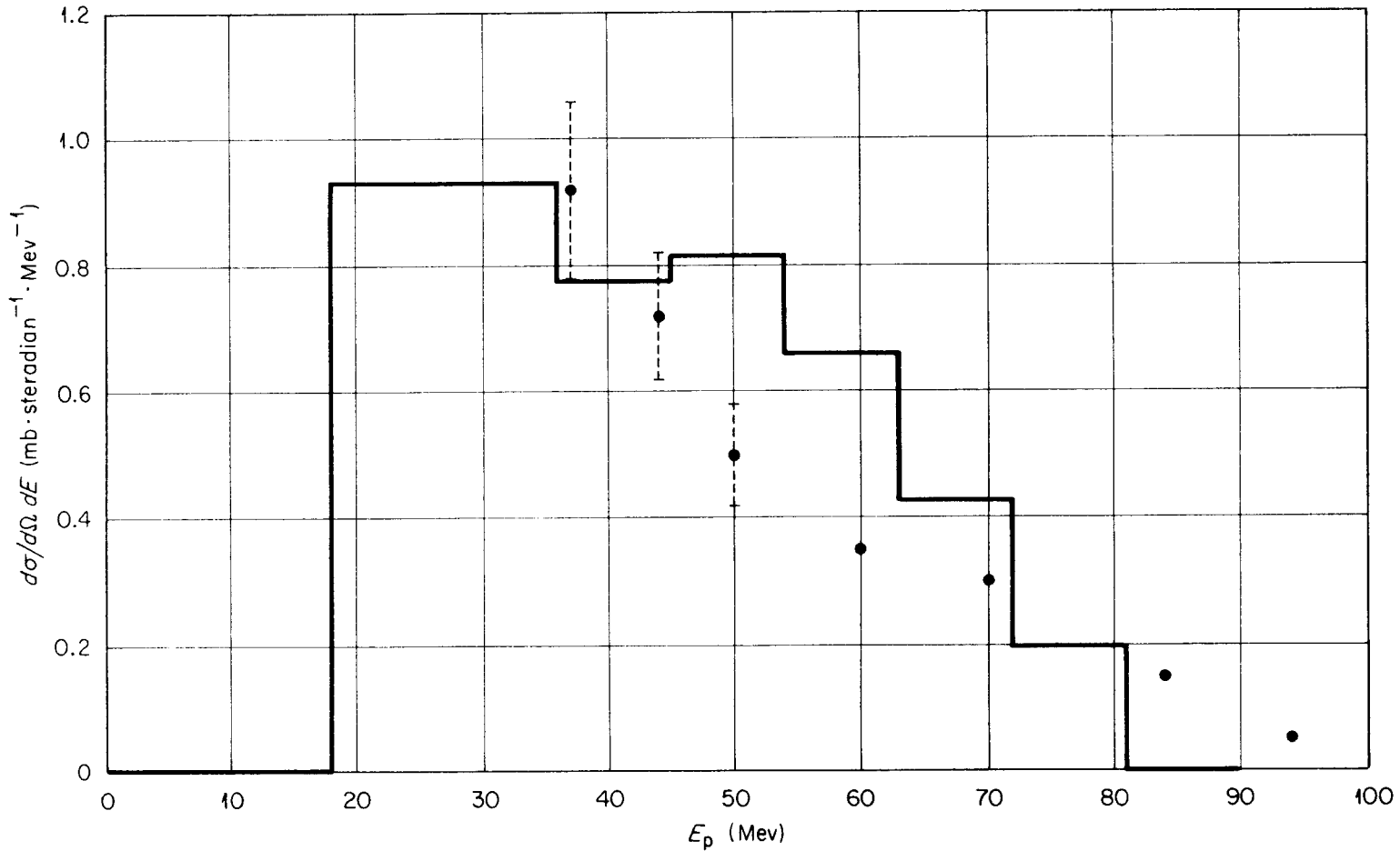


Figure 40. Proton Spectra at  $45^\circ$  for Protons with Energies Greater than 20 Mev from 90-Mev Neutrons on Copper. Points: experimental results of Hadley and York [J. Hadley and H. York, Phys. Rev. 80, 345 (1950)]; solid lines: calculated spectrum of protons emitted in the angular interval from  $36^\circ$  to  $54^\circ$ .

UNCLASSIFIED  
ORNL-LR-DWG 70318

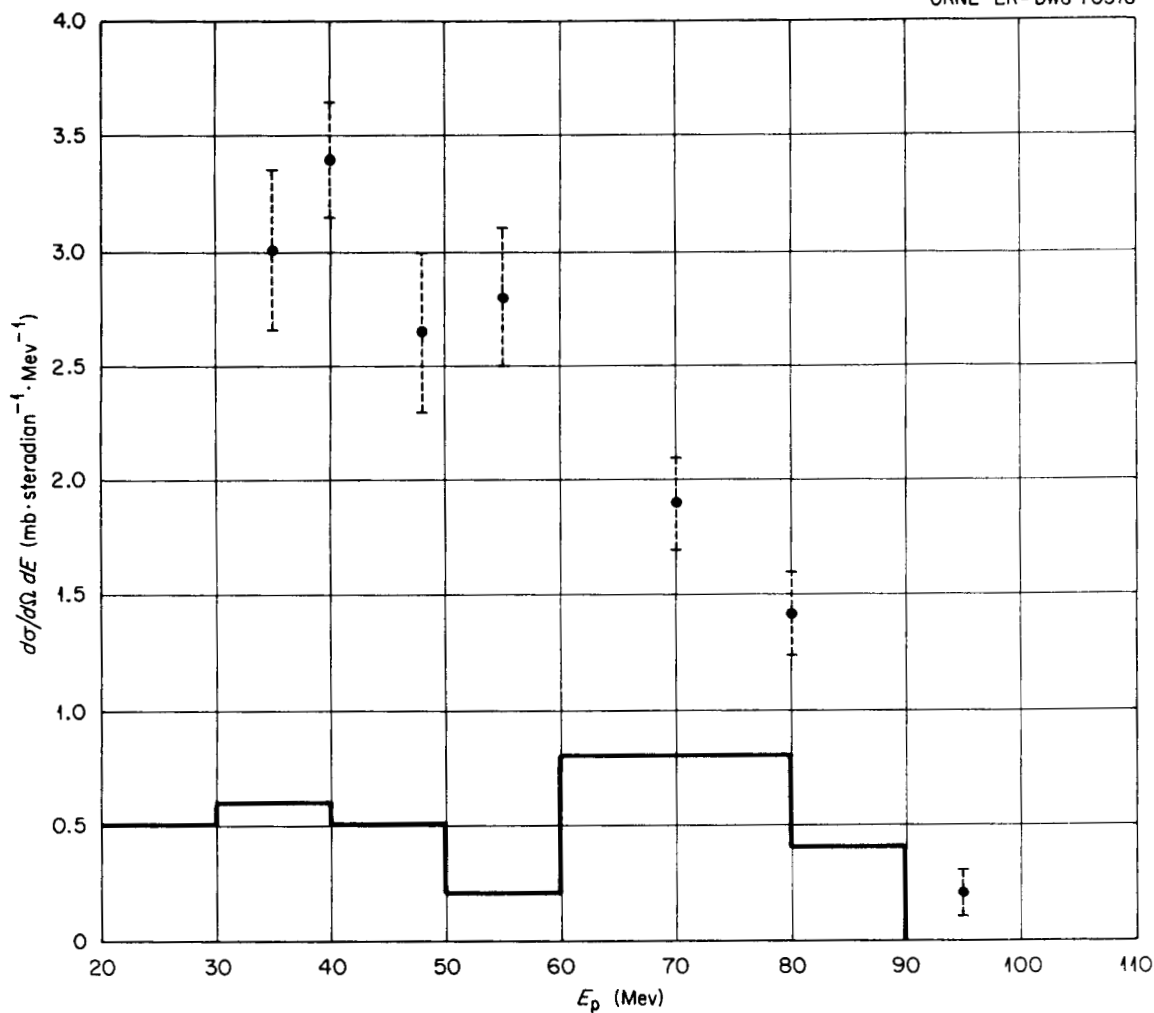


Figure 41. Proton Spectrum for a Uniform Nuclear Density Distribution. Solid lines: calculated spectrum of protons emitted in the angular interval  $0^{\circ}$  to  $15^{\circ}$ ; points: experimental values of Hadley and York [J. Hadley and H. York, Phys. Rev. 80, 345 (1950)]; for protons emitted at  $0^{\circ}$ . The case is 90-Mev neutrons on copper.

UNCLASSIFIED  
ORNL-LR-DWG 70320

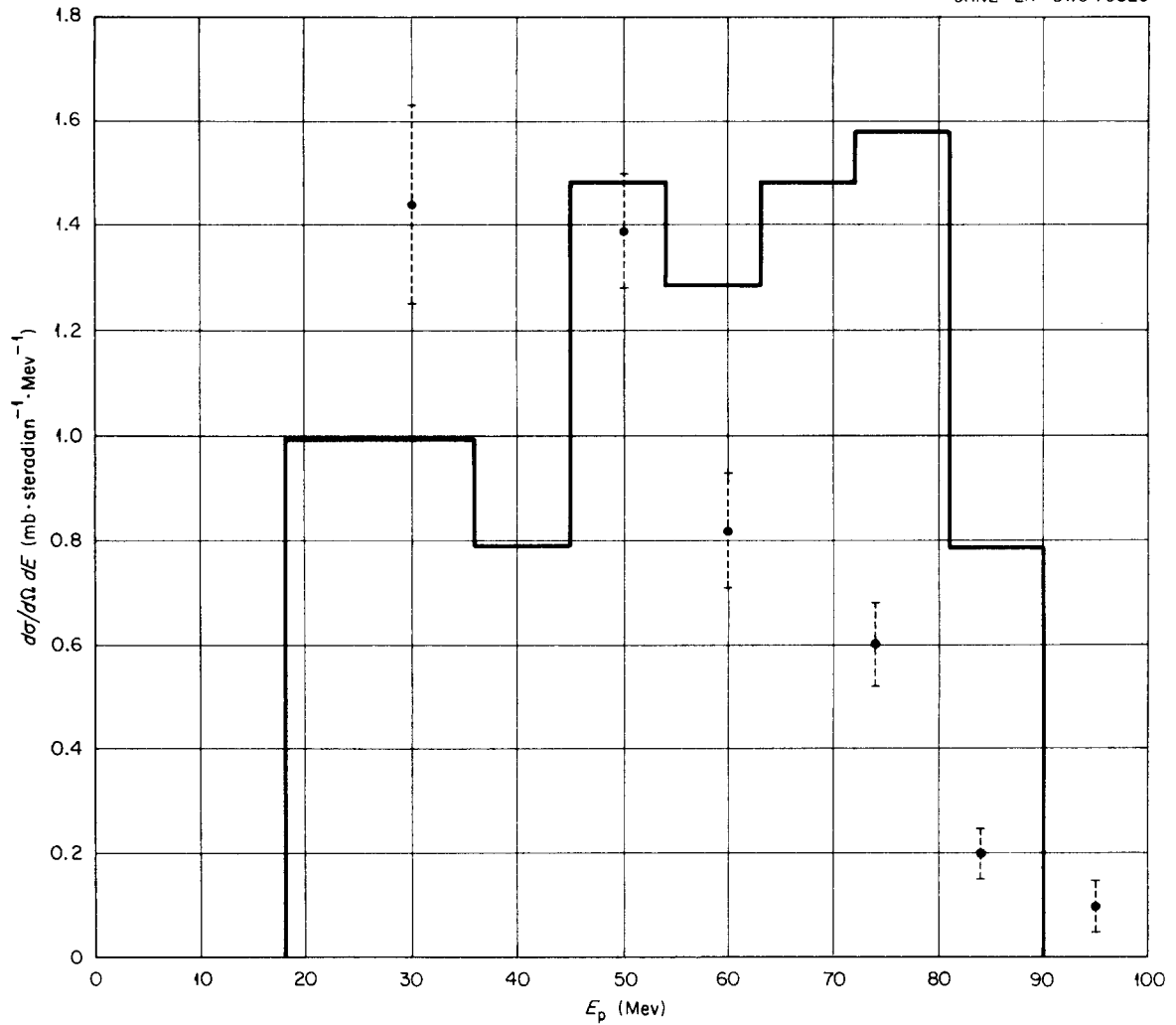


Figure 42. Proton Spectra at  $25^\circ$  for Protons with Energies Greater than 20 Mev from 90-Mev Neutrons on Lead. Points: experimental results of Hadley and York [J. Hadley and H. York, Phys. Rev. 80, 345 (1950)]; solid lines: calculated spectrum of protons emitted in the angular interval from  $15^\circ$  to  $35^\circ$ .

UNCLASSIFIED  
ORNL-LR-DWG 70319

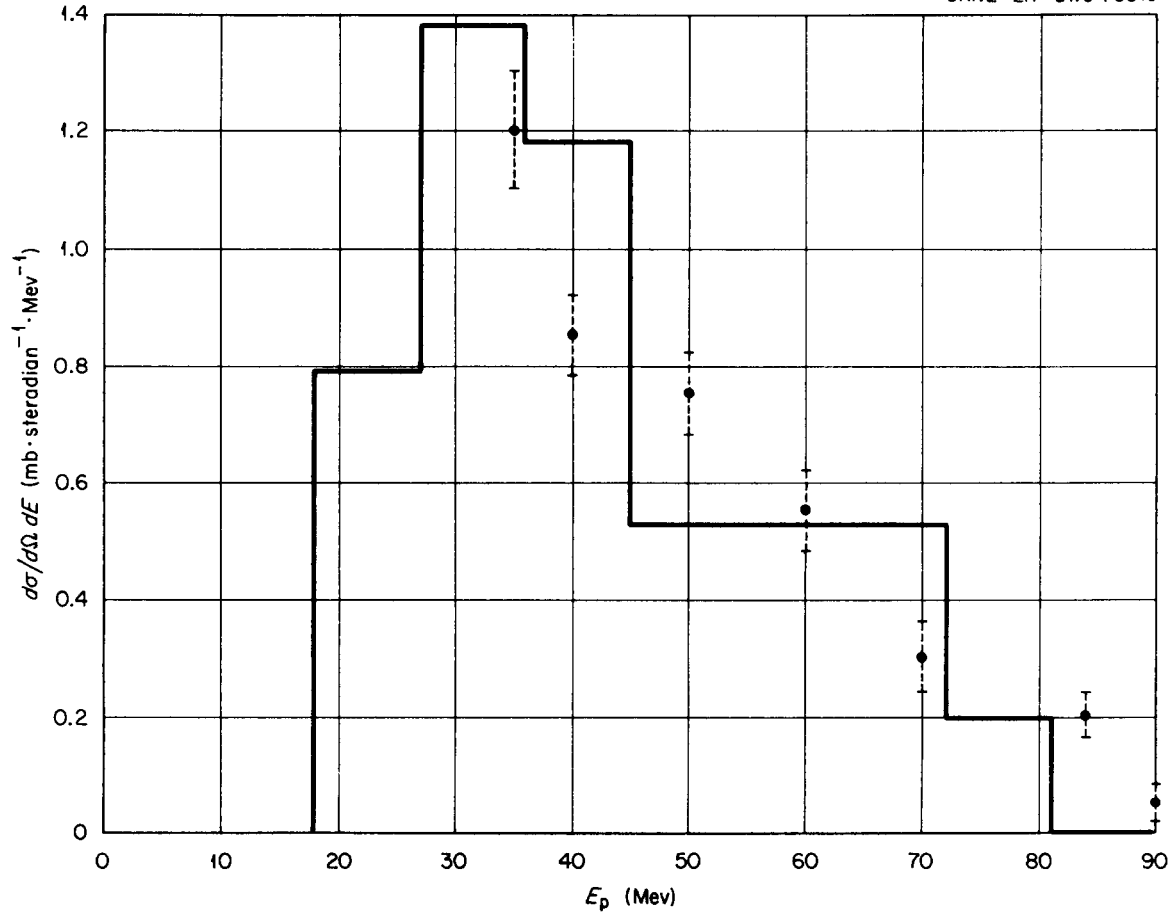


Figure 43. Proton Spectra at  $45^\circ$  for Protons with Energies Greater than 20 Mev from 90-Mev Neutrons on Lead. Points: experimental results of Hadley and York [J. Hadley and H. York, Phys. Rev. 80, 345 (1950)]; solid lines: calculated spectrum of protons emitted in the angular interval from  $36^\circ$  to  $54^\circ$ .

UNCLASSIFIED  
ORNL-LR-DWG 70186

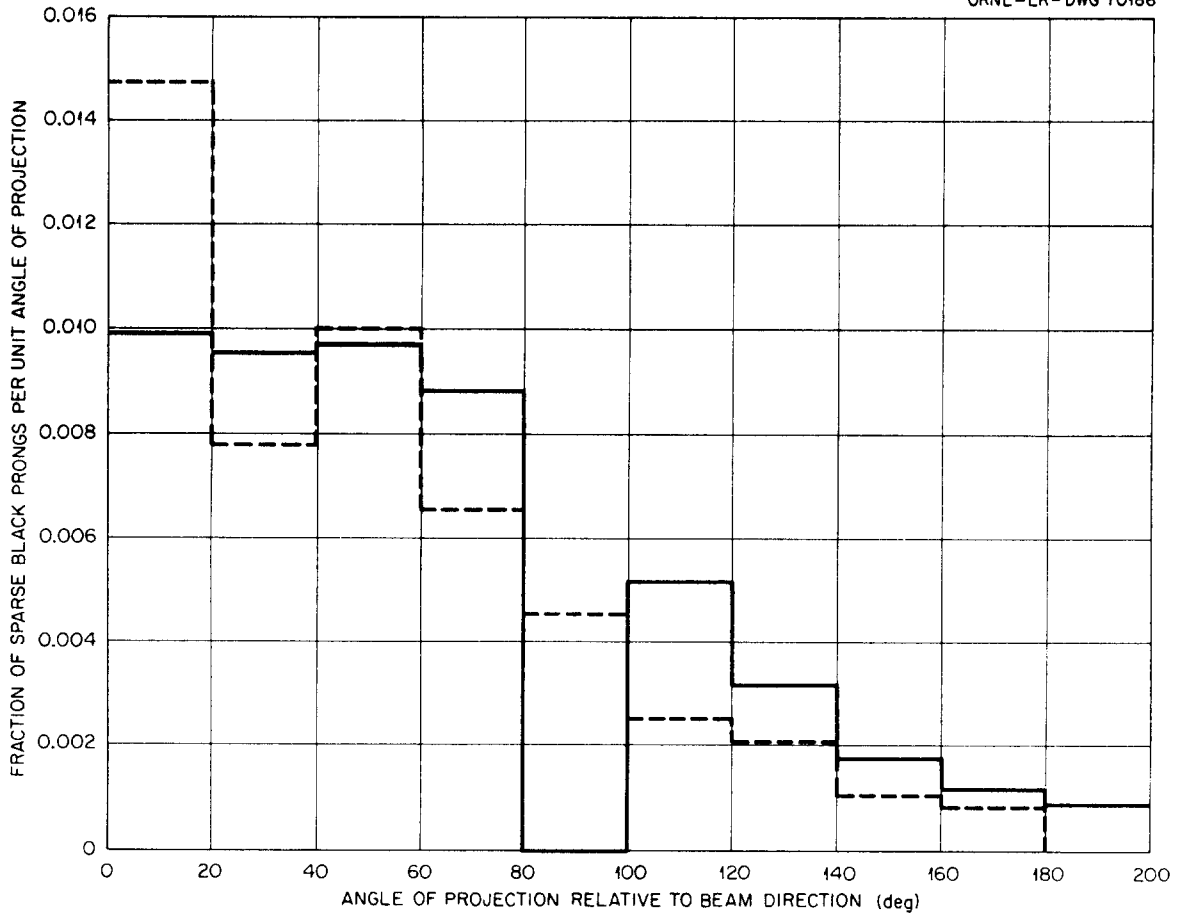


Figure 44. Angular Distribution of Sparse Black Prongs from 375-Mev Protons on Heavy Emulsion Nuclei. Dashed lines: experimental results of Bernardini et al. [G. Bernardini, E. T. Booth, and S. J. Lindenbaum, Phys. Rev. 85, 826 (1952)]; solid lines: calculated distribution for protons emitted with energies from 30 to 100 Mev for 375-Mev protons on Ru<sup>100</sup>.

Page 101: Note: The solid line between 100 and 200 deg should be shifted to the left so that it represents the region between 80 and 180 deg. That is, the dip to zero between 80 and 100 deg is non-existent.

UNCLASSIFIED  
ORNL-LR-DWG 70187

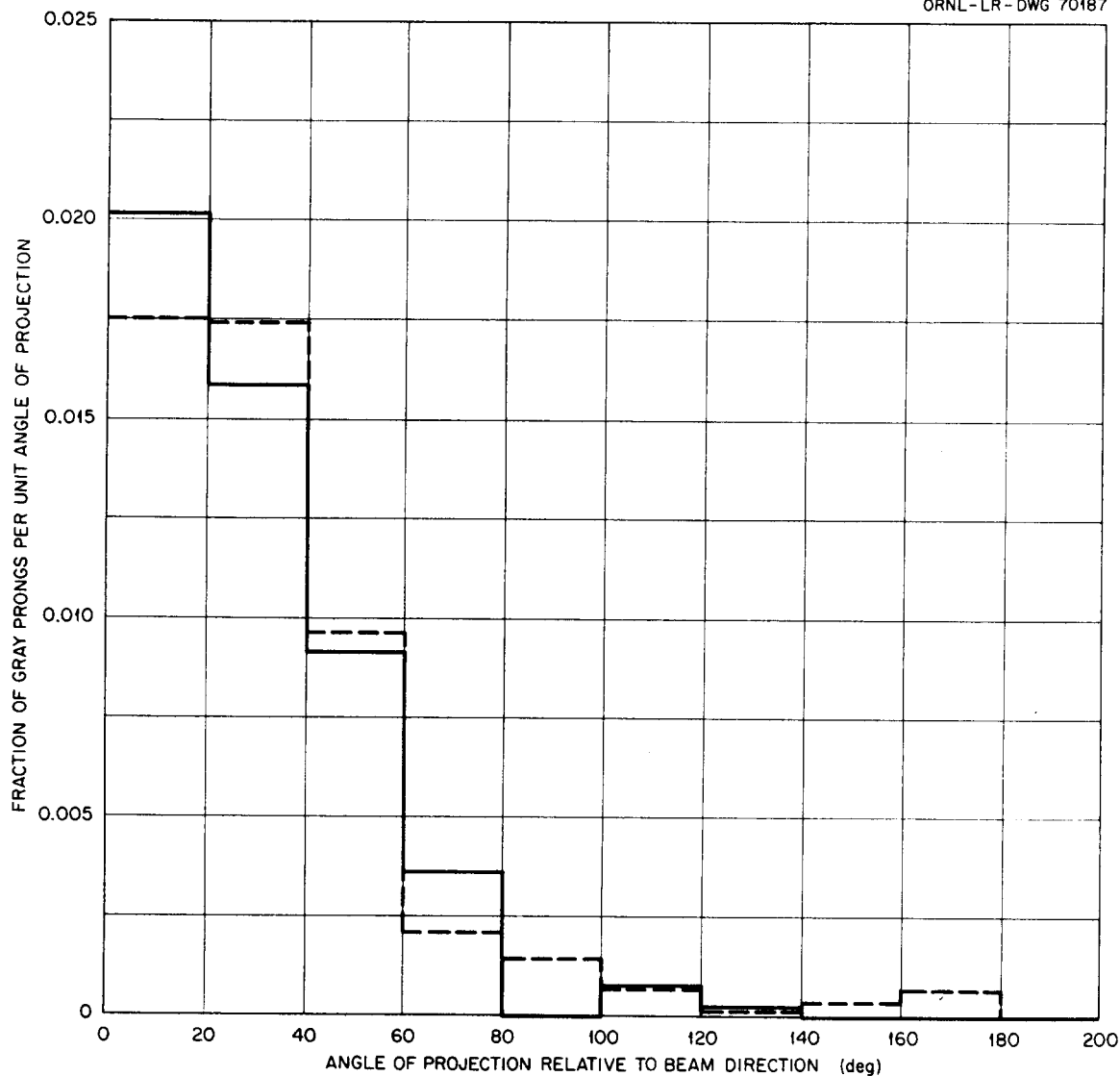


Figure 45. Angular Distribution of Gray Prongs from 375-Mev Protons on Heavy Emulsion Nuclei. Dashed lines: experimental results of Bernardini et al. [G. Bernardini, E. T. Booth, and S. J. Lindenbaum, Phys. Rev. 85, 826 (1952)]; solid lines: calculated distribution for protons emitted with energies from 100 to 375 Mev for 375-Mev protons on Ru<sup>100</sup>.

Page 102: Note: The solid line between 100 and 200 deg should be shifted to the left so that it represents the region between 80 and 180 deg. That is, the dip to zero between 80 and 100 deg is non-existent.

UNCLASSIFIED  
ORNL-LR-DWG 70421

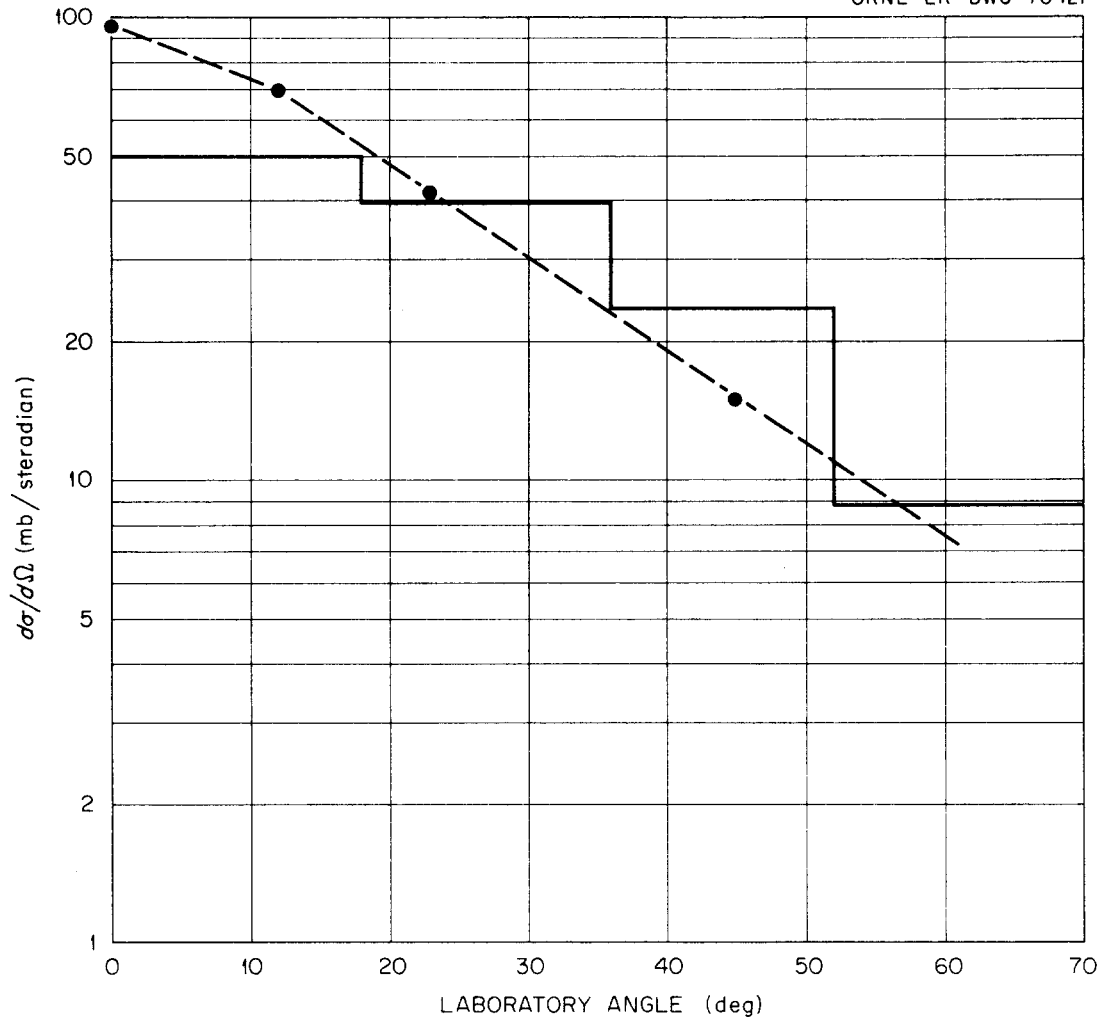


Figure 46. Angular Distribution of Protons with Energies Greater than 20 Mev from 90-Mev Neutrons on Carbon. Dashed curve: experimental results of Hadley and York [J. Hadley and H. York, Phys. Rev. 80, 345 (1950)]; solid lines: calculated distribution.

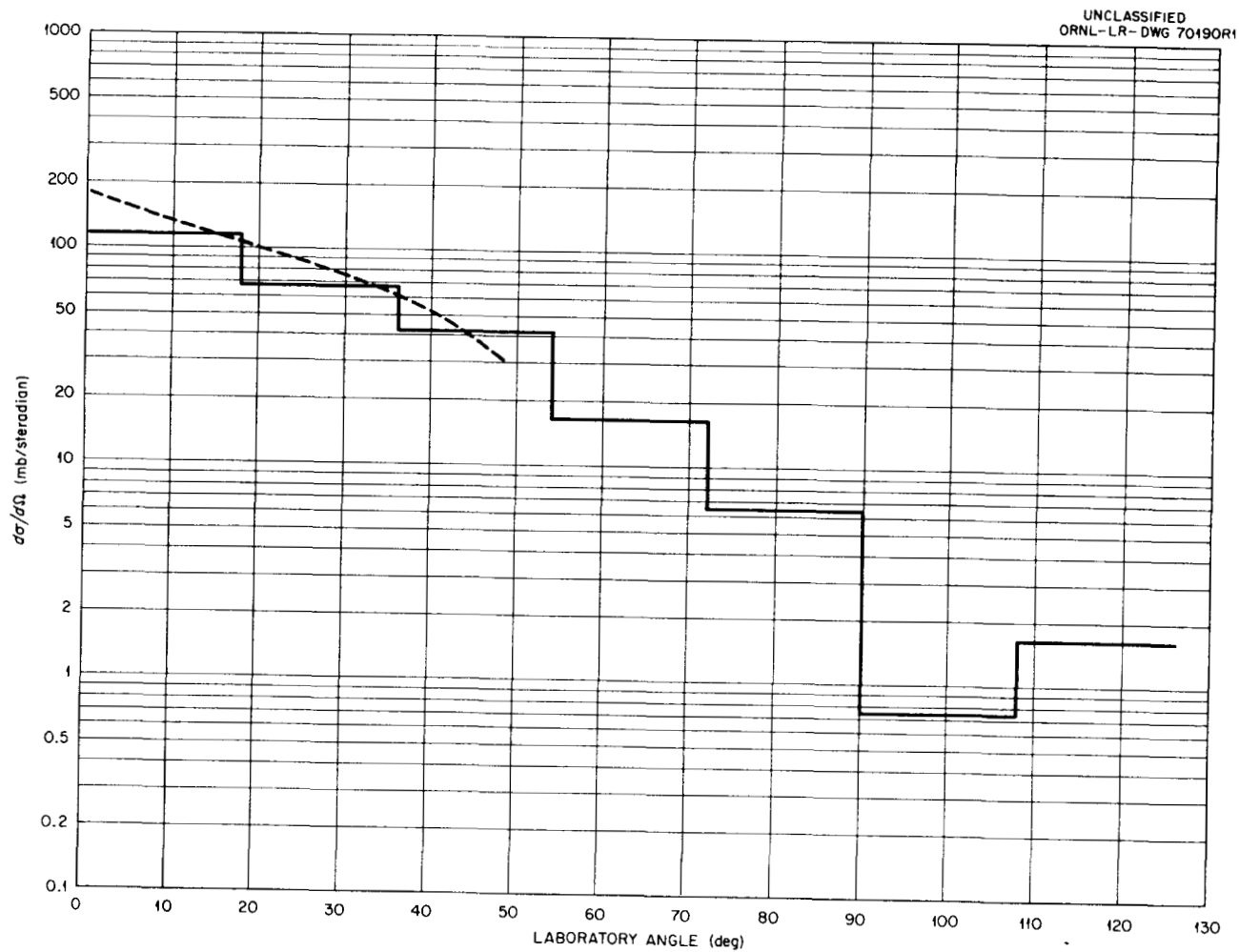


Figure 47. Angular Distribution of Protons with Energies Greater than 20 Mev from 90-Mev Neutrons on Copper. Dashed curve: experimental results of Hadley and York [J. Hadley and H. York, Phys. Rev. 80, 345 (1950)]; solid lines: calculated distribution.

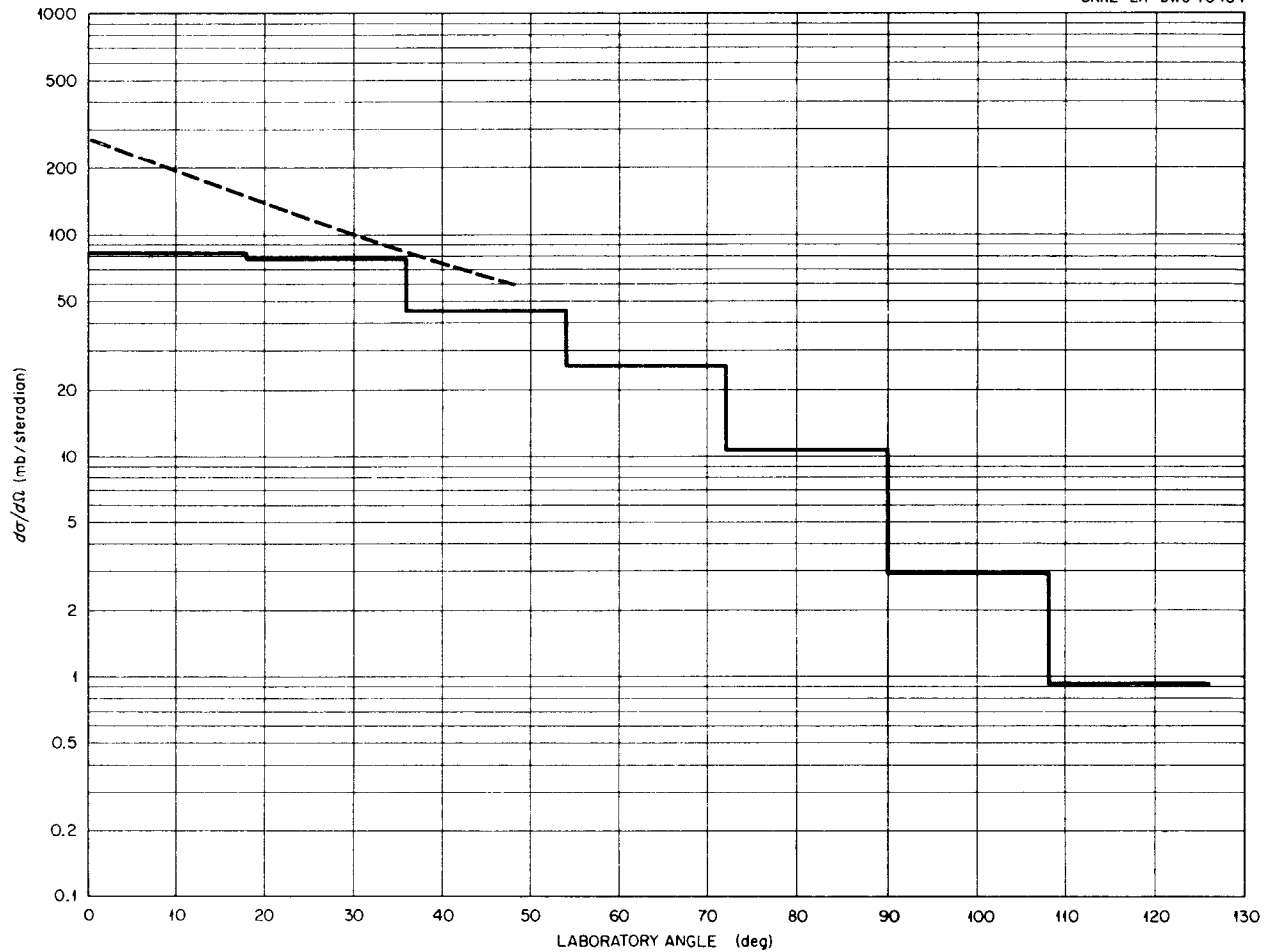


Figure 48. Angular Distribution of Protons with Energies Greater than 20 Mev from 90-Mev Neutrons on Lead. Dashed curve: experimental results of Hadley and York [J. Hadley and H. York, Phys. Rev. 80, 345 (1950)]; solid lines: calculated distribution.

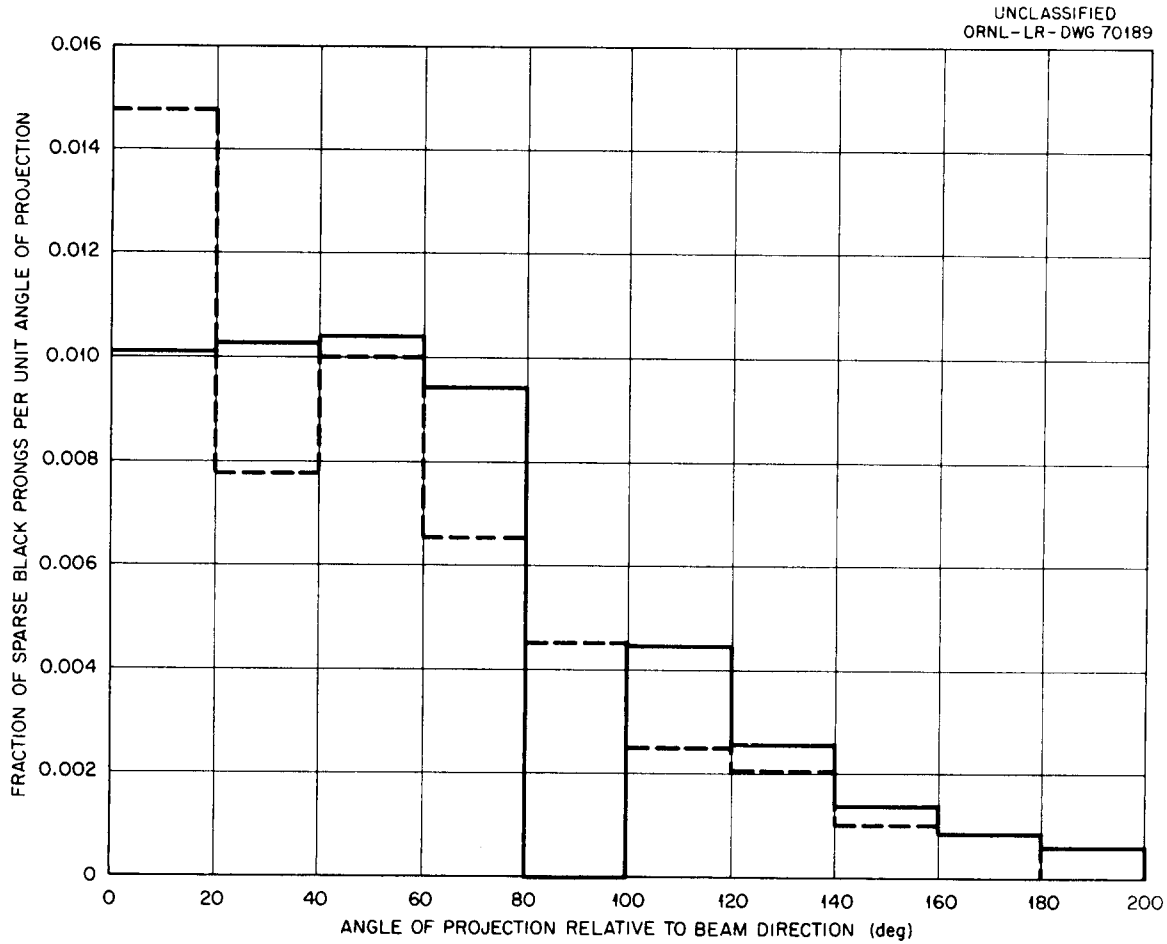


Figure 49. Angular Distribution of Sparse Black Prongs from 300-Mev Neutrons on Heavy Emulsion Nuclei. Dashed lines: experimental results of Bernardini et al. [G. Bernardini, E. T. Booth, and S. J. Lindenbaum, Phys. Rev. 85, 826 (1952)]; solid lines: calculated distribution for protons emitted with energies from 30 to 100 Mev for 300-Mev neutrons on Ru<sup>100</sup>.

Page 106: Note: The solid line between 100 and 200 deg should be shifted to the left so that it represents the region between 80 and 180 deg. That is, the dip to zero between 80 and 100 deg is non-existent.

UNCLASSIFIED  
ORNL-LR-DWG 70188

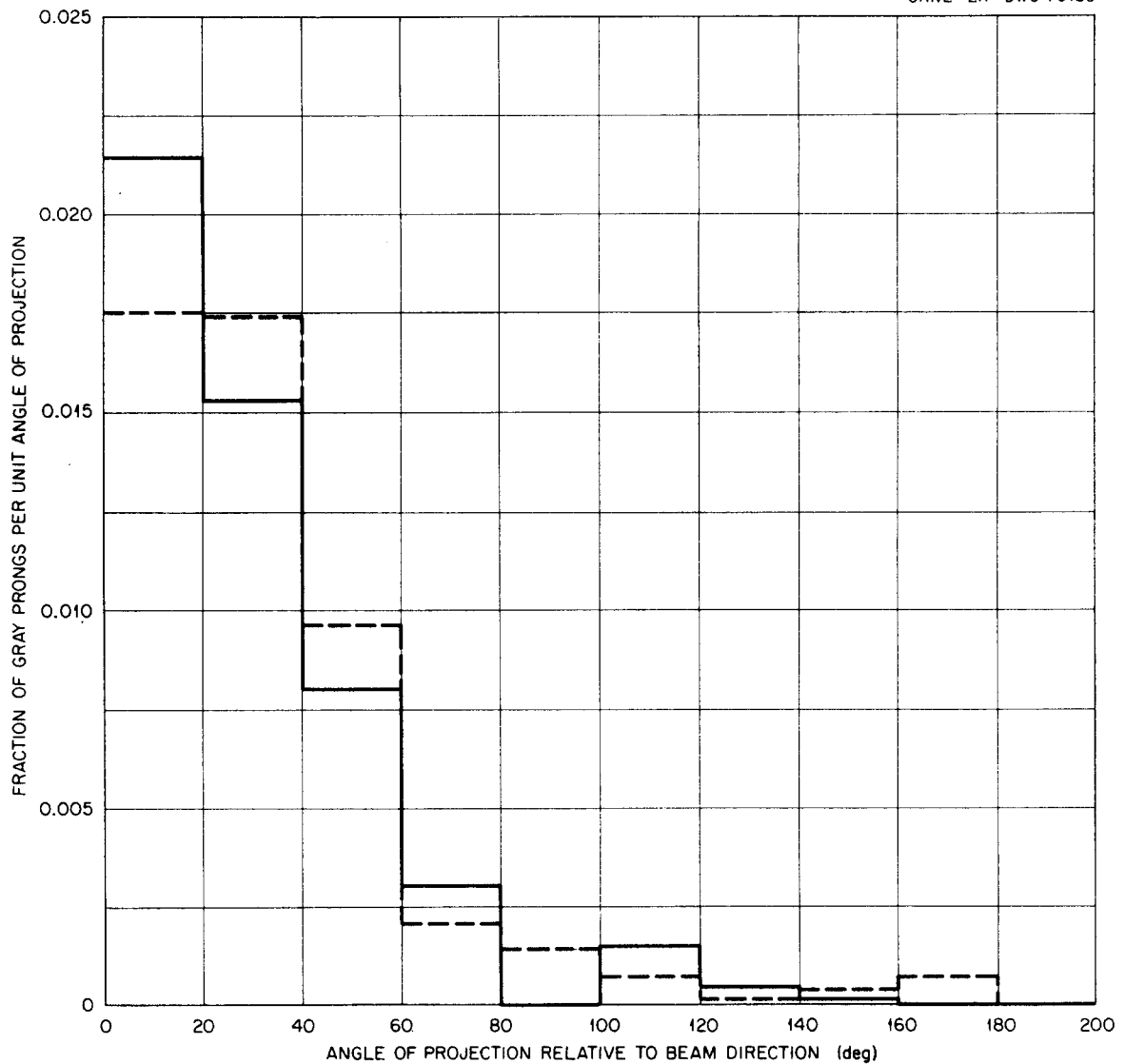


Figure 50. Angular Distribution of Gray Prongs from 300-Mev Neutrons on Heavy Emulsion Nuclei. Dashed lines: experimental results of Bernardini et al. [G. Bernardini, E. T. Booth, and S. J. Lindenbaum, Phys. Rev. 85, 826 (1952)]; solid lines: calculated distribution for protons emitted with energies from 100 to 300 Mev for 300-Mev neutrons on Ru<sup>100</sup>.

Page 107: Note: The solid line between 100 and 200 deg should be shifted to the left so that it represents the region between 80 and 180 deg. That is, the dip to zero between 80 and 100 deg is non-existent.

UNCLASSIFIED  
ORNL-LR-DWG 70423

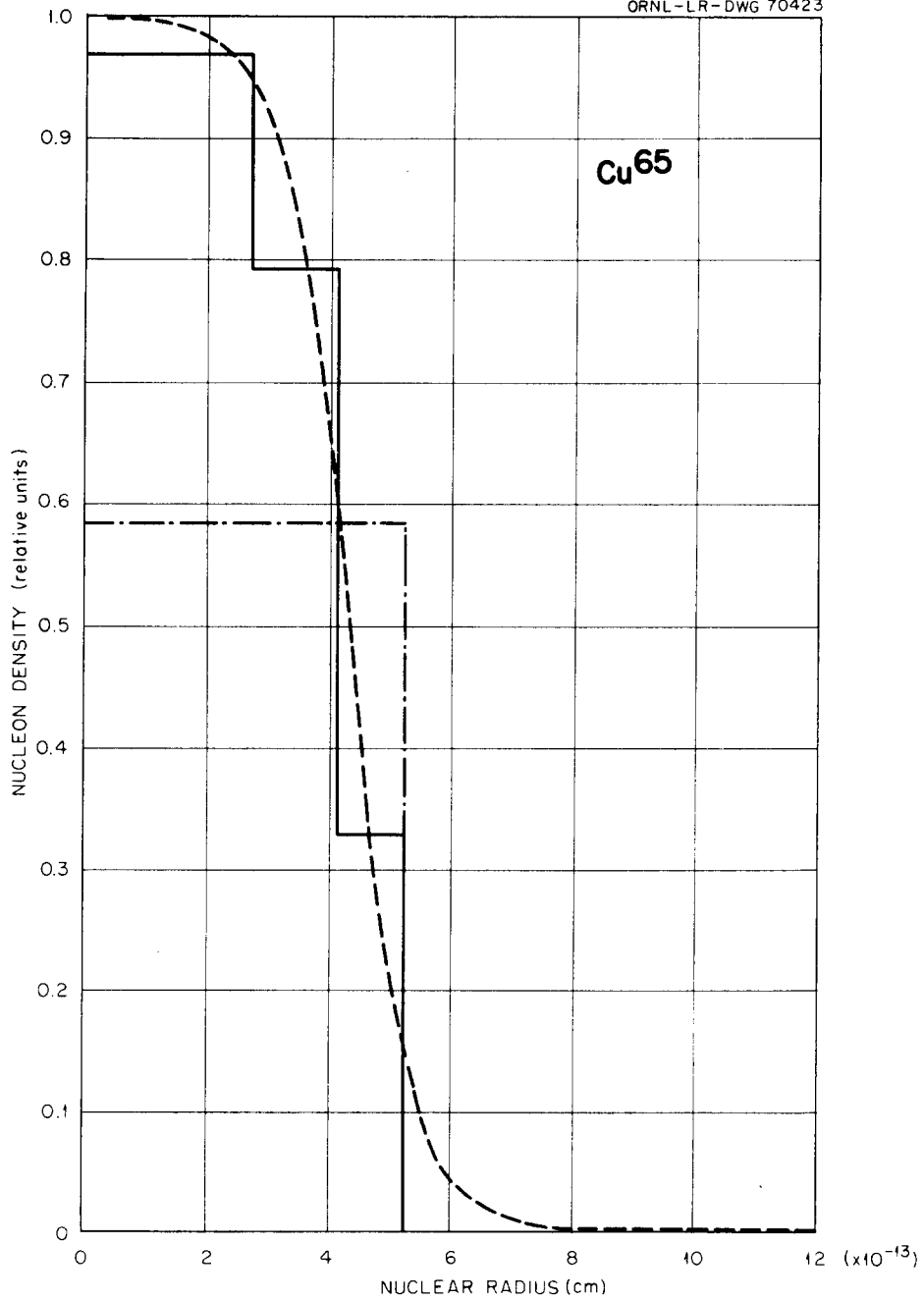


Figure 51. Nucleon Density Distributions Within the Nucleus When the Nuclear Radius Is Assumed To Be Small. Solid lines: nonuniform nucleon density distribution within the nucleus; dash-dotted lines: uniform nucleon density distribution within the nucleus; dashed curve: experimental curve of Hofstadter [R. Hofstadter, Revs. Modern Phys. 28, 214 (1956)].

UNCLASSIFIED  
ORNL-LR-DWG 70424

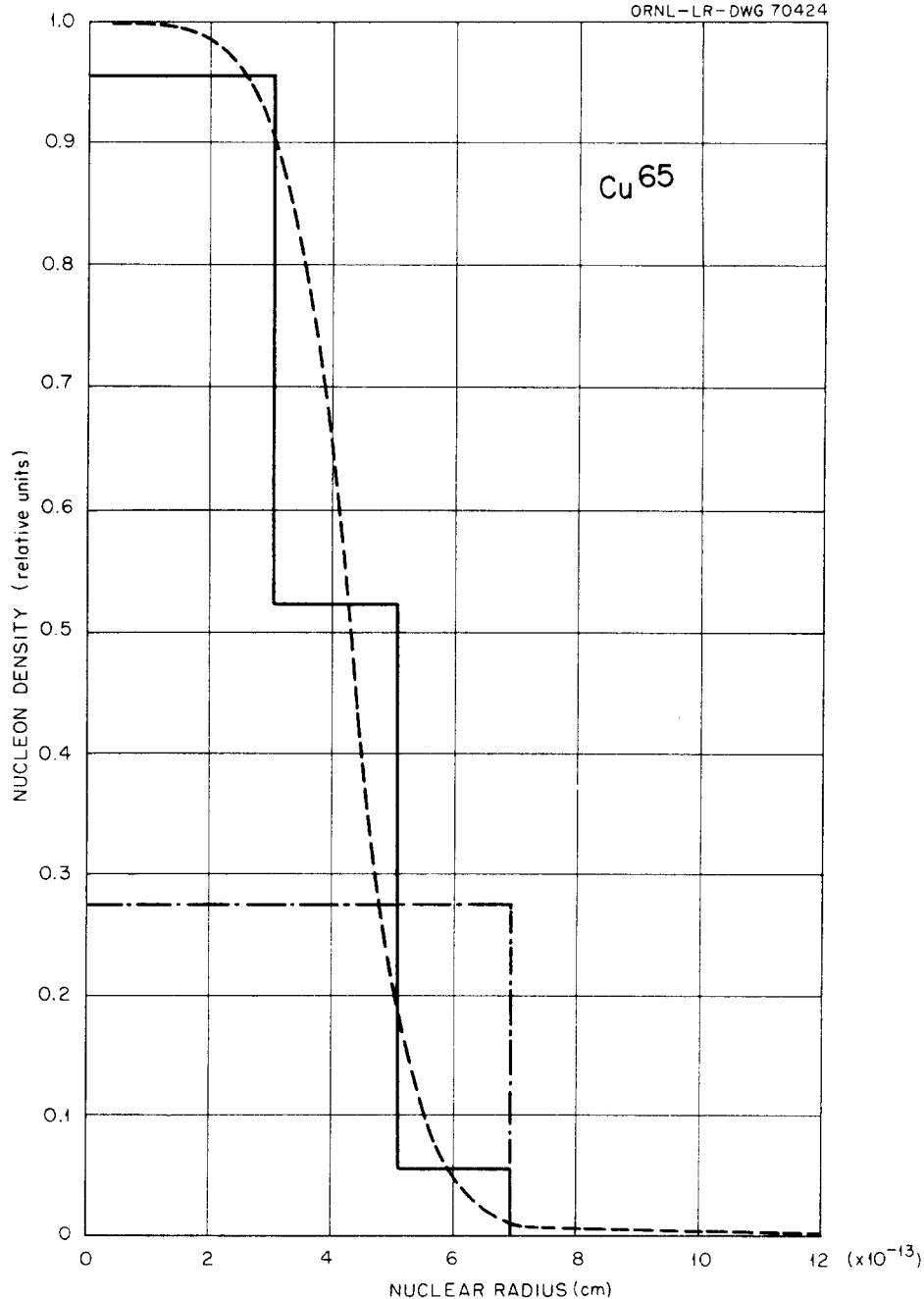


Figure 52. Nucleon Density Distributions Within the Nucleus When the Nuclear Radius Is Assumed To Be Medium. Solid lines: nonuniform nucleon density distribution within the nucleus; dash-dotted lines: uniform nucleon density distribution within the nucleus; dashed curve: experimental curve of Hofstadter [R. Hofstadter, Revs. Modern Phys. 28, 214 (1956)].

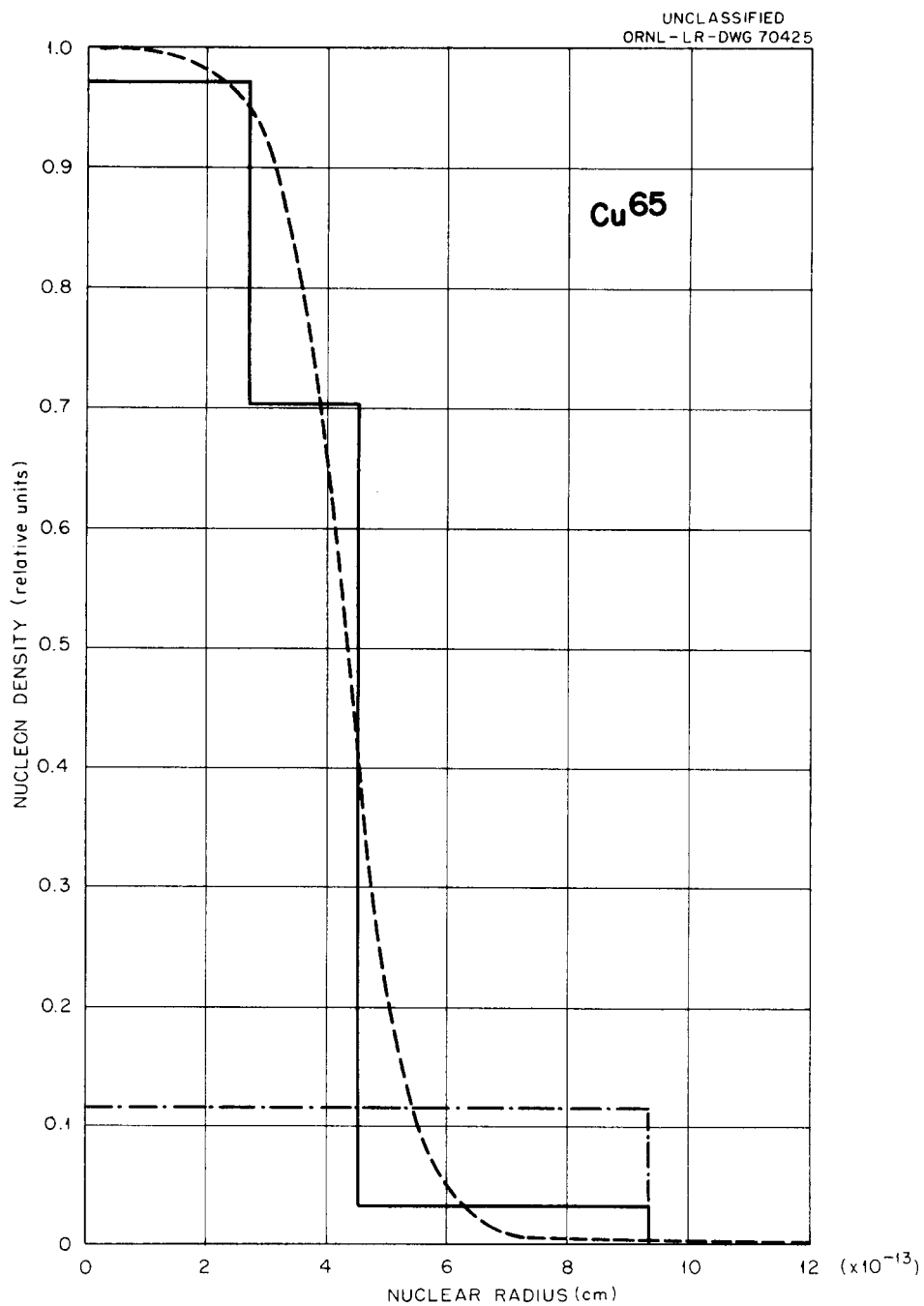


Figure 53. Nucleon Density Distributions Within the Nucleus When the Nuclear Radius Is Assumed To Be Large. Solid lines: nonuniform nucleon density distribution within the nucleus; dash-dotted lines: uniform nucleon density distribution within the nucleus; dashed curve: experimental curve of Hofstadter [R. Hofstadter, *Revs. Modern Phys.* 28, 214 (1956)].

UNCLASSIFIED  
ORNL-LR-DWG 70426

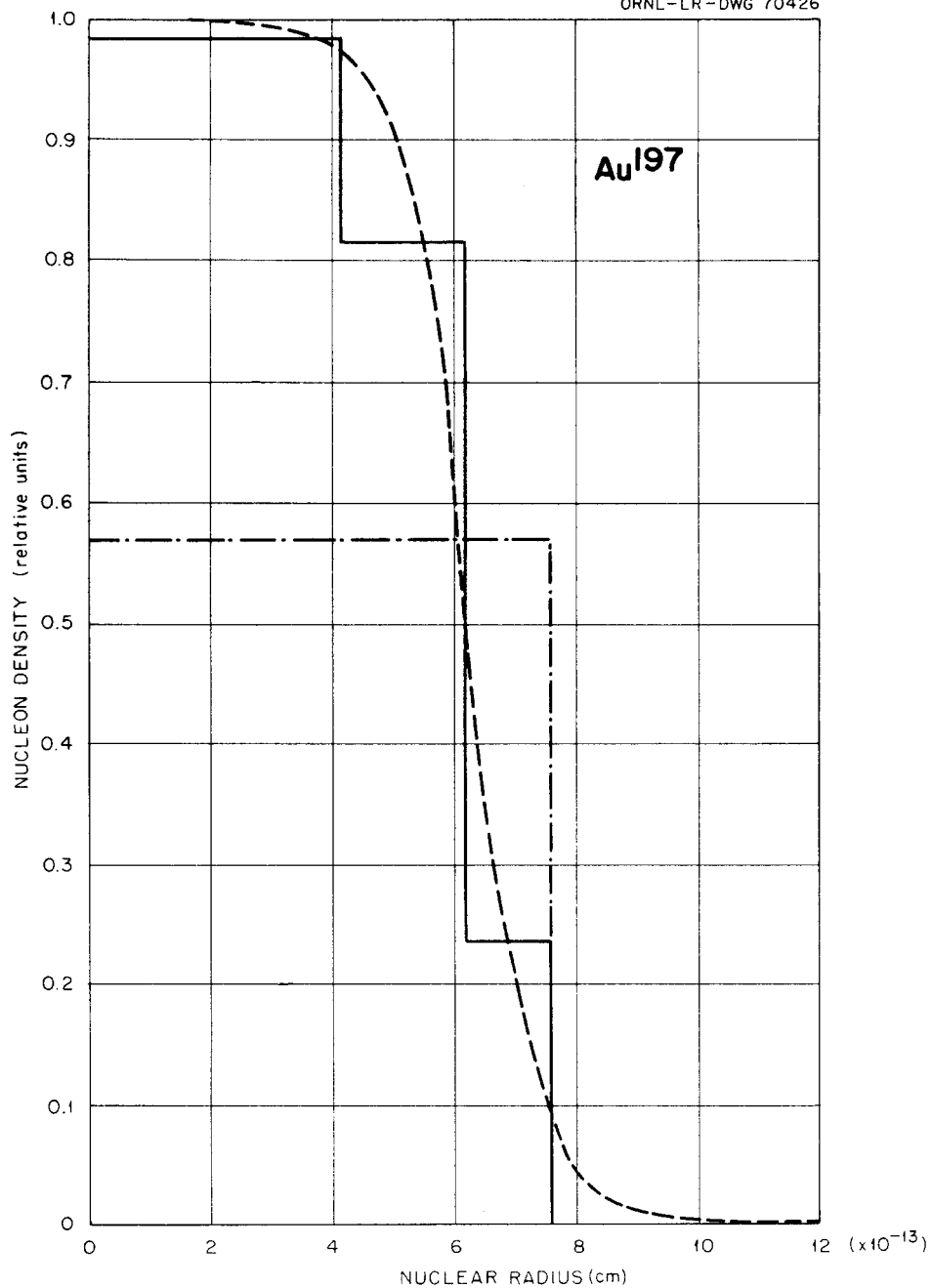


Figure 54. Nucleon Density Distributions Within the Nucleus When the Nuclear Radius Is Assumed To Be Small. Solid lines: nonuniform nucleon density distribution within the nucleus; dash-dotted lines: uniform nucleon density distribution within the nucleus; dashed curve: experimental curve of Hofstadter [R. Hofstadter, *Revs. Modern Phys.* 28, 214 (1956)].

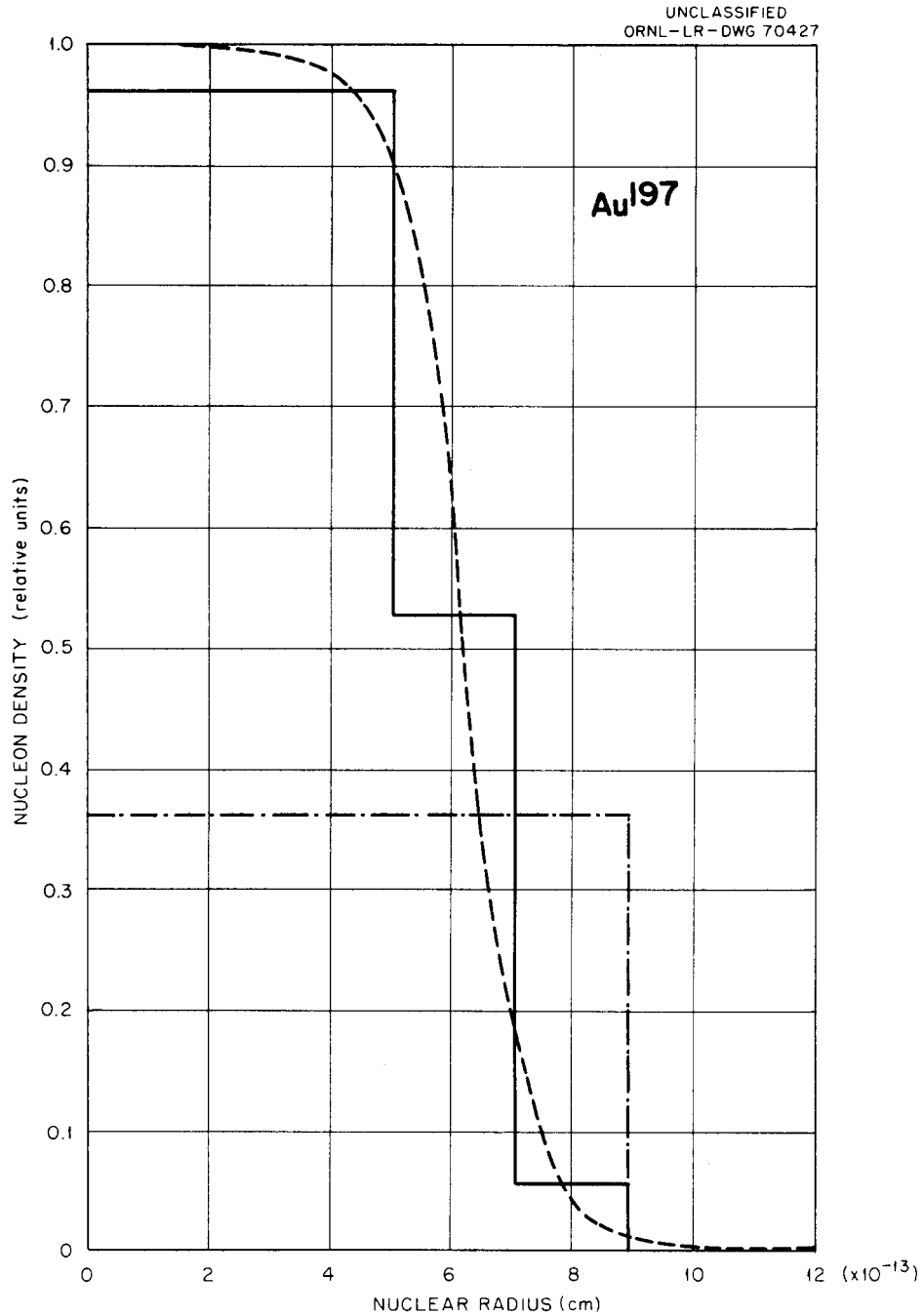


Figure 55. Nucleon Density Distributions Within the Nucleus When the Nuclear Radius Is Assumed To Be Medium. Solid lines: nonuniform nucleon density distribution within the nucleus; dash-dotted lines: uniform nucleon density distribution within the nucleus; dashed curve: experimental curve of Hofstadter [R. Hofstadter, *Revs. Modern Phys.* 28, 214 (1956)].

UNCLASSIFIED  
ORNL -LR- DWG 70428

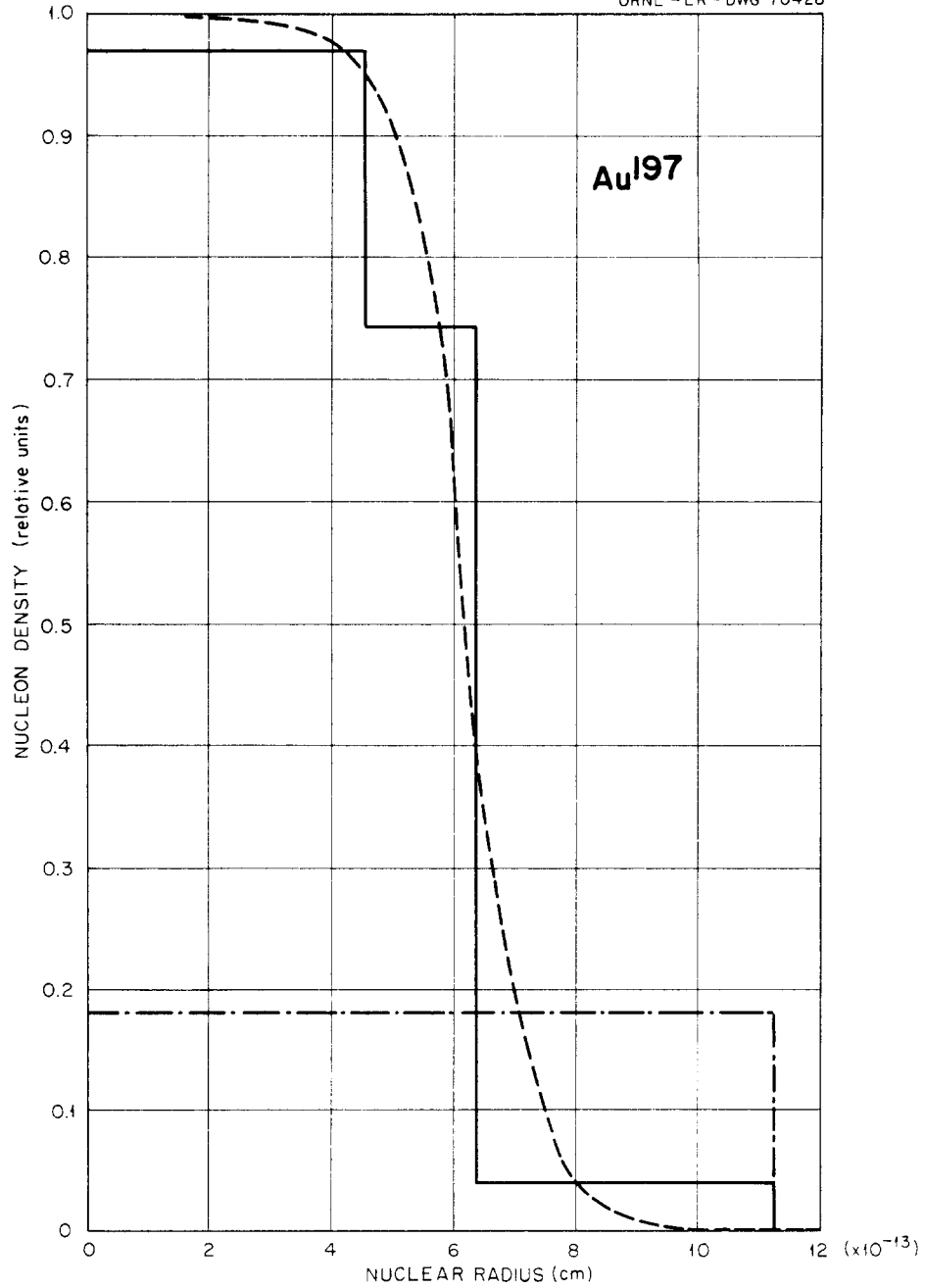


Figure 56. Nucleon Density Distributions Within the Nucleus When the Nuclear Radius Is Assumed To Be Large. Solid lines: nonuniform nucleon density distribution within the nucleus; dash-dotted lines: uniform nucleon density distribution within the nucleus; dashed curve: experimental curve of Hofstadter [R. Hofstadter, Revs. Modern Phys. 28, 214 (1956)].

## CHAPTER VI

### COMPARISONS WITH EXPERIMENT: INCIDENT PIONS

The experimental data for  $\pi$ -meson interactions with nuclei is not as extensive as that for nucleons. The majority of the work referred to here was performed in Russia. The preliminary remarks made prior to the comparisons with experimental data for incident nucleons also apply here.

#### I. NONELASTIC CROSS SECTIONS

The comparisons between calculated and experimental nonelastic cross sections are given in Table XII. The agreement is fair, but not as good or consistent as the same comparisons for incident nucleons. The calculations tend to overestimate the total nonelastic cross section for some of the lightest elements. When the absorption cross section was reduced by 50 per cent at all energies, the nonelastic cross section decreased only about 5 to 10 per cent; thus the discrepancies were not accounted for in this way. The effect of the absorption cross section is small at incident particle energies of about 200 Mev, because it is a small fraction of the resonance cross section at this energy, and its effect is relatively small at lower energies because the nucleus becomes more transparent there.

#### II. ENERGY SPECTRUM FOR NONELASTIC SCATTERING

The comparisons of the calculated and experimental data for the non-elastic scattering of pions on nuclei are given in Figures 57 through 71.

TABLE XII  
CALCULATED AND EXPERIMENTAL TOTAL NONELASTIC  
CROSS SECTIONS FOR INCIDENT PIONS

Pion	Energy (Mev)	Target	Nonelastic Cross Section (mb)	
			Calculated <sup>a</sup>	Experimental
$\pi^+$	195	Li	324 $\pm$ 10	226 $\pm$ 18 <sup>b</sup>
	195	C	455 $\pm$ 11	325 $\pm$ 26 <sup>b</sup>
	270		358 $\pm$ 10	296 $\pm$ 35 <sup>c</sup> - 28
	50	Pb	1563 $\pm$ 26	1620 <sup>d</sup>
$\pi^-$	125	C	458 $\pm$ 11	308 $\pm$ 43 <sup>e</sup>
	150		478 $\pm$ 11	430 $\pm$ 42 <sup>f</sup>
	225		423 $\pm$ 11	346 $\pm$ 21 <sup>g</sup>
	225	Al	653 $\pm$ 14	596 $\pm$ 30 <sup>g</sup>
	225	Cu	1038 $\pm$ 19	1058 $\pm$ 45 <sup>g</sup>
	225	Sn	1471 $\pm$ 20	1550 $\pm$ 70 <sup>g</sup>
	125	Pb	2062 $\pm$ 29	2477 $\pm$ 385 <sup>e</sup>
	150		2145 $\pm$ 29	2490 $\pm$ 160 <sup>f</sup>
	225		1993 $\pm$ 29	2290 $\pm$ 90 <sup>g</sup>

<sup>a</sup>Errors indicated apply for a confidence coefficient of 68 per cent.

<sup>b</sup>N. I. Petrov, V. G. Ivanov, V. A. Rusakov, Soviet Phys. -JETP 10, 682 (1960).

<sup>c</sup>W. Kan Chang et al., Soviet Phys. -JETP 8, 625 (1959).

<sup>d</sup>Calculated from the mean free path in nuclear matter given by G.Saphir, Phys. Rev. 104, 535 (1956).

<sup>e</sup>J. O. Kessler and L. M. Lederman, Phys. Rev. 94, 689 (1954).

<sup>f</sup>R. H. Miller, Nuovo Cimento 6, 882 (1957).

<sup>g</sup>V. G. Ivanov et al., Soviet Phys. -JETP 4, 992 (1957).

Figures 57 through 62 are illustrations containing the comparisons with emulsion work for scattering into wide angular intervals. The calculations indicate a reasonable consistency with the data. The cross-section peaks shift from the high-energy end to the low-energy end of the spectrum as the angular intervals into which the particles are scattered are taken from the forward to the backward direction. The data are fairly coarse and not much more can be said of the comparisons.

In Figure 62 there is a high-energy peak in the experimental spectrum<sup>1</sup> which results from the inclusion in the data of all two-prong small-energy-loss events which do not satisfy the author's criterion for elastic scattering with a free proton in the emulsion. He calls these events pseudo-elastic, and they are not clearly nonelastic collisions with heavy emulsion nuclei.

One of the discrepancies of the calculations of Metropolis et al. with experiment occurred in the shape of the nonelastic pion spectrum in various directions for the case of 150-Mev  $\pi^-$  on carbon and lead. The experiment<sup>2</sup> indicated that the peaks in the spectrum were at much lower energies than those predicted by the calculations. Among the possible sources suggested for the discrepancy was the lack of a pion potential in the previous model or the lack of a diffuse nuclear edge or both. The discrepancy at scattering angles of ninety degrees and one hundred thirty-eight degrees for 150-Mev  $\pi^-$  on lead was examined in this calculation and

---

<sup>1</sup>B. Willot-Chemel, Ann. Phys. (France) 6, 703 (1961).

<sup>2</sup>R. H. Miller, Nuovo Cimento 6, 882 (1957).

found to persist even with the improved model. The results are given in Figures 63 through 68 where at each scattering angle six different nuclear configurations were used to determine their effect. The configurations tried were of the same type described in Chapter V in the section on (p,pn) cross sections, namely, two different nucleon density distributions for each of three outer nuclear radii. As the outer nuclear radius is increased the peaks in the spectrum shift to somewhat higher energies while as the density is changed from a nonuniform to a uniform distribution the peaks shift a little to the lower energies. None of the shifts are sufficient to account for the discrepancy, however.

The calculation was repeated with the standard configuration and the pion absorption cross section reduced by 50 per cent at all energies. The results indicate that the peaks for the two angles remain at about the same position, but they become a little sharper. It was thought that reducing the low-energy pion absorption cross section would enhance the escape of low-energy pions, but indications from the calculation are that most of the pions escape after relatively few collisions. The data from the experiments imply a means of large energy transfer between the pion and the nucleus, which is not accounted for in the calculations.

Another discrepancy between the results of the previous calculations and experimental data is in the spectrum of nonelastic  $\pi^-$  scattered into the backward hemisphere for the case of 162-Mev  $\pi^-$  on heavy emulsion nuclei.

This discrepancy was not very great, but it was mentioned by Metropolis et al.<sup>3</sup> as one which might be overcome by the inclusion of a pion potential. This case was examined using six configurations of the type just mentioned, and the comparisons are illustrated in Figures 69 through 71. The effect of the radius is larger than the effect of the nucleon density distribution, but for nuclear radii of the size used by Metropolis et al. (small radius in the present notation) the shift is in the right direction from the previous work. In this case the comparison is best with the small nuclear radii (Figure 69), but is quite reasonable even with the standard configuration (Figure 70).

### III. ANGULAR DISTRIBUTION OF NONELASTIC PION SCATTERING

Figures 72 through 78 contain the comparisons with experiment for the angular distributions of the pions scattered in nonelastic collisions.

The comparison with data of Kessler and Lederman<sup>4</sup> is illustrated in Figures 72 and 73 for 125-Mev  $\pi^-$  on carbon and lead, respectively. The distributions are for  $\pi^-$  which have lost more than 40 Mev of energy. The data on lead again illustrates the fact that there is a means of large-energy transfer to the nucleus which is not represented by simple particle-particle collisions. The experimental distribution is relatively flat from zero to about one hundred twenty degrees, indicating that in a significant fraction of these events the emitted pion leaves isotropically.

---

<sup>3</sup>See ref. 8, Chapter I.

<sup>4</sup>J. O. Kessler and L. M. Lederman, Phys. Rev. 94, 689 (1954).

Comparisons for 195-Mev  $\pi^+$  on lithium and carbon (Figures 74 and 75) indicate a fair agreement between the calculated and experimental results. The calculated lithium spectrum has been multiplied by the ratio of experimental to calculated nonelastic cross sections in order to better compare the shapes of the distributions.

The experimental angular distribution of nonelastically scattered pions of all energies from 162-Mev  $\pi^-$  on heavy emulsion nuclei was in disagreement with the results of the previous work. This disagreement was investigated here by using the six nuclear configurations mentioned before, and the results are shown in Figures 76 through 78. Here again the size of the nucleus, rather than the nucleon density distribution, has the greatest effect on the results. In this case the data using the nucleus with the largest radius gives the best agreement (Figure 78) but results using the standard configuration are in good agreement also (Figure 77).

#### IV. PION ABSORPTION

The energy spectrum of protons from slow-pion absorption in heavy emulsion nuclei was measured by Azimov.<sup>5</sup> Slow-pion absorption was simulated by calculating the case of 1-Mev pions on  $\text{Ru}^{100}$ . Clearly the calculation for anything but pion absorption is not valid at this energy, and even for pion absorption it is a rough approximation. The reason that it has some validity is that at this energy the reactions within the nucleus are mostly absorption reactions. The nucleons which are involved

---

<sup>5</sup>S. A. Azimov et al., Soviet Phys.-JETP 4, 632 (1957).

in the pion absorption have sufficient energy after the reaction ( $\sim 70$  Mev) to justify the use of the cascade approach used here to determine their subsequent collision histories.

If all of the events occurred at the surface of the nucleus then this approach would have no validity; however, the transparency at this energy is so high ( $\sim 72$  per cent) that the distribution of absorption events within the nucleus should not lead to results which are noticeably different from a uniform distribution. Comparisons were made with the measured spectrum for proton energies greater than 15 Mev for two nuclear configurations: the standard configuration and the small-radius uniform-nucleon-density configuration. The experimental spectrum decreases more rapidly with energy than the calculated spectrum from either configuration (Figure 79).

This was investigated further in a calculation made under the assumption that all  $\pi^-$  were absorbed on n-p pairs so that protons could escape only when they had suffered collisions with the neutrons produced by the absorption. The spectrum in this case was in excellent agreement with the experimental spectrum.

This illustrates a somewhat frustrating difficulty in many of the comparisons made for incident pions, for one set of assumptions may yield reasonable comparisons with one type of data while the same set leads to very poor comparisons with another type. The best path is difficult to find here.

The average number of protons per absorption emitted with energy greater than 30 Mev is calculated here to be 0.10. It was calculated by

Metropolis et al. to be 0.18. If one applies the values estimated by Menon et al.<sup>6</sup> for the fraction of absorptions in heavy emulsion nuclei leading to "starless" tracks (31 starless tracks for every 54 producing stars) to the data of Azimov, one obtains 0.13 fast protons per absorption from the experiment. The value of Metropolis et al. is higher than the one calculated here because they assumed that  $\pi^-$  absorption took place with n-p pairs and p-p pairs with equal probability,<sup>7</sup> while in the present work the probabilities were taken as 0.73 and 0.27, respectively. If one assumes that all absorption takes place with n-p pairs, then the number of fast protons emitted per absorption is calculated to be 0.05. This assumption led to the spectrum that compared best with the experiment.

A comparison of the calculated and experimental angular distributions of two protons resulting from the absorption of 50-Mev  $\pi^+$  on carbon is shown in Figure 80. It illustrates the claim of almost all experimentalists who measure this type of data that there are mechanisms by which a pion is absorbed other than the simple two-particle cluster mechanism.

The calculated and experimental  $\pi^+$  absorption cross sections for beryllium are shown here and indicate a reasonable agreement.

---

<sup>6</sup>M. G. K. Menon, H. Muirhead, and O. Rachat, *Phil. Mag.* 41, 583 (1950).

<sup>7</sup>J. M. Miller, private communication.

$\pi^+$ Energy (Mev)	Pion Absorption Cross Section (mb)	
	Calculated	Experimental <sup>8</sup>
20	58	56 $\pm$ 9
30	63	74 $\pm$ 13
40	67	96 $\pm$ 20

### V. PION REACTIONS INVOLVING CHARGE EXCHANGE

The largest discrepancies between calculated and experimental data in this report involve the charge exchange cross section, as can be demonstrated by the following:

Pion	Energy (Mev)	Target	Pion Charge Exchange Cross Section (mb)	
			Calculated	Experimental
$\pi^+$	50	Pb	206	27 $\pm$ 19 (Ref. 9)
$\pi^-$	125	C	61	20 $\pm$ 20 (Ref. 4) - 10
$\pi^-$	125	Pb	215	100 $\pm$ 80 (Ref. 4) - 40

There can be considerable error in the results of Saphir<sup>9</sup> since he observed only two charge exchange scattering events out of a total of 277 acceptable events.

---

<sup>8</sup>F. H. Tenney and J. Tinlot, Phys. Rev. 92, 974 (1953).

<sup>9</sup>G. Saphir, Phys. Rev. 104, 535 (1956).

<sup>10</sup>N. I. Petrov, V. G. Ivanov, and V. A. Rusakov, Soviet Phys.-JETP 10, 682 (1960).

Another set of data that can be examined is the sum of the charge exchange and absorption cross sections:

<u>Pion</u>	<u>Energy (Mev)</u>	<u>Target</u>	<u>Charge Exchange Plus Absorption Cross Sections (mb)</u>	
			<u>Calculated</u>	<u>Experimental</u>
$\pi^+$	195	Li	142	$164 \pm 16$ (Ref. 10)
$\pi^+$	78	C	174	$195 \pm 20$ (Ref. 11)
	195		205	$203 \pm 22$ (Ref. 10)
	270		146	$165 \pm 34$ (Ref. 12) - 22
$\pi^+$	50	Pb	930	$880 \pm 73$ (Ref. 9)
$\pi^-$	125	C	206	$220 \pm 40$ (Ref. 4)
$\pi^-$	150	C	209	$192 \pm 34$ (Ref. 2)
$\pi^-$	125	Pb	923	$1840 \pm 350$ (Ref. 4)
$\pi^-$	150	Pb	957	$380 \pm 310$ (Ref. 2)

Except for the last two entries, the agreement between the calculated and experimental values is very good. The experimental cross section of 1840 mb for 125-Mev  $\pi^-$  on lead is published as a "star and stops" cross section which includes absorption, charge exchange, and nonelastic collisions where the scattered particle is emitted with small energy. The

---

<sup>11</sup>R. G. Sulukvadze and D. Neagu, Soviet Phys.-JETP 14, 59 (1962).

<sup>12</sup>W. Kan Chang et al., Soviet Phys.-JETP 8, 625 (1959).

calculated results do not include the latter events and the discrepancy indicates that there might be a considerable number of them.

Other measurements involving the charge exchange cross section were those of Blinov et al.,<sup>13</sup> where the ratios of the charge exchange to geometric cross sections and the ratios of absorption to geometric cross sections were measured for  $\pi^+$  on freons ( $\text{CCl}_2\text{F}_2$  and  $\text{CClF}_3$ ). Calculations were done on  $\text{F}^{19}$  and compared with the experiments and the results are indicated below.

<u>Energy (Mev)</u>	<u>Ratio of Charge Exchange to Absorption Cross Section</u>	
	<u>Calculated</u>	<u>Experimental</u>
77	0.39	0.11
136	0.47	0.12
224	0.51	0.24
283	0.57	0.26

Here again a consistently higher charge exchange cross section is predicted by the calculation.

One final experiment that illustrates this point once more is an experiment on  $\pi^+$  production from 308-Mev  $\pi^-$  on carbon by Krivitskii and Reut.<sup>14</sup> They assumed that all the  $\pi^+$  came from pion production and measured

---

<sup>13</sup>G. A. Blinov et al., Soviet Phys.-JETP 8, 609 (1959).

<sup>14</sup>V. V. Krivitskii and A. A. Reut, Doklady Akad. Nauk. S.S.S.R. 112, 232 (1957).

the differential  $\pi^+$  cross section at ninety degrees to be  $0.21 \pm 0.11$  mb/sr. Assuming the production to be isotropic, they calculated the total cross section for producing  $\pi^+$  as  $2.6 \pm 1.3$  mb. Predictions from the calculation, where  $\pi^+$  are produced by two charge exchange events, are that the total cross section for producing  $\pi^+$  is 8 mb and the differential cross section at ninety degrees is 0.84 mb/sr. Both values are higher than the measurements and pion production is not included.

This discrepancy between the calculations and experiments for charge exchange reactions is difficult to reconcile, for on a particle-particle basis this cross section is quite large. If one considers all pion-proton reactions to occur by means of the  $T = 3/2$  state only, then simple isotopic spin analysis indicates that for  $\pi^-$ -p scattering the charge exchange cross section should be  $2/3$  of the total cross section. This is best illustrated in Figure 8.

A comparison of the measured charge exchange cross section at a few energies with those which were used in the calculation and were calculated from the phase shifts is given here. This is merely meant to illustrate the validity of the cross sections that were used.

<u><math>\pi^-</math> Energy (Mev)</u>	<u>Charge Exchange Cross Section (mb)</u>	
	<u>Calculated from Phase Shifts</u>	<u>Measured</u>
230	32.2	$30.4 \pm 1.3$
290	21.1	$18.2 \pm 0.8$

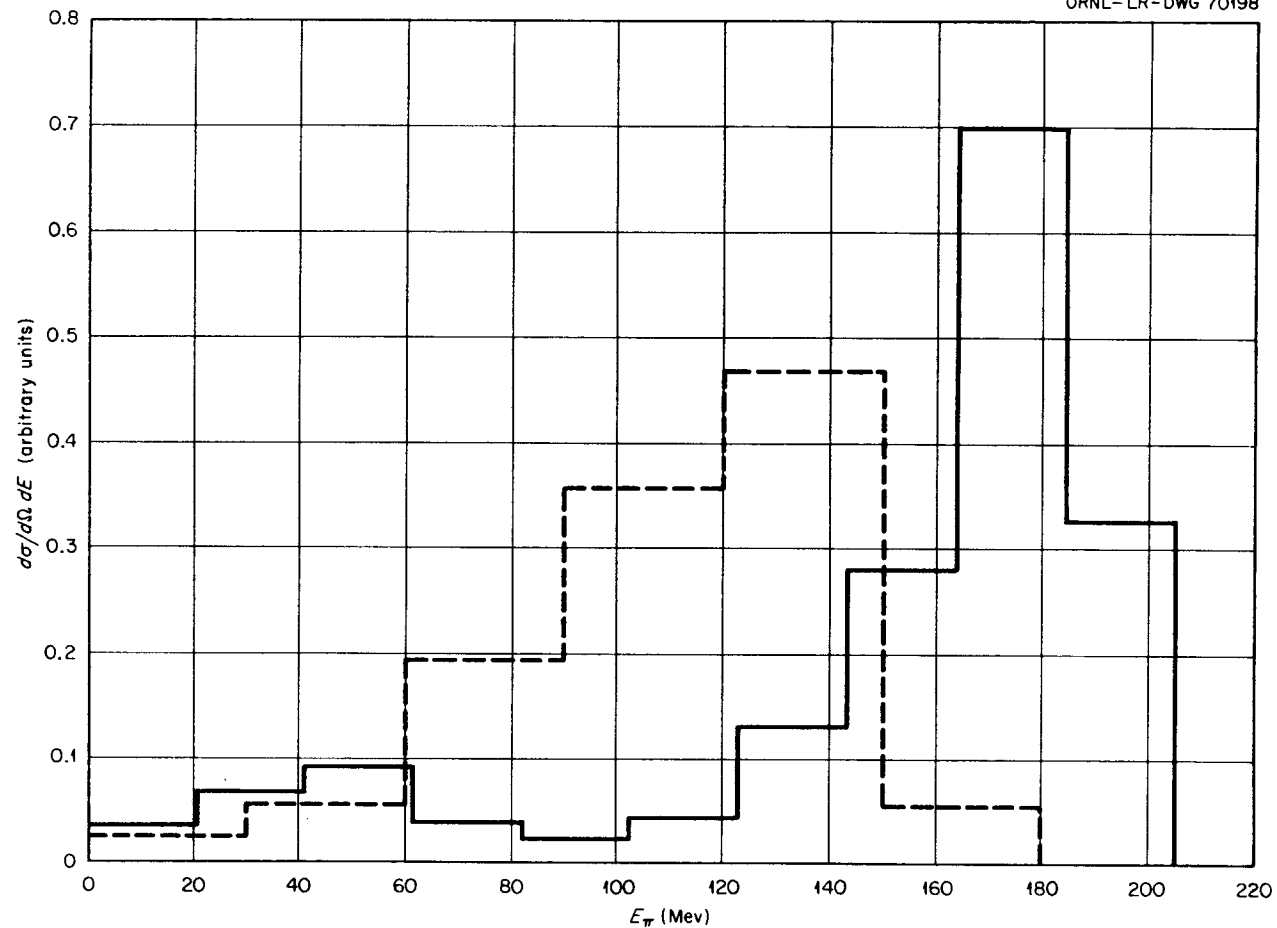


Figure 57. Energy Spectra of Nonelastic  $\pi^+$  Emitted in the Angular Interval  $0^\circ$  to  $60^\circ$  from 195-Mev  $\pi^+$  on Lithium and Carbon. Dashed lines: experimental results of Petrov et al. [N. I. Petrov, V. G. Ivanov, and V. A. Rusakov, Soviet Phys.-JETP 10, 682 (1960)]; solid lines: calculated spectrum. Units of the ordinate scale are arbitrary.

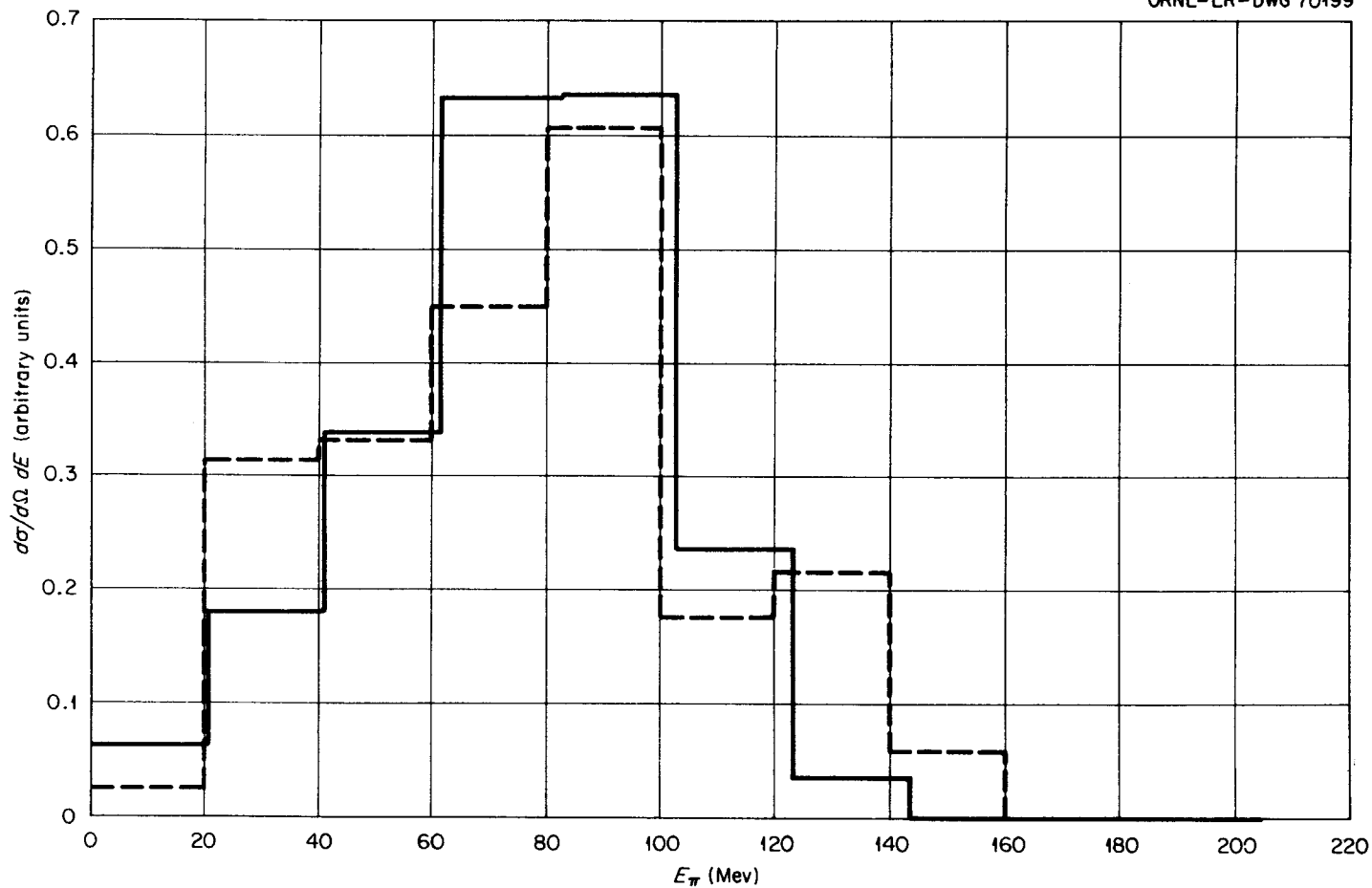


Figure 58. Energy Spectra of Nonelastic  $\pi^+$  Emitted in the Angular Interval  $120^\circ$  to  $180^\circ$  from 195-Mev  $\pi^+$  on Lithium and Carbon. Dashed lines: experimental results of Petrov et al. [N. I. Petrov, V. G. Ivanov, and V. A. Rusakov, Soviet Phys.-JETP 10, 682 (1960)]; solid lines: calculated spectrum. Units of the ordinate scale are arbitrary.

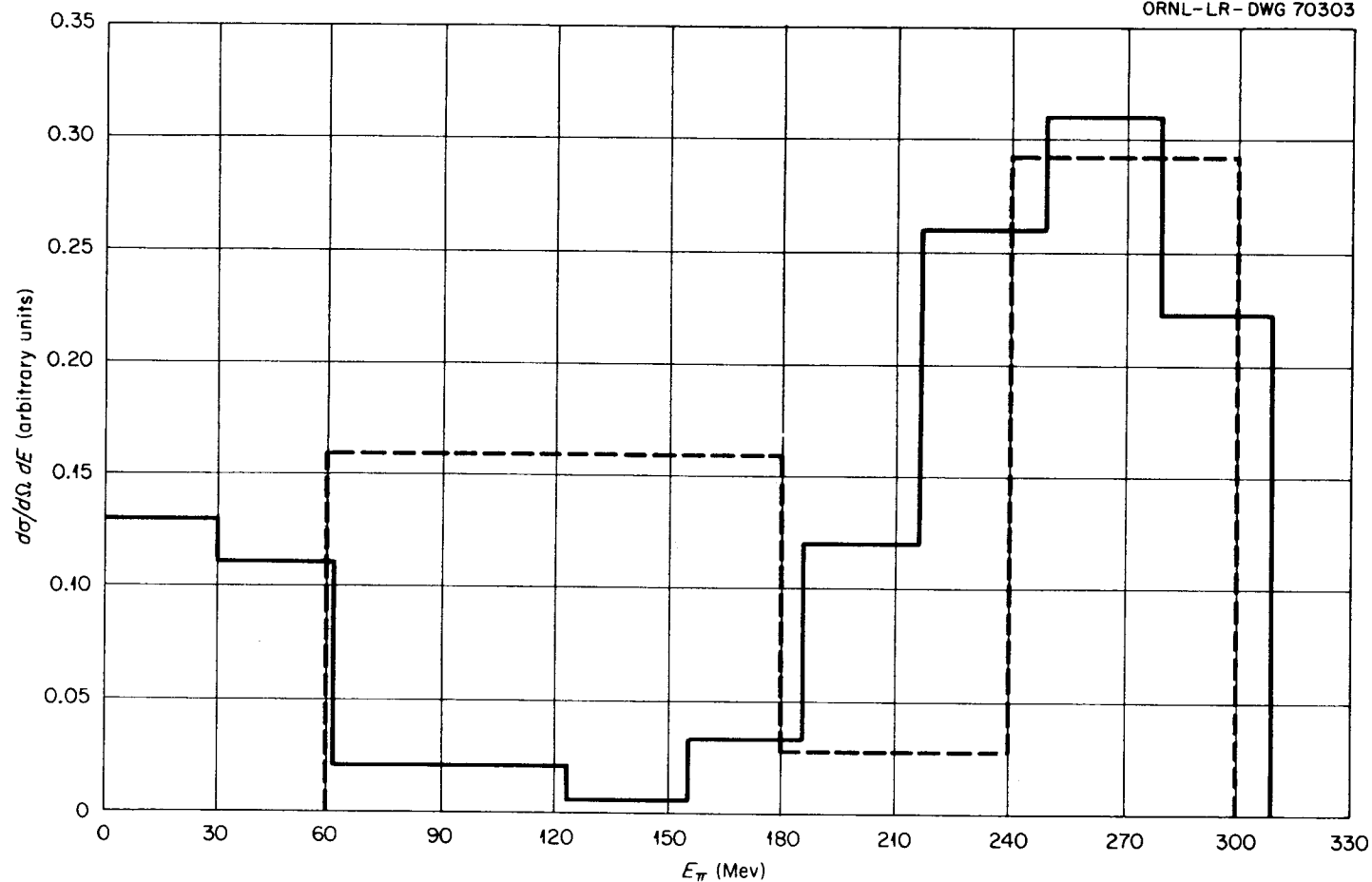


Figure 59. Energy Spectra of Nonelastic  $\pi^-$  Emitted into the Angular Interval  $0^\circ$  to  $60^\circ$  from 300-Mev  $\pi^-$  on Heavy Emulsion Nuclei. Dashed lines: experimental values of Chemel [B. Willot-Chemel, Ann. Phys. (France) 6, 703 (1961)]; solid lines: calculated values for 300-Mev  $\pi^-$  on  $\text{Ru}^{100}$ . Units of the ordinate scale are arbitrary.

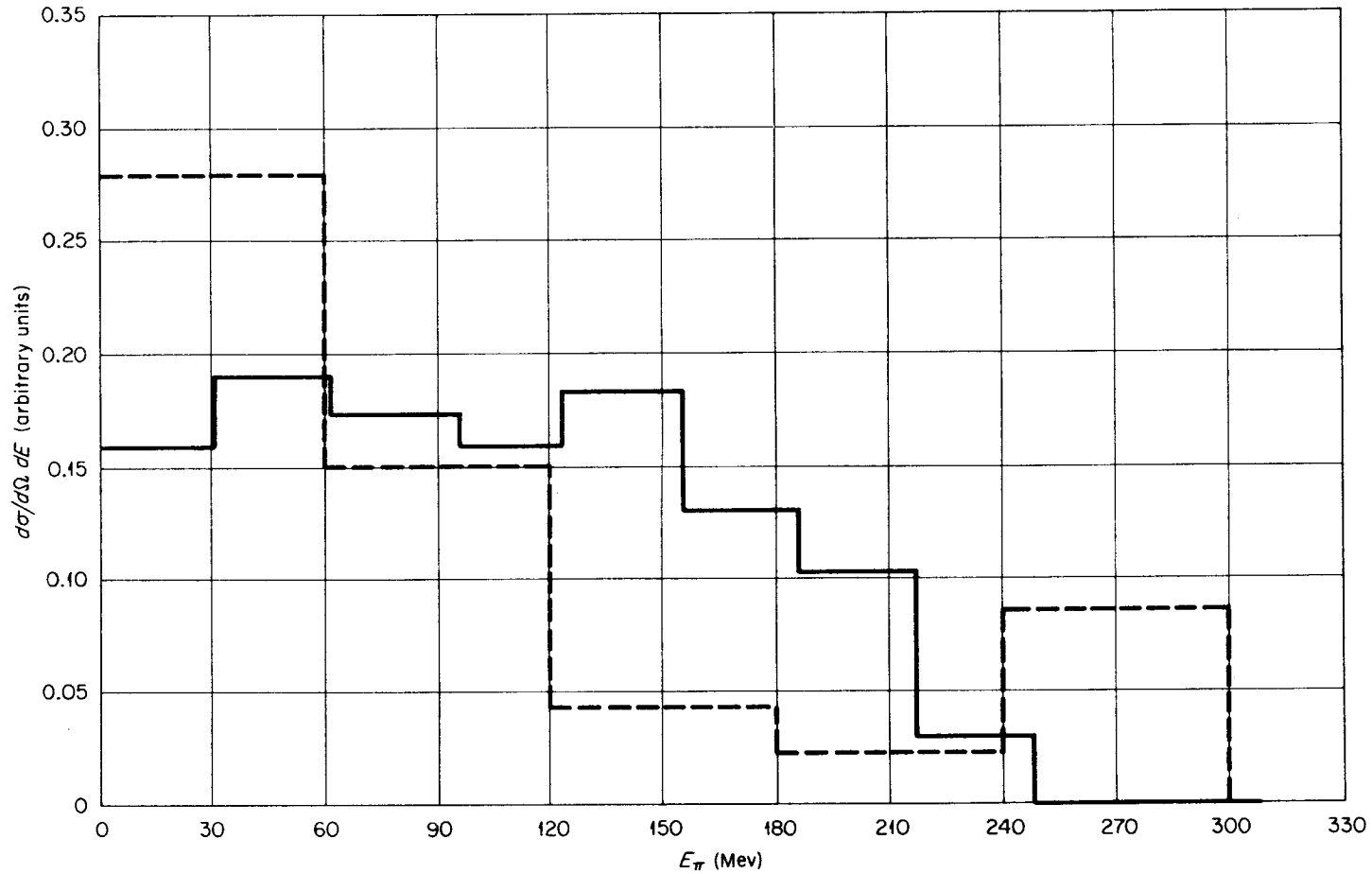


Figure 60. Energy Spectra of Nonelastic  $\pi^-$  Emitted Into the Angular Interval  $60^\circ$  to  $120^\circ$  from 300-Mev  $\pi^-$  on Heavy Emulsion Nuclei. Dashed lines: experimental values of Chemel (B. Willot-Chemel, Ann. Phys. (France) 6, 703 (1961)]; solid lines: calculated values for 300-Mev  $\pi^-$  on  $\text{Ru}^{100}$ . Units of the ordinate scale are arbitrary.

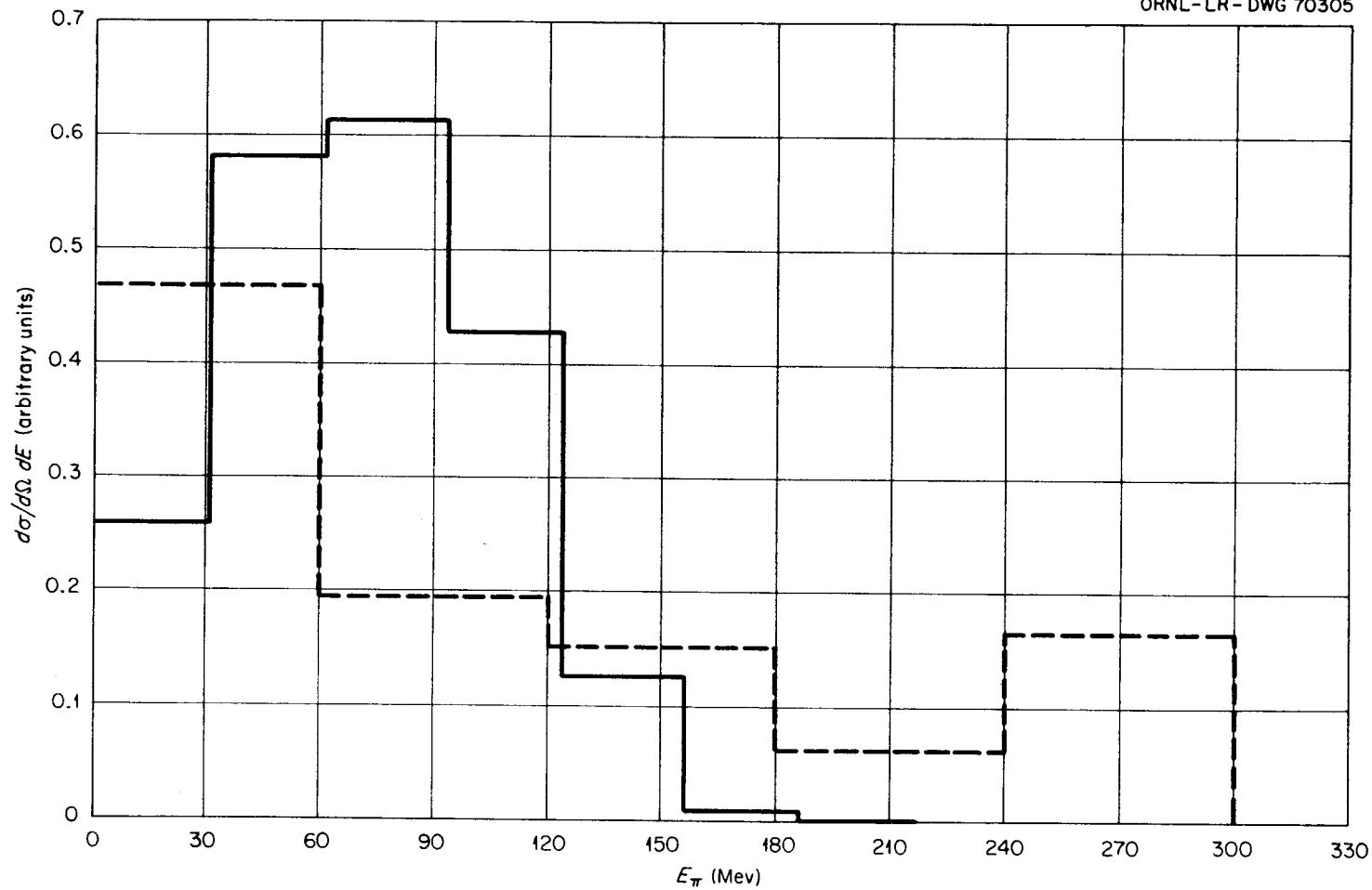


Figure 61. Energy Spectra of Nonelastic  $\pi^-$  Emitted Into the Angular Interval  $120^\circ$  to  $180^\circ$  from 300-Mev  $\pi^-$  on Heavy Emulsion Nuclei. Dashed lines: experimental values of Chemel [B. Willot-Chemel, Ann. Phys. (France) 6, 703 (1961)]; solid lines: calculated values for 300-Mev  $\pi^-$  on  $\text{Ru}^{100}$ . Units of the ordinate scale are arbitrary.

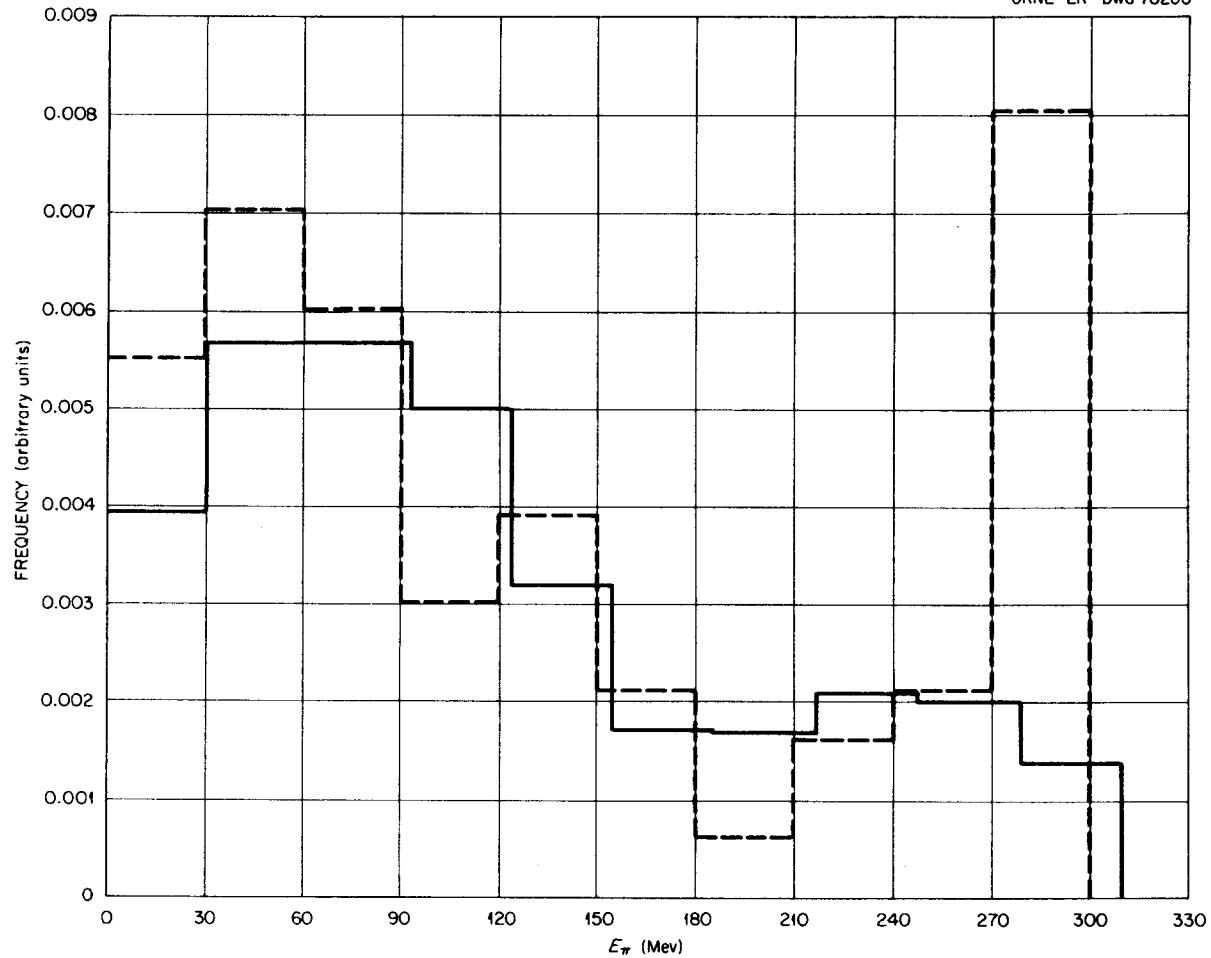


Figure 62. Energy Spectra of Nonelastic  $\pi^-$  from 300-Mev  $\pi^-$  on Heavy Emulsion Nuclei. Dashed lines: experimental results of Chemel [B. Willot-Chemel, Ann. Phys. (France) 6, 703 (1961)]; solid lines: calculated nonelastic  $\pi^-$  spectrum for 300-Mev  $\pi^-$  on  $\text{Ru}^{100}$ . Units of the ordinate scale are arbitrary.

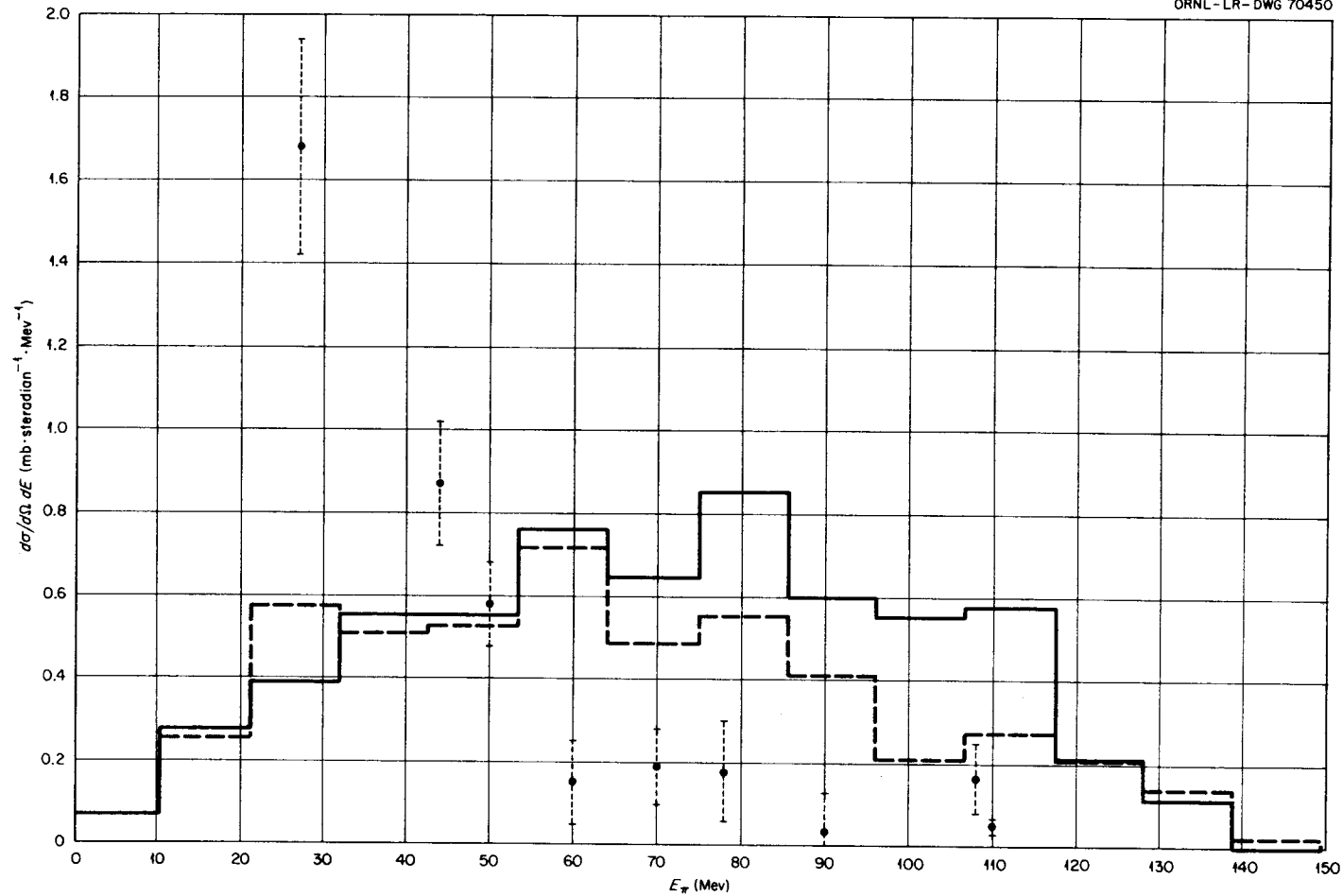


Figure 63. Nonelastic  $\pi^-$  Spectra at  $90^\circ$  from 150-Mev  $\pi^-$  on Lead. Calculated spectra for  $\pi^-$  in the interval  $78^\circ$  to  $102^\circ$  for nucleus with small radius. Solid lines: nonuniform nucleon density distribution within the nucleus; dashed lines: uniform density distribution; points: experimental values of Miller [R. H. Miller, Nuovo cimento 6, 882 (1957)].

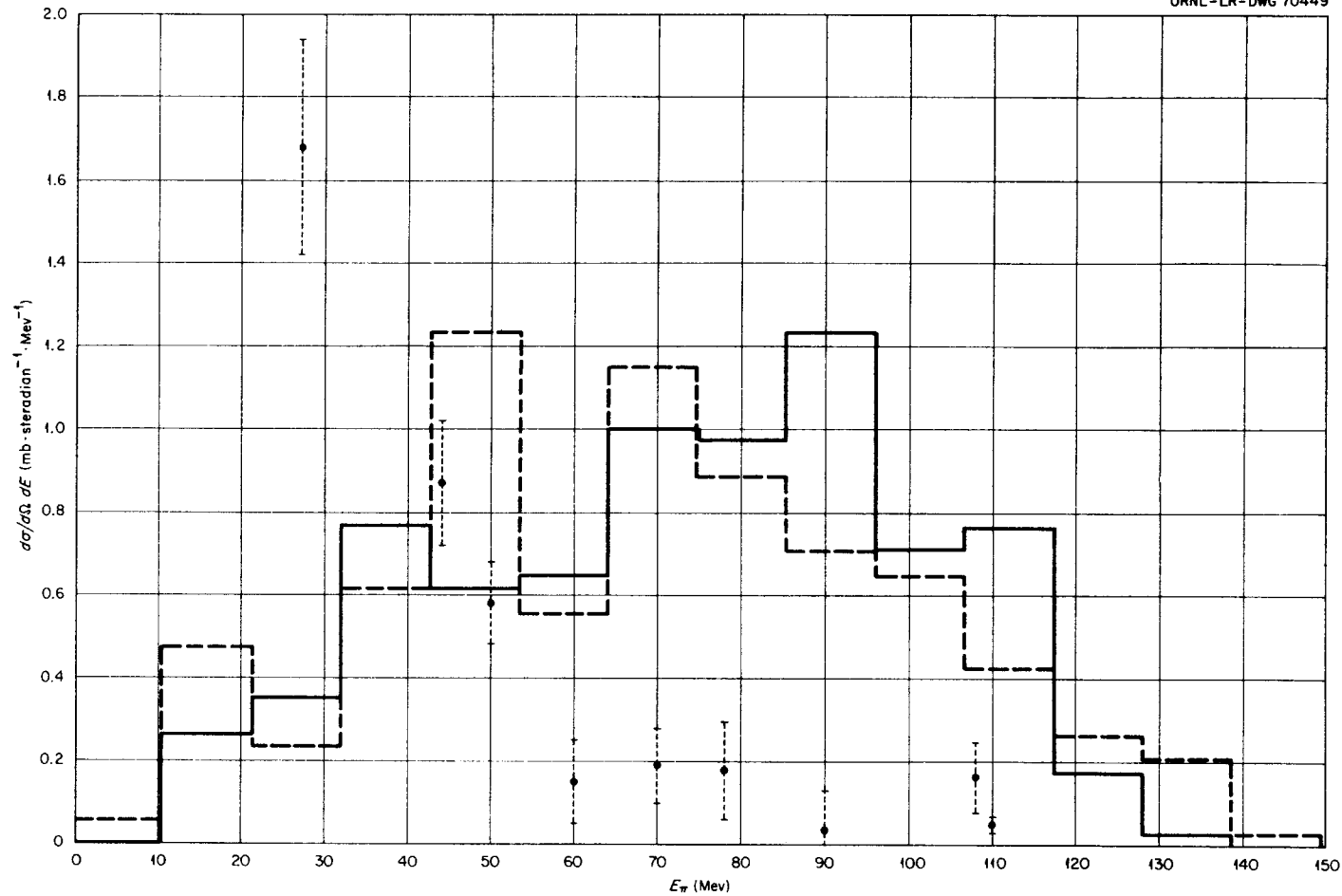


Figure 64. Nonelastic  $\pi^-$  Spectra at  $90^\circ$  from 150-Mev  $\pi^-$  on Lead. Calculated spectra for  $\pi^-$  in the interval  $78^\circ$  to  $102^\circ$  for nucleus with medium radius. Solid lines: nonuniform nucleon density distribution within the nucleus; dashed lines: uniform density distribution; points: experimental values of Miller [R. H. Miller, Nuovo cimento 6, 882 (1957)].

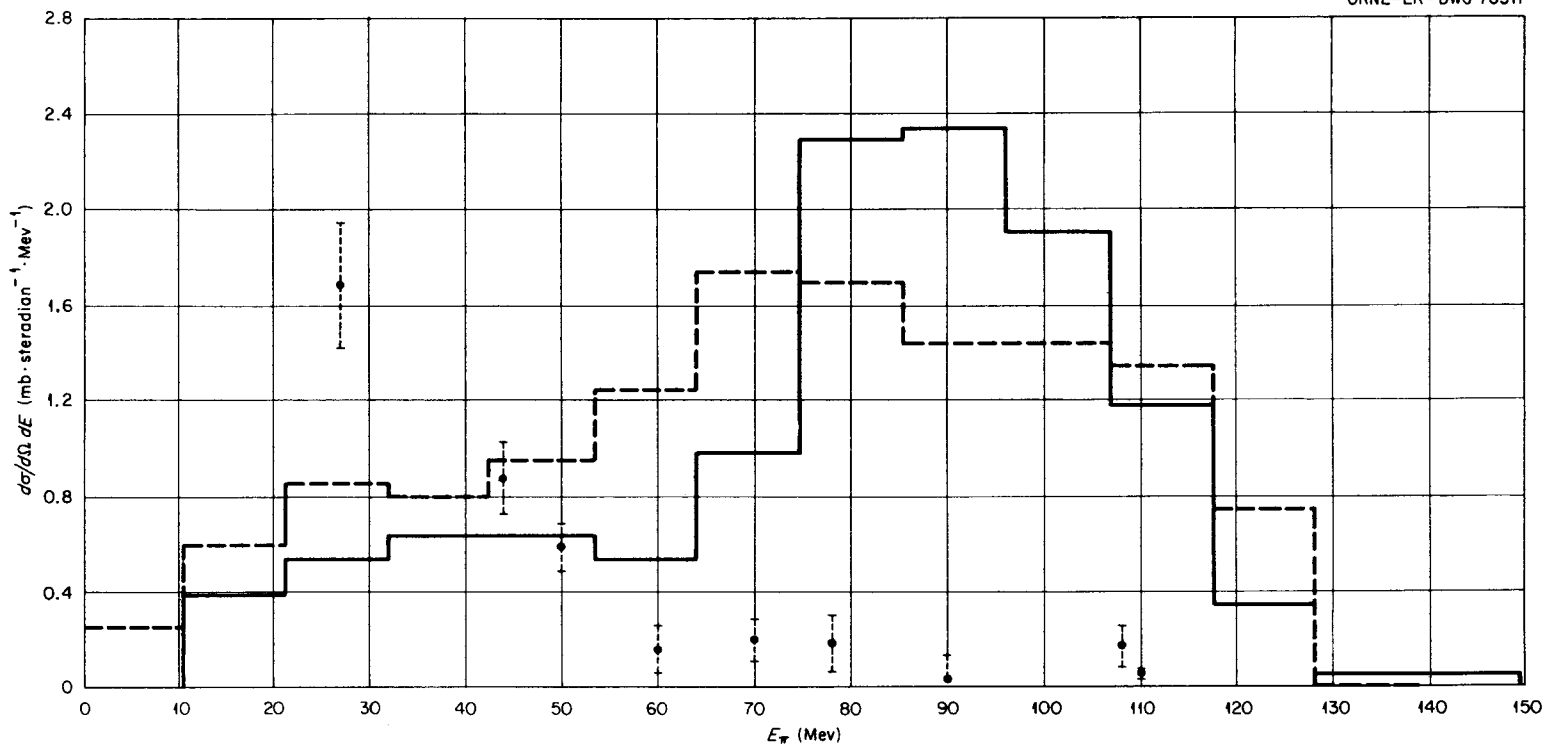


Figure 65. Nonelastic  $\pi^-$  Spectra at  $90^\circ$  from 150-Mev  $\pi^-$  on Lead. Calculated spectra for  $\pi^-$  in the interval  $78^\circ$  to  $102^\circ$  for nucleus with large radius. Solid lines: nonuniform nucleon density distribution within the nucleus; dashed lines: uniform density distribution; points: experimental values of Miller [R. H. Miller, *Nuovo cimento* 6, 882 (1957)].

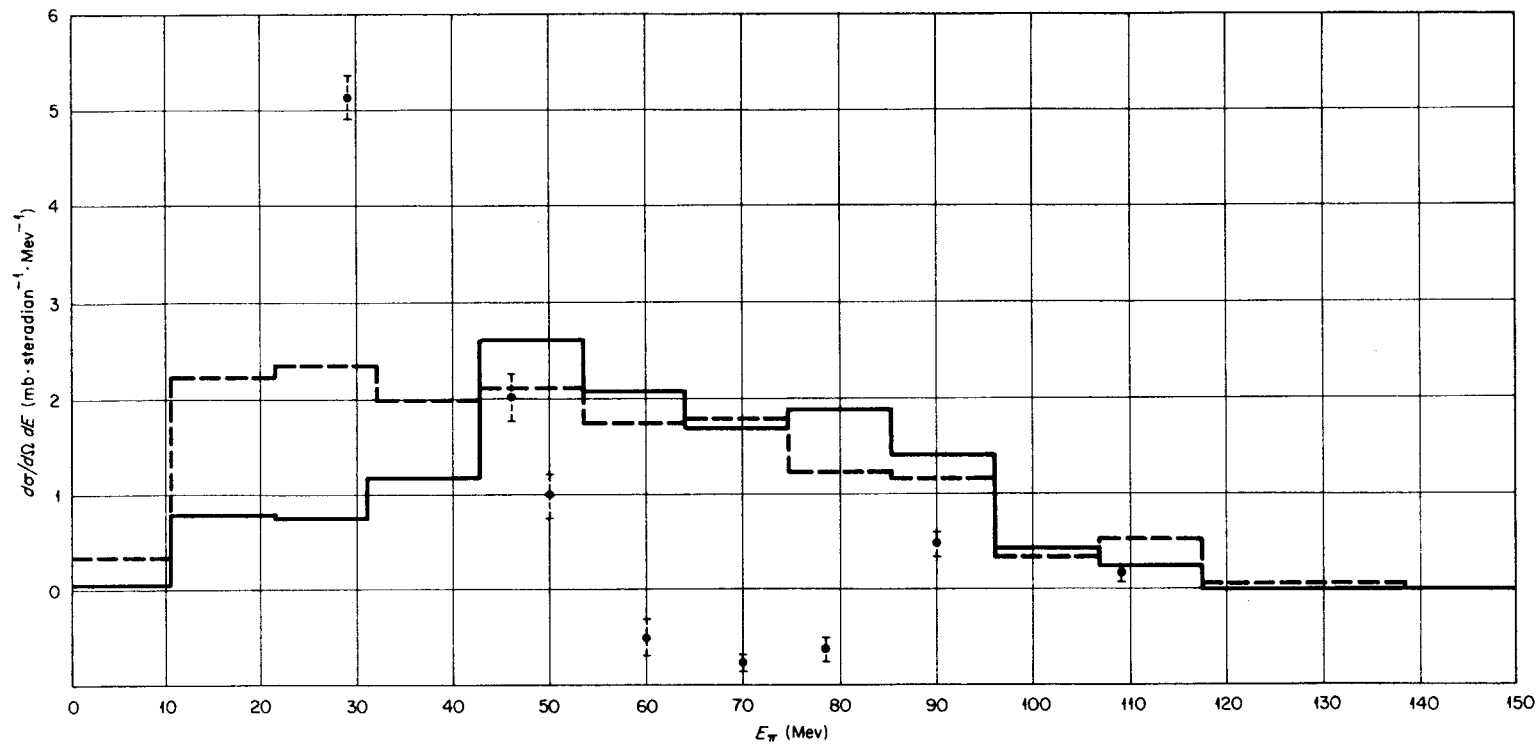


Figure 66. Nonelastic  $\pi^-$  Spectra at  $138^\circ$  from 150-Mev  $\pi^-$  on Lead. Calculated spectra for  $\pi^-$  in the interval  $130^\circ$  to  $148^\circ$  for nucleus with small radius. Solid lines: nonuniform nucleon density distribution within the nucleus; dashed lines: uniform density distribution; points: experimental values of Miller [R. H. Miller, Nuovo cimento 6, 882 (1957)].

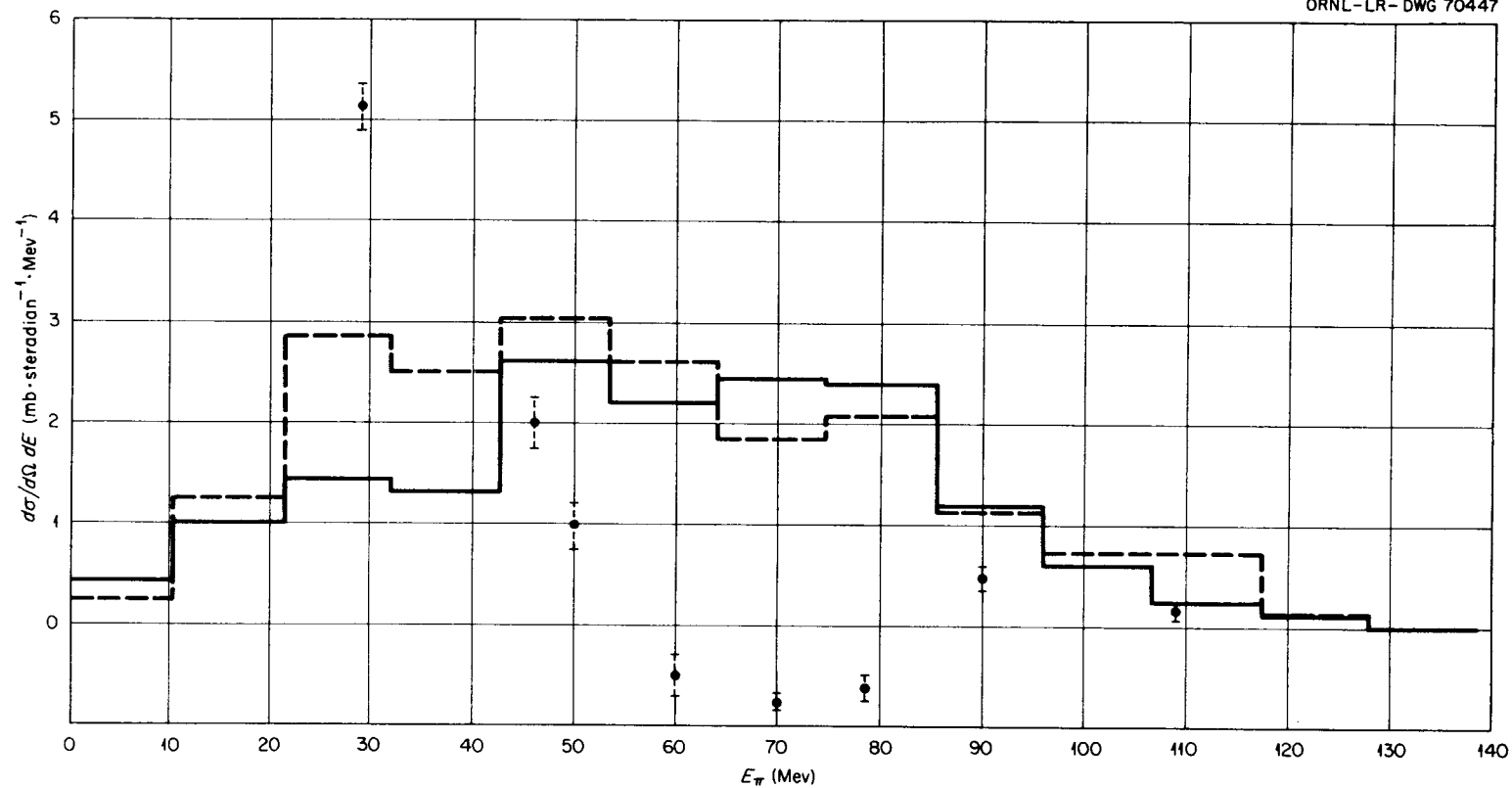


Figure 67. Nonelastic  $\pi^-$  Spectra at  $138^\circ$  from 150-Mev  $\pi^-$  on Lead. Calculated spectra for  $\pi^-$  in the interval  $130^\circ$  to  $148^\circ$  for nucleus with medium radius. Solid lines: nonuniform nucleon density distribution within the nucleus; dashed lines: uniform density distribution; points: experimental values of Miller [R. H. Miller, Nuovo cimento 6, 882 (1957)].

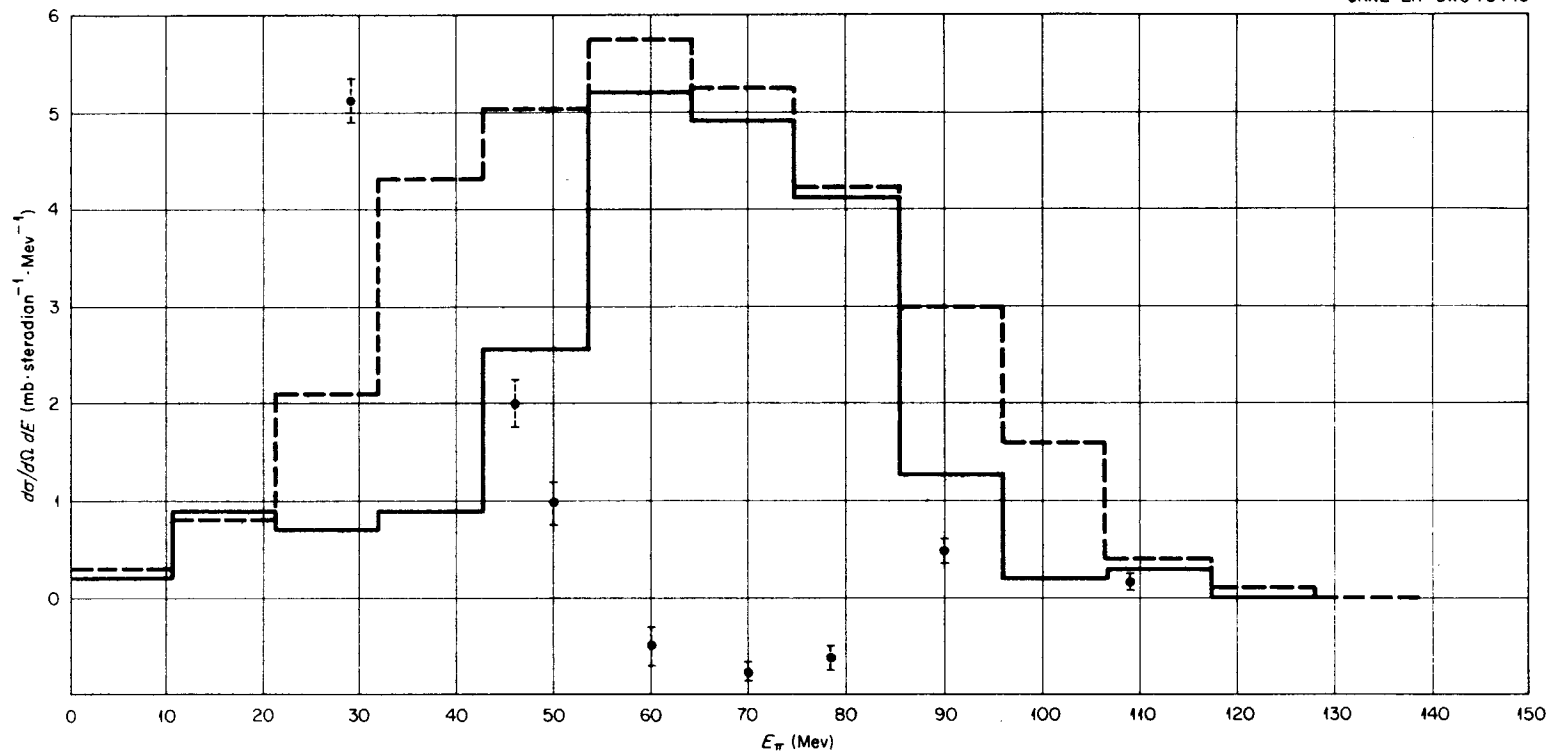


Figure 68. Nonelastic  $\pi^-$  Spectra at  $138^\circ$  from 150-Mev  $\pi^-$  on Lead. Calculated spectra for  $\pi^-$  in the interval  $130^\circ$  to  $148^\circ$  for nucleus with large radius. Solid lines: nonuniform nucleon density distribution within the nucleus; dashed lines: uniform distribution; points: experimental values of Miller [R. H. Miller, Nuovo cimento 6, 882 (1957)].

UNCLASSIFIED  
ORNL-LR-DWG 70453

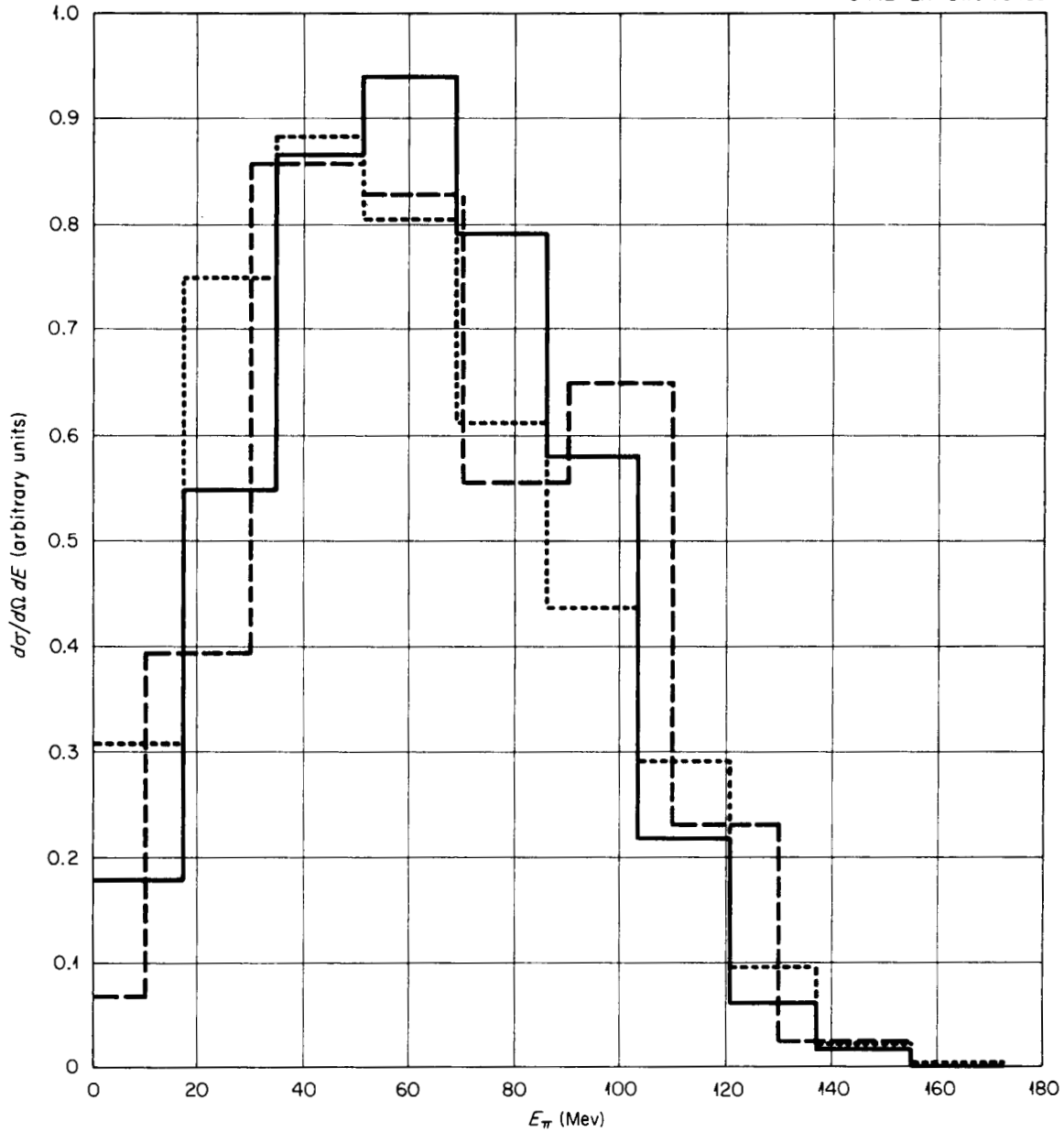


Figure 69. Nonelastic Spectrum for  $\pi^-$  Emitted Into the Backward Hemisphere from 162-Mev  $\pi^-$  on Heavy Emulsion Nuclei. Calculated values are for 162-Mev  $\pi^-$  on  $\text{Ru}^{100}$  with a small nuclear radius. Solid lines: nonuniform nucleon density distribution within the nucleus; dotted lines: uniform nucleon density distributions; dashed lines: experimental results of Nikolskii et al. [B. A. Nikolskii, L. P. Kudrin, and S. A. Ali-Zade, Soviet Phys. - JETP 5, 93 (1957)]. The units of the ordinate scale are arbitrary.

UNCLASSIFIED  
ORNL-LR-DWG 70456

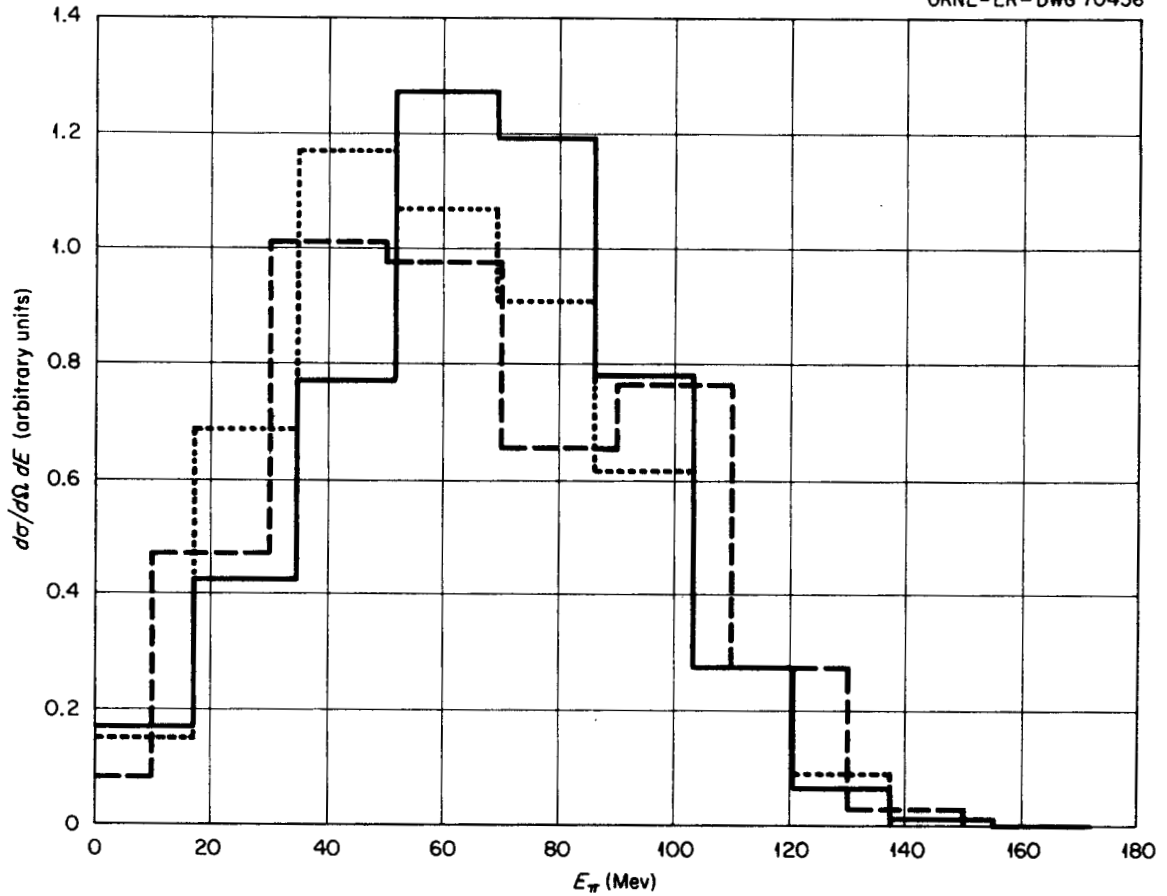


Figure 70. Nonelastic Spectrum for  $\pi^-$  Emitted Into the Backward Hemisphere from 162-Mev  $\pi^-$  on Heavy Emulsion Nuclei. Calculated values are for 162-Mev  $\pi^-$  on  $\text{Ru}^{100}$  with a medium nuclear radius. Solid lines: nonuniform nucleon density distribution within the nucleus; dotted lines: uniform nucleon density distribution; dashed lines: experimental results of Nikolskii et al. [B. A. Nikolskii, L. P. Kudrin, and S. A. Ali-Zade, Soviet Phys.-JETP 5, 93 (1957)]. The units of the ordinate scale are arbitrary.

UNCLASSIFIED  
ORNL-LR-DWG 70455

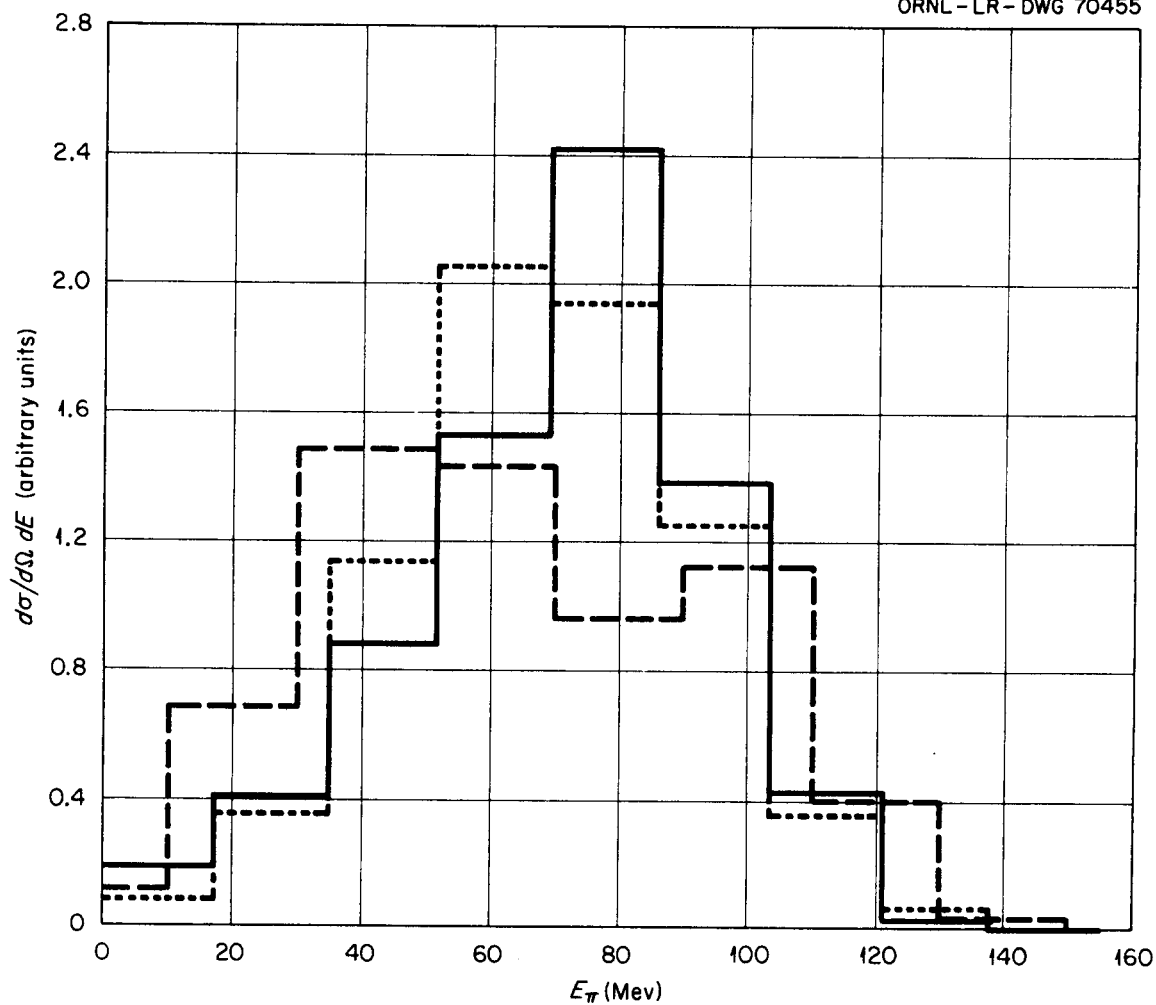


Figure 71. Nonelastic Spectrum for  $\pi^-$  Emitted Into the Backward Hemisphere from 162-Mev  $\pi^-$  on Heavy Emulsion Nuclei. Calculated values are for 162-Mev  $\pi^-$  on  $\text{Ru}^{100}$  with a large nuclear radius. Solid lines: nonuniform nucleon density distribution within the nucleus; dotted lines: uniform nucleon density distribution; dashed lines: experimental results of Nikolskii et al. [B. A. Nikolskii, L. P. Kudrin, and S. A. Ali-Zade, Soviet Phys.-JETP 5, 93 (1957)]. The units of the ordinate scale are arbitrary.

UNCLASSIFIED  
ORNL-LR-DWG 70309

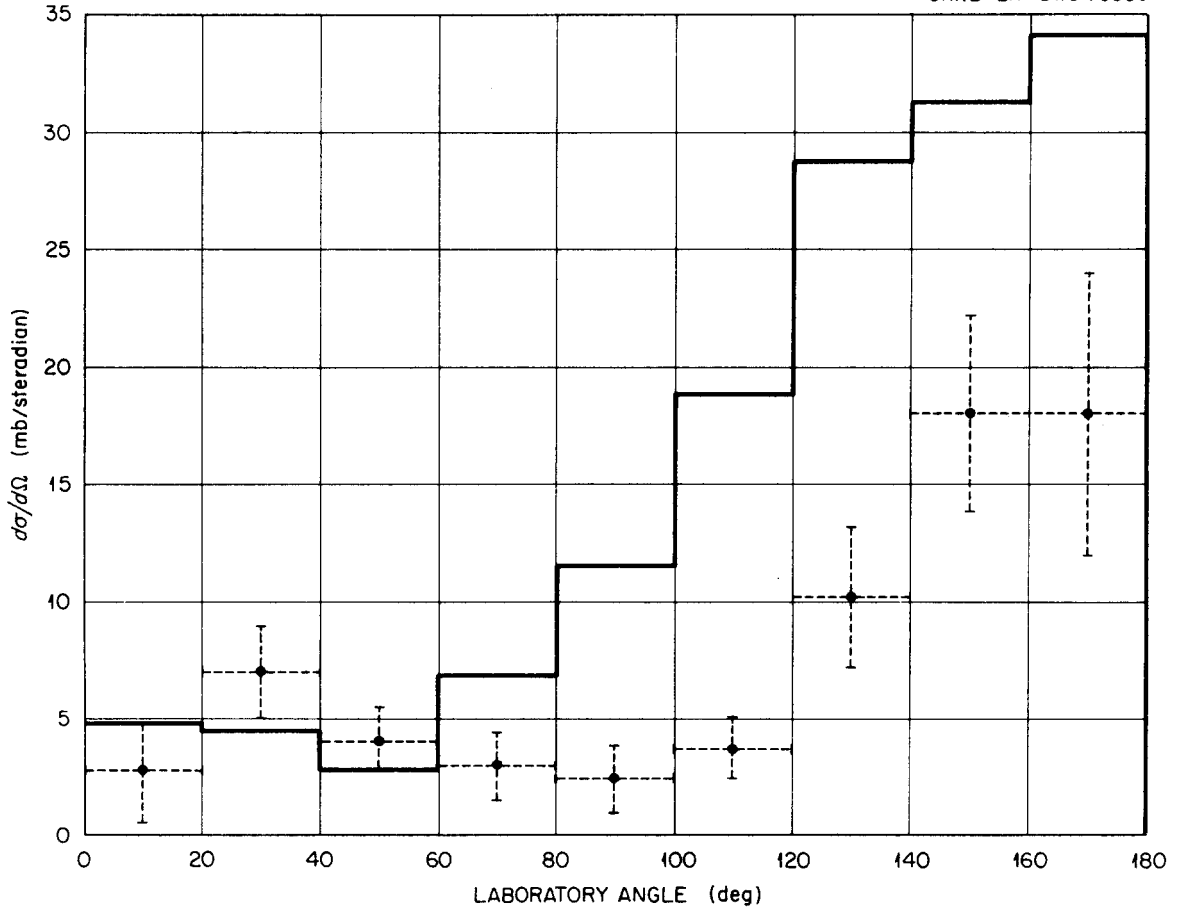


Figure 72. Angular Distribution of Nonelastic  $\pi^-$  Scattered with Energy Loss Greater than 40 Mev for 125-Mev  $\pi^-$  on Carbon. Points: experimental values of Kessler and Lederman [J. O. Kessler and L. M. Lederman, Phys. Rev. 94, 689 (1954)]; solid lines: calculated distribution.

UNCLASSIFIED  
ORNL-LR-DWG 70310

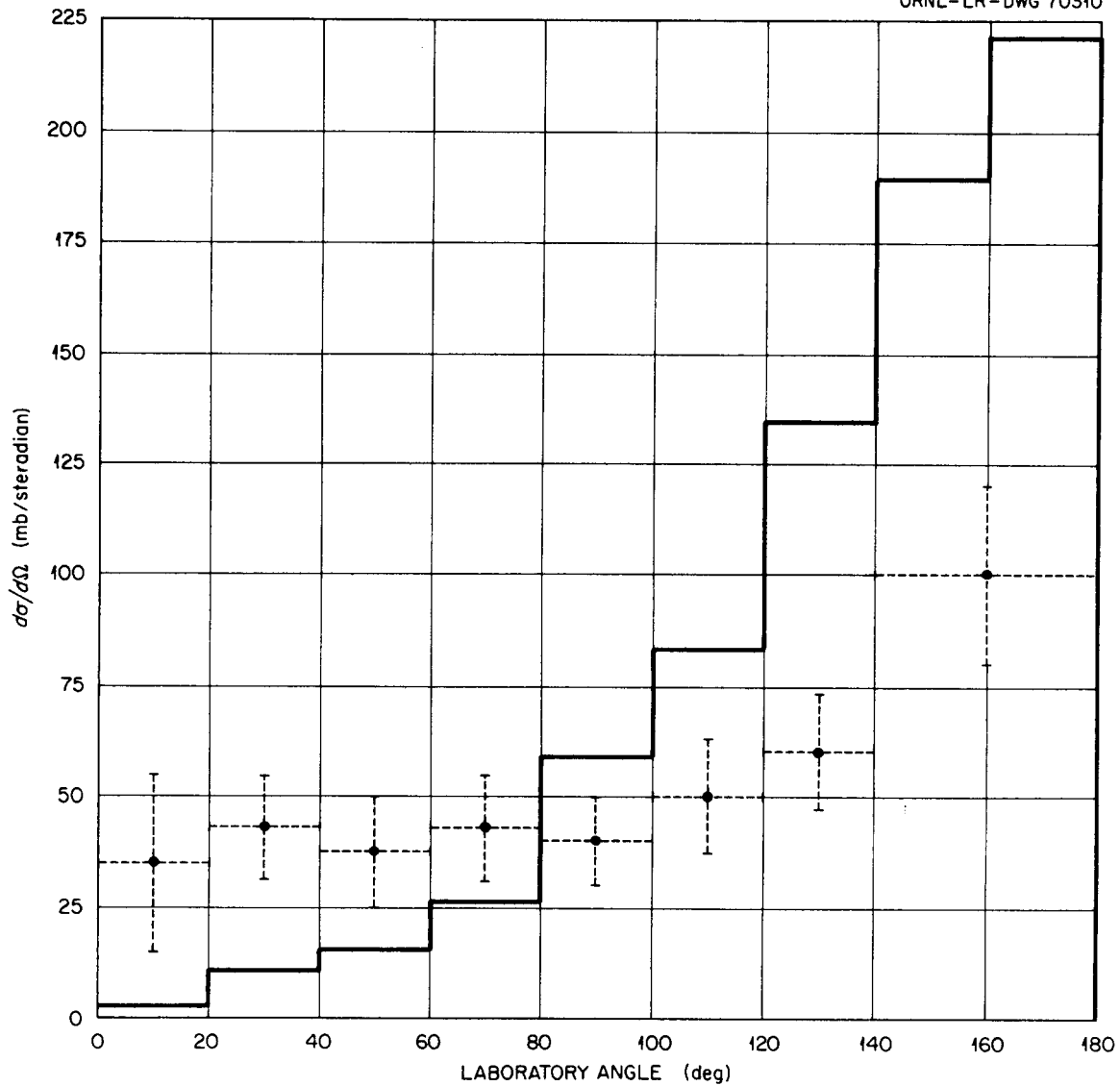


Figure 73. Angular Distribution of Nonelastic  $\pi^-$  Scattered with Energy Loss Greater than 40 Mev for 125-Mev  $\pi^-$  on Lead. Points: experimental values of Kessler and Lederman [J. O. Kessler and L. M. Lederman, Phys. Rev. 94, 689 (1954)]; solid lines: calculated distribution.

UNCLASSIFIED  
ORNL-LR-DWG 70308

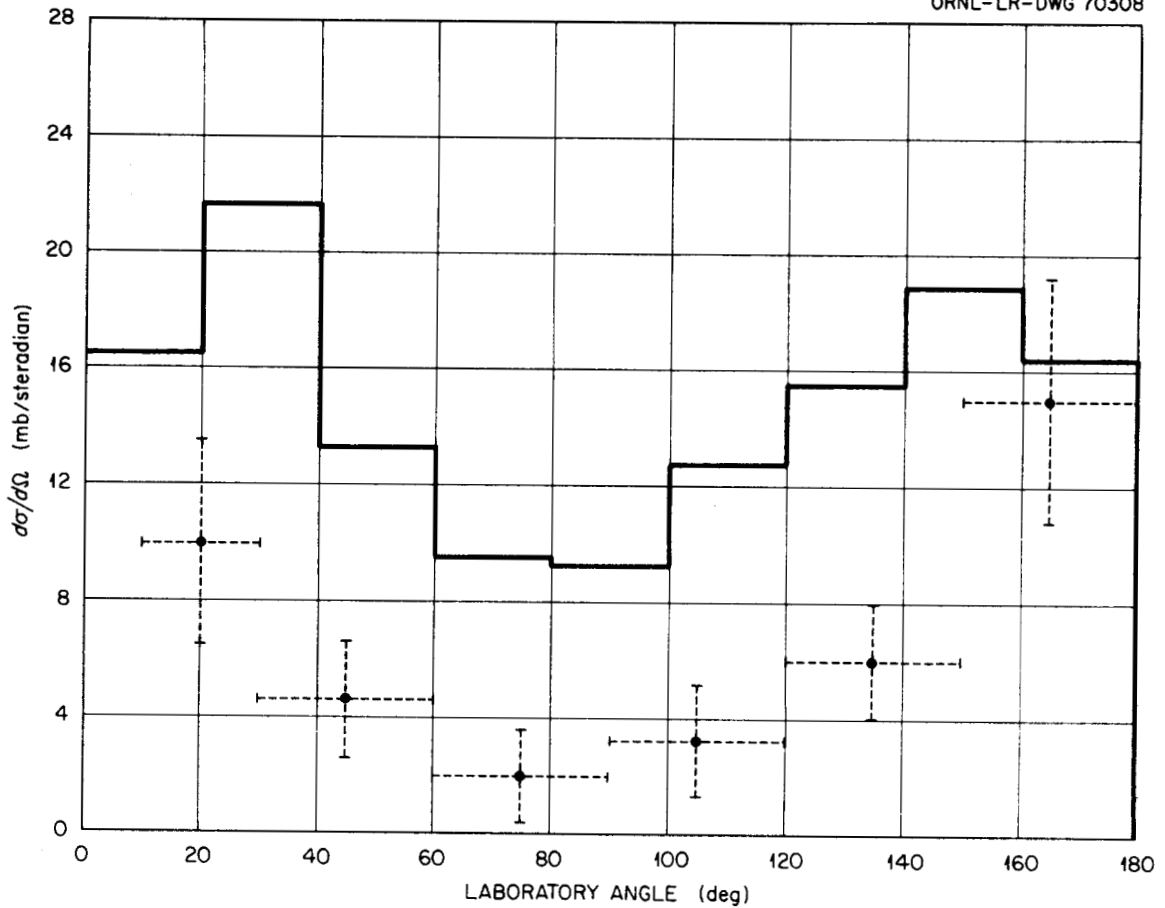


Figure 74. Angular Distribution of Nonelastic  $\pi^+$  from 195-MeV  $\pi^+$  on Lithium. Points: experimental values of Petrov et al. [N. I. Petrov, V. G. Ivanov, and V. A. Rusakov, Soviet Phys.-JETP 10, 682 (1960)]; solid lines: calculated  $\pi^+$  spectrum reduced by the ratio of the experimental to the calculated total nonelastic cross section.

UNCLASSIFIED  
ORNL-LR-DWG 70307

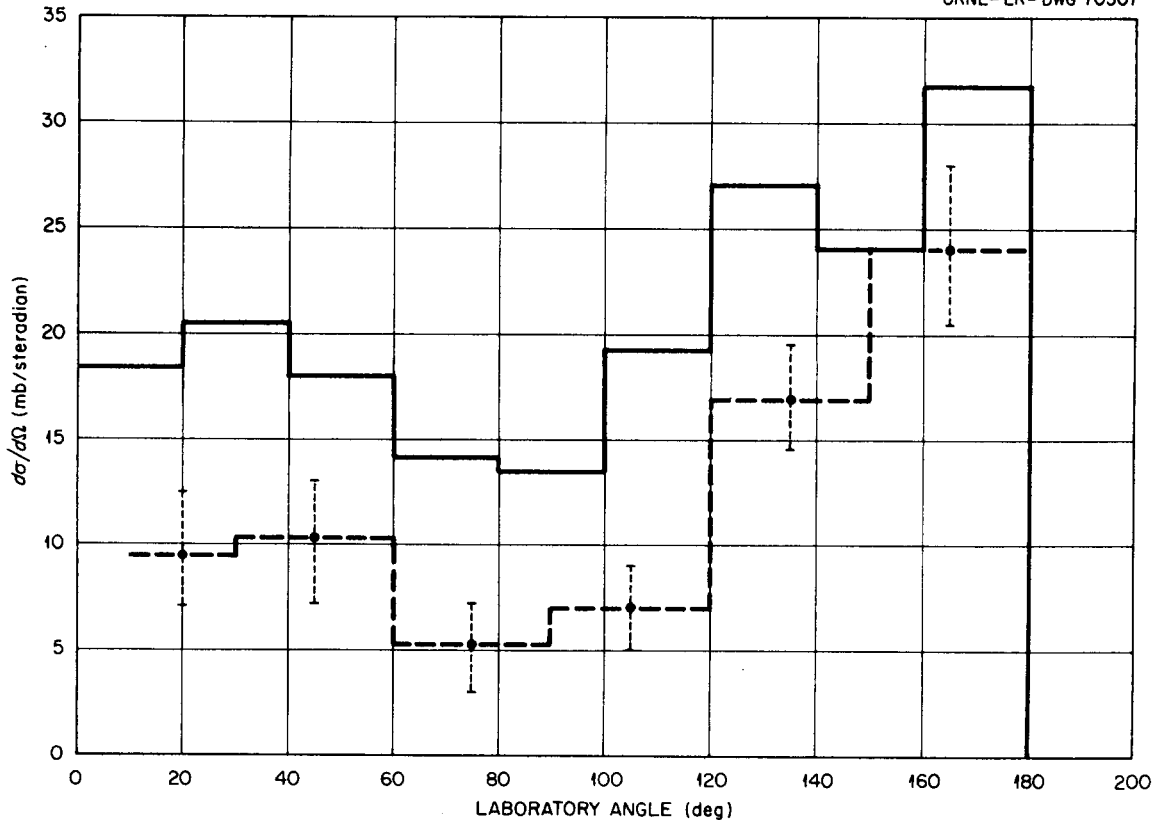


Figure 75. Angular Distribution of Nonelastic  $\pi^+$  from 195-MeV  $\pi^+$  on Carbon. Points: experimental values of Petrov et al. [N. I. Petrov, V. G. Ivanov, and V. A. Rusakov, Soviet Phys.-JETP 10, 682 (1960)]; solid lines: calculated spectrum.

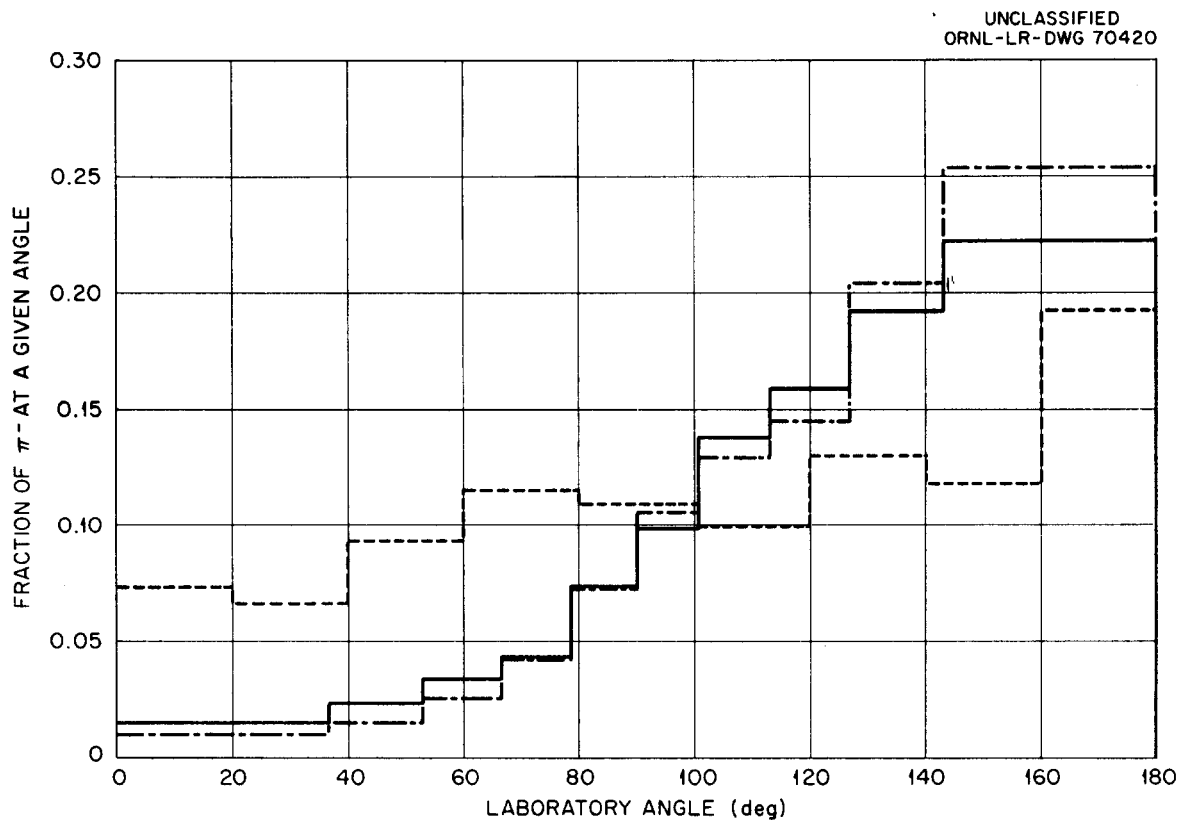


Figure 76. Angular Distribution of Nonelastic  $\pi^-$  from 162-Mev  $\pi^-$  on Heavy Emulsion Nuclei. Calculated distribution for nucleus with small radius. Dashed lines: experimental values of Nikolskii *et al.* [B. A. Nikolskii, L. P. Kudrin, and S. A. Ali-Zade, Soviet Phys.-JETP 5, 93 (1957)]; solid lines: calculated spectra for a nonuniform nucleon density distribution within the nucleus; dash-dotted lines: uniform nucleon density distribution.

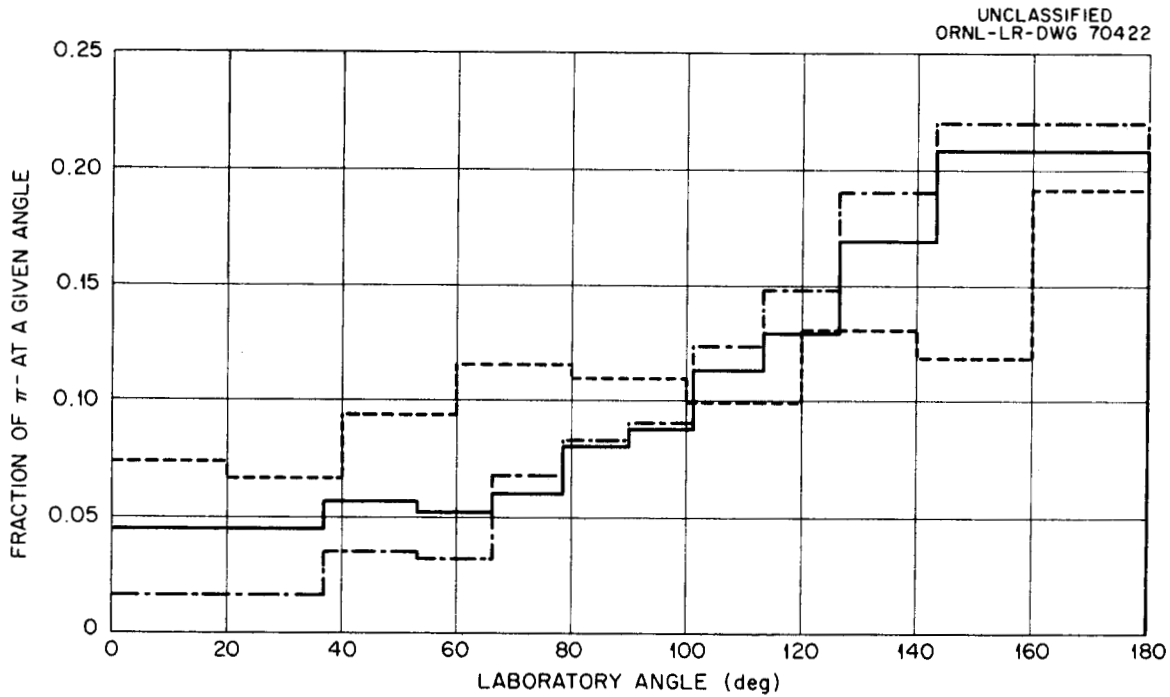


Figure 77. Angular Distribution of Nonelastic  $\pi^-$  from 162-Mev  $\pi^-$  on Heavy Emulsion Nuclei. Calculated distribution for nucleus with medium radius. Dashed lines: experimental values of Nikolskii et al. [B. A. Nikolskii, L. P. Kudrin, and S. A. Ali-Zade, Soviet Phys. JETP 5, 93 (1957)]; solid lines: calculates spectra for a nonuniform nucleon density distribution within the nucleus; dashed-dotted lines: uniform nucleon density distribution.

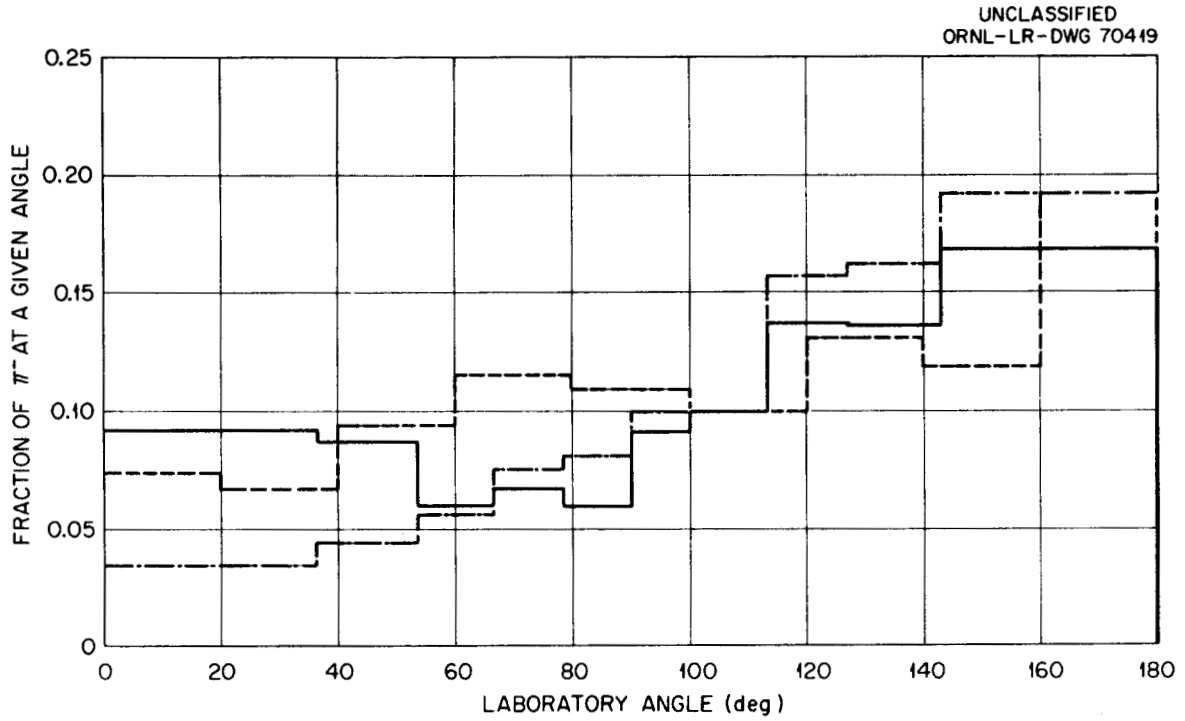


Figure 78. Angular Distribution of Nonelastic  $\pi^-$  from 162-Mev  $\pi^-$  on Heavy Emulsion Nuclei. Calculated distribution for nucleus with large radius. Dashed lines: experimental values of Nikolskii et al. [B. A. Nikolskii, L. P. Kudrin, and S. A. Ali-Zade, Soviet Phys. JETP 5, 93 (1957)]; solid lines: calculated spectra for a nonuniform nucleon density distribution within the nucleus; dash-dotted lines: uniform nucleon density distribution.

UNCLASSIFIED  
ORNL-LR-DWG 70433

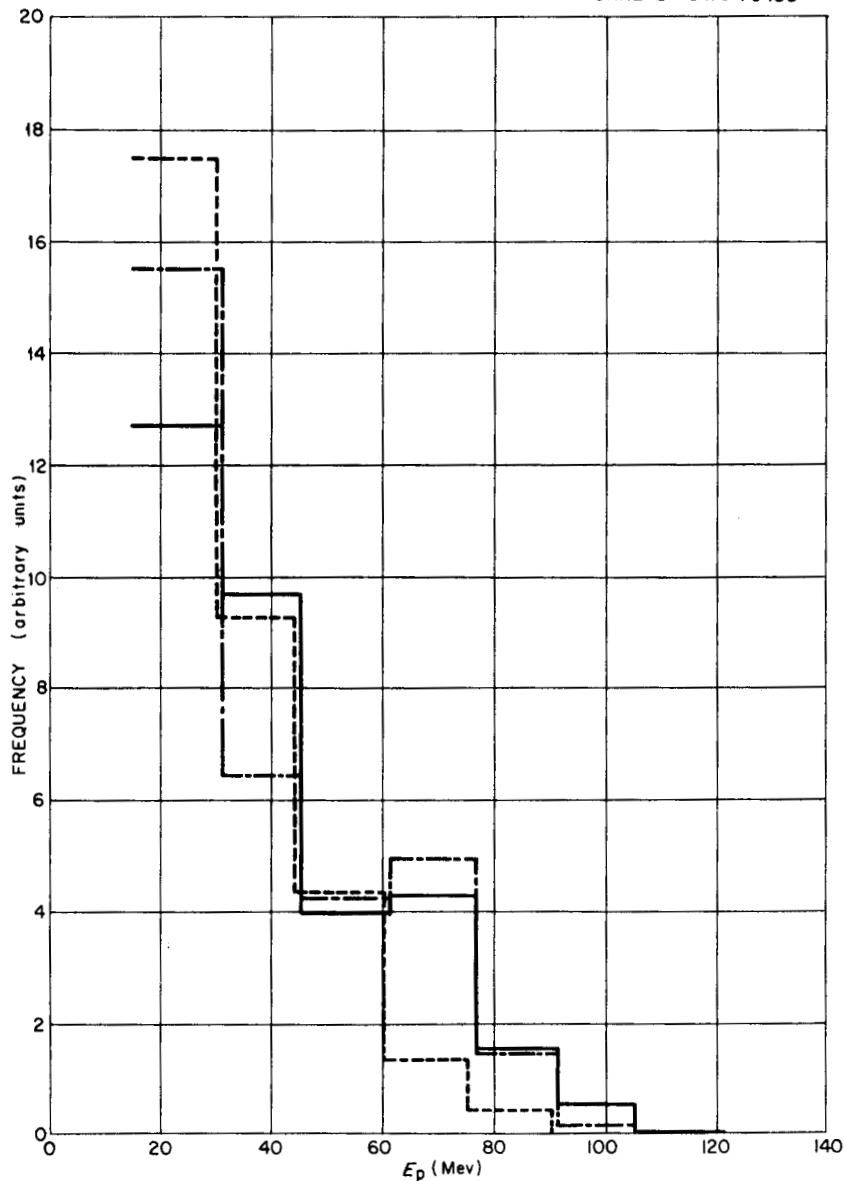


Figure 79. Energy Spectra of Protons with Energies Greater than 15 Mev for Slow  $\pi^-$  Absorption on Heavy Emulsion Nuclei. Calculated values are for 1-Mev  $\pi^-$  on  $\text{Ru}^{100}$ . Solid lines: calculated spectrum for standard nuclear configuration, i.e., medium radius, nonuniform nuclear density distribution within the nucleus; dash-dotted lines: calculated spectrum for small radius configuration with uniform nucleon density distribution within the nucleus; dashed lines: experimental results of Azimov et al. [S. A. Azimov et al., Soviet Phys.-JETP 4, 632 (1957)]. The units of the ordinate scale are arbitrary.

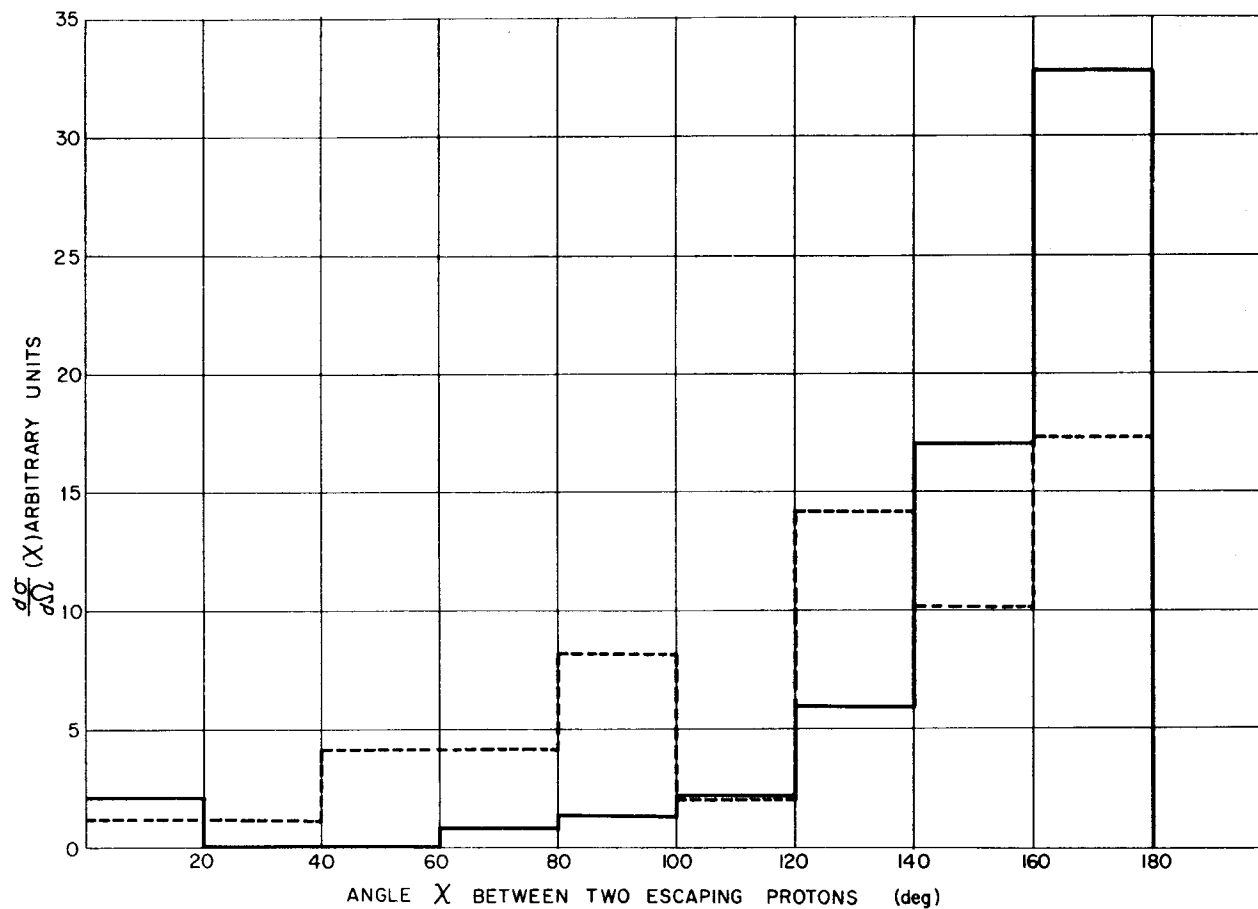


Figure 80. Angular Distribution of Two-Prong Stars as a Function of the Angle Between Them. Prongs result from 50-Mev  $\pi^+$  absorption on carbon. Solid lines: calculated values; dashed lines: experimental values of Laberrigue *et al.* [J. Laberrigue, M. P. Balandine, and S. J. Otvinovski, J. phys. radium 21, 54 (1960)]. The units of the ordinate scale are arbitrary.

## VI. ERRORS

The only error limits that were indicated for the calculated values were those for the total nonelastic cross sections and the (p,pn) cross sections. In these cases they are the limits of the standard 68 per cent confidence interval (plus and minus one standard deviation). The interval associated with the total nonelastic cross sections represent the smallest statistical deviation to be expected from any calculated quantity presented here.

The standard statistical error limits are not included with the other quantities because these error limits are not very meaningful in the opinion of the author and others. The standard error limit represents only the degree of confidence, i.e., the chance that if the calculation were repeated again the estimated mean value would lie between the errors indicated. Nothing at all can be ascertained about the magnitude of the deviation of the estimated mean value from the true mean value of the calculation. On the other hand, experimental error limits are generally meant to bracket the value of the quantity being questioned.

Another difference between the errors associated with experimental measurements and statistical calculations is that in the latter every pertinent event is counted, while generally in the former only a very small fraction of all the pertinent events which actually occur are recorded. The number of source events in the experiment are extremely large compared to those of the calculation so that if one has the same "statistics" in both cases (i.e., number of successful counts) the experimental results are more stable than the calculated values.

The error limits associated with the calculated average excitation energies are about  $\pm 30$  per cent.

A good rule of thumb for estimating the reproducibility of the calculated histograms is to draw an imaginary smooth curve through the histograms and note the deviations from this curve.

## CHAPTER VII

### SUMMARY AND CONCLUSIONS

The range of the cases that have been used in examining this model has been quite extensive. The energies considered for the incident particles have varied from about 50 to 350 Mev while the targets considered have essentially spanned the periodic table.

The following general statements can be made about the degree of validity or limits of application of the approach: With a few exceptions, calculations using the model seem to be capable of reproducing most of the experimental data for the cascade process within or close to the experimental error for incident nucleons. This applies for incident nucleon energies in the range from about 50 to 350 Mev on all but the very lightest elements ( $A < 12$ ). The exceptions are: (a) The cascade particle energy spectrum in the forward direction ( $\lesssim$  twenty degrees) for light- to medium-weight elements for nucleon energies below about 100 Mev; for this case a high-energy peak is predicted where none is observed. (b) The differential nonelastic cross section in the far forward direction ( $\lesssim$  twenty degrees) for nucleon energies of about 100 Mev on heavy elements; the experimental values are higher than those predicted by the calculation.

One cannot make these general statements for cases involving incident pions. The best that can be said for the reactions involving these particles is that the gross features of the reactions should be predicted reasonably well. In demanding specific detailed information, the breakdown of the

predictions occurs for much wider boundaries in the case of incident pions than in the case of nucleons.

One of the reasons for this may be the influence of the  $\pi^+p$  resonance at 200 Mev. The cross section is quite large, which might invalidate the assumption of complete incoherency of the pion-nucleon scattering reactions within the nucleus. The resonance is in the middle of the energy region under test, and escaping its influence is difficult. The prime reason for tabulating the cross sections at such narrow energy intervals (20 Mev) was to attempt to account for the energy dependence of the reactions near the resonance as accurately as possible.

In regard to the nuclear configuration, the conclusion is that in going from a uniform nucleon density distribution within the nucleus to a nonuniform distribution (diffuse nuclear edge) the bulk of the effect comes from the increased nuclear dimensions while the shape of the distribution yields second-order effects. These latter effects are larger for the heaviest nuclei.

It is concluded that only rough predictions for radiochemical cross sections of the type (p,pn) (one- or two-particle emissions) can be made with the combined cascade and evaporation calculation for particle energies in the range considered. These cross sections are extremely sensitive to the nuclear model.

There are three experiments which would be pertinent to some of the discrepancies observed in these comparisons. One would be a check on the symmetry of the results of fast-particle multiplicities when fairly heavy elements are bombarded by neutrons and protons of about the same energy.

Another would be a careful measurement of the pion charge exchange cross section for a few energies and targets. The third would be a measure of the spectrum and multiplicities of the cascade nucleons emitted when pions are inelastically scattered from nuclei. This would help in determining the means by which pions lose so much energy in inelastic scattering collisions with the nuclei, a loss which is not predicted accurately by the free particle-particle concept.

The calculation could be improved by including refraction effects at the nuclear surface and by allowing pion absorption to take place on other clusters besides the two-particle ones included here.

## BIBLIOGRAPHY

## BIBLIOGRAPHY

### BOOKS AND REPORTS

- Bailey, L. E., Angle and Energy Distributions of Charged Particles from the High Energy Nuclear Bombardment of Various Elements, University of California Radiation Laboratory Report, UCRL-3334 (March 1, 1956).
- Bethe, H. A., and F. de Hoffmann, Mesons and Fields, Vol. 2 (Row, Peterson and Company, Evanston, 1955).
- Blatt, J. M., and V. E. Weisskopf, Theoretical Nuclear Physics (John Wiley and Sons, New York, 1952).
- Dresner, L., EVAP - A FORTRAN Program for Calculating the Evaporation from Excited Compound Nuclei, Oak Ridge National Laboratory Report ORNL-CF-61-12-30 (December 19, 1961).
- Gell-Mann, M., and K. M. Watson, Annual Review of Nuclear Science, Vol. 4 (Annual Reviews, Inc., Stanford, 1954).
- Gross, E., Absolute Neutron Spectra from 190-Mev Proton Bombardment of Uranium, University of California Radiation Laboratory Report UCRL-3337 (March 8, 1956).
- Gross, E., The Absolute Yield of Low Energy Neutrons from 190-Mev Proton Bombardment of Gold, Silver, Nickel, Aluminum, and Carbon, University of California Radiation Laboratory Report UCRL-3330 (February 29, 1956).
- Hofman, J. A., Neutrons Ejected from Nuclei by 50-Mev Protons. Cambridge: A Ph.D. Thesis submitted to the Faculty of Arts and Sciences of Harvard University (August, 1952).
- Hughes, D. J., and R. B. Schwartz, Neutron Cross Sections, Brookhaven National Laboratory Report, BNL-325 (July 1, 1958).
- Kahn, Herman, Applications of Monte Carlo, Atomic Energy Commission Report AECU-3259 (April 19, 1954).
- Schiff, L. I., Quantum Mechanics, 2nd ed. (McGraw-Hill, Inc., New York, 1955).
- Zerby, C. D., R. B. Curtis, and H. W. Bertini, The Relativistic Doppler Problem, Oak Ridge National Laboratory Report, ORNL-CF-61-7-20 (July 12, 1961).

JOURNALS

- Anderson, H. L. et al., Phys. Rev. 91, 155 (1953).
- Ashkin, J. et al., Phys. Rev. 96, 1104 (1954).
- Azhgirey, L. S. et al., Nuclear Phys. 13, 258 (1959).
- Azimov, S. A. et al., Soviet Phys.-JETP 4, 632 (1957).
- Beretta, L., C. Ville, and F. Ferrari, Nuovo Cimento 12, 5499 (1954).
- Bernardini, G., E. T. Booth, and S. J. Lindenbaum, Phys. Rev. 88, 1017 (1952).
- Blatt, J. M., and L. C. Biedenharn, Revs. Modern Phys. 24, 258 (1952).
- Blinov, G. A. et al., Soviet Phys.-JETP 8, 609 (1959).
- Brueckner, K. A., R. Serber, and K. M. Watson, Phys. Rev. 84, 258 (1951).
- Burrowes, H. C. et al., Phys. Rev. Letters 2, 119 (1959).
- Caris, J. C. et al., Phys. Rev. 122, 262 (1961).
- Cassels, J. M. et al., Phil. Mag. 42, 215 (1951).
- Chamberlain, O., E. Segre', and C. Wiegand, Phys. Rev. 83, 923 (1951).
- Chamberlain, O., and J. D. Garrison, Phys. Rev. 95, 1349(L) (1954).
- Chang, W. Kan et al., Soviet Phys.-JETP 8, 625 (1959).
- Chen, F. F., C. P. Leavitt, and A. M. Shapiro, Phys. Rev. 103, 211 (1956).
- Cladis, J. B., W. N. Hess, and B. J. Moyer, Phys. Rev. 87, 425 (1952).
- Cook, L. J. et al., Phys. Rev. 75, 7 (1949).
- Cool, R., O. Piccioni, and D. Clark, Phys. Rev. 103, 1082 (1956).
- De Juren, J., and B. J. Moyer, Phys. Rev. 81, 919 (1951).
- De Juren, J., and N. Knable, Phys. Rev. 77, 606 (1950).
- De Sabbata, V., E. Monarisi, and G. Puppi, Nuovo Cimento 10, 1704 (1953).

- Dostrovsky, I., Z. Fraenkel, and G. Friedlander, Phys. Rev. 116, 683 (1959).
- Dowell, J. D. et al., Proc. Phys. Soc. 75, Pt. 1, 24 (1960).
- Fowler, W. B. et al., Phys. Rev. 103, 1479 (1956).
- Frank, R. M., J. L. Gammel, and K. M. Watson, Phys. Rev. 101, 891 (1956).
- Fujii, T. A., Phys. Rev. 113, 695 (1959).
- Goldberger, M. L., Phys. Rev. 74, 1268 (1948).
- Hadley, J. et al., Phys. Rev. 75, 351 (1949).
- Hess, W. N., Revs. Modern Phys. 30, 368 (1958).
- Hofstadter, R., Revs. Modern Phys. 28, 214 (1956).
- Hodgson, P. E., Nucl. Phys. 21, 21 (1960).
- Ivanova, N. S., and I. I. P'anov, Soviet Phys.-JETP 4, 367 (1957).
- Ivanova, V. G. et al., Soviet Phys.-JETP 4, 922 (1957).
- Jannelli, S., and F. Mizzaneres, Nuovo Cimento 4, S939 (1956).
- Kessler, J. O., and L. M. Lederman, Phys. Rev. 94, 689 (1954).
- Krivitskii, V. V., and A. A. Reut, Doklady Akad. Nauk. S.S.S.R. 112, 232 (1957).
- Kruse, U. E., J. M. Teem, and N. F. Ramsey, Phys. Rev. 101, 1079 (1956).
- Laberrigue, J., M. P. Balandine, and S. J. Otvinovski, J. phys. radium 21, 54 (1960).
- Lindenbaum, S. J., and L. C. L. Yuan, Phys. Rev. 100, 306 (1955).
- McManus, H., W. T. Sharp, and H. Gellman, Phys. Rev. 93, 924A (1954).
- Meadows, J. W., Phys. Rev. 98, 744 (1955).
- Menon, M. G. K., H. Muirhead, and O. Rachat, Phil. Mag. 41, 583 (1950).
- Metropolis, N. et al., Phys. Rev. 110, 185 (1958). Part I. Low-Energy Studies.

- Metropolis, N. et al., Phys. Rev. 110, 185 (1958). Part II. Low-Energy Studies.
- Millburn, G. P. et al., Phys. Rev. 95, 1268 (1954).
- Miller, R. H., Nuovo Cimento 6, 882 (1957).
- Nedzel, A. V., Phys. Rev. 94, 174 (1954).
- Nikolskii, B. A., L. P. Kudrin, and S. A. Ali-Zade, Soviet Phys.-JETP 5, (1957).
- Orear, J., Phys. Rev. 100, 288 (1955).
- Ostroumov, V. I., Soviet Phys.-JETP 5, 12 (1957).
- Petrov, N. I., V. G. Ivanov, and V. A. Rusakov, Soviet Phys.-JETP 10, 682 (1960).
- Salukvadze, R. G., and D. Neagu, Soviet Phys.-JETP 14, 59 (1962).
- Saphir, G., Phys. Rev. 104, 535 (1956).
- Serber, R., Phys. Rev. 72, 1114 (1947).
- Smith, L. W., A. W. McReynolds, and G. Snow, Phys. Rev. 97, 1186 (1955).
- Strauch, K., and F. Titus, Phys. Rev. 104, 191 (1956).
- Temmer, G. M., Phys. Rev. 83, 1067 (1951).
- Tenney, F. H., and J. Tinlot, Phys. Rev. 92, 974 (1953).
- Tomasini, A., Nuovo Cimento 3, 160 (1956).
- Wilcox, J. M., and B. J. Moyer, Phys. Rev. 99, 875 (1955).
- Willot-Chemel, B., Ann. Phys. 6, 703 (1961).
- Yule, H. P., and A. Turkevich, Phys. Rev. 118, 1591 (1960).
- Zerby, C. D., Phys. Rev. 124, 2029 (1961).
- Zoki, S. O. et al., Phys. Rev. Letters 4, 533 (1960).

## APPENDIX A

### DERIVATION OF THE PION-NUCLEON DIFFERENTIAL SCATTERING CROSS SECTIONS IN TERMS OF THE PHASE SHIFTS

The symbols that will be used are defined as follows:

- J  $\equiv$  Total angular momentum quantum number,
- M  $\equiv$  Magnetic quantum number for total angular momentum,
- $l$   $\equiv$  Orbital angular momentum quantum number,
- s  $\equiv$  Spin angular momentum quantum number,
- T  $\equiv$  Isotopic spin quantum number,
- m  $\equiv$  Magnetic quantum number for  $l$ , s, or T (designated by a subscript),
- X  $\equiv$  Two-particle spin wave function,
- $\Omega$   $\equiv$  Isotopic spin wave function,
- k  $\equiv$  The wave number multiplied by  $2\pi$  in the center-of-mass system of  
the incident and scattered particle,
- C  $\equiv$  Vector addition coefficients.

When the phase shifts are used in the description of scattering reactions, they give the difference in phase between the asymptotic forms of an undisturbed incident plane wave and the solutions to the wave equation. This approach is generally used in the analysis of collisions between spinless particles interacting through spherically symmetric potentials.<sup>1</sup> When this is done the asymptotic form of the solution to the wave equation is written as

---

<sup>1</sup>L. I. Schiff, Quantum Mechanics (McGraw-Hill, Inc., New York, 1955) 2nd ed., p. 103.

$$\psi \rightarrow \sum_{\ell} \frac{A_{\ell}}{(kr)^{\ell}} \frac{1}{2i} \left[ e^{i(kr - \frac{\ell\pi}{2} + \delta_{\ell})} - e^{-i(kr - \frac{\ell\pi}{2} + \delta_{\ell})} \right] P_{\ell}(\cos\theta),$$

where  $P_{\ell}(\cos\theta)$  are the Legendre polynomials. The asymptotic form of the incident plane wave is

$$\text{Plane Wave} \rightarrow \sum_{\ell} \frac{(2\ell + 1) i^{\ell}}{2ikr} \left[ e^{i(kr - \frac{\ell\pi}{2})} - e^{-i(kr - \frac{\ell\pi}{2})} \right] P_{\ell}(\cos\theta).$$

The spherical scattered wave is obtained from the equation

$$f \frac{e^{ikr}}{r} = \psi - \text{Plane Wave},$$

which leads to

$$f = \frac{1}{2ik} \sum_{\ell} (2\ell + 1) (e^{2i\delta_{\ell}} - 1) P_{\ell}(\cos\theta).$$

The derivation to this point is a standard one and it is given in Schiff.<sup>2</sup>

The term  $A_{\ell}$ , where

$$A_{\ell} = \frac{e^{2i\delta_{\ell}} - 1}{2i},$$

is referred to as the scattering amplitude of the  $\ell^{\text{th}}$  partial wave.

A generalization of this approach can be made for pion-nucleon scattering if one places two restrictions on the forces: (1) the range of the force is finite and (2)  $T$  is a good quantum number.  $\ell$  is a good

---

<sup>2</sup>Ibid.

quantum number for the following reasons: The pion has zero spin and consequently the spin angular momentum quantum number for the pion-nucleon system is  $1/2$  (the spin of the nucleon). Therefore, for each  $J$  value there are two possible  $l$  values ( $l_1 = J + 1/2$ ,  $l_2 = J - 1/2$ ), but the parity of the  $l$  values is not the same since the possible  $l$  values differ by one. Since  $J$  is a good quantum number and parity is a good quantum number, there can be only one  $l$  value present in a given pure state; hence  $l$  remains unchanged in the reaction. The set of good quantum numbers is then  $J$ ,  $M$ ,  $l$ ,  $s$ ,  $T$ , and  $m_T$ . This implies that there is no mixing between these states in the initial plane wave and the same states in the scattered wave. If  $l$ , for example, were not a good quantum number one would have to account for the contributions to each  $l$  state of the scattered wave from all of the  $l$  states in the incident wave. One would then have to formulate the problem in terms of a more general  $S$  matrix.<sup>3</sup> With the restrictions on the quantum numbers and range of the forces, a general solution to the wave equation for large distances can then be written as a sum of terms, each given by

$$\psi_\alpha = \frac{A_\alpha}{(kr)} \frac{1}{2i} \left[ e^{i(kr - \frac{l\pi}{2} + \delta_\alpha)} - e^{-i(kr - \frac{l\pi}{2} + \delta_\alpha)} \right] y_{Jl s}^M \Omega_{M_T}^T,$$

where  $\alpha$  represents the quantum numbers  $J$ ,  $M$ ,  $l$ ,  $s$ ,  $T$ , and  $m_T$ .

$$y_{Jl s}^M = \sum_{m_s} \sum_{m_l = M - m_s} C(l s J; m_l m_s M) Y_l^{m_l} X_{m_s}^s$$

---

<sup>3</sup>J. M. Blatt and L. C. Biedenharn, *Revs. Modern Phys.* 24, 258 (1952).

and  $Y_{\ell}^m$  are the spherical harmonics.<sup>4</sup>

The incident plane wave can be written as

$$e^{i\vec{k}\cdot\vec{r}} \chi_{m_{s_0}}^{s_0} \sum_{T} C(T_1 T_2 T; m_{T_1} m_{T_2} m_{T_0}) \Omega_{m_{T_0}}^T$$

$$= \sqrt{4\pi} \sum_{T} \sum_{\ell=0}^{\infty} C(T_1 T_2 T; m_{T_1} m_{T_2} m_{T_0}) (2\ell + 1)^{1/2} i^{\ell} j_{\ell}(kr) Y_{\ell}^0 \chi_{m_{s_0}}^{s_0} \Omega_{m_{T_0}}^T,$$

where

$$Y_{\ell}^0 = \sqrt{\frac{2\ell + 1}{4\pi}} P_{\ell}(\cos\theta),$$

and  $T_1, T_2, m_{T_1}, m_{T_2}$  are the isotopic spin quantum numbers of the pion and nucleon. The functions  $j_{\ell}(kr)$  are the spherical Bessel functions.<sup>5</sup> The subscript 0 refers to quantum numbers of the initial state.

The quantity  $Y_{\ell}^0 \chi_{m_{s_0}}^{s_0}$  can be expressed in terms of J and M by

$$Y_{\ell}^0 \chi_{m_{s_0}}^{s_0} = \sum_{J=|l-s_0|}^{l+s_0} C(l s_0 J; 0 m_{s_0} M_0) y_{J l s_0}^{M_0}.$$

Then, to simplify the notation, let

$$C(T) = C(T_1 T_2 T; m_{T_1} m_{T_2} m_{T_0})$$

$$C(J) = C(l s_0 J; 0 m_{s_0} M_0)$$

and in these terms the initial plane wave can be written

<sup>4</sup>J. M. Blatt and V. F. Weiskopf, Theoretical Nuclear Physics (John Wiley and Sons, New York, 1952), p. 783.

<sup>5</sup>Schiff, op. cit., p. 77.

$$\begin{aligned}
 & e^{i\bar{k}\cdot\bar{r}} \chi_{m_{s_0}}^{s_0} \sum_T C(T) \Omega_{m_{T_0}}^T \\
 &= \sqrt{4\pi} \sum_T \sum_{\ell=0}^{\infty} \sum_{J=|l-s_0|}^{l+s_0} (2\ell+1)^{1/2} i^\ell j_\ell(kr) C(T) C(J) y_{Jl s_0}^{M_0} \Omega_{m_{T_0}}^T.
 \end{aligned}$$

For large r

$$\begin{aligned}
 \text{Plane Wave} \rightarrow & \sqrt{4\pi} \sum_T \sum_{\ell=0}^{\infty} \sum_{J=|l-s_0|}^{l+s_0} (2\ell+1)^{1/2} \frac{i^\ell}{kr} \frac{1}{2i} \\
 & \left[ e^{i(kr - \frac{l\pi}{2})} - e^{-i(kr - \frac{l\pi}{2})} \right] C(T) C(J) y_{Jl s_0}^{M_0} \Omega_{m_{T_0}}^T.
 \end{aligned}$$

The scattered wave is obtained from the expression

$$\begin{aligned}
 f \frac{e^{ikr}}{r} &= \sum_{\alpha} \psi_{\alpha} - \text{Plane Wave} \\
 &= \sum_{\substack{M, l, T, \\ m_T, s}} \sum_{J=|l-s|}^{l+s} \frac{A_{\alpha}}{kr} \frac{1}{2i} \left[ e^{i(kr - \frac{l\pi}{2} + \delta_{\alpha})} \right. \\
 & \quad \left. - e^{-i(kr - \frac{l\pi}{2} + \delta_{\alpha})} \right] y_{Jl s}^M \Omega_{m_T}^T
 \end{aligned}$$

$$- \sqrt{4\pi} \sum_{T, l} \sum_{J=|l-s_0|}^{l+s_0} (2l+1)^{1/2} \frac{i^l}{kr} \frac{1}{2i} \left[ e^{i(kr - \frac{l\pi}{2})} - e^{-i(kr - \frac{l\pi}{2})} \right] C(T) C(J) y_{Jl s_0}^{M_0} \Omega_{m_{T_0}}^T.$$

$A_\alpha = 0$  when  $s \neq s_0$ ,  $M \neq M_0$ , and  $m_T \neq m_{T_0}$ , since each of these is a good quantum number.

The expression on the left of the equal sign contains terms in  $e^{ikr}$  only; therefore, the terms containing  $e^{-ikr}$  on the right must be equal to zero.

This will be true when

$$A_\alpha e^{-i(kr - \frac{l\pi}{2} + \delta_\alpha)} = \sqrt{4\pi} (2l+1)^{1/2} i^l e^{-i(kr - \frac{l\pi}{2})} C(T) C(J).$$

Making use of the fact that  $(-i)^l = e^{-i \frac{l\pi}{2}}$ , one finds that the coefficient of  $\frac{e^{ikr}}{r}$  in the scattered wave is given by

$$f = \sum_{l, T} \sum_{J=|l-s_0|}^{l+s_0} \sqrt{4\pi} (2l+1)^{1/2} i^l C(T) C(J) (-i)^l \frac{(e^{2i\delta_\alpha} - 1)}{2ik} y_{Jl s_0}^{M_0} \Omega_{m_{T_0}}^T,$$

where

$$y_{Jl s_0}^{M_0} = \sum_{m_s} \sum_{m_l = M_0 - m_s} C(l s_0 J; m_l m_s M_0) Y_l^{m_l} X_{m_s}^{s_0}.$$

Let

$$C(s_0) = C(l s_0 J; m_l m_s M_0)$$

$$a_\alpha = \frac{e^{2i\delta_\alpha} - 1}{2i}.$$

Then

$$f = \frac{1}{k} \sum_{l, T} \sum_{J=|l-s_0|}^{l+s_0} \sum_{m_s} \sum_{m_l=M-m_s} \sqrt{4\pi} (2l+1)^{1/2}$$

$$a_\alpha C(T) C(J) C(s_0) Y_l^m \chi_{m_s}^{s_0} \Omega_{m_{T_0}}^T.$$

The isotopic spin part of the scattered wave must now be written in terms of observable final states.

Let  $T_3$  and  $T_4$  be the isotopic spin quantum numbers of the final state particles, and let  $N$  represent the isotopic spin wave function for one particle. Then

$$\Omega_{m_{T_0}}^T = \sum_{m_{T_3}} \sum_{m_{T_4}=m_{T_0}-m_{T_3}} C(T_3 T_4 T; m_{T_3} m_{T_4} m_{T_0}) N_{m_{T_3}}^{T_3} N_{m_{T_4}}^{T_4}.$$

Let

$$C(T_F) = C(T_3 T_4 T; m_{T_3} m_{T_4} m_{T_0});$$

then

$$f = \frac{\sqrt{4\pi}}{k} \sum_{\ell, T} \sum_{J=|\ell-s_0|}^{\ell+s_0} \sum_{\substack{m_s \\ m_\ell}} \sum_{\substack{m_{T_3} \\ m_{T_4}}} (2\ell + 1)^{1/2} \\ a_\alpha c(T) c(J) c(s_0) c(T_F) Y_\ell^{m_\ell} \chi_{m_s}^{s_0} N_{m_{T_3}}^{T_3} N_{m_{T_4}}^{T_4}.$$

The cross section as the sum over the final states is obtained by setting

$$\frac{d\sigma}{d\Omega} = (f^*f),$$

where the term on the right represents the inner product for the spin and isotopic spin functions. Then

$$\frac{d\sigma}{d\Omega} = \frac{4\pi}{k^2} \sum_{\substack{m_s \\ m_\ell}} \sum_{\substack{M_{T_3} \\ M_{T_4}}} \left| \sum_{\ell, T} \sum_{J=|\ell-s_0|}^{\ell+s_0} (2\ell + 1)^{1/2} a_\alpha c(T) c(J) c(s_0) c(T_F) Y_\ell^{m_\ell} \right|^2.$$

An examination of the final results of this analysis indicates that the differential cross section is the same for each initial spin projection, and therefore there is no need to average over initial states.

In the work that follows, the cross sections for the various pion-nucleon reactions will be expressed in terms of the phase shifts for S and

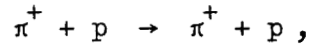
P state scattering only. In the energy range below about 300 Mev the contributions from D states is small.<sup>6</sup>

The subscripts on the scattering amplitudes of the partial waves and the corresponding phase shifts will be the same as those used by Anderson et al.,<sup>7</sup> i.e., a single subscript implies an S state and the subscript will be twice the isotopic spin; a double subscript implies a P state and the first subscript will be twice the isotopic spin of the state and the second will be twice the total angular momentum.

The spherical harmonics used are

$$\begin{aligned}
 Y_0^0 &= \frac{1}{\sqrt{4\pi}} & Y_1^0 &= \sqrt{\frac{3}{4\pi}} \cos\theta \\
 Y_1^1 &= -\sqrt{\frac{3}{8\pi}} \sin\theta e^{i\phi} & Y_1^{-1} &= \sqrt{\frac{3}{8\pi}} \sin\theta e^{-i\phi}.
 \end{aligned}$$

For the reaction



the initial and final quantum numbers involved are

$$\begin{array}{llll}
 T_1 = 1 & m_{T_1} = 1 & T = \frac{3}{2} & m_{T_0} = \frac{3}{2} \\
 T_2 = \frac{1}{2} & m_{T_2} = \frac{1}{2} & s_0 = \frac{1}{2} & m_{s_0} = \frac{1}{2} \\
 T_3 = 1 & m_{T_3} = 1 & & M_0 = \frac{1}{2} \\
 T_4 = \frac{1}{2} & m_{T_4} = \frac{1}{2} & & 
 \end{array}$$

---

<sup>6</sup>H. A. Bethe and F. deHoffman, Mesons and Fields (Row Peterson and Co., Evanston, 1955), Vol. II, p. 63.

<sup>7</sup>H. L. Anderson et al., Phys. Rev. 91, 155 (1953).

$m_{s_0}$  is set equal to  $\frac{1}{2}$  arbitrarily. Then

$$\begin{aligned} \frac{d\sigma}{d\Omega} (\pi^+ + p) = \frac{4\pi}{k^2} \left\{ \left| a_3 Y_0^0 + a_{31} \sqrt{3} \left[ c \left( 1 \frac{1}{2} \frac{1}{2} ; 0 \frac{1}{2} \frac{1}{2} \right) \right]^2 Y_1^0 \right. \right. \\ \left. \left. + a_{33} \sqrt{3} \left[ c \left( 1 \frac{1}{2} \frac{3}{2} ; 0 \frac{1}{2} \frac{1}{2} \right) \right]^2 Y_1^0 \right|^2 \right. \\ \left. + \left| a_{31} \sqrt{3} c \left( 1 \frac{1}{2} \frac{1}{2} ; 0 \frac{1}{2} \frac{1}{2} \right) c \left( 1 \frac{1}{2} \frac{1}{2} ; 1 - \frac{1}{2} \frac{1}{2} \right) Y_1^1 \right. \right. \\ \left. \left. + a_{33} \sqrt{3} c \left( 1 \frac{1}{2} \frac{3}{2} ; 0 \frac{1}{2} \frac{1}{2} \right) c \left( 1 \frac{1}{2} \frac{3}{2} ; 1 - \frac{1}{2} \frac{1}{2} \right) Y_1^1 \right|^2 \right\}. \end{aligned}$$

The terms within the first set of absolute value symbols contribute to the "direct" scattering; those within the second set make up the "spin-flip" scattering. When the algebra is carried out the result is

$$\begin{aligned} \frac{d\sigma}{d\Omega} (\pi^+ + p) = \frac{1}{k^2} \left\{ \frac{1}{2} [2 - \cos 2\delta_3 - \cos 2(\delta_{33} - \delta_{31})] \right. \\ \left. + \frac{1}{2} [2 \cos 2(\delta_{33} - \delta_3) + \cos 2(\delta_{31} - \delta_3) - 3 \cos 2\delta_3 \right. \\ \left. - 2 \cos 2\delta_{33} - \cos 2\delta_{31} + 3] \cos \theta \right. \\ \left. + \frac{3}{2} [2 + \cos 2(\delta_{33} - \delta_{31}) - 2 \cos 2\delta_{33} \right. \\ \left. - \cos 2\delta_{31}] \cos^2 \theta \right\}. \end{aligned}$$

In  $\pi^- + p$  scattering, both the elastic and charge exchange cross sections are obtained when the sum is taken over the final isotopic spin states. The set of quantum numbers to be used are

$$\begin{array}{lll}
 T_1 = 1 & m_{T_1} = -1 & m_{T_0} = -\frac{1}{2} \\
 T_2 = \frac{1}{2} & m_{T_2} = \frac{1}{2} & s_0 = \frac{1}{2} \quad m_{s_0} = \frac{1}{2} \\
 T_3 = 1 & m_{T_3} = \begin{cases} -1 \\ 0 \end{cases} & M_0 = \frac{1}{2} \\
 T_4 = \frac{1}{2} & m_{T_4} = \begin{cases} \frac{1}{2} \\ -\frac{1}{2} \end{cases} & 
 \end{array}$$

For  $\pi^- + p$  scattering,

$$\begin{aligned}
 \frac{d\sigma}{d\Omega} = & \frac{4\pi}{k^2} \left\{ a_3 \left[ c \left( 1 \frac{1}{2} \frac{3}{2}; -1 \frac{1}{2} - \frac{1}{2} \right) \right]^2 Y_0^0 + a_1 \left[ c \left( 1 \frac{1}{2} \frac{1}{2}; -1 \frac{1}{2} - \frac{1}{2} \right) \right]^2 Y_0^0 \right. \\
 & + a_{31} \sqrt{3} \left[ c \left( 1 \frac{1}{2} \frac{3}{2}; -1 \frac{1}{2} - \frac{1}{2} \right) c \left( 1 \frac{1}{2} \frac{1}{2}; 0 \frac{1}{2} \frac{1}{2} \right) \right]^2 Y_1^0 \\
 & + a_{11} \sqrt{3} \left[ c \left( 1 \frac{1}{2} \frac{1}{2}; -1 \frac{1}{2} - \frac{1}{2} \right) c \left( 1 \frac{1}{2} \frac{1}{2}; 0 \frac{1}{2} \frac{1}{2} \right) \right]^2 Y_1^0 \\
 & + a_{33} \sqrt{3} \left[ c \left( 1 \frac{1}{2} \frac{3}{2}; -1 \frac{1}{2} - \frac{1}{2} \right) c \left( 1 \frac{1}{2} \frac{3}{2}; 0 \frac{1}{2} \frac{1}{2} \right) \right]^2 Y_1^0 \\
 & \left. + a_{13} \sqrt{3} \left[ c \left( 1 \frac{1}{2} \frac{1}{2}; -1 \frac{1}{2} - \frac{1}{2} \right) c \left( 1 \frac{1}{2} \frac{3}{2}; 0 \frac{1}{2} \frac{1}{2} \right) \right]^2 Y_1^0 \right\}^2
 \end{aligned}$$

$$\begin{aligned}
 & + \left| a_{31} \sqrt{3} \left[ c \left( 1 \frac{1}{2} \frac{3}{2} ; -1 \frac{1}{2} - \frac{1}{2} \right) \right]^2 c \left( 1 \frac{1}{2} \frac{1}{2} ; 0 \frac{1}{2} \frac{1}{2} \right) c \left( 1 \frac{1}{2} \frac{1}{2} ; 1 - \frac{1}{2} \frac{1}{2} \right) Y_1^1 \right. \\
 & + a_{11} \sqrt{3} \left[ c \left( 1 \frac{1}{2} \frac{1}{2} ; -1 \frac{1}{2} - \frac{1}{2} \right) \right]^2 c \left( 1 \frac{1}{2} \frac{1}{2} ; 0 \frac{1}{2} \frac{1}{2} \right) c \left( 1 \frac{1}{2} \frac{1}{2} ; 1 - \frac{1}{2} \frac{1}{2} \right) Y_1^1 \\
 & + a_{33} \sqrt{3} \left[ c \left( 1 \frac{1}{2} \frac{3}{2} ; -1 \frac{1}{2} - \frac{1}{2} \right) \right]^2 c \left( 1 \frac{1}{2} \frac{3}{2} ; 0 \frac{1}{2} \frac{1}{2} \right) c \left( 1 \frac{1}{2} \frac{3}{2} ; 1 - \frac{1}{2} \frac{1}{2} \right) Y_1^1 \\
 & + a_{13} \sqrt{3} \left[ c \left( 1 \frac{1}{2} \frac{1}{2} ; -1 \frac{1}{2} - \frac{1}{2} \right) \right]^2 c \left( 1 \frac{1}{2} \frac{3}{2} ; 0 \frac{1}{2} \frac{1}{2} \right) c \left( 1 \frac{1}{2} \frac{3}{2} ; 1 - \frac{1}{2} \frac{1}{2} \right) Y_1^1 \Big|^2 \\
 & + \left| a_3 c \left( 1 \frac{1}{2} \frac{3}{2} ; -1 \frac{1}{2} - \frac{1}{2} \right) c \left( 1 \frac{1}{2} \frac{3}{2} ; 0 - \frac{1}{2} - \frac{1}{2} \right) Y_0^0 \right. \\
 & + a_1 c \left( 1 \frac{1}{2} \frac{1}{2} ; -1 \frac{1}{2} - \frac{1}{2} \right) c \left( 1 \frac{1}{2} \frac{1}{2} ; 0 - \frac{1}{2} - \frac{1}{2} \right) Y_0^0 \\
 & + a_{31} \sqrt{3} c \left( 1 \frac{1}{2} \frac{3}{2} ; -1 \frac{1}{2} - \frac{1}{2} \right) \left[ c \left( 1 \frac{1}{2} \frac{1}{2} ; 0 \frac{1}{2} \frac{1}{2} \right) \right]^2 c \left( 1 \frac{1}{2} \frac{3}{2} ; 0 - \frac{1}{2} - \frac{1}{2} \right) Y_1^0 \\
 & + a_{11} \sqrt{3} c \left( 1 \frac{1}{2} \frac{1}{2} ; -1 \frac{1}{2} - \frac{1}{2} \right) \left[ c \left( 1 \frac{1}{2} \frac{1}{2} ; 0 \frac{1}{2} \frac{1}{2} \right) \right]^2 c \left( 1 \frac{1}{2} \frac{1}{2} ; 0 - \frac{1}{2} - \frac{1}{2} \right) Y_1^0 \\
 & + a_{33} \sqrt{3} c \left( 1 \frac{1}{2} \frac{3}{2} ; -1 \frac{1}{2} - \frac{1}{2} \right) \left[ c \left( 1 \frac{1}{2} \frac{3}{2} ; 0 \frac{1}{2} \frac{1}{2} \right) \right]^2 c \left( 1 \frac{1}{2} \frac{3}{2} ; 0 - \frac{1}{2} - \frac{1}{2} \right) Y_1^0 \\
 & + a_{13} \sqrt{3} c \left( 1 \frac{1}{2} \frac{1}{2} ; -1 \frac{1}{2} - \frac{1}{2} \right) \left[ c \left( 1 \frac{1}{2} \frac{3}{2} ; 0 \frac{1}{2} \frac{1}{2} \right) \right]^2 c \left( 1 \frac{1}{2} \frac{1}{2} ; 0 - \frac{1}{2} - \frac{1}{2} \right) Y_1^0 \Big|^2
 \end{aligned}$$

$$\begin{aligned}
 & + |a_{31}| \sqrt{3} c \left( 1 \frac{1}{2} \frac{3}{2}; -1 \frac{1}{2} - \frac{1}{2} \right) c \left( 1 \frac{1}{2} \frac{1}{2}; 0 \frac{1}{2} \frac{1}{2} \right) c \left( 1 \frac{1}{2} \frac{1}{2}; 1 - \frac{1}{2} \frac{1}{2} \right) \\
 & \quad \times c \left( 1 \frac{1}{2} \frac{3}{2}; 0 - \frac{1}{2} - \frac{1}{2} \right) Y_1^1 \\
 & + a_{11} \sqrt{3} c \left( 1 \frac{1}{2} \frac{1}{2}; -1 \frac{1}{2} - \frac{1}{2} \right) c \left( 1 \frac{1}{2} \frac{1}{2}; 0 \frac{1}{2} \frac{1}{2} \right) c \left( 1 \frac{1}{2} \frac{1}{2}; 1 - \frac{1}{2} \frac{1}{2} \right) \\
 & \quad \times c \left( 1 \frac{1}{2} \frac{1}{2}; 0 - \frac{1}{2} - \frac{1}{2} \right) Y_1^1 \\
 & + a_{33} \sqrt{3} c \left( 1 \frac{1}{2} \frac{3}{2}; -1 \frac{1}{2} - \frac{1}{2} \right) c \left( 1 \frac{1}{2} \frac{3}{2}; 0 \frac{1}{2} \frac{1}{2} \right) c \left( 1 \frac{1}{2} \frac{3}{2}; 1 - \frac{1}{2} \frac{1}{2} \right) \\
 & \quad \times c \left( 1 \frac{1}{2} \frac{3}{2}; 0 - \frac{1}{2} - \frac{1}{2} \right) Y_1^1 \\
 & + a_{13} \sqrt{3} c \left( 1 \frac{1}{2} \frac{1}{2}; -1 \frac{1}{2} - \frac{1}{2} \right) c \left( 1 \frac{1}{2} \frac{3}{2}; 0 \frac{1}{2} \frac{1}{2} \right) c \left( 1 \frac{1}{2} \frac{3}{2}; 1 - \frac{1}{2} \frac{1}{2} \right) \\
 & \quad \times c \left( 1 \frac{1}{2} \frac{1}{2}; 0 - \frac{1}{2} - \frac{1}{2} \right) Y_1^1 \left. \right\}^2.
 \end{aligned}$$

The first two pairs of absolute value signs represent the elastic scattering, and the last two pairs represent the charge exchange scattering. The first set in each pair represents the direct scattering, and the second set in each pair represents the spin-flip scattering.

The cross section for the  $\pi^- + p$  elastic scattering expressed in terms of the phase shifts is

$$\begin{aligned}
 \frac{d\sigma}{d\Omega} = \frac{1}{k^2} & \left\{ \frac{1}{9} \left[ 6 + \cos 2(\delta_1 - \delta_3) - \frac{3}{2} \cos 2\delta_3 - 3 \cos 2\delta_1 + \cos 2(\delta_{33} - \delta_{13}) \right. \right. \\
 & - 2 \cos 2(\delta_{11} - \delta_{13}) - \cos 2(\delta_{31} - \delta_{13}) - \cos 2(\delta_{11} - \delta_{33}) \\
 & \left. \left. - \frac{1}{2} \cos 2(\delta_{31} - \delta_{33}) + \cos 2(\delta_{31} - \delta_{11}) \right] \right. \\
 & + \frac{1}{9} \left[ 13.5 + \frac{1}{2} \cos 2(\delta_{31} - \delta_3) + \cos 2(\delta_{11} - \delta_3) + \cos 2(\delta_{33} - \delta_3) \right. \\
 & + 2 \cos 2(\delta_{13} - \delta_3) + \cos 2(\delta_{31} - \delta_1) + 2 \cos 2(\delta_{11} - \delta_1) \\
 & + 2 \cos 2(\delta_{33} - \delta_1) + 4 \cos 2(\delta_{13} - \delta_1) - \frac{9}{2} \cos 2\delta_3 \\
 & \left. \left. - 9 \cos 2\delta_1 - \frac{3}{2} \cos 2\delta_{31} - 3 \cos 2\delta_{11} - 3 \cos 2\delta_{33} - 6 \cos 2\delta_{13} \right] \cos \theta \right. \\
 & + \frac{1}{3} \left[ 8 + \frac{1}{2} \cos 2(\delta_{33} - \delta_{31}) + \cos 2(\delta_{13} - \delta_{31}) - \frac{3}{2} \cos 2\delta_{31} \right. \\
 & + \cos 2(\delta_{33} - \delta_{11}) + 2 \cos 2(\delta_{13} - \delta_{11}) - 3 \cos 2\delta_{11} \\
 & \left. \left. + \cos 2(\delta_{33} - \delta_{13}) - 3 \cos 2\delta_{33} - 6 \cos 2\delta_{13} \right] \cos^2 \theta \right\} .
 \end{aligned}$$

The cross section for  $\pi^- + p$  charge exchange scattering expressed in terms of the phase shifts is

$$\begin{aligned}
 \frac{d\sigma}{d\Omega} = \frac{1}{k^2} & \left\{ \frac{1}{9} \left[ 3 - \cos 2(\delta_3 - \delta_1) + \cos 2(\delta_{33} - \delta_{11}) - \cos 2(\delta_{31} - \delta_{11}) \right. \right. \\
 & - \cos 2(\delta_{13} - \delta_{11}) - \cos 2(\delta_{33} - \delta_{31}) + \cos 2(\delta_{13} - \delta_{31}) \\
 & \left. \left. - \cos 2(\delta_{13} - \delta_{33}) \right] \right. \\
 & + \frac{1}{9} \left[ \cos 2(\delta_{31} - \delta_3) - \cos 2(\delta_{11} - \delta_3) + 2 \cos 2(\delta_{33} - \delta_3) \right. \\
 & - 2 \cos 2(\delta_{13} - \delta_3) - \cos 2(\delta_{31} - \delta_1) + \cos 2(\delta_{11} - \delta_1) \\
 & \left. - 2 \cos 2(\delta_{33} - \delta_1) + 2 \cos 2(\delta_{13} - \delta_1) \right] \cos \theta \\
 & + \frac{1}{3} \left[ 1 + \cos 2(\delta_{33} - \delta_{31}) - \cos 2(\delta_{13} - \delta_{31}) - \cos 2(\delta_{33} - \delta_{11}) \right. \\
 & \left. + \cos 2(\delta_{13} - \delta_{11}) - \cos 2(\delta_{13} - \delta_{33}) \right] \cos^2 \theta \left. \right\} .
 \end{aligned}$$

By using the same procedure, one finds that the cross sections for the following reactions are equal:

For charge exchange scattering,

$$\frac{d\sigma}{d\Omega} (\pi^- + p) = \frac{d\sigma}{d\Omega} (\pi^+ + n) = \frac{d\sigma}{d\Omega} (\pi^0 + p) = \frac{d\sigma}{d\Omega} (\pi^0 + n) .$$

For elastic scattering,

$$\frac{d\sigma}{d\Omega} (\pi^- + p) = \frac{d\sigma}{d\Omega} (\pi^+ + n)$$

$$\frac{d\sigma}{d\Omega} (\pi^+ + p) = \frac{d\sigma}{d\Omega} (\pi^- + n)$$

$$\frac{d\sigma}{d\Omega} (\pi^0 + p) = \frac{d\sigma}{d\Omega} (\pi^0 + n).$$

The cross section for  $\pi^0 + p$  elastic scattering is the only one remaining that needs to be expressed in terms of the phase shifts.

The initial and final state quantum numbers for this reaction are

$$\begin{array}{llll} T_1 = 1 & m_{T_1} = 0 & & m_{T_0} = \frac{1}{2} \\ T_2 = \frac{1}{2} & m_{T_2} = \frac{1}{2} & s_0 = \frac{1}{2} & m_{s_0} = \frac{1}{2} \\ T_3 = 1 & m_{T_3} = 0 & & M_0 = \frac{1}{2} \\ T_4 = \frac{1}{2} & m_{T_4} = \frac{1}{2} & & \end{array}$$

and the cross section for elastic scattering is

$$\begin{aligned} \frac{d\sigma}{d\Omega} = \frac{4\pi}{k^2} & \left\{ a_3 c \left( 1 \frac{1}{2} \frac{3}{2} ; 0 \frac{1}{2} \frac{1}{2} \right) c \left( 1 \frac{1}{2} \frac{3}{2} ; 0 \frac{1}{2} \frac{1}{2} \right) Y_0^0 \right. \\ & + a_1 \left[ c \left( 1 \frac{1}{2} \frac{1}{2} ; 0 \frac{1}{2} \frac{1}{2} \right) \right]^2 Y_0^0 \\ & + a_{31} \sqrt{3} \left[ c \left( 1 \frac{1}{2} \frac{3}{2} ; 0 \frac{1}{2} \frac{1}{2} \right) \right]^2 \left[ c \left( 1 \frac{1}{2} \frac{1}{2} ; 0 \frac{1}{2} \frac{1}{2} \right) \right]^2 Y_1^0 \end{aligned}$$

$$\begin{aligned}
 & + a_{11} \sqrt{3} \left[ c \left( 1 \frac{1}{2} \frac{1}{2} ; 0 \frac{1}{2} \frac{1}{2} \right) \right]^2 \left[ c \left( 1 \frac{1}{2} \frac{1}{2} ; 0 \frac{1}{2} \frac{1}{2} \right) \right]^2 Y_1^0 \\
 & + a_{33} \sqrt{3} \left[ c \left( 1 \frac{1}{2} \frac{3}{2} ; 0 \frac{1}{2} \frac{1}{2} \right) \right]^2 \left[ c \left( 1 \frac{1}{2} \frac{3}{2} ; 0 \frac{1}{2} \frac{1}{2} \right) \right]^2 Y_1^0 \\
 & + a_{13} \sqrt{3} \left[ c \left( 1 \frac{1}{2} \frac{1}{2} ; 0 \frac{1}{2} \frac{1}{2} \right) \right]^2 \left[ c \left( 1 \frac{1}{2} \frac{3}{2} ; 0 \frac{1}{2} \frac{1}{2} \right) \right]^2 Y_1^0 \Big|^2 \\
 & + \left| a_{31} \sqrt{3} \left[ c \left( 1 \frac{1}{2} \frac{3}{2} ; 0 \frac{1}{2} \frac{1}{2} \right) \right]^2 c \left( 1 \frac{1}{2} \frac{1}{2} ; 0 \frac{1}{2} \frac{1}{2} \right) c \left( 1 \frac{1}{2} \frac{1}{2} ; 1 - \frac{1}{2} \frac{1}{2} \right) Y_1^1 \right. \\
 & + a_{11} \sqrt{3} \left[ c \left( 1 \frac{1}{2} \frac{1}{2} ; 0 \frac{1}{2} \frac{1}{2} \right) \right]^2 c \left( 1 \frac{1}{2} \frac{1}{2} ; 0 \frac{1}{2} \frac{1}{2} \right) c \left( 1 \frac{1}{2} \frac{1}{2} ; 1 - \frac{1}{2} \frac{1}{2} \right) Y_1^1 \\
 & + a_{33} \sqrt{3} \left[ c \left( 1 \frac{1}{2} \frac{3}{2} ; 0 \frac{1}{2} \frac{1}{2} \right) \right]^2 c \left( 1 \frac{1}{2} \frac{3}{2} ; 0 \frac{1}{2} \frac{1}{2} \right) c \left( 1 \frac{1}{2} \frac{3}{2} ; 1 - \frac{1}{2} \frac{1}{2} \right) Y_1^1 \\
 & \left. + a_{13} \sqrt{3} \left[ c \left( 1 \frac{1}{2} \frac{1}{2} ; 0 \frac{1}{2} \frac{1}{2} \right) \right]^2 c \left( 1 \frac{1}{2} \frac{3}{2} ; 0 \frac{1}{2} \frac{1}{2} \right) c \left( 1 \frac{1}{2} \frac{3}{2} ; 1 - \frac{1}{2} \frac{1}{2} \right) Y_1^1 \right|^2 \Big\} .
 \end{aligned}$$

In terms of the phase shifts,

$$\begin{aligned}
 \frac{d\sigma}{d\Omega} = \frac{1}{k^2} \Big\{ & \frac{1}{9} \left[ 6 + \cos 2(\delta_1 - \delta_3) - 3 \cos 2\delta_3 - \frac{3}{2} \cos 2\delta_1 - \frac{1}{2} \cos 2(\delta_{11} - \delta_{13}) \right. \\
 & - \cos 2(\delta_{31} - \delta_{13}) + \cos 2(\delta_{33} - \delta_{13}) + \cos 2(\delta_{31} - \delta_{11}) \\
 & \left. - \cos 2(\delta_{33} - \delta_{11}) - 2 \cos 2(\delta_{33} - \delta_{31}) \right] \Big\} .
 \end{aligned}$$

$$\begin{aligned}
 & + \frac{1}{9} \left[ \cos 2(\delta_{11} - \delta_3) + 2 \cos 2(\delta_{31} - \delta_3) + 2 \cos 2(\delta_{13} - \delta_3) \right. \\
 & \quad + 4 \cos 2(\delta_{33} - \delta_3) - 9 \cos 2\delta_3 + \frac{1}{2} \cos 2(\delta_{11} - \delta_1) \\
 & \quad + \cos 2(\delta_{31} - \delta_1) + \cos 2(\delta_{13} - \delta_1) + 2 \cos 2(\delta_{33} - \delta_1) \\
 & \quad - 4.5 \cos 2\delta_1 - \frac{3}{2} \cos 2\delta_{11} - 3 \cos 2\delta_{31} \\
 & \quad \left. - 3 \cos 2\delta_{13} - 6 \cos 2\delta_{33} + 13.5 \right] \cos \theta \\
 & + \frac{1}{3} \left[ 8 + \frac{1}{2} \cos 2(\delta_{13} - \delta_{11}) + \cos 2(\delta_{33} - \delta_{11}) - 1.5 \cos 2\delta_{11} \right. \\
 & \quad + \cos 2(\delta_{13} - \delta_{31}) + 2 \cos 2(\delta_{33} - \delta_{31}) - 3 \cos 2\delta_{31} \\
 & \quad \left. + \cos 2(\delta_{33} - \delta_{13}) - 3 \cos 2\delta_{13} - 6 \cos 2\delta_{33} \right] \cos^2 \theta \}.
 \end{aligned}$$

## APPENDIX B

### TWO-PARTICLE RELATIVISTIC KINEMATICS

The equations derived below are the ones used to describe the kinematics of the particle-particle collisions that are assumed to occur within the nucleus. Although the approach is a standard one, the equations for the reactions involved are difficult to find in the literature, so they are given here. The equations give the momentum and energy of the collision products for a reaction in which the known quantities are the masses of the initial and final particles, the scattering angles in the center of mass system, and the momenta of the initial particles. A system of units is used in which  $h = c = 1$ .

The symbols that are used are defined as follows: the unprimed quantities refer to the laboratory frame; the primed quantities refer to the moving frame. The subscripts 1 and 2 refer to the initial particles; subscripts 3 and 4 refer to the final particles. The subscripts  $\parallel$  and  $\perp$  indicate parallel and perpendicular components of a vector.

$\bar{V} \equiv$  Velocity of moving frame,

$\bar{r} \equiv$  Spatial vector,  $\bar{r}(x, y, z)$ ,

$t \equiv$  Time,

$m \equiv$  Rest mass,

$\bar{p} \equiv$  Momentum,  $\bar{p}(p_x, p_y, p_z)$ ,

$E \equiv$  Total energy ( $E = \sqrt{p^2 + m^2}$ ).

In the standard relativistic transformation where the moving frame is traveling in the  $z$  direction with speed  $V$  and where the coordinate axes of the fixed frame and the moving frame are parallel, the  $z$  and  $t$  components of a four-vector transform as

$$z' = \frac{z - Vt}{\sqrt{1 - V^2}},$$

$$t' = \frac{t - Vz}{\sqrt{1 - V^2}}.$$

One can generalize from this to the case of a moving frame with velocity  $\bar{V}$  for any orientation of the two sets of axes by writing down the transformation equations of a vector  $\bar{r}$  in terms of its components parallel and perpendicular to  $\bar{V}$  :

$$\bar{r}'_{\parallel} = \frac{\bar{r}_{\parallel} - \bar{V}t}{\sqrt{1 - V^2}}, \quad \bar{r}'_{\perp} = \bar{r}_{\perp},$$

$$t' = \frac{t - \bar{r} \cdot \bar{V}}{\sqrt{1 - V^2}}.$$

In order to express all quantities in terms of  $\bar{r}$ ,  $\bar{V}$ , and  $t$ , one can write

$$\bar{r}_{\parallel} = \frac{(\bar{r} \cdot \bar{V})}{V} \frac{\bar{V}}{V},$$

$$\begin{aligned} \bar{r}_{\perp} &= \bar{r} - \bar{r}_{\parallel} \\ &= \bar{r} - \left( \frac{\bar{r} \cdot \bar{V}}{V^2} \right) \bar{V}, \end{aligned}$$

$$\bar{r}'_{\parallel} = \frac{(\bar{r} \cdot \bar{V}) \frac{\bar{V}}{v^2} - \bar{V}t}{\sqrt{1 - v^2}}, \quad \bar{r}'_{\perp} = \bar{r} - (\bar{r} \cdot \bar{V}) \frac{\bar{V}}{v^2},$$

$$\bar{r}' = \bar{r}'_{\parallel} + \bar{r}'_{\perp} = \bar{r} + \frac{(\bar{r} \cdot \bar{V}) \bar{V}}{v^2} \left[ \frac{1}{\sqrt{1 - v^2}} - 1 \right] - \frac{\bar{V}t}{\sqrt{1 - v^2}},$$

$$t' = \frac{t - (\bar{r} \cdot \bar{V})}{\sqrt{1 - v^2}}.$$

The components of the four-momentum vector transform like those of the space-time vector; hence for the particles involved in a collision one can write

$$\bar{p}'_1 = \bar{p}_1 + \frac{\bar{V}(\bar{p}_1 \cdot \bar{V})}{v^2} \left( \frac{1}{\sqrt{1 - v^2}} - 1 \right) - \frac{\bar{V}E_1}{\sqrt{1 - v^2}}; \quad E'_1 = \frac{E_1 - \bar{p}_1 \cdot \bar{V}}{\sqrt{1 - v^2}},$$

$$\bar{p}'_2 = \bar{p}_2 + \frac{\bar{V}(\bar{p}_2 \cdot \bar{V})}{v^2} \left( \frac{1}{\sqrt{1 - v^2}} - 1 \right) - \frac{\bar{V}E_2}{\sqrt{1 - v^2}}; \quad E'_2 = \frac{E_2 - \bar{p}_2 \cdot \bar{V}}{\sqrt{1 - v^2}}.$$

To find the velocity of the frame that represents the center-of-mass system, the C system (more correctly the center of momentum system), one sets

$$\bar{p}'_1 + \bar{p}'_2 = 0$$

and solves for  $\bar{V}$ .

$$(\bar{p}_1 + \bar{p}_2) + \frac{\bar{V}[(\bar{p}_1 + \bar{p}_2) \cdot \bar{V}]}{v^2} \left( \frac{1}{\sqrt{1 - v^2}} - 1 \right) - \frac{\bar{V}(E_1 + E_2)}{\sqrt{1 - v^2}} = 0.$$

Let

$$\bar{p} = \bar{p}_1 + \bar{p}_2 \quad E = E_1 + E_2 \quad E' = E'_1 + E'_2.$$

The transformation for the energy gives

$$E' = \frac{E - \bar{p} \cdot \bar{V}}{\sqrt{1 - v^2}}.$$

The inverse transformation gives

$$E = \frac{E'}{\sqrt{1 - v^2}},$$

from which

$$\bar{p} \cdot \bar{V} = E - E(1 - v^2) = EV^2.$$

Then

$$\bar{p} + EV \left( \frac{1}{\sqrt{1 - v^2}} - 1 \right) - \frac{EV}{\sqrt{1 - v^2}} = 0$$

and

$$\bar{V} = \frac{\bar{p}}{E} = \frac{\bar{p}_1 + \bar{p}_2}{E_1 + E_2}.$$

The total energy in the C system expressed in terms of the initial quantities is

$$E' = E \sqrt{1 - V^2} = E \sqrt{1 - (p^2/E^2)} = \sqrt{E^2 - p^2} = \sqrt{(E_1 + E_2)^2 - (\bar{p}_1 + \bar{p}_2)^2}$$

$$= \sqrt{2(E_1 E_2 - \bar{p}_1 \cdot \bar{p}_2) + m_1^2 + m_2^2} .$$

The final energy of the collision products in the C system can be expressed in terms of the known quantities. To do this one begins from the condition

$$\bar{p}_3' + \bar{p}_4' = 0 .$$

Then

$$E_3' = \sqrt{P^2 + m_3^2} , \quad E_4' = \sqrt{P^2 + m_4^2} ,$$

where  $P = |\bar{p}_3'|$  and

$$P^2 + m_3^2 = (E' - E_4')^2 = (E')^2 + P^2 + m_4^2 - 2E'E_4' ,$$

or

$$E_4' = \frac{(E')^2 + m_4^2 - m_3^2}{2E'} .$$

Similarly

$$E_3' = \frac{(E')^2 + m_3^2 - m_4^2}{2E'} .$$

In order to express the momenta of the collision products in terms of the scattering angles  $\theta$  and  $\phi$  in the C system, it is convenient to define a system whose unit vectors  $\hat{x}$ ,  $\hat{y}$ , and  $\hat{z}$  are defined by

$$\bar{p}'_1 = p'_1 \hat{z}, \quad \bar{v} = \alpha \hat{x} + \beta \hat{z}, \quad \bar{p}'_1 \times \bar{v} = \delta \hat{y},$$

where

$$\alpha = \sqrt{v^2 - \beta^2}, \quad \beta = \frac{1}{p'_1} \bar{p}'_1 \cdot \bar{v}, \quad \delta = \alpha p'_1.$$

The unit vectors are then given by

$$\hat{x} = \frac{1}{\alpha} \bar{v} - \frac{\beta}{\alpha p'_1} \bar{p}'_1, \quad \hat{y} = \frac{1}{\alpha p'_1} \bar{p}'_1 \times \bar{v}, \quad \hat{z} = \frac{1}{p'_1} \bar{p}'_1,$$

and in terms of these

$$\begin{aligned} \bar{p}'_3 &= p'_3 (\sin\theta \cos\phi \hat{x} + \sin\theta \sin\phi \hat{y} + \cos\theta \hat{z}) \\ &= p'_3 \left[ \frac{1}{\alpha} \sin\theta \cos\phi \bar{v} + \left( \cos\theta - \frac{\beta}{\alpha} \sin\theta \cos\phi \right) \frac{1}{p'_1} \bar{p}'_1 \right. \\ &\quad \left. + \frac{1}{\alpha p'_1} \sin\theta \sin\phi (\bar{p}'_1 \times \bar{v}) \right]. \end{aligned}$$

Then using the inverse transformations

$$\begin{aligned} E_3 &= \frac{E'_3 + \bar{p}'_3 \cdot \bar{v}}{\sqrt{1 - v^2}} \\ &= \frac{E}{E'} \left\{ E'_3 + p'_3 \left[ \left( \cos\theta - \frac{\beta}{\alpha} \sin\theta \cos\phi \right) \beta + \frac{v^2}{\alpha} \sin\theta \cos\phi \right] \right\} \\ &= \frac{E}{E'} \left[ E'_3 + p'_3 (\beta \cos\theta + \alpha \sin\theta \cos\phi) \right], \end{aligned}$$

$$\bar{p}_3 = \bar{p}'_3 + \frac{\bar{V}(\bar{p}'_3 \cdot \bar{V})}{v^2} \left( \frac{1}{\sqrt{1-v^2}} - 1 \right) + \frac{\bar{V} E'_3}{\sqrt{1-v^2}},$$

$$E_4 = E - E_3, \quad \bar{p}_4 = (\bar{p}_1 + \bar{p}_2) - \bar{p}_3.$$

## APPENDIX C

### SAMPLING TECHNIQUE FOR DETERMINING DISTANCE OF TRAVEL BETWEEN COLLISIONS, TYPE OF COLLISION, AND MOMENTUM OF STRUCK PARTICLE

The basic sampling technique of the entire calculation is that in which the point of collision, the type of collision, and the momentum of the struck particle is determined for a particle moving with relativistic velocity through a sea of protons and a sea of neutrons, each with a given momentum distribution. The sampling technique and the proof of its validity in its most general form is given by Zerby et al.<sup>1</sup> The description and proof of the sampling technique that does not include pion absorption is given here, and the slight modification in the technique needed for the inclusion of pion absorption will be described at the end of this section. With a few exceptions the symbols used will be the same as those used in the complete treatment.<sup>1</sup> The primed symbols will refer to the frame of reference in which the struck particle is at rest; the unprimed symbols will refer to the laboratory system. The units will be such that  $\hbar = c = 1$ . Other symbols are defined as follows:

$E_i$  = Total energy of the incident particle,

$\bar{p}_i$  = Momentum of the incident particle,

$m$  = Mass of the incident particle,

---

<sup>1</sup>C. D. Zerby, R. B. Curtis, and H. W. Bertini, The Relativistic Doppler Problem, Oak Ridge National Laboratory Report ORNL-CF-61-7-20 (July 12, 1961).

$\rho$  = Density of incident particles,

$\bar{j}$  = Incident current

$$= \rho \times (\bar{p}_i / E_i),$$

$E_k$  = Kinetic energy of the incident particle,

$E$  = Total energy of a nucleon in the sea,

$\bar{p}$  = Momentum of a nucleon in the sea,

$M$  = Mass of a nucleon in the sea,

$[N(\bar{p}) d\bar{p}]$  = Nucleons per unit volume in  $d\bar{p}$ ,

$\sigma(E_k')$  = Microscopic cross section at the energy of the incident particle  
measured in the primed frame,

$\bar{V}$  = Velocity of the primed frame

$$= \bar{p}/E,$$

$dR$  = Reaction rate per unit volume in  $d\bar{p}$ ,

$\Sigma$  = Macroscopic cross section.

There are two special effects here which must be accounted for:

They are the exclusion principle and the relativistic effects. The exclusion principle is accounted for by using a cross section,  $\sigma^f$ , defined by

$$\sigma^f = \int_{\Omega_f} \frac{d\sigma}{d\Omega} d\Omega,$$

where  $\Omega_f$  is the solid angle into which the particles can scatter and leave the nucleons with energy greater than the Fermi energy; i.e.,  $\sigma^f$  is the cross section for allowed collisions only. In contrast

$$\sigma = \int_{\Omega} \frac{d\sigma}{d\Omega} d\Omega,$$

where  $\Omega$  represents all solid angles. The simplest way to account for the relativistic effects is to express the reaction rate for one type of reaction,  $\ell$ , in terms of the system in which the struck particle is at rest. For allowed collisions this is simply

$$dR'_{\ell} = |\bar{j}'| \sigma_{\ell}^f(E'_k) [N_{\ell}(\bar{p}) d\bar{p}]',$$

which gives the reactions per unit volume per unit time. However, the quantity  $\Delta x \Delta y \Delta z \Delta t$  is invariant under Lorentz transformations, so that the expression represents the reaction rate in the laboratory system also. The macroscopic cross section for allowed collisions in the laboratory system for the reaction,  $\ell$ , is then defined by

$$dR_{\ell}(\bar{p}) = |\bar{j}| d\Sigma_{\ell}^f = dR'_{\ell}$$

for an incident particle at a given energy.

The expression for the total reaction rate is

$$dR(\bar{p}) = \sum_{\ell} dR_{\ell}(\bar{p}).$$

The expression from which the type of reaction and the momentum of the struck particle are to be sampled is given by the normalized distribution function,  $g(\bar{p})$ , where

$$g(\bar{p}) d\bar{p} = \frac{1}{K} dR(\bar{p}) = \frac{\sum_{\ell} |\bar{j}'| \sigma_{\ell}^f(E_k') [N_{\ell}(\bar{p}) d\bar{p}]}{|\bar{j}| \Sigma^f},$$

in which K, the normalization constant, is

$$\begin{aligned} K &= \int dR(\bar{p}) = \sum_{\ell} \int |\bar{j}'| \sigma_{\ell}^f(E_k') [N_{\ell}(\bar{p}) d\bar{p}] \\ &= \sum_{\ell} \int |\bar{j}| d\Sigma_{\ell}^f = |\bar{j}| \sum_{\ell} \Sigma_{\ell}^f = |\bar{j}| \Sigma^f. \end{aligned}$$

A rejection technique is now used that will yield the proper distribution function for the distance traveled. Very briefly it involves first choosing x from a distribution function  $\Sigma^m e^{-\Sigma^m x}$ , where  $1/\Sigma^m$  gives a shorter mean free path than the true mean free path. Then  $\bar{p}$  and the type of reaction is selected from  $g(\bar{p})$  with a certain probability of rejection. When there is a rejection, a new distance x is chosen from  $\Sigma^m e^{-\Sigma^m x}$ . The procedure is repeated until one obtains an acceptance of the choice of  $\bar{p}$  and the type of reaction whereupon all the x's that were selected are added together to give the distance traveled before the collision.

One must first express  $g(\bar{p})$  in terms of quantities that are known in the laboratory system. One notes that the current,  $\bar{j}$ , and density,  $\rho$ , make up a four-vector that transforms like the momentum and energy four-vector.<sup>2</sup> Thus

$$\bar{j}' = \bar{j} + \frac{\bar{V}(\bar{j} \cdot \bar{V})}{v^2} \left( \frac{1}{\sqrt{1-v^2}} - 1 \right) - \frac{\rho \bar{V}}{\sqrt{1-v^2}}.$$

---

<sup>2</sup>See Appendix B.

Note that the density of incident particles,  $\rho$ , does not enter explicitly since

$$\bar{j} = \rho \bar{v}_1 = \rho \frac{\bar{p}_1}{E_1},$$

and therefore in the ratio  $|\bar{j}'|/|\bar{j}|$  the density cancels out.

To determine  $E'_k$ , consider

$$\bar{v} = \frac{\bar{p}}{E}; \quad \sqrt{1 - v^2} = \sqrt{\frac{E^2 - p^2}{E^2}} = \frac{M}{E}.$$

Then

$$\begin{aligned} E'_k &= E'_i - m = \frac{E_i - \bar{p}_i \cdot \bar{v}}{\sqrt{1 - v^2}} - m \\ &= \frac{E_i E - \bar{p}_i \cdot \bar{p}}{M} - m. \end{aligned}$$

$[N(\bar{p}) d\bar{p}]'$  can be expressed in terms of laboratory quantities by using the relation

$$\Delta x' \Delta y' \Delta z' = \frac{\Delta x \Delta y \Delta z}{\sqrt{1 - v^2}},$$

from which

$$[N(\bar{p}) d\bar{p}]' = N(\bar{p}) d\bar{p} \sqrt{1 - v^2} = \frac{M}{E} N(\bar{p}) d\bar{p}.$$

In developing the rejection technique the following function is used:

$$\frac{\sum^f}{\sum^m} g(\bar{p}) d\bar{p}, \quad \frac{\sum^f}{\sum^m} \leq 1,$$

where  $\Sigma^m$  will be defined presently. The function will now be written in a form suitable for a rejection technique:

$$\begin{aligned} \frac{\Sigma^f}{\Sigma^m} g(\bar{p}) d\bar{p} &= \frac{\Sigma^f}{\Sigma^m} \cdot \frac{1}{|\bar{j}| \Sigma^f} \cdot \sum_{\ell} |\bar{j}'| \sigma_{\ell}^f(E'_k) \frac{M}{E} N_{\ell}(\bar{p}) d\bar{p} \\ &= \sum_{\ell} \frac{\frac{1}{|\bar{j}|} \left[ |\bar{j}'| \sigma_{\ell}(E'_k) \frac{M}{E} \right] N_{\ell}^{\circ}}{\Sigma^m} \cdot \frac{\left[ |\bar{j}'| \sigma_{\ell}(E'_k) \frac{M}{E} \right]}{\left[ |\bar{j}'| \sigma_{\ell}(E'_k) \frac{M}{E} \right]_m} \cdot \frac{\sigma_{\ell}^f(E'_k)}{\sigma_{\ell}(E'_k)} \cdot \frac{N_{\ell}(\bar{p}) d\bar{p}}{N_{\ell}^{\circ}}, \end{aligned}$$

where

$$\left[ |\bar{j}'| \sigma_{\ell}(E'_k) \frac{M}{E} \right]_m \geq \text{maximum of } \left[ |\bar{j}'| \sigma_{\ell}(E'_k) \frac{M}{E} \right],$$

$$N_{\ell}^{\circ} = \int N_{\ell}(\bar{p}) d\bar{p},$$

$$\Sigma_{\ell}^m = \frac{\left[ |\bar{j}'| \sigma_{\ell}(E'_k) \frac{M}{E} \right]_m N_{\ell}^{\circ}}{|\bar{j}|},$$

$$\Sigma^m = \sum_{\ell} \Sigma_{\ell}^m.$$

The steps in the technique for one collision proceed as follows:

1. Choose  $x$  from the function  $\Sigma^m e^{-\Sigma^m x}$ .
2. Select a reaction,  $l$ , with a probability given by  $(\Sigma_l^m / \Sigma^m)$ .
3. Select  $\bar{p}$  from the distribution function

$$\frac{N_l(\bar{p}) d\bar{p}}{N_l^0}$$

4. Tentatively accept  $l$  and  $\bar{p}$  if a random number,  $R$ , is such that

$$R \leq \frac{\left[ |\bar{J}'| \sigma_l(E'_k) \frac{M}{E} \right]}{\left[ |\bar{J}'| \sigma_l(E'_k) \frac{M}{E} \right]_m};$$

otherwise reject  $l$  and  $\bar{p}$  and start again at 1.

5. If  $l$  and  $\bar{p}$  are tentatively accepted, sample from the angular distribution of the reaction  $l$  at energy  $E'_k$  and calculate the final energy of each nucleon. Test to see if these energies are greater than the Fermi energy. If it is, accept  $l$  and  $\bar{p}$ ; if it is not reject  $l$  and  $p$ . The probability of acceptance for this test is

$$\frac{\sigma_l^f(E'_k)}{\sigma_l(E'_k)}$$

If there is a rejection start again at 1; if there is an acceptance add all of the  $x$ 's that were selected in going through step 1 for this collision. The sum of the  $x$ 's gives the distance traveled for the collision.

It will now be demonstrated that this technique yields the proper frequency distributions for the variables selected.

The probability of selecting the type of reaction,  $l$ , and having it accepted is given by

$$\begin{aligned} \frac{\sum_l^m}{\sum^m} \int \frac{N_l(\bar{p}) \, d\bar{p}}{N_l^0} \cdot \frac{\left[ |\bar{j}'| \sigma_l(E'_k) \frac{M}{E} \right]}{\left[ |\bar{j}'| \sigma_l(E'_k) \frac{M}{E} \right]_m} \cdot \frac{\sigma_l^f(E'_k)}{\sigma_l(E'_k)} \\ = \frac{1}{|\bar{j}| \sum^m} \int |\bar{j}'| \sigma_l^f(E'_k) [N(\bar{p}) \, d\bar{p}] \\ = \frac{\sum_l^f}{\sum^m} ; \end{aligned}$$

i.e., the probability of selecting and accepting a reaction,  $l$ , is proportional to the macroscopic cross section for allowed collisions of that reaction.

Now given the reaction,  $l$ , the probability of selecting and accepting a momentum,  $\bar{p}$ , for one of the struck nucleons in the sea is

$$\frac{N_l(\bar{p}) \, d\bar{p}}{N_l^0} \cdot \frac{\left[ |\bar{j}'| \sigma_l(E'_k) \frac{M}{E} \right]}{\left[ |\bar{j}'| \sigma_l(E'_k) \frac{M}{E} \right]_m} \cdot \frac{\sigma_l^f(E'_k)}{\sigma_l(E'_k)} = \frac{dR_l(\bar{p})}{|\bar{j}| \sum_l^m} ;$$

i.e.,  $\bar{p}$  is selected from a function that represents the reaction rate for a given reaction.

The distribution obtained for the distance traveled is obtained by considering the following: The distance traveled between collisions,  $z$ , is given by the sum of the  $x$ 's obtained by sampling from  $\sum^m e^{-\sum^m x}$ . If one

were to sample from the distribution  $n$  times and add the  $x$ 's to give  $z$ , the distribution in  $z$  would be<sup>3</sup>

$$\frac{z^{(n-1)}}{(n-1)!} (\Sigma^m)^n e^{-\Sigma^m z}.$$

In the rejection technique the probability of an acceptance of all quantities on the first attempt is given by

$$\sum_l \frac{\Sigma^f}{\Sigma^m} = \frac{\Sigma^f}{\Sigma^m}.$$

The probability of having  $(n - 1)$  rejections with an acceptance on the  $n^{\text{th}}$  attempt is given by

$$\frac{\Sigma^f}{\Sigma^m} \left(1 - \frac{\Sigma^f}{\Sigma^m}\right)^{n-1}.$$

Therefore the distance traveled will be distributed as

$$\begin{aligned} \sum_{n=1}^{\infty} \frac{\Sigma^f}{\Sigma^m} \left(1 - \frac{\Sigma^f}{\Sigma^m}\right)^{n-1} \frac{z^{n-1}}{(n-1)!} (\Sigma^m)^n e^{-\Sigma^m z} &= \Sigma^f e^{-\Sigma^m z} \left[ \sum_{n=0}^{\infty} (\Sigma^m - \Sigma^f)^n \frac{z^n}{n!} \right] \\ &= \Sigma^f e^{-\Sigma^m z} \left[ e^{(\Sigma^m - \Sigma^f)z} \right] \\ &= \Sigma^f e^{-\Sigma^f z}, \end{aligned}$$

---

<sup>3</sup>Herman Kahn, Applications of Monte Carlo, Atomic Energy Commission Report AECU-3259 (April 19, 1954) p. 44.

which is the distribution required for the distance traveled.

The technique works with a slight modification when pion absorption is included. By the nature of its derivation the pion absorption cross section is independent of the momentum of the nucleons in the nucleus, and, in order to take this reaction into account, one sets

$$\Sigma_{\text{abs}}^f = N_{\text{abs}}^0 \sigma_{\text{abs}}^f = N_{\text{abs}}^0 \sigma_{\text{abs}}$$

and

$$\Sigma_{\text{abs}}^m = N_{\text{abs}}^0 \sigma_{\text{abs}}'$$

so that when the absorption reaction is selected the probability for it being accepted is unity.

Appendix D

LIST OF TABLES

TABLE	PAGE
I. Representative Values of the Semiempirical Parameters Used to Describe the Nucleon-Nucleon Differential Scattering Cross Sections .....	20
II. Pion Absorption Cross Section Per Proton in Nuclear Matter .....	30
III. Calculated and Experimental Total Nonelastic Cross Sections for Incident Protons .....	47
IV. Calculated and Experimental Total Nonelastic Cross Sections for Incident Neutrons .....	49
V. Average Excitation Energy (Mev) for 190-Mev Incident Protons on Various Nuclei .....	52
VI. Comparison of Calculated and Experimental Mean Prong Numbers for 375-Mev Protons on Heavy Emulsion Nuclei .....	57
VII. Comparison of Calculated and Experimental Mean Prong Numbers for 300-Mev Neutrons on Heavy Emulsion Nuclei .....	58
VIII. Gray Prong Distribution for 375-Mev Protons on Heavy Emulsion Nuclei .....	59
IX. Fast Prong Distribution for Heavy Emulsion Nuclei .....	60
X. Cross Sections for the $\text{Cu}^{65}(\text{p,pn})\text{Cu}^{64}$ Reaction and for the Total Nonelastic Scattering as a Function of Proton Energy and Nuclear Configuration .....	63

TABLE

PAGE

XI.	Cross Sections for the $\text{Au}^{197}(\text{p},\text{pn})\text{Au}^{196}$ Reaction and for the Total Nonelastic Scattering as a Function of Proton Energy and Nuclear Configuration .....	64
-----	---	----

Appendix E

LIST OF FIGURES

FIGURE	PAGE
1. A Comparison of Various Nucleon Density Distributions for Nucleons Inside the Nucleus.	
— Standard three-region configuration	
- - - Uniform distribution	
- - - Hofstadter's curve [R. Hofstadter, Revs. Modern Phys. <u>28</u> , 214 (1956)] .....	10
2. Momentum Distribution of Nucleons Inside the Nucleus.	
— Composite distribution from three zero-temperature Fermi energy distributions	
- - - Maxwell-Boltzmann distribution with $kT$ value of 15 Mev .....	12
3. Nucleon Potential vs Nuclear Radius for a Typical Nucleus.	
B.E. is the fixed binding energy of the loosest nucleon ....	14
4. Proton-Proton Total and Elastic Cross Sections vs. Energy.	
○ U. E. Kruse, J. M. Teem, and N. F. Ramsey, Phys. Rev. <u>101</u> , 1079 (1956); ● O. Chamberlain and J. D. Garrison, Phys. Rev. <u>95</u> , 1349(L) (1954); △ O. Chamberlain, E. Segre <sup>1</sup> , and C. Wiegand, Phys. Rev. <u>83</u> , 923 (1951); ▲ F. F. Chen, C. P. Leavitt, and A. M. Shapiro, Phys. Rev. <u>103</u> , 211 (1956); □ L. W. Smith, A. W. McReynolds, and G. Snow, Phys. Rev. <u>97</u> , 1186 (1955); ■ W. B. Fowler <u>et al.</u> , Phys. Rev. <u>103</u> , 1479 (1956).....	16
5. Neutron-Proton Total Cross Sections vs Energy.	
● L. J. Cook <u>et al.</u> , Phys. Rev. <u>75</u> , 7 (1949); □ J. Hadley <u>et al.</u> , Phys. Rev. <u>75</u> , 351 (1949); ◆ J. DeJuren and N. Knable, Phys. Rev. <u>77</u> , 606 (1950); △ J. DeJuren and	

FIGURE	PAGE
B. J. Moyer, Phys. Rev. <u>81</u> , 919 (1951); ▲ A. V. Nedzel, Phys. Rev. <u>94</u> , 174 (1954); ● F. F. Chen, C. P. Leavitt, and A. M. Shapiro, Phys. Rev. <u>103</u> , 211 (1956).....	17
6. Phase Shifts for Pion-Proton Scattering vs Pion Laboratory Energy [J. Orear, Phys. Rev. <u>100</u> , 288 (1955)].....	24
7. $\pi^+$ -Proton and $\pi^-$ -Proton Total Cross Sections vs Energy. ●, ▲ H. L. Anderson <u>et al.</u> , Phys. Rev. <u>91</u> , 155 (1953); ■ S. J. Lindenbaum and L. C. L. Yuan, Phys. Rev. <u>100</u> 306 (1955); ▲, □ R. Cool, O. Piccioni, and D. Clark, Phys. Rev. <u>103</u> , 1082 (1956); ○ J. Ashkin <u>et al.</u> , Phys. Rev. <u>96</u> , 1104 (1954); ▽ H. C. Burrowes <u>et al.</u> , Phys. Rev. Letters <u>2</u> , 119 (1959).....	27
8. Calculated Pion-Proton Cross Sections vs Pion Energy. $\sigma_t(\pi^0)$ , Total cross section for $\pi^0 + p$ scattering; $\sigma_D(\pi^0)$ , Cross section for $\pi^0 + p$ elastic scattering; $\sigma_t(\pi^-)$ , Experimental $\pi^- + p$ total cross section included for comparison purposes; $\sigma_x$ , Cross section for $\pi^- + p$ , $\pi^+ + n$ , $\pi^0 + p$ , and $\pi^0 + n$ exchange scattering; $\sigma_D(\pi^-)$ , Cross section for $\pi^- + p$ elastic scattering .....	28
9. Neutron Spectra at $0^\circ$ from 50-Mev Protons on Carbon. Dashed curve: Hofmann's experimental results [J. A. Hofmann, <u>Neutrons Ejected from Nuclei by 50-Mev Protons</u> , A Ph.D. Thesis submitted to the Faculty of Arts and Sciences of	

FIGURE	PAGE
Harvard University, Cambridge (August, 1952)]; solid lines: calculated spectrum for neutrons emitted in the angular interval $0^{\circ}$ to $11^{\circ}$ .....	66
10. Neutron Spectra at $16^{\circ}$ from 50-Mev Protons on Carbon. Dashed curve: Hofmann's experimental results [J. A. Hofmann, <u>Neutrons Ejected from Nuclei by 50-Mev Protons</u> , A Ph.D. Thesis submitted to the Faculty of Arts and Sciences of Harvard University, Cambridge (August, 1952)]; solid lines: calculated spectrum for neutrons emitted in the angular interval $5^{\circ}$ to $25^{\circ}$ .....	67
11. Neutron Spectra at $0^{\circ}$ from 50-Mev Protons on Lead. Dashed curve: Hofmann's experimental results [J. A. Hoffman, <u>Neutrons Ejected from Nuclei by 50-Mev Protons</u> , A Ph.D. Thesis submitted to the Faculty of Arts and Sciences of Harvard University, Cambridge (August, 1952)]; solid lines: calculated spectrum for neutrons emitted in the interval $0^{\circ}$ to $10^{\circ}$ .....	68
12. Neutron Spectra at $16^{\circ}$ from 50-Mev Protons on Lead. Dashed curve: Hofmann's experimental results [J. A. Hofmann, <u>Neutrons Ejected from Nuclei by 50-Mev Protons</u> , A Ph.D. Thesis submitted to the Faculty of Arts and Sciences of Harvard University, Cambridge (August, 1952)]; solid lines: calculated spectra for neutrons emitted in the angular interval $5^{\circ}$ to $25^{\circ}$ .....	69

FIGURE	PAGE
13. Proton Spectra at $40^\circ$ from 96-Mev Protons on Carbon. Dashed curve: experimental results of Strauch and Titus [K. Strauch and F. Titus, Phys. Rev. <u>104</u> , 191 (1956)]; solid lines: calculated spectrum of protons emitted in the angular interval $30^\circ$ to $50^\circ$ .....	70
14. Proton Spectra at $40^\circ$ from 96-Mev Protons on Fluorine. Dashed curve: experimental results of Strauch and Titus [K. Strauch and F. Titus, Phys. Rev. <u>104</u> , 191 (1956)]; solid lines: calculated spectrum of protons emitted in the angular interval $30^\circ$ to $50^\circ$ .....	71
15. Proton Spectra at $40^\circ$ from 96-Mev Protons on Aluminum. Dashed curve: experimental results of Strauch and Titus [K. Strauch and F. Titus, Phys. Rev. <u>104</u> , 191 (1956)]; solid lines: calculated spectrum of protons emitted in the angular interval $30^\circ$ to $50^\circ$ .....	72
16. Proton Spectra at $40^\circ$ from 96-Mev Protons on Copper. Dashed curve: experimental results of Strauch and Titus [K. Strauch and F. Titus, Phys. Rev. <u>104</u> , 191 (1956)]; solid lines: calculated spectrum of protons emitted in the angular interval $30^\circ$ to $50^\circ$ .....	73
17. Proton Spectra at $40^\circ$ from 96-Mev Protons on Silver. Dashed curve: experimental results of Strauch and Titus [K. Strauch and F. Titus, Phys. Rev. <u>104</u> , 191 (1956)]; solid lines: calculated spectrum of protons emitted in the angular interval $30^\circ$ to $50^\circ$ .....	74

FIGURE	PAGE
18. Proton Spectra at $40^\circ$ from 96-Mev Protons on Bismuth. Dashed curve: experimental results of Strauch and Titus [K. Strauch and F. Titus, Phys. Rev. <u>104</u> , 191 (1956)]; solid lines: calculated spectrum of protons emitted in the angular interval $30^\circ$ to $50^\circ$ .....	75
19. Neutron Spectra at $2.5^\circ$ from 171-Mev Protons on Carbon. Dashed curve: experimental results of Cassels <u>et al.</u> [J. M. Cassels <u>et al.</u> , Phil. Mag. <u>42</u> , 215 (1951)]; solid lines: calculated spectrum of neutrons emitted in the angular interval $0^\circ$ to $15^\circ$ . The units of the ordinate scale are arbitrary .....	76
20. Neutron Spectra at $2.5^\circ$ from 171-Mev Protons on Uranium. Dashed curve: experimental results of Cassels <u>et al.</u> [J. M. Cassels <u>et al.</u> , Phil. Mag. <u>42</u> , 215 (1951)]; solid lines: calculated spectrum of neutrons emitted in the angular interval $0^\circ$ to $15^\circ$ . The units of the ordinate scale are arbitrary. ....	77
21. Proton Spectra from $0^\circ$ to $65^\circ$ for 190-Mev Protons on Aluminum. Dashed curve: experimental results of Bailey [L. E. Bailey, <u>Angle and Energy Distributions of</u> <u>Charged Particles from the High Energy Nuclear Bombardment</u> <u>of Various Elements</u> , University of California Radiation Laboratory Report UCRL-3334 (March 1, 1956)]; solid lines: calculated spectrum .....	78

FIGURE

PAGE

22. Proton Spectra from  $46^\circ$  to  $65^\circ$  for 190-Mev Protons on Aluminum. Error bars: experimental results of Bailey [L. E. Bailey, Angle and Energy Distributions of Charged Particles from the High Energy Nuclear Bombardment of Various Elements, University of California Radiation Laboratory Report UCRL-3334 (March 1, 1956)]; solid lines: calculated spectrum..... 79
23. Proton Spectra from  $102^\circ$  to  $117^\circ$  for 190-Mev Protons on Aluminum. Points: experimental results of Bailey [L. E. Bailey, Angle and Energy Distributions of Charged Particles from the High Energy Nuclear Bombardment of Various Elements, University of California Radiation Laboratory Report UCRL-3334 (March 1, 1956)]; solid lines: calculated spectrum..... 80
24. Proton Spectra from  $100^\circ$  to  $180^\circ$  for 190-Mev Protons on Aluminum. Dashed curve: experimental results of Bailey [L. E. Bailey, Angle and Energy Distributions of Charged Particles from the High Energy Nuclear Bombardment of Various Elements, University of California Radiation Laboratory Report UCRL-3334 (March 1, 1956)]; solid lines: calculated spectrum..... 81

FIGURE	PAGE
25. Proton Spectra from $0^{\circ}$ to $65^{\circ}$ for 190-Mev Protons on Nickel. Dashed curve: experimental results of Bailey [L. E. Bailey, <u>Angle and Energy Distributions of Charged Particles from the High Energy Nuclear Bombardment of Various Elements</u> , University of California Radiation Laboratory Report UCRL-3334 (March 1, 1956)]; solid lines: calculated spectrum.....	82
26. Proton Spectra from $46^{\circ}$ to $65^{\circ}$ for 190-Mev Protons on Nickel. Error bars: experimental results of Bailey [L. E. Bailey, <u>Angle and Energy Distributions of Charged Particles from the High Energy Nuclear Bombardment of Various Elements</u> , University of California Radiation Laboratory Report UCRL-3334 (March 1, 1956)]; solid lines: calculated spectrum.....	83
27. Proton Spectra from $102^{\circ}$ to $117^{\circ}$ for 190-Mev Protons on Nickel. Error bars: experimental results of Bailey [L. E. Bailey, <u>Angle and Energy Distributions of Charged Particles from the High Energy Nuclear Bombardment of Various Elements</u> , University of California Radiation Laboratory Report UCRL-3334 (March 1, 1956)]; solid lines: calculated spectrum .....	84
28. Proton Spectra from $100^{\circ}$ to $180^{\circ}$ for 190-Mev Protons on Nickel. Dashed curve: experimental results of Bailey [L. E. Bailey, <u>Angle and Energy Distributions of Charged Particles from the High Energy Nuclear Bombardment of Various Elements</u> ,	

FIGURE	PAGE
University of California Radiation Laboratory Report UCRL-3334 (March 1, 1956)]; solid lines: calculated spectrum .....	85
29. Proton Spectra from $0^{\circ}$ to $65^{\circ}$ for 190-Mev Protons on Gold. Dashed curve: experimental results of Bailey [L. E. Bailey, <u>Angle and Energy Distributions of Charged Particles from the High Energy Nuclear Bombardment of Various Elements</u> , University of California Radiation Laboratory Report UCRL-3334 (March 1, 1956)]; solid lines: calculated spectrum.....	86
30. Proton Spectra from $46^{\circ}$ to $65^{\circ}$ for 190-Mev Protons on Gold. Points: experimental results of Bailey [L. E. Bailey, <u>Angle and Energy Distributions of Charged Particles from the High Energy Nuclear Bombardment of Various Elements</u> , University of California Radiation Laboratory Report UCRL-3334 (March 1, 1956)]; solid lines: calculated spectrum.....	87
31. Proton Spectra from $102^{\circ}$ to $117^{\circ}$ for 190-Mev Protons on Gold. Points: experimental results of Bailey [L. E. Bailey, <u>Angle and Energy Distributions of Charged Particles from the High Energy Nuclear Bombardment of Various Elements</u> , University of California Radiation Laboratory Report UCRL-3334 (March 1, 1956)]; solid lines: calculated spectrum.....	88

FIGURE	PAGE
32. Proton Spectra from $100^{\circ}$ to $180^{\circ}$ for 190-Mev Protons on Gold. Dashed curve: experimental results of Bailey [L. E. Bailey, <u>Angle and Energy Distributions of Charged Particles from the High Energy Nuclear Bombardment of Various Elements</u> , University of California Radiation Laboratory Report UCRL-3334 (March 1, 1956)]; solid lines: calculated spectrum.....	89
33. Proton Spectra at $90^{\circ}$ from 240-Mev Protons on Carbon. Points: experimental values of Temmer [G. M. Temmer, Phys. Rev. <u>83</u> , 1067 (1951)]; solid curve: calculated spectrum for protons emitted in the angular interval $70^{\circ}$ to $110^{\circ}$ .....	90
34. Proton Spectra at $30^{\circ}$ from 340-Mev Protons on Carbon. Dashed curve: experimental spectrum of Cladis <u>et al.</u> [J. B. Cladis, W. N. Hess, and B. J. Moyer, Phys. Rev. <u>87</u> , 425 (1952)]; solid lines: calculated spectrum of protons emitted in the angular interval $20^{\circ}$ to $40^{\circ}$ . The units of the ordinate scale are arbitrary.....	91
35. Proton Spectra at $0^{\circ}$ for Protons with Energies Greater Than 20 Mev from 90-Mev Neutrons on Carbon. Points: experimental results of Hadley and York [J. Hadley and H. York, Phys. Rev. <u>80</u> , 345 (1950)]; solid lines: calculated spectrum of protons emitted in the angular interval from $0^{\circ}$ to $25^{\circ}$ .....	92

FIGURE	PAGE
36. Proton Spectra at $12^\circ$ for Protons with Energies Greater than 20 Mev from 90-Mev Neutrons on Carbon. Points: experimental results of Hadley and York [J. Hadley and H. York, Phys. Rev. <u>80</u> , 345 (1950)]; solid lines: calculated spectrum of protons emitted in the angular interval from $9^\circ$ to $15^\circ$ .....	93
37. Proton Spectra at $45^\circ$ for Protons with Energies Greater Than 20 Mev from 90-Mev Neutrons on Carbon. Points: experimental results of Hadley and York [J. Hadley and H. York, Phys. Rev. <u>80</u> , 345 (1950)]; solid lines: calculated spectrum of protons emitted in the angular interval from $36^\circ$ to $54^\circ$ .....	94
38. Proton Spectra at $0^\circ$ for Protons with Energies Greater Than 20 Mev from 90-Mev Neutrons on Copper. Points: experimental results of Hadley and York [J. Hadley and H. York, Phys. Rev. <u>80</u> , 345 (1950)]; solid lines: calculated spectrum of protons emitted in the angular interval from $0^\circ$ to $20^\circ$ .....	95
39. Proton Spectra at $12^\circ$ for Protons with Energies Greater Than 20 Mev from 90-Mev Neutrons on Copper. Points: experimental results of Hadley and York [J. Hadley and H. York, Phys. Rev. <u>80</u> , 345 (1950)]; solid lines: calculated spectrum of protons emitted in the angular interval from $9^\circ$ to $15^\circ$ .....	96

FIGURE	PAGE
40. Proton Spectra at $45^\circ$ for Protons with Energies Greater Than 20 Mev from 90-Mev Neutrons on Copper. Points: experimental results of Hadley and York [J. Hadley and H. York, Phys. Rev. <u>80</u> , 345 (1950)]; solid lines: calculated spectrum of protons emitted in the angular interval from $36^\circ$ to $54^\circ$ .....	97
41. Proton Spectrum for a Uniform Nuclear Density Distribution. Solid lines: calculated spectrum of protons emitted in the angular interval $0^\circ$ to $15^\circ$ ; points: experimental values of Hadley and York [J. Hadley and H. York, Phys. Rev. <u>80</u> , 345 (1950)]; for protons emitted at $0^\circ$ . The case is 90-Mev neutrons on copper.....	98
42. Proton Spectra at $25^\circ$ for Protons with Energies Greater Than 20 Mev from 90-Mev Neutrons on Lead. Points: experimental results of Hadley and York [J. Hadley and H. York, Phys. Rev. <u>80</u> , 345 (1950)]; solid lines: calculated spectrum of protons emitted in the angular interval from $15^\circ$ to $35^\circ$ .....	99
43. Proton Spectra at $45^\circ$ for Protons with Energies Greater than 20 Mev from 90-Mev Neutrons on Lead. Points: experimental results of Hadley and York [J. Hadley and H. York, Phys. Rev. <u>80</u> , 345 (1950)]; solid lines: calculated spectrum of protons emitted in the angular interval from $36^\circ$ to $54^\circ$ ....	100

FIGURE	PAGE
44. Angular Distribution of Sparse Black Prongs from 375-Mev Protons on Heavy Emulsion Nuclei. Dashed lines: experimental results of Bernardini <u>et al.</u> [G. Bernardini, E. T. Booth, and S. J. Lindenbaum, Phys. Rev. <u>85</u> , 826 (1952)]; solid lines: calculated distribution for protons emitted with energies from 30 to 100 Mev for 375-Mev protons on Ru <sup>100</sup> .....	101
45. Angular Distribution of Gray Prongs from 375-Mev Protons on Heavy Emulsion Nuclei. Dashed lines: experimental results of Bernardini <u>et al.</u> [G. Bernardini, E. T. Booth, and S. J. Lindenbaum, Phys. Rev. <u>85</u> , 826 (1952)]; solid lines: calculated distribution for protons emitted with energies from 100 to 375 Mev for 375-Mev protons on Ru <sup>100</sup> .....	102
46. Angular Distribution of Protons with Energies Greater Than 20 Mev from 90-Mev Neutrons on Carbon. Dashed curve: experimental results of Hadley and York [J. Hadley and H. York, Phys. Rev. <u>80</u> , 345 (1950)]; solid lines: calculated distribution .....	103
47. Angular Distribution of Protons with Energies Greater than 20 Mev from 90-Mev Neutrons on Copper. Dashed curve: experimental results of Hadley and York [J. Hadley and H. York, Phys. Rev. <u>80</u> , 345 (1950)]; solid lines: calculated distribution.....	104

FIGURE	PAGE
48. Angular Distribution of Protons with Energies Greater than 20 Mev from 90-Mev Neutrons on Lead. Dashed curve: experimental results of Hadley and York [J. Hadley and H. York, Phys. Rev. <u>80</u> , 345 (1950)]; solid lines: calculated distribution .....	105
49. Angular Distribution of Sparse Black Prongs from 300-Mev Neutrons on Heavy Emulsion Nuclei. Dashed lines: experimental results of Bernardini <u>et al.</u> [G. Bernardini, E. T. Booth, and S. J. Lindenbaum, Phys. Rev. <u>85</u> , 826 (1952)]; solid lines: calculated distribution for protons emitted with energies from 30 to 100 Mev for 300-Mev neutrons on Ru <sup>100</sup> .....	106
50. Angular Distribution of Gray Prongs from 300-Mev Neutrons on Heavy Emulsion Nuclei. Dashed lines: experimental results of Bernardini <u>et al.</u> [G. Bernardini, E. T. Booth, and S. J. Lindenbaum, Phys. Rev. <u>85</u> , 826 (1952)]; solid lines: calculated distribution for protons emitted with energies from 100 to 300 Mev for 300-Mev Neutrons on Ru <sup>100</sup> .....	107
51. Nucleon Density Distributions Within the Nucleus When the Nuclear Radius Is Assumed To Be Small. Solid lines: non-uniform nucleon density distribution within the nucleus; dash-dotted lines: uniform nucleon density distribution within the nucleus; dashed curve: experimental curve of Hofstadter [R. Hofstadter, Revs. Modern Phys. <u>28</u> , 214 (1956)].....	108

FIGURE	PAGE
52. Nucleon Density Distributions Within the Nucleus When the Nuclear Radius Is Assumed To Be Medium. Solid lines: nonuniform nucleon density distribution within the nucleus; dash-dotted lines: uniform nucleon density distribution within the nucleus; dashed curve: experimental curve of Hofstadter [R. Hofstadter, Revs. Modern Phys. <u>28</u> , 214 (1956)].....	109
53. Nucleon Density Distributions Within the Nucleus When the Nuclear Radius Is Assumed To Be Large. Solid lines: nonuniform nucleon density distribution within the nucleus; dash-dotted lines: uniform nucleon density distribution within the nucleus; dashed curve: experimental curve of Hofstadter [R. Hofstadter, Revs. Modern Phys. <u>28</u> , 214 (1956)] .....	110
54. Nucleon Density Distributions Within the Nucleus When the Nuclear Radius Is Assumed To Be Small. Solid lines: nonuniform nucleon density distribution within the nucleus; dash-dotted lines: uniform nucleon density distribution within the nucleus; dashed curve: experimental curve of Hofstadter [R. Hofstadter, Revs. Modern Phys. <u>28</u> , 214 (1956)] .....	111
55. Nucleon Density Distributions Within the Nucleus When the Nuclear Radius Is Assumed To Be Medium. Solid lines:	

FIGURE	PAGE
nonuniform nucleon density distribution within the nucleus; dash-dotted lines: uniform nucleon density distribution within the nucleus; dashed curve: experimental curve of Hofstadter [R. Hofstadter, Revs. Modern Phys. <u>28</u> , 214 (1956)] .....	112
56. Nucleon Density Distributions Within the Nucleus When the Nuclear Radius Is Assumed To Be Large. Solid lines: non-uniform nucleon density distribution within the nucleus; dash-dotted lines: uniform nucleon density distribution within the nucleus; dashed curve: experimental curve of Hofstadter [R. Hofstadter, Revs. Modern Phys. <u>28</u> , 214 (1956)] .....	113
57. Energy Spectra of Nonelastic $\pi^+$ Emitted in the Angular Interval $0^\circ$ to $60^\circ$ from 195-Mev $\pi^+$ on Lithium and Carbon. Dashed lines: experimental results of Petrov <u>et al.</u> [N. I. Petrov, V. G. Ivanov, and V. A. Rusakov, Soviet Phys.-JETP <u>10</u> , 682 (1960)]; solid lines: calculated spectrum. Units of the ordinate scale are arbitrary.....	126
58. Energy Spectra of Nonelastic $\pi^+$ Emitted in the Angular Interval $120^\circ$ to $180^\circ$ from 195-Mev $\pi^+$ on Lithium and Carbon. Dashed lines: experimental results of Petrov <u>et al.</u> [N. I. Petrov, V. G. Ivanov, and V. A. Rusakov, Soviet Phys.-JETP <u>10</u> , 682 (1960)]; solid lines: calculated spectrum. Units of the ordinate scale are arbitrary.....	127

FIGURE	PAGE
59. Energy Spectra of Nonelastic $\pi^-$ Emitted Into the Angular Interval $0^\circ$ to $60^\circ$ from 300-Mev $\pi^-$ on Heavy Emulsion Nuclei. Dashed lines: experimental values of Chemel [B. Willot-Chemel, Ann. Phys. (France) <u>6</u> , 703 (1961)]; solid lines: calculated values for 300-Mev $\pi^-$ on Ru <sup>100</sup> . Units of the ordinate scale are arbitrary .....	128
60. Energy Spectra of Nonelastic $\pi^-$ Emitted Into the Angular Interval $60^\circ$ to $120^\circ$ from 300-Mev $\pi^-$ on Heavy Emulsion Nuclei. Dashed lines: experimental values of Chemel [B. Willot-Chemel, Ann. Phys. (France) <u>6</u> , 703 (1961)]; solid lines: calculated values for 300-Mev $\pi^-$ on Ru <sup>100</sup> . Units of the ordinate scale are arbitrary.....	129
61. Energy Spectra of Nonelastic $\pi^-$ Emitted Into the Angular Interval $120^\circ$ to $180^\circ$ from 300-Mev $\pi^-$ on Heavy Emulsion Nuclei. Dashed lines: experimental values of Chemel [B. Willot-Chemel, Ann. Phys. (France) <u>6</u> , 703 (1961)]; solid lines: calculated values for 300-Mev $\pi^-$ on Ru <sup>100</sup> . Units of the ordinate scale are arbitrary.....	130
62. Energy Spectra of Nonelastic $\pi^-$ from 300-Mev $\pi^-$ on Heavy Emulsion Nuclei. Dashed lines: experimental results of Chemel [B. Willot-Chemel, Ann. Phys. (France) <u>6</u> , 703 (1961)]; solid lines: calculated nonelastic $\pi^-$ spectrum for 300-Mev $\pi^-$ on Ru <sup>100</sup> . Units of the ordinate scale are arbitrary.....	131

FIGURE

PAGE

63. Nonelastic  $\pi^-$  Spectra at  $90^\circ$  from 150-Mev  $\pi^-$  on Lead.  
Calculated spectra for  $\pi^-$  in the interval  $78^\circ$  to  $102^\circ$   
for nucleus with small radius. Solid lines: non-  
uniform nucleon density distribution within the nucleus;  
dashed lines: uniform density distribution; points:  
experimental values of Miller [R. H. Miller, Nuovo Cimento  
6, 882 (1957)] ..... 132
64. Nonelastic  $\pi^-$  Spectra at  $90^\circ$  from 150-Mev  $\pi^-$  on Lead.  
Calculated spectra for  $\pi^-$  in the interval  $78^\circ$  to  $102^\circ$  for  
nucleus with medium radius. Solid lines: nonuniform  
nucleon density distribution within the nucleus; dashed  
lines: uniform density distribution; points: experimental  
values of Miller [R. H. Miller, Nuovo Cimento 6, 882  
(1957)] ..... 133
65. Nonelastic  $\pi^-$  Spectra at  $90^\circ$  from 150-Mev  $\pi^-$  on Lead.  
Calculated spectra for  $\pi^-$  in the interval  $78^\circ$  to  $102^\circ$   
for nucleus with large radius. Solid lines: nonuniform  
nucleon density distribution within the nucleus; dashed  
lines: uniform density distribution; points: experi-  
mental values of Miller [R. H. Miller, Nuovo Cimento  
6, 882 (1957)] ..... 134

FIGURE	PAGE
66. Nonelastic $\pi^-$ Spectra at $138^\circ$ from 150-Mev $\pi^-$ on Lead. Calculated spectra for $\pi^-$ in the interval $130^\circ$ to $148^\circ$ for nucleus with small radius. Solid lines: nonuniform nucleon density distribution within the nucleus; dashed lines: uniform density distribution; points: experi- mental values of Miller [R. H. Miller, Nuovo Cimento <u>6</u> , 882 (1957)] .....	135
67. Nonelastic $\pi^-$ Spectra at $138^\circ$ from 150-Mev $\pi^-$ on Lead. Calculated spectra for $\pi^-$ in the interval $130^\circ$ to $148^\circ$ for nucleus with medium radius. Solid lines: nonuniform nucleon density distribution within the nucleus; dashed lines: uniform density distribution; points: experi- mental values of Miller [R. H. Miller, Nuovo Cimento <u>6</u> , 882 (1957)].....	136
68. Nonelastic $\pi^-$ Spectra at $138^\circ$ from 150-Mev $\pi^-$ on Lead. Calculated spectra for $\pi^-$ in the interval $130^\circ$ to $148^\circ$ for nucleus with large radius. Solid lines: nonuniform nucleon density distribution within the nucleus; dashed lines: uniform distribution; points: experimental values of Miller [R. H. Miller, Nuovo Cimento <u>6</u> , 882 (1957)].....	137

69. Nonelastic Spectrum for  $\pi^-$  Emitted into the Backward Hemisphere from 162-Mev  $\pi^-$  on Heavy Emulsion Nuclei. Calculated values are for 162-Mev  $\pi^-$  on  $Ru^{100}$  with a small nuclear radius. Solid lines: nonuniform nucleon density distribution within the nucleus; dotted lines: uniform nucleon density distributions; dashed lines: experimental results of Nikolskii et al [B. A. Nikolskii, L. P. Kudrin, and S. A. Ali-Zade, Soviet Phys.-JETP 5, 93 (1957)]. The units of the ordinate scale are arbitrary ..... 138
70. Nonelastic Spectrum for  $\pi^-$  Emitted into the Backward Hemisphere from 162-Mev  $\pi^-$  on Heavy Emulsion Nuclei. Calculated values are for 162-Mev  $\pi^-$  on  $Ru^{100}$  with a medium nuclear radius. Solid lines: nonuniform nucleon density distribution within the nucleus; dotted lines: uniform nucleon density distribution; dashed lines: experimental results of Nikolskii et al. [B. A. Nikolskii, L. P. Kudrin, and S. A. Ali-Zade, Soviet Phys.-JETP 5, 93 (1957)]. The units of the ordinate scale are arbitrary ..... 139
71. Nonelastic Spectrum for  $\pi^-$  Emitted into the Backward Hemisphere from 162-Mev  $\pi^-$  on Heavy Emulsion Nuclei. Calculated values are for 162-Mev  $\pi^-$  on  $Ru^{100}$  with a large nuclear radius. Solid lines: nonuniform nucleon density distribution within the nucleus; dotted lines: uniform nucleon density distribution; dashed lines: experimental results of Nikolskii et al.

FIGURE	PAGE
[B. A. Nikolskii, L. P. Kudrin, and S. A. Ali-Zade, Soviet Phys.-JETP <u>5</u> , 93 (1957)]. The units of the ordinate scale are arbitrary.....	140
72. Angular Distribution of Nonelastic $\pi^-$ Scattered with Energy Loss Greater than 40 Mev for 125-Mev $\pi^-$ on Carbon. Points: experimental values of Kessler and Lederman [J. O. Kessler and L. M. Lederman, Phys. Rev. <u>94</u> , 689 (1954)]; solid lines: calculated distribution.....	141
73. Angular Distribution of Nonelastic $\pi^-$ Scattered with Energy Loss Greater than 40 Mev for 125-Mev $\pi^-$ on Lead. Points: experimental values of Kessler and Lederman [J. O. Kessler and L. M. Lederman, Phys. Rev. <u>94</u> , 689 (1954)]; solid lines: calculated distribution. ....	142
74. Angular Distribution of Nonelastic $\pi^+$ from 195-Mev $\pi^+$ on Lithium. Points: experimental values of Petrov <u>et al.</u> [N. I. Petrov, V. G. Ivanov, and V. A. Rusakov, Soviet Phys.-JETP <u>10</u> , 682 (1960)]; solid lines: calculated $\pi^+$ spectrum reduced by the ratio of the experimental to the calculated total nonelastic cross section.....	143
75. Angular Distribution of Nonelastic $\pi^+$ from 195-Mev $\pi^+$ on Carbon. Points: experimental values of Petrov <u>et al.</u> [N. I. Petrov, V. G. Ivanov, and V. A. Rusakov, Soviet Phys.-JETP <u>10</u> , 682 (1960)]; solid lines: calculated spectrum.....	144

FIGURE	PAGE
76. Angular Distribution of Nonelastic $\pi^-$ from 162-Mev $\pi^-$ on Heavy Emulsion Nuclei. Calculated distribution for nucleus with small radius. Dashed lines: experimental values of Nikolskii <u>et al.</u> [B. A. Nikolskii, L. P. Kudrin, and S. A. Ali-Zade, Soviet Phys.-JETP <u>5</u> , 93 (1957)]; solid lines: calculated spectra for a non-uniform nucleon density distribution within the nucleus; dash-dotted lines: uniform nucleon density distribution .....	145
77. Angular Distribution of Nonelastic $\pi^-$ from 162-Mev $\pi^-$ on Heavy Emulsion Nuclei. Calculated distribution for nucleus with medium radius. Dashed lines: experimental values of Nikolskii <u>et al.</u> [B. A. Nikolskii, L. P. Kudrin, and S. A. Ali-Zade, Soviet Phys.-JETP <u>5</u> , 93 (1957)]; solid lines: calculated spectra for a nonuniform nucleon density distribution within the nucleus; dash-dotted lines: uniform nucleon density distribution .....	146
78. Angular Distribution of Nonelastic $\pi^-$ from 162-Mev $\pi^-$ on Heavy Emulsion Nuclei. Calculated distribution for nucleus with large radius. Dashed lines: experimental values of Nikolskii <u>et al.</u> [B. A. Nikolskii, L. P. Kudrin, and S. A. Ali-Zade, Soviet Phys.-JETP <u>5</u> , 93 (1957)];	

FIGURE	PAGE
solid lines: calculated spectra for a nonuniform nucleon density distribution within the nucleus; dash-dotted lines: uniform nucleon density distribution .....	147
79. Energy Spectra of Protons with Energies Greater than 15 Mev for Slow $\pi^-$ Absorption on Heavy Emulsion Nuclei. Calculated values are for 1-Mev $\pi^-$ on Ru <sup>100</sup> . Solid lines: calculated spectrum for standard nuclear configuration, i.e., medium radius, nonuniform nuclear density distribution within the nucleus; dash-dotted lines: calculated spectrum for small radius configuration with uniform nucleon density distribution within the nucleus; dashed lines: experimental results of Azimov <u>et al.</u> [S. A. Azimov <u>et al.</u> , Soviet Phys.-JETP <u>4</u> , 632 (1957)]. The units of the ordinate scale are arbitrary.....	148
80. Angular Distribution of Two-Prong Stars as a Function of the Angle Between Them. Prongs result from 50-Mev $\pi^+$ absorption on carbon. Solid lines: calculated values; dashed lines: experimental values of Laberrigue <u>et al.</u> [J. Laberrigue, M. P. Balandine, and S. J. Otvinovski, J. phys. radium <u>21</u> , 54 (1960)]. The units of the ordinate scale are arbitrary.....	149

#### ACKNOWLEDGEMENT

The author would like to express his sincerest appreciation to Dr. C. D. Zerby for suggesting the problem, and for the many time-consuming discussions concerning all of its aspects.

Dr. R. B. Curtis participated in some of the preliminary calculations and was available for discussion at all times. His help is also gratefully acknowledged.

Finally the author is indebted to Dr. T. A. Welton for agreeing to become an advisor in this work and for suggesting that the calculation (which will be continued to higher incident particle energies) be submitted in present form as a fulfillment of the thesis requirements of the University of Tennessee.



ORNL-3383  
UC-32 - Mathematics and Computers  
TID-4500 (19th ed.)

INTERNAL DISTRIBUTION

- |                                     |                                 |
|-------------------------------------|---------------------------------|
| 1. Biology Library                  | 47. C. E. Larson                |
| 2-3. Central Research Library       | 48. M. H. Lietzke               |
| 4. Reactor Division Library         | 49. F. K. McGowan               |
| 5-6. ORNL - Y-12 Technical Library  | 50. A. Meyer                    |
| Document Reference Section          | 51. J. J. Pinajian              |
| 7-31. Laboratory Records Department | 52. C. A. Preskitt              |
| 32. Laboratory Records, ORNL R.C.   | 53. M. J. Skinner               |
| 33. F. S. Alsmiller                 | 54. J. A. Swartout              |
| 34. R. G. Alsmiller, Jr.            | 55. J. E. Turner                |
| 35-39. H. W. Bertini                | 56. A. M. Weinberg              |
| 40. E. P. Blizard                   | 57. C. D. Zerby                 |
| 41. R. R. Coveyou                   | 58. A. Zucker                   |
| 42. E. Eichler                      | 59. R. A. Charpie (consultant)  |
| 43. C. B. Fulmer                    | 60. P. F. Gast (consultant)     |
| 44. M. L. Halbert                   | 61. R. F. Taschek (consultant)  |
| 45. W. H. Jordan                    | 62. T. J. Thompson (consultant) |
| 46. W. E. Kinney                    |                                 |

EXTERNAL DISTRIBUTION

63. L. Jackson Laslett, Chief, High Energy Physics Branch, Division of Research, U.S. Atomic Energy Commission, Washington 25, D.C.
64. Richard B. Curtis, Indiana University, Bloomington, Indiana
65. Herman J. Schaefer, U.S. Naval School of Aviation, Pensacola, Florida
66. S. P. Shen, New York University, New York, New York
67. E. A. Cosbie, Argonne National Laboratory, Argonne, Illinois
- 68-72. University of California Radiation Laboratory, Berkeley (1 copy each to B. J. Moyer, R. Wallace, W. Patterson, C. Sondhaus, and C. Tobias)
- 73-76. Stanford Linear Accelerator Center, Stanford University, Stanford, California (1 copy each to K. G. Dedrick, H. DeStaebler, Jr., R. F. Mozley, and W. K. H. Panofsky)
77. M. Stanley Livingston, Cambridge Electron Accelerator, Cambridge 38, Massachusetts
- 78-79. NASA, Goddard Space Flight Center, Greenbelt, Maryland (1 copy each to Wilmot N. Hess and Frank McDonald)
- 80-81. Bendix Systems Division, Ann Arbor, Michigan (1 copy each to O. L. Tiffany and Keith More)
- 82-83. University of Tennessee, Knoxville, Tennessee (1 copy each to R. L. Childers and W. M. Bugg)
84. Aaron Galonsky, Midwestern Universities Research Association, Madison 5, Wisconsin
- 85-90. Brookhaven National Laboratory, Upton, Long Island, New York (1 copy each to F. P. Cowan, S. J. Lindenbaum, G. Friedlander, Y. Shimamoto, Catherine Chen, and J. R. Grover)

91. H. B. Knowles, Yale University, Sloane Laboratory, New Haven, Connecticut
- 92-98. General Dynamics/Fort Worth, Texas (1 copy each to R. A. Miller, R. French, N. Schaeffer, C. F. Johnson, T. W. Deveries, T. J. Roch, and S. Dominey)
- 99-100. Department of Commerce, National Bureau of Standards, Washington, D.C. (1 copy each to J. H. Hubbell and M. J. Berger)
101. J. M. Miller, Chemistry Department, Columbia University, New York, New York
102. A. Turkevich, Enrico Fermi Institute of Nuclear Studies, University of Chicago, Chicago, Illinois
103. J. H. Roberts, Physics Department, Northwestern University, Evanston, Illinois
104. John P. Neissel, Electrical Engineering Laboratory, General Electric Company, Schenectady 5, New York
105. Sol Krasner, Office of Naval Research, Washington 25, D.C.
106. E. V. Vaughan, Dept. 716-612, Atomics International, Canoga Park, California
107. Harry Schulte, Bellcomm, Inc., Washington, D.C.
- 108-109. Advanced Research Corporation, Lafayette, Indiana (1 copy each to W. M. Schofield and E. C. Smith)
110. R. V. Glowczwski, McDonnell Aircraft, St. Louis, Missouri
111. R. A. Glass, Lockheed Missiles and Space Company, Palo Alto, California
112. G. A. Whan, The University of New Mexico, Albuquerque, New Mexico
113. K. D. George, Reactor Requirements Office, Picatinny Arsenal, Dover, New Jersey
114. Fred L. Keller, Aerospace Corporation, El Segundo, California
115. D. H. Robey, General Dynamics/Astronautics, San Diego, California
116. Wright H. Langham, Los Alamos Scientific Laboratory, Los Alamos, New Mexico
- 117-120. NASA, Langley Field, Virginia (1 copy each to L. F. Vosteen, W. C. Hulton, T. Foelsche, and J. E. Duberg)
121. David Langford, Pratt and Whitney Aircraft, East Hartford 8, Connecticut
- 122-125. NASA, Manned Space Craft Center, Houston, Texas (1 copy each to R. H. Steelle, C. Warren, W. L. Gill, and L. N. McMillion)
- 126-127. NASA, Washington, D.C. (1 copy each to J. W. Keller and Lt. Col. Joseph Conner)
- 128-129. NASA, Huntsville, Alabama (1 copy each to Russell Shelton and H. E. Stern)
- 130-134. North American Aviation, Downey, California (1 copy each to E. R. Beever, K. R. Pinckney, G. E. Laubach, L. Clark, and M. R. Kinsler)
135. J. P. T. Pearman, National Academy of Sciences, Washington, D.C.
136. D. W. Drawbaugh, Westinghouse Electric Company, Pittsburgh, Pennsylvania
- 137-138. USAF Aerospace Medical Center, Brooks Air Force Base, Texas (1 copy each to Lt. Col. Ralph G. Allen, Jr., and Col. John E. Pickering)
139. Charles Hill, Lockheed Aircraft, Marietta, Georgia

- 140-141. Jet Propulsion Laboratory, Pasadena, California (1 copy each to R. V. Meghreblian and D. F. Spencer)
- 142-143. Boeing Aircraft Company, Seattle, Washington (1 copy each to D. L. Dye and J. C. Noyes)
- 144. E. M. Finkelman, Grumman Aircraft, Bethpage, New York
- 145. Phil Mittleman, United Nuclear Corporation, White Plains, New York
- 146. Ray Aronson, Technical Research Group, Syossett, New York
- 147. Richard Madey, Republic Aviation Corporation, Farmingdale, Long Island, New York
- 148-149. Lewis Research Center, Cleveland, Ohio (1 copy each to I. M. Karp and R. I. Hildebrand)
- 150-152. The Martin Company, Baltimore 3, Maryland (1 copy each to S. Russak, A. J. Beck, and E. Divita)
- 153-155. Northrup Space Laboratory, Los Angeles, California (1 copy each to M. C. Chapman, R. E. Fortney, and S. H. Levine)
- 156. E. O. Berdahl, Scientific Advisor (Systems), TDX1A, Wright-Patterson Air Force Base, Ohio
- 157-162. WADC, Dayton, Ohio (1 copy each to Capt. R. F. Cooper, C. A. Dempsey, Maj. J. F. Dinwiddie, T. J. McGuire, L. Pittman, and J. Speakman)
- 163. Robert E. Cote, Argonne National Laboratory, 9700 South Cass Avenue, Argonne, Illinois
- 164. Hermann J. Donnert, Nuclear Defense Laboratory, Army Chemical Center, Maryland
- 165. Stanley C. Fultz, Lawrence Radiation Laboratory, P. O. Box 808, Livermore, California
- 166. Erwin R. Gaerttner, Linac Building, Rensselaer Polytechnic Institute, Troy, New York
- 167. Herbert Goldstein, 242 Mudd Building, Columbia University, New York 27, New York
- 168. Phillip B. Hemmig, Division of Reactor Development, U.S. Atomic Energy Commission, Washington 25, D.C.
- 169. Bowen R. Leonard, Jr., Building 326, 300 Area, General Electric Company, Richland, Washington
- 170. Leon J. Lidofsky, 328 Mudd Building, Columbia University, New York 27, New York
- 171. Michael S. Moore, Phillips Petroleum Company, Atomic Energy Division, Idaho Falls, Idaho
- 172. Henry W. Newson, Department of Physics, Duke University, Durham, North Carolina
- 173. Gerald C. Phillips, Department of Physics, Rice University, Houston 1, Texas
- 174. George L. Rogosa, Physics and Mathematics Branch, Division of Research, U.S. Atomic Energy Commission, Washington 25, D.C.
- 175. Vance L. Sailor, Brookhaven National Laboratory, Upton, L.I., New York
- 176. Erwin F. Shrader, Case Institute of Technology, 10900 Euclid Avenue, Cleveland 6, Ohio
- 177. John R. Stehn, Brookhaven National Laboratory, Upton, L.I., New York
- 178. Jacob Benveniste, Lawrence Radiation Laboratory, P. O. Box 808, Livermore, California

179. Ben C. Diven, P Division, Los Alamos Scientific Laboratory,  
Los Alamos, New Mexico
180. Rex G. Fluharty, Phillips Petroleum Company, Atomic Energy  
Division, Idaho Falls, Idaho
181. William W. Havens, Jr., Pegram Nuclear Physics Laboratory,  
Columbia University, New York 27, New York
182. George A. Kolstad, Physics and Mathematics Branch, Division of  
Research, U.S. Atomic Energy Commission, Washington 25, D.C.
183. Alan B. Smith, Reactor Engineering Division, Argonne National  
Laboratory, 9700 South Cass Avenue, Argonne, Illinois
184. Max L. Yeater, Linac Building, Rensselaer Polytechnic  
Institute, Troy, New York
185. Research and Development Division, AEC, ORO
- 186-795. Given distribution as shown in TID-4500 (19th ed.) under  
Mathematics and Computers category (75 copies - OTS)